Colour 85

CRANFIELD INSTITUTE OF TECHNOLOGY

SCHOOL OF AUTOMOTIVE STUDIES

Ph.D. THESIS

H. KURT-ELLI

THE MECHANICS OF THE STEERED WHEELS OF A ROAD VEHICLE

Supervisor: Professor J R Ellis

May, 1982

ABSTRACT

Modern road vehicle suspension and steering systems may generally be classed as multi-loop spatial mechanisms, designed with links constrained and interconnected in such a manner as to attempt a preferred and prescribed motion of the steered wheels with regard to the inputs to the system. The mechanism incorporates elastic and damping elements and is terminated to the ground surface via the tyres. The complete system may be modelled as a multi-body system with spatial kinematics. This work demonstrates an analysis and simulation of the mechanics of a double wishbone/rack and pinion suspension and steering system modelled as a multi-body system.

A 3-dimensional Newton-Euler based approach employing vector and matrix notation is used in deriving the coupled set of non-linear equations of motion, and these together with the kinematic equations of constraint are cast in state space form, and numerical solutions sought using a digital computer. The kinematic equations are derived from the velocity loop equations for the model, and deal with the so-called redundant degrees-of-freedom arising in models of this type in a completely general manner. The tyre, shock absorber, main spring, and steering gear are modelled from empirical data. A feature of the work is that the complete set of equations need not be excessively manipulated manually, and that use of a set of specially written computer program routines allows a numerical formulation of the equations in the machine, enabling the main program to be written from inspection of the 'raw' equations. Large displacements and therefore changes of geometry are considered, with the provision for partial numerical linearization of the geometric aspects if required. The kinematic behaviour of the model is also described.

A supporting experimental programme of work with a vehicle on a rolling drum rig has been conducted in parallel to the simulation work. And results indicate good correlation between theory and experiment at low frequencies of vibration.

ACKNOWLEDGEMENTS

The author wishes to thank Professor J R Ellis for the opportunity to conduct the research and also for his guidance and encouragement throughout the project.

Thanks are also due to many members of the School of Automotive Studies who assisted with the project, and in particular to Jerry Ames and Richard Jones who were involved with the experimental work.

The suspension and steering components were supplied by the Ford Motor Company, and this is gratefully acknowledged.

Finally, to Mrs Eileen Denton and Mrs Julie Saunders warm thanks for their assistance in preparing this thesis.

CONTENTS

LIST OF ILLUSTRATIONS

Figure No.

NOTATION

t	time
$\dot{}$	$\frac{d}{dt}$
o	vector dot product
x	vector cross product
f	function of
P_K	point K
$(\underline{i}, \underline{j}, \underline{k})$	unit vectors along axes of inertial frame of reference
$(\underline{e}_x, \underline{e}_y, \underline{e}_z)$	unit vectors along axes of orthogonal frame of reference fixed in a link.
$\bar{r}_K$	position vector of P_K
$\bar{V}_K$	velocity vector of P_K
$\bar{A}_K$	acceleration vector of P_K
$\bar{W}_K$	angular velocity vector of link-K
$\bar{\alpha}_K$	angular acceleration vector of link-K
(x_K, y_K, z_K)	co-ordinates of P_K in the inertial axis set
(VKX,VKY,VKZ)	components of $\bar{V}_K$ in the inertial axis set
(AKX,AKY,AKZ)	components of $\bar{A}_K$ in the inertial axis set
(WKX,WKY,WKZ)	components of $\bar{W}_K$ in the inertial axis set
(αKX,αKY,αKZ)	components of $\bar{\alpha}_K$ in the inertial axis set
$\bar{\lambda}_{L,M}$	unit vector from P_L to P_M
$L_{L,M}$	distance between P_L and P_M
$\vec{I,J}$	vector path from P_I to P_J
$\bar{F}_K$	force vector at P_K
$\bar{M}_K$	moment vector at P_K
$\Sigma(\bar{M})_K$	sum of moments about P_K
g	gravitational constant

m_K, M_K	mass of link-K
$\bar{r}_{G/K}$	position vector of centre of mass of link-K
$\bar{V}_{G/K}$	velocity vector of centre of mass of link-K
$\bar{A}_{G/K}$	acceleration vector of centre of mass of link-K
T_K	transformation matrix between the inertial axis set and the body fixed axis set in link-K
I_K	inertia tensor of link-K defined about the body fixed axis set
$I_{6,7}$	moment of inertia of link-A about axis through P_6 and P_7
$I_{8,9}$	moment of inertia of link-C about axis through P_8 and P_9
$\bar{F}_T$	tyre force vector
$\bar{M}_T$	tyre moment vector
(FTX,FTY,FTZ), (FX,FY,FZ)	components of $\bar{F}_T$ in the inertial axis set.
(MTX,MTY,MTZ), (MX,MY,MZ)	components of $\bar{M}_T$ in the inertial axis set.
Δf	frequency bandwidth of analysis
$\hat{\gamma}^2$	ordinary coherence function
n	number of averages used in the evaluation of frequency response functions.

Other symbols are defined as they appear and in the context in which they are used.

CHAPTER 1 INTRODUCTION

SUMMARY

The primary functions of suspension and steering systems in road vehicles are described, and the importance of gaining a proper understanding of the mechanics of the steered wheels indicated. A review of previous work in this area of study is presented, a specific need identified, and an objective for the present study correspondingly undertaken. The chapter is concluded with some general comments concerning the thesis.

1.1. INTRODUCTION

Modern road vehicles are constructed with many different types of suspension and steering systems. The primary functions of these units may readily be listed. Suspension systems are required to provide guidance for the relative motion between road wheel and vehicle body, and for springing and damping the vehicle movements. Steering systems are required to enable the vehicle driver to influence the motion of the steered wheels and in doing so provide some degree of directional control of the vehicle. These units are essentially spatial mechanisms containing springing and damping elements. Both systems are incorporated at the front end of vehicles, attempting to control the motion of the steered wheels, and it is this assembly of parts which is hence collectively referred to as the suspension and steering system of a vehicle.

The foregoing description of suspension and steering system functions indicates the strong influence that the performance of these systems has on the ride and handling qualities of the vehicle as a whole. This naturally makes knowledge of the system behaviour highly desirable. Additionally, it is known that vibration of the suspension and steering system may occur largely independently of the vehicle dynamics, thus making such knowledge desirable in its own right. In considering these facts, the importance of understanding the mechanics of the steered wheels of a road vehicle becomes clear. Here, understanding the mechanics of the steered wheels infers developing the necessary techniques to be able to usefully analyse and predict system behaviour under given conditions. This ability may be of considerable value to the engineer by providing more information on which a design may be based, and consequently improving the probability of producing an optimum design. The continuing increase in complexity of vehicle designs suggests that the appreciation and need for these design tools will grow, and in accordance with this, the requirement for more comprehensive analyses increasingly recognised. It is in response to this requirement that the present study has been undertaken.

Cursory examination of some typical suspension and steering systems isolated from the vehicle body reveals some of the problems confronting the engineering analyst. These may conveniently be divided into two main categories; the first associated with the mechanics of the main system mechanism and the second with the mechanics of the various complementary sub-systems. The pneumatic tyre, shock absorber, and other such elements which may be considered distinct from the main system mechanism are all regarded as falling under this heading of sub-systems. Problems apparent in the first of these categories are considered initially. The main system mechanism may be thought of as a collection of links incorporating elastic and damping elements and interconnected in a manner that results in the mechanism having certain required kinematic properties. This is the classic representation of a mechanism. When considered to operate in this particular mode of a well defined mechanism, two problems of analysis may immediately be cited. The first of these being that of finding the relationships between the set of degree-of-freedom variables and the in general larger set of kinematic variables assignable to the individual links, and the second being that of accounting for the inherent non-linearity of the mechanics due to the motion related change in geometry that may occur

in the mechanism. This view of mechanism mechanics is based on the simplifying assumption that the links may be modelled as rigid bodies. Naturally, further difficulties arise in circumstances where the individual links may not be modelled as rigid body components of the mechanism, since these production items are quite often formed with complex shapes and therefore not readily amenable for analysis. Problems of analysis similar to this last type may also be found when considering the sub-system mechanics. However, while it may be difficult to formulate an adequate analytical model for some sub-systems, it is generally possible to synthesize a simple mathematical model using empirically determinable parameters, and subsequently provide an acceptable simulation of the real behaviour. This is not the case with the tyre, and it happens that the task of modelling this particular sub-system proves to be the major difficulty in this second category. The complexity of the structure and behaviour of the tyre are such that a comprehensive analysis has yet to be presented. And although various analyses which serve to illustrate certain aspects of tyre performance have been produced, the inability to call upon more comprehensive models is in fact a serious limitation common to all work involving this item.

A reasonable view of the state of the art in this area of applied mechanics may be obtained upon inspection of the more widely known published material. And, as the development of the self-propelled road vehicle spans many years, it is not surprising to find that a considerable amount of work has been reported. A brief review of the more recently published works is given next.

1.2. PREVIOUS WORK

It is convenient to separate discussion of past work into two areas. The first deals with methods of analysis of mechanisms in general and, because of the particular relevance to this thesis, concentrates mainly on those methods utilizing vector mathematics. The second deals with work directly related to vehicle suspensions, steering systems, and components of these systems.

Waldron (1) presents a survey of known techniques of analysis for spatial mechanisms, and includes references to material published up till 1970. A section of this survey is devoted to those methods employing vectors, and reference is made here to the paper by Staph (2) which demonstrates the ease with which kinematic information may be calculated when vector analysis is used. Chace (3) provides a review of some requisite vector mathematics before demonstrating its application to the kinematic analyses of several mechanisms. Emphasis is placed here on the use of spherical co-ordinates (in expressing unit vectors) and selection of appropriate reference frames. Ellis (4) demonstrates the use of simple vector algebra to obtain the linear velocity relationships in various linkages. When expressed in matrix format, a similarity with control theory is shown, with the geometry and velocities of the linkage forming one side of the equation and the driving velocities the other. Rectangular co-ordinates are used throughout, and some rules to aid formulation of these velocity relationships are provided.

A method of simulating the dynamics of planar systems using a Newtonian

vector mechanics formulation is described by Timm and Ellis (5). The simulation is essentially achieved by solving the differential equations of motion simultaneously with the kinematic equations of constraint, integrating the derivative kinematic variables, and feeding these back to drive the mechanism. This procedure is carried out using a digital computer, and a discussion of some aspects of a computer simulation language suitable for this type of application is included. An example problem that demonstrates this approach to simulating the dynamics of constrained planar mechanical systems is also provided. This approach is further reinforced by Timm et al(6) in a later paper. Begg (7) follows a similar procedure when simulating the mechanics of a spatial 4-bar mechanism which has two revolute pairs and two spherical pairs and is commonly denoted symbolically by RSSR. A feature of the RSSR mechanism is the so-called redundant degree-of-freedom of the link joining the two spherical pairs, and various aspects of the effects of this have been investigated. Some experimental results are provided, enabling comparison with the simulated behaviour to be made.

This period of development in mechanisms study, as with many other branches of engineering, is marked by the increasing use and influence of digital computers. And clearly, one of the direct consequences of this was the early realization by researchers of the possibilities of implementing a general purpose computer-aided design analysis system. Such a system would be capable of automatically formulating an analytical model for a particular mechanism, and would for instance, only require input data specifying the topology of the mechanism in order to simulate its kinematics. Several programs appear to have been developed along these lines by the mid-1970's; probably the best known being IMP (Integrated Mechanisms Program), reported by Sheth and Uicker (8). The techniques employed in this particular program are based on network theory, and matrix and energy methods of analysis. Uicker (9) provides a more detailed exposition of the type of formulation involved by deriving the Lagrange equations for a generalised multi-degree-of-freedom spatial mechanism under the influence of time varying external forces. And Livermore (10) explains the further use of matrix methods in determining equilibrium configurations of spring-restrained mechanisms.

In passing it may be noted that a feature common to all of the generalized programs appears to be the very large computer storage requirement. Finally, in considering the general simulation of multi-degree-of-freedom dynamic models, it may be of importance to include the effects of Coulomb friction, and the recommendations for the implementation of this non-linearity provided by Heller et al (11) may be of interest in this respect.

An over-view of the dynamics of the vehicle and its associated components may be obtained by studying the work of Ellis (12). This work includes a discussion on various design aspects of different suspension systems and steering systems, as well as demonstrating a manner in which kinematic analyses of such systems may be performed. A discussion on steering system vibrations is also included. Some of the essential ideas from various analyses in this work may also be found reproduced by Dorgham (13) who otherwise fails to meet his own prime investigation objective of providing a coherent account of road wheel mechanics.

The behaviour of suspensions during vehicle body motions is of obvious

importance in vehicle dynamics studies, and Hales (14) presents an early analytical account of the motion relationships for simplified models of various systems. The work considers 2-dimensional models with rigid tyres that maintain point contact with the ground but may slip, and examines the constrained motions of the wheel in relationship to the motions of the vehicle body. Ellis (15) extends the analysis to consider 3-dimensional models, and is supported by Butler (16) who provides verifying experimental results from a mechanical test rig.

The value of vibration testing vehicles and vehicle components is now generally accepted, and the practice of such testing widely adopted among the major tyre and vehicle manufacturers. An early account of the type of facilities that are more commonly found today was given by Gough et al (17) in 1965. A description of various test and data analysis procedures associated with the use of vibrators and rolling drums in laboratory testing is included.

One particular type of steering system vibration that has been investigated by many researchers is termed shimmy, and refers to the unwanted oscillations of the steered wheels about their steering axes. A historical background of the automobile shimmy problem is outlined by La Barre and Mills (18) who also demonstrate an analysis for the dynamics of a model suspension and steering system. Podgorski (19) investigates the shimmy phenomenon in a single wheel system using a set of linearized equations of motion, and includes geometric considerations of having wheel wobble and out of round in the analysis. And Dödlbacher (20) describes the use of a nineteen degree-of-freedom vibration model to determine the degree of influence certain factors have on shimmy.

A procedure that may aid the optimization of suspension designs is described by Hardenberg et al (21). The method developed is described with respect to a linear vibration model of a suspension, and recommendations are made which aim to reduce the transmission of road-generated vibration into the vehicle body. Recognition of the fact that suspensions may be more formally regarded and better modelled as multi-body systems consisting of rigid bodies, springs, dampers, and joints is made by Schielen (22) who also provides a general discussion on the dynamical analysis of suspension systems. The concept of a multi-body system is also utilized by Mormon (23) when modelling a front suspension unit. And although the model used here does not appear to allow for wheel rotation and omits representation of a complete steering system, it is nevertheless one of the most realistic of models of a suspension unit. Orlandea and Chace (24) adopt a similar model when demonstrating the ability of the generalised ADAMS (Automatic Dynamic Analysis of Mechanical Systems) computer program to simulate vehicle suspension mechanics.

The importance of the tyre component in studies of this type is well recognised and confirmed by the numerous publications that may be found on the subject. A monograph on the mechanics of pneumatic tyres, edited by Clark (25), provides an evaluation of the field up to 1971. The use of limited analyses to illustrate certain aspects of tyre behaviour has already been stated, and the most frequently encountered of these analyses are those which describe the vertical and steering responses of the tyre. An example of the synthesis of a model using the Four Pole Parameter Method and suitable for the

simulation of the vertical behaviour of a non-rolling tyre is given by Overton et al (26). The model assumes point contact with the ground and lumped parameter representation of tyre properties. Models used in steering response studies are normally restricted to considering the generation of lateral forces and self aligning torques only, and Rogers and Brewer (27) give an example of this type of modelling. In general, tyre equations employed in simulation studies need not be based on models which are even partially physically representative of the tyre, and in fact the group of models derived entirely from experimental data forms a substantial part of the family of all tyre models. The disadvantage with this particular type of modelling is of course that very little understanding of tyre behaviour may be achieved, and theoretical models are important from this point of view. The most commonly formulated tyre theories are those based on the string models, and a discussion of these is given by Pacejka (28) and Sharp and Jones (29).

The usefulness of point contact tyre models in studies considering the presence of rough ground may be expected to be severely limited, as these are unable to account for the enveloping qualities of the tyre. And in simulations of vehicles traversing rough ground, and employing point contact models for simplicity, this factor is usually compensated by inputing a modified ground profile. In broad terms this modification may be thought of as a filtering operation that smoothes the actual road profile. Captain et al (30) discuss this particular procedure, and also provide a comparison of the performance of several tyre models in this type of simulation.

The tyre models employed in the various works referred to here are generally useful in circumstances where the inertial effects of the tyre are not important, and this review is concluded with references to two papers which deal with tyre behaviour when this is not the case. The first is by Potts and Csora (31) who discuss the state of the art in tyre vibration studies as it stood in 1973. And the second is by Potts et al (32) who describe a vibration analysis of a radial tyre modelled as a thin ring on an elastic foundation; a comparison of some theoretical and experimental results is also provided.

1.3. CONCLUSIONS AND STATEMENT OF PRESENT OBJECTIVE

It is apparent from the literature that analytical studies concerned with the mechanics of the steered wheels of road vehicles fall into two categories. These relate essentially to the different levels of assumption made during the model synthesis process. The first category contains the simplest models possible, usually employing a lumped parameter approach to modelling, and incorporating inherent assumptions concerning the kinematics of the mechanism, thus eliminating the need for any difficult geometric reasoning. The corresponding analyses are quite often linear, and generally present very little difficulty in formulation. The usefulness of these models is restricted to certain limited vibration studies. The models in the second category assume that suspension and steering systems may be modelled as multi-body systems consisting of rigid body links with distributed mass properties, and inter-connected with springs, dampers and joints. The usually non-linear analysis associated with this type of model allows for a more precise description of the spatial kinematics of the mechanism. This type of modelling may be expected to result in a more realistic simulation

of behaviour, but the additional complexity involved in the formulation of such models is generally not insignificant, and it is probably for this reason that an analysis of a complete suspension and steering system has not been published. The application of the large generalised mechanisms analysis programs to problems in this area have been limited, and their value not proven; additionally the high computing requirements may be a distinct impediment to some potential users.

The modelling of the tyre component is seen to present major difficulties, and examination of the literature reveals that only partial analyses of simple tyre models have been developed. And finally, it is noted that no theoretical analysis of link elasticity appears to have been included in any of the published works.

In conclusion, with regard to the published work in this area, it may be seen that a complete analysis of a suspension and steering system modelled as a multy-body system with spatial kinematics has not been presented. The objective of the present work is to demonstrate the modelling of a complete suspension and steering system as a spatial mechanism (or multi-body system), and develop suitable procedures of analysis and simulation to enable study of the mechanics of the steered wheels to be made.

1.4. SOME COMMENTS ON THE THESIS

The main thesis work is done in relation to a double wishbone suspension with rack and pinion steering. The primary reason for this selection is that this system is currently one of the commonest of the more complex systems employed in vehicles and in its composition demonstrates many of the characteristics encountered in mechanisms used in road vehicles for this purpose. Secondarily, in being such a popular type, acquisition of a suitable unit would not be a problem. A mathematical description of a basic suspension and steering system model of this type is given in the main thesis; additional complexities that may be introduced into this basic model are discussed in Appendix B. Analysis of the basic model is described in two separate chapters: the main mechanism mechanics being treated in one, and the mechanics of the various sub-systems being treated in the other.

The suspension and steering system model is considered isolated from the vehicle body for the purpose of analysis, and the attachment points are considered stationary with respect to an inertial frame of reference. For brevity, the analysis is demonstrated only for one side of the suspension and steering system model, the extension to both sides being direct and simple. Similarly, for reasons of conciseness, vector and matrix notation is used extensively in the analysis. It may be noted that the use of vectors also alleviates the need for 3-dimensional geometric reasoning and this is especially useful in analysing spatial mechanisms of this type.

In the later stages of this work, a procedure was developed making the traditional need of manipulating equations so that coefficients of unknown variables could be stated explicitly in terms of system parameters unnecessary. This procedure is implemented by use of a set

of specially written computer program routines leading to a numerical formulation of the equations in the computer. However, where more explicit formulations have been worked through prior to developing this technique and are potentially useful to other investigators, these are included in the thesis.

CHAPTER 2 THE MECHANICS OF THE MAIN SUSPENSION AND STEERING MECHANISM MODEL

SUMMARY

A model of a double wishbone suspension and rack and pinion steering system is described. A set of equations which may be used to determine displacements of the mechanism model from a known reference position is derived, and the difficulty introduced by the so-called redundant degrees of freedom of the mechanism described. Various kinematic relationships are derived, and a Newtonian vector mechanics approach is employed to derive the set of equations concerned with the dynamics of the individual links within the mechanism. Vector and matrix notation is used extensively in the analyses, and reference is made to the application of the methods developed to other models.

2.1. INTRODUCTION

An arrangement of a suspension and steering system of the double wishbone and rack and pinion type is illustrated in Fig.1. The components shown here may be seen to be attached to a sub-frame, which is normally in turn bolted onto the vehicle body. This sub-frame is modelled as a rigid body whose position remains unchanged with respect to an inertial frame of reference. The inertial axis set employed is right handed, and its orientation with respect to the ground is shown in Fig.1, and again in Fig.2 which also shows the axes orientation with respect to a complete vehicle system. The X-axis is pointed along the forward direction of the vehicle and the Z-axis intersects the ground in a perpendicular manner. The unit vectors ($\underline{i}$, $\underline{j}$, $\underline{k}$) along the axes of this frame are also shown. A more detailed view of the suspension and steering system is shown in Figs. 3 and 4, and a representation of the basic suspension and steering mechanism model to be analysed is given in Fig.5.

The configuration of the mechanism is defined by the position vectors of several numbered points in the model. These may be seen to either define positions of kinematic pair centres, locate axes that constrain possible link motions, or simply to provide additional reference points that fully define the orientation of a particular link. Effective force and moment vectors acting on links and arising from interaction with sub-systems are referred to various points in the model, and these are similarly labelled using the numbering procedure. The links themselves are labelled using the letters A through F, and brief descriptions of these are included in the illustration. The purpose served by most of the numbered points is clear, although an explanation of all of these is given now for completeness. The points P_1 and P_{12} locate the spin axis of the disc and wheel relative to the stub axle, with P_{12} located at the geometric centre of the wheel. Points P_{18} and P_{19} are fixed in the inertial frame of reference and define the direction of any possible rack motion, and points P_{14} and P_{15} provide the additional reference positions to define the orientation of the links F and D respectively. Some forces and moments effectively acting on the links are referred to points P_{10}, P_{11}, P_{13}, and P_{20}, and these are due to interaction with the main spring, shock absorber, tyre and steering gear sub-systems respectively. More clearly, points P_2, P_3, P_4, and P_5 may be seen to locate the positions of spherical joint centres. And points P_6 and P_7, and P_8 and P_9 may be seen to locate the axes of possible rotation for the upper and lower wishbone links respectively; these four points are stationary with respect to the inertial axis set. The points attached to pair centres may, by definition, be considered to be part of either of the two links inter-connected by the joint.

The links in the model are rigid, as are the bushes, and these are inter-connected with frictionless revolute and spherical joints. The rack and rack housing are considered to form a prismatic pair. Gravitational forces are assumed to be perpendicular to the ground, and acting at the centre of gravity of each of the links; the centres are assumed to be fixed in relation to each of the respective bodies. In respect of this model, the disc and wheel may be considered as a single unit, and this combination is hence simply referred to as the wheel.

The number of degrees of freedom of such models may be determined by subtracting the number of independent kinematic constraint equations that may be formulated from the number of co-ordinates that are necessary to fully specify the configuration of the individual links of the mechanism. This is however, generally, a lengthy procedure for multi-body systems of this and greater complexity, and the definition given by Pars (33) may be usefully employed in such instances. This is that 'the number of velocity-components that can be given arbitrary values' in a system 'is the number of degrees of freedom of the system'. Following this definition, it is apparent from the model illustrated in Fig.5 that the mechanism has four degrees of freedom; these are rack speed ($\dot{s}$), coupler spin velocity ($\dot{\theta}$), wheel spin velocity (W), and upper wishbone link spin velocity ($\dot{\psi}$). It is noted that the lower wishbone link spin velocity ($\dot{\phi}$) may have been selected equally arbitrarily in place of the upper wishbone link spin velocity ($\dot{\psi}$). The analysis of the model is divided into three sections dealing with the position, kinematics, and dynamics of the mechanism, and a few explanatory comments are made here prior to the analysis.

It is to be expected that a position analysis would normally describe the change in configuration of a system from a known reference position given the displacement-component values measured from the reference position and associated with the degrees of freedom. And, although this may be done in part, a peculiarity of mechanisms containing so-called redundant degrees of freedom (such as the coupler and wheel spin velocities) is that this process may not in general be readily completed. The problem is that the particular velocity-component variables usually assigned to these degrees of freedom may not in general be integrated to yield meaningful displacement-component variables. Here, this is due to the possible change in direction of the axis of rotation associated with the degree of freedom, which eliminates the possibility of selecting a fixed reference line from which angular displacements may be measured. It is noted however that this may be due to the properties of the particular co-ordinate system selected.

Kinematic analyses generally provide a description of the velocities and accelerations of individual mechanism links as a function of the degree-of-freedom velocity-component and acceleration-component values of the system. The resulting relationships are usually a set of coupled equations in the degree-of-freedom variables and the unknown kinematic motion variables of the system. In certain cases, limited relationships between certain of the degree-of-freedom variables and link motion variables may be obtained. And physical consideration of the basic mechanism model adopted for this work indicates that this is the case here. The most obvious of these is the clear relationship between the upper and lower wishbone link motions.

A Newtonian approach employing vector and matrix notation is used in the dynamic analysis of the model. General relationships of importance are developed prior to the application of these equations to the individual links. And a description of the transformation of vectors between different axis sets is also included.

2.2. POSITION ANALYSIS

2.2.1. Rack position

The steering rack position may be fully determined by specifying the position vector of P_5, which is

$$\bar{r}_5 = \bar{r}_5\ (s = 0) + s.\bar{\lambda}_{18,19} \qquad (2.1)$$

where $\bar{r}_5$ (s = 0) is the reference position vector of P_5, and is the position from which the displacement s to P_5 is measured, (see Fig. 6(a)).

2.2.2. Upper wishbone link position

The upper wishbone link position may be fully determined by specifying the position vector of P_3. Fig 6(b) shows the link in its reference position from which the angular displacement (ψ) of the link is measured. The locus of P_3 is a circle centred at a point (P_Q) somewhere on the revolute pair axis, and in a plane perpendicular to this axis of rotation. A local axis set which is right handed and fixed in the reference frame is defined by unit vectors ($\underline{\ell}$, $\underline{m}$, $\underline{n}$), where

$$\underline{\ell} \equiv \bar{\lambda}_{6,7} \qquad (2.2(a))$$

$$\underline{m} = [\ \bar{r}_3(\psi = 0) - \bar{r}_Q\ ]/L_{3,Q} \qquad (2.2(b))$$

$$\underline{n} = \underline{\ell} \times \underline{m} \qquad (2.2(c))$$

And these only require knowledge of $\bar{r}_Q$ to be evaluated: $L_{3,Q}$ is the distance between P_3 and P_Q and, as with all distances between pairs of points fixed in a rigid link, is a constant of the system. The distance between P_6 and P_Q is $L_{6,Q}$ and this may be evaluated directly by resolving the vector ($\bar{r}_3 - \bar{r}_6$) along the unit vector $\underline{\ell}$,

$$L_{6,Q} = (\bar{r}_3 - \bar{r}_6) \circ \underline{\ell}$$

$$= \ell_x\ (x_3 - x_6) + \ell_y\ (y_3 - y_6) + \ell_z\ (z_3 - z_6)$$

The position vector of P_Q is then given by

$$\bar{r}_Q = \bar{r}_6 + L_{6,Q} \cdot \underline{\ell}$$

$$\therefore \quad \bar{r}_Q = \bar{r}_6 + [\ell_x\ (x_3 - x_6) + \ell_y\ (y_3 - y_6) + \ell_z (z_3 - z_6)]\ \underline{\ell} \qquad (2.3)$$

And $L_{3,Q}$ may now be evaluated using the reference position for P_3; the triad of unit vectors ($\underline{\ell}$, $\underline{m}$, $\underline{n}$) may also now be completely evaluated. Referring to Fig 6(c), the position of P_3 may now be stated as a function of ψ :

$$\overline{r}_3 = \overline{r}_Q + (L_{3,Q} \cos\psi)\ \underline{m} + (L_{3,Q} \sin\psi)\ \underline{n} \qquad (2.4)$$

2.2.3. Position vectors of remaining spherical pair centres

Given the degree-of-freedom displacement-component value s and angle of rotation ψ from the known mechanism reference position, it is seen that the rack and upper wishbone link positions may be determined. The corresponding positions of the remaining spherical pair centres to be located are those of points P_2 and P_4.

Considering the position of point P_2, the distances between P_2 and three known positions, namely those of P_3, P_8, and P_9, are system constants and impose the necessary constraints on $\overline{r}_2$ for its co-ordinates to be evaluated. The three constraint equations for P_2 are:

$$(x_2 - x_3)^2 + (y_2 - y_3)^2 + (z_2 - z_3)^2 = L^2_{2,3}$$

$$(x_2 - x_8)^2 + (y_2 - y_8)^2 + (z_2 - z_8)^2 = L^2_{2,8}$$

$$(x_2 - x_9)^2 + (y_2 - y_9)^2 + (z_2 - z_9)^2 = L^2_{2,9}$$

Each of these equations constrain P_2 to lie on the surface of a sphere centred at each of the known reference positions with the appropriate constant radius value. The problem of locating P_2 may therefore be thought of as evaluating the position of intersection of three spheres. And given that $\overline{r}_2$ may be evaluated, then this may in turn be used as a reference position, together with $\overline{r}_3$ and $\overline{r}_5$, to locate the remaining spherical pair centre at point P_4 in a similar fashion.

An iterative numerical procedure is often used in solving algebraic equations of this type, and Paul (34) gives a good account of the general use of the popular Newton-Raphson algorithm for solving a set of algebraic equations. The application of this method to the solution of the intersection of three spheres is demonstrated in appendix C. An analytical solution may also be obtained for the particular set of three equations encountered here, and a general description of this is presented next.

2.2.4. Analytical solution to the intersection of three spheres

Referring to Fig 7, the general problem may be re-stated as follows; the positions of three reference points P_1, P_2, and P_3 are known with respect to the frame O'X'Y'Z', the distances between a point P and these reference positions are also known, and it is required that the position of P(x', y', z') be located. The three constraint equations are

$$(x' - x_1')^2 + (y' - y_1')^2 + (z' - z_1')^2 = L_1^2$$

$$(x' - x_2')^2 + (y' - y_2')^2 + (z' - z_2')^2 = L_2^2$$

$$(x' - x_3')^2 + (y' - y_3')^2 + (z' - z_3')^2 = L_3^2$$

An algebraic solution may be effected if a co-ordinate transformation is made. The new frame OXYZ is simply a translation of the original frame to P_1, which now becomes the new origin, the co-ordinates may be evaluated using

$$x_i = x_i' - x_1'$$

$$y_i = y_i' - y_1'$$

$$z_i = z_i' - z_1' \qquad \text{for } i = 1, 2, 3.$$

The constraint equations for the co-ordinates of P(x, y, z) in the new frame may be written as

$$x^2 + y^2 + z^2 = L_1^2 \qquad (2.5(a))$$

$$(x - x_2)^2 + (y - y_2)^2 + (z - z_2)^2 = L_2^2 \qquad (2.5(b))$$

$$(x - x_3)^2 + (y - y_3)^2 + (z - z_3)^2 = L_3^2 \qquad (2.5(c))$$

Expanding equation (2.5(b))

$$x^2 - 2xx_2 + x_2^2 + y^2 - 2yy_2 + y_2^2 + z^2 - 2zz_2 + z_2^2 = L_2^2$$

Substituting equation (2.5(a)) and re-arranging

$$x_2x + y_2y + z_2z = \frac{1}{2}(L_1^2 - L_2^2 + x_2^2 + y_2^2 + z_2^2) \qquad (2.6(a)$$

Similarly for equation (2.5(c))

$$x_3x + y_3y + z_3z = \frac{1}{2}(L_1^2 - L_3^2 + x_3^2 + y_3^2 + z_3^2) \qquad (2.6(b))$$

It is noted that the two algebraic equations (2.6) are linear in the variables x, y and z, and therefore that two of these variables may be found as linear functions of the third variable. And in fact the method of solution to be followed is to evaluate two such linear functions, each relating one of the variables as a function of this third variable, and then substitute these relationships into equation (2.5(a)). The resulting equation may then be solved for the third variable. The other two variables are found working backwards. The procedure is demonstrated

by working through one possible procedure, that of initially finding x and y as a function of z. Letting

$$k_1 = \frac{1}{2}(L_1^2 - L_2^2 + x_2^2 + y_2^2 + z_2^2) \qquad (2.7(a))$$

$$k_2 = \frac{1}{2}(L_1^2 - L_3^2 + x_3^2 + y_3^2 + z_3^2) \qquad (2.7(b))$$

substituting equations (2.7) into (2.6), and putting into matrix format

$$\begin{bmatrix} x_2 & y_2 \\ x_3 & y_3 \end{bmatrix} \cdot \begin{bmatrix} x \\ y \end{bmatrix} = \begin{bmatrix} (k_1 - z_2 z) \\ (k_2 - z_3 z) \end{bmatrix}$$

And following the rules of matrix algebra

$$\begin{bmatrix} x \\ y \end{bmatrix} = \frac{1}{D_1} \begin{bmatrix} y_3 & -y_2 \\ -x_3 & x_2 \end{bmatrix} \begin{bmatrix} (k_1 - z_2 z) \\ (k_2 - z_3 z) \end{bmatrix}$$

$$= \frac{1}{D_1} \begin{bmatrix} \{ y_3 (k_1 - z_2 z) - y_2 (k_2 - z_3 z) \} \\ \{ -x_3 (k_1 - z_2 z) + x_2 (k_2 - z_3 z) \} \end{bmatrix}$$

provided $D_1 \neq 0$, where the determinant, D_1, is defined by

$$D_1 = x_2 . y_3 - y_2 . x_3 \qquad (2.8)$$

Letting

$$k_3 = (y_3 . k_1 - y_2 . k_2)/D_1 \qquad (2.9(a))$$

$$k_4 = (y_2 . z_3 - y_3 z_2)/D_1 \qquad (2.9(b))$$

$$k_5 = (x_2 . k_2 - x_3 . k_1)/D_1 \qquad (2.9(c))$$

$$k_6 = (x_3 . z_2 - x_2 . z_3)/D_1 \qquad (2.9(d))$$

It follows then that the linear functions respectively relating x and y as a function of z are

$$x = k_3 + k_4 . z \qquad (2.10(a))$$

$$y = k_5 + k_6 . z \qquad (2.10(b))$$

Substituting equations (2.10) into (2.5(a))

$$(k_3 + k_4 . z)^2 + (k_5 + k_6 . z)^2 + z^2 = L_1^2$$

$$\therefore \quad z^2 [1 + k_4^2 + k_6^2] + z [2 . (k_3 . k_4 + k_5 . k_6)]$$

$$+ [k_3^2 + k_5^2 - L_1^2] = 0 \qquad (2.11)$$

Letting

$$k_7 = 1 + k_4^2 + k_6^2 \qquad (2.12(a))$$

$$k_8 = 2\,(k_3k_4 + k_5k_6) \qquad (2.12(b))$$

$$k_9 = k_3^2 + k_5^2 - L_1^2 \qquad (2.12(c))$$

equation (2.11) becomes

$$k_7\, z^2 + k_8\, z + k_9 = 0$$

and

$$z = (-k_8 \pm k_{10})/(2k_7) \qquad (2.13)$$

where

$$k_{10} = \sqrt{(k_8^2 - 4\, k_7k_9)} \qquad (2.14)$$

It may thus be seen that, in general, there may be two distinct positions in space which satisfy the three constraint equations, and this is in accord with physical consideration of the constraints, that is that in general a circle results when any two spheres fully intersect and a maximum of two distinct points may then result on the further full intersection of this circle with a third sphere. Equation (2.13) yields up to two solutions for the z co-ordinate, and the corresponding x and y values may be evaluated by use of equations (2.10). These may then be simply transformed to the original axis set O'X'Y'Z'.

In considering the displacement of the mechanism from its known reference position, a criterion is needed to select the appropriate solution from the possible set of two distinct positions. The procedure adopted here is to select the position whose distance to the original position is a minimum; for large displacements from the reference position, this is implemented in stages yielding up-dated intermediate solutions at each step until the total mechanism displacement is achieved.

One of the steps involved in this analytical solution of the three constraint equations is to cast x and y as a function of z, and this was found to be possible provided $D_1 \neq 0$, however, it is perfectly possible that this may not be the case and this is considered now. In passing, it is noted that the condition that $D_1 = 0$ corresponds to the situation where the points resulting from projecting P_2 and P_3 on the xy-plane both lie on a straight line drawn from P_1. Now the decision to adopt z as the independent variable and to seek a solution for this variable first was an arbitrary one, and any of the other two variables could have equally been selected, each yielding different conditons on (x_2, y_2, z_2) and (x_3, y_3, z_3) for which the procedure outlined may be used. The position is summarised by the following; re-writing the equation set (2.6)

$$x_2 x + y_2 y + z_2 z = k_1$$

$$x_3 x + y_3 y + z_3 z = k_2$$

then in general three similar routes are possible

1)
$$\begin{bmatrix} x_2 & y_2 \\ x_3 & y_3 \end{bmatrix} \begin{bmatrix} x \\ y \end{bmatrix} = \begin{bmatrix} (k_1 & - z_2 z) \\ (k_2 & - z_3 z) \end{bmatrix}$$

from which $x, y = f(z)$ provided $D_1 \neq 0$, where

$D_1 = x_2 y_3 - y_2 x_3$

2)
$$\begin{bmatrix} x_2 & z_2 \\ x_3 & z_3 \end{bmatrix} \begin{bmatrix} x \\ z \end{bmatrix} = \begin{bmatrix} (k_1 & - y_2 y) \\ (k_2 & - y_3 y) \end{bmatrix}$$

from which $x, z = f(y)$ provided $D_2 \neq 0$, where

$D_2 = x_2 z_3 - z_2 x_3$

3)
$$\begin{bmatrix} y_2 & z_2 \\ y_3 & z_3 \end{bmatrix} \begin{bmatrix} y \\ z \end{bmatrix} = \begin{bmatrix} (k_1 & - x_2 x) \\ (k_2 & - x_3 x) \end{bmatrix}$$

from which $y,z = f(x)$ provided $D_3 \neq 0$, where

$D_3 = y_2 z_3 - z_2 y_3$

Then provided that all three determinants are not zero, then at least one of these routes may be adopted, and a solution sought in a directly analogous manner to that demonstrated.

The condition that $D_1 = D_2 = D_3 = 0$ may be investigated by noting that

$$\bar{r}_2 \times \bar{r}_3 = \begin{vmatrix} \underline{i} & \underline{j} & \underline{k} \\ x_2 & y_2 & z_2 \\ x_3 & y_3 & z_3 \end{vmatrix}$$

$$= \underline{i} (y_2 z_3 - z_2 y_3) + \underline{j} (x_2 z_3 - z_2 x_3)$$

$$+ \underline{k} (x_2 y_3 - y_2 x_3)$$

$$= D_3 \underline{i} + D_2 \underline{j} + D_1 \underline{k}$$

Then

$$D_1 = D_2 = D_3 = 0$$

$$\Rightarrow \quad \bar{r}_2 \times \bar{r}_3 = \bar{0}$$

But

$$|\bar{r}_2 \times \bar{r}_3| = |\bar{r}_2| \, |\bar{r}_3| \sin \theta$$

where θ is the angle between the two vectors; now the three reference

points P_1, P_2, and P_3 must by definition be distinct, and since $\bar{r}_2$ and $\bar{r}_3$ are the vectors from P_1 to P_2 and P_3 respectively, then

$$|\bar{r}_2| \neq 0 \quad \text{and} \quad |\bar{r}_3| \neq 0$$

$$\therefore \quad \sin\theta = 0$$

$$\therefore \quad \theta = 0, \pm\pi, \pm 2\pi, \ldots\ldots$$

This means that the three reference points must all lie on a straight line. This condition is illustrated in Fig.8, and from this it can be seen that unless the required point of intersection is itself on the line, then an infinite number of solutions is possible. These solutions describe a circle centred on the line, and in a plane perpendicular to the line. The locus of P is outlined by rotation of the three constraining links about the line joining P_1, P_2, and P_3. In considering the application of this analysis to mechanisms, this condition corresponds to the mechanism position not being adequately described by the constraints, and is therefore not considered any further. And finally, in the specific case of a unique solution existing, where P is known to be located on the line, then its position is easily found by selecting the co-ordinate set common to any two of the equations.

$$\bar{r}_p = \pm L_1 \bar{\lambda}_{1,3}$$

$$\bar{r}_p = \pm L_2 \bar{\lambda}_{1,3} + \bar{r}_2$$

$$\bar{r}_p = \pm L_3 \bar{\lambda}_{1,3} + \bar{r}_3$$

2.2.5. Coupler position

Having located the spherical pair centres at P_4 and P_5, only the orientation of the coupler (link-D) about its spin axis remains to be described. P_{15} is part of this link and its position may be used to describe this orientation provided it does not lie on the line passing through points P_4 and P_5. The locus of P_{15} is a circle centred on the line through P_4 and P_5 at P_Q, where

$$\bar{r}_Q = \bar{r}_4 + L_{4,Q} \bar{\lambda}_{4,5}$$

and

$$L_{4,Q} = (\bar{r}_{15} - \bar{r}_4) \circ \bar{\lambda}_{4,5}$$

and these may be evaluated from the mechanism reference position. There are two equations of constraint on $\bar{r}_{15}$

$$(\bar{r}_{14} - \bar{r}_4) \circ \lambda_{4,5} = L_{4,Q}$$

$$|\bar{r}_{15} - r_4| = L_{4,15}$$

Letting

$$\bar{\lambda}_{4,5} = \lambda_x \underline{i} + \lambda_y \underline{j} + \lambda_z \underline{k}$$

Then the constraint equations become

$$(x_{15} - x_4)\lambda_x + (y_{15} - y_4)\lambda_y + (z_{15} - z_4)\lambda_z = L_{4,Q} \qquad (2.15(a))$$

$$(x_{15} - x_4)^2 + (y_{15} - y_4)^2 + (z_{15} - z_4)^2 = L_{4,15}^2 \qquad (2.15(b))$$

The x, y, or z co-ordinate of P_{15} may in general be arbitrarily chosen as the independent variable from which the other two are to be evaluated using the two constraint equations; provided $\lambda_y \neq 0$, then z may be selected:

from equation (2.15(a))

$$(y_{15} - y_4)^2 = \left(\frac{\{L_{4,Q} - (z_{15} - z_4)\,\lambda_z\}}{\lambda_y} - (x_{15} - x_4)\left(\frac{\lambda_x}{\lambda_y}\right) \right)^2$$

substituting this into equation (2.15(b)) and simplifying

$$\left[1 + \left(\frac{\lambda_x}{\lambda_y}\right)^2\right](x_{15} - x_4)^2 - \left[2A\left(\frac{\lambda_x}{\lambda_y}\right)\right](x_{15} - x_4) +$$

$$+ \left[A^2 + (z_{15} - z_4)^2 - L^2_{4,15}\right] = 0 \qquad (2.16)$$

where

$$A = \left[L_{4,Q} - (z_{15} - z_4)\,\lambda_z\right] / \lambda_y$$

And equation (2.16) may be solved to yield two solutions of x_{15} for a given value of z_{15} ; corresponding solutions of y_{15} may then be evaluated using equation (2.15(a)). Correct selection of one of these possible solutions may then be made by inspection.

If $\lambda_y = 0$, and if $\lambda_x \neq 0$, equations (2.15(a)) will yield a solution for x_{15} as a function of z_{15} immediately, and the corresponding solutions for y_{15} may be obtained from equation (2.15(b)). Finally, if

$$\lambda_x = \lambda_y = 0$$

$$\Leftrightarrow \quad \bar{\lambda}_{4,5} = \frac{(z_5 - z_4)}{|z_5 - z_4|}\,\underline{k}$$

$$\therefore \quad z_{15} = z_4 + L_{4,Q}\frac{(z_5 - z_4)}{|z_5 - z_4|}$$

Substituting into equation (2.15(b))

$$(x_{15} - x_4)^2 + (y_{15} - y_4)^2 = L^2_{4,15} - L^2_{4,Q}$$

And either x_{15} or y_{15} may then be used as the independent variable.

2.2.6. Wheel position

The analysis of the intersection of three spheres may be used to locate the wheel spin axis by evaluating the positions of points P_1 and P_{12}; the three reference points being P_2, P_3, and P_4. And the orientation of the wheel about this spin axis may be described in an analogous manner to that adopted for the coupler, with P_{14} acting as the locating point fixed in the wheel system.

2.2.7. Position vectors of more than three points on a link

Given that the positions of three points on a link are known, then provided these do not all lie on a straight line, the position vector of an arbitrary point fixed in this link may be defined in relation to the locations of these points. Considering the rigid body shown in Fig. 9, provided the vectors $(\bar{r}_2 - \bar{r}_1)$ and $(\bar{r}_3 - \bar{r}_1)$ are not co-parallel, the position of a fourth point may be located by using

$$\bar{r}_4 = \left[(\bar{r}_2 - \bar{r}_1) \times (\bar{r}_3 - \bar{r}_1)\right] + \bar{r}_1 \qquad (2.17)$$

P_4 being, by definition, out of the plane containing P_1, P_2 and P_3. These four points may be used to form an axis set from which the relative position of an arbitrary point (P_Q) fixed in the body may be easily calculated for any subsequent angular orientation of the body. The position vector of P_Q is

$$\bar{r}_Q = \bar{r}_1 + a(\bar{r}_2 - \bar{r}_1) + b.(\bar{r}_3 - \bar{r}_1) + c.(\bar{r}_4 - \bar{r}_1) \qquad (2.18)$$

And the constants a, b and c may be found by using the reference position values for $\bar{r}_1$, $\bar{r}_2$, $\bar{r}_3$, and $\bar{r}_Q$; the corresponding vector $\bar{r}_4$ being evaluated from equation (2.17). The vector equation (2.18), with the reference position values substituted may be resolved into the three scalar components

$$x_Q = x_1 + a(x_2 - x_1) + b(x_3 - x_1) + c(x_4 - x_1)$$

$$y_Q = y_1 + a(y_2 - y_1) + b(y_3 - y_1) + c(y_4 - y_1)$$

$$z_Q = z_1 + a(z_2 - z_1) + b(z_3 - z_1) + c(z_4 - z_1)$$

And putting these into matrix format

$$\begin{bmatrix} (x_2 - x_1) & (x_3 - x_1) & (x_4 - x_1) \\ (y_2 - y_1) & (y_3 - y_1) & (y_4 - y_1) \\ (z_2 - z_1) & (z_3 - z_1) & (z_4 - z_1) \end{bmatrix} \begin{bmatrix} a \\ b \\ c \end{bmatrix} = \begin{bmatrix} (x_Q - x_1) \\ (y_Q - y_1) \\ (z_Q - z_1) \end{bmatrix} \qquad (2.19)$$

The matrix equation (2.19) may then be solved for the constants a, b, and c.

2.3. KINEMATIC ANALYSIS

2.3.1. Preliminary note

An equivalent form of the velocity loop equations commonly used in kinematic analyses is employed here in the analysis of the suspension and steering mechanism model. The procedure relies on the fact that the velocity of a point on a rigid link relative to another point on the link is dependent only on the angular velocity of the body and the relative displacement vector between the two points. Referring to Fig. 10, $\bar{W}_k$ is the angular velocity of the link-K relative to the frame OXYZ, and $\bar{\alpha}_k$ is the angular acceleration, then

$$\bar{V}_2 = \bar{V}_1 + \left[\bar{W}_k \times (\bar{r}_2 - \bar{r}_1)\right] \qquad (2.20)$$

Differentiating this yields

$$\bar{A}_2 = \bar{A}_1 + \left[\bar{W}_k \times (\bar{V}_2 - \bar{V}_1)\right] + \left[\bar{\alpha}_k \times (\bar{r}_2 - \bar{r}_1)\right] \qquad (2.21)$$

The various limited relationships between the degree-of-freedom velocity-component and acceleration-component variables and the link motion variables are obtained by making use of the equivalent displacement constraint equation between any two fixed points (P_1, P_2) in a rigid link, that is,

$$(\bar{r}_2 - \bar{r}_1) \circ (\bar{r}_2 - \bar{r}_1) = L_{1,2}^2$$

Differentiating this yields

$$2.\ (\bar{r}_2 - \bar{r}_1) \circ (\bar{V}_2 - \bar{V}_1) = 0$$

And this may be re-stated as

$$\bar{\lambda}_{1,2} \circ \bar{V}_2 = \bar{\lambda}_{1,2} \circ \bar{V}_1 \qquad (2.22)$$

which is simply a statement constraining the relative velocity between P_1 and P_2 along the inter-connecting line $\vec{1,2}$ to be zero. An equivalent equation between accelerations may be obtained by differentiating equation (2.22) and re-arranging,

$$\bar{\lambda}_{1,2} \circ (\bar{V}_2 - \bar{V}_1) + \bar{\lambda}_{1,2} \circ (\bar{A}_2 - \bar{A}_1) = 0 \qquad (2.23)$$

A description of the vector algebra and mechanics employed here may be found in many good texts, among these, the book by Capildeo(35) is mentioned here because of its inclusion of a range of worked application problems which are particularly useful.

2.3.2. General velocity relationships

The mechanism model is re-drawn in Fig.11 for clarity; all vectors are defined with respect to the right-handed axis set OXYZ. The points numbered 6, 7, 8, 9, 16, 17, 18, 19 and 20 are stationary with respect to this frame of reference. And the velocity-components $\dot{s}$, $\dot{\theta}$, $\dot{\psi}$, $\dot{\theta}$, and W are defined to be positive in the directions indicated. Given this, the angular velocity of link-A is

$$\overline{W}_A = \dot{\psi}\ \overline{\lambda}_{6,7}$$

$$= \dot{\psi}\left[\left(\frac{x_7 - x_6}{L_{6,7}}\right)\underline{i} + \left(\frac{y_7 - y_6}{L_{6,7}}\right)\underline{j} + \left(\frac{z_7 - z_6}{L_{6,7}}\right)\underline{k}\right]$$

$$= (WAX)\ \underline{i} + (WAY)\ \underline{j} + (WAZ)\ \underline{k}$$

Similarly for link-C

$$\overline{W}_C = \dot{\phi}\ \overline{\lambda}_{8,9}$$

The angular velocity of the wheel is considered separately and the general relationship required concerning the rest of the mechanism may be expressed as

$$\overline{W}_B,\ \dot{\phi},\ \overline{W}_D = f\ (\dot{s},\ \dot{\psi},\ \dot{\theta})$$

This may be obtained by equating the velocities of various points in the mechanism evaluated from the different kinematic routes possible. The velocity of P_2 via $6\vec{,}3$ and $3\vec{,}2$ is

$$\overline{V}_2 = \left[\overline{W}_A \times (\overline{r}_3 - \overline{r}_6)\right] + \left[\overline{W}_B \times (\overline{r}_2 - \overline{r}_3)\right]$$

And via $8\vec{,}2$

$$\overline{V}_2 = \left[\overline{W}_C \times (\overline{r}_2 - \overline{r}_8)\right]$$

Equating the two equations for $\overline{V}_2$ yields

$$\left[\overline{W}_A \times (\overline{r}_3 - \overline{r}_6)\right] + \left[\overline{W}_B \times (\overline{r}_2 - \overline{r}_3)\right] = \left[\overline{W}_C \times (\overline{r}_2 - \overline{r}_8)\right] \quad (2.24)$$

The velocity of P_5 via $6\vec{,}3$, $3\vec{,}4$, and $4\vec{,}5$ is

$$\overline{V}_5 = \left[\overline{W}_A \times (\overline{r}_3 - \overline{r}_6)\right] + \left[\overline{W}_B \times (\overline{r}_4 - \overline{r}_3)\right] + \left[\overline{W}_D \times (\overline{r}_5 - \overline{r}_4)\right]$$

And also, evaluated directly relative to the rack housing

$$\overline{V}_5 = \dot{s}\ \overline{\lambda}_{18,19}$$

Equating the two equations for $\overline{V}_5$ yields

$$[\overline{W}_A \times (\overline{r}_3 - \overline{r}_6)] + [\overline{W}_B \times (\overline{r}_4 - \overline{r}_3)]$$

$$+ [\overline{W}_D \times (\overline{r}_5 - \overline{r}_4)] = \dot{s}\,\overline{\lambda}_{18,19} \qquad (2.25)$$

And because of the rotational freedom of the link-D about the axis through P_4 and P_5, the further constraint equation concerning the angular velocity of this link must be utilised, that is

$$\overline{W}_D \circ \overline{\lambda}_{4,5} = \dot{\theta} \qquad (2.26)$$

Equations (2.24) and (2.25) may each be resolved into three component scalar equations and together with equation (2.26) form a sufficient set of equations to evaluate the required velocity relationships. Substituting for $\overline{W}_A = \dot{\psi}\,\overline{\lambda}_{6,7}$ and $\overline{W}_C = \dot{\phi}\,\overline{\lambda}_{8,9}$, expanding, re-arranging, simplifying, and putting into matrix format yeilds the matrix equation (2.27) which is in a form suitable for numerical calculation of the required velocity relationships. The matrix [A] referred to in this equation is defined in equation (2.28), and the set of defined geometric functions (G) is given in the equation set (2.29). Numerical solution of the matrix equation (2.27) may be achieved by a number of well known methods, and for given degree-of-freedom velocity-component values yields the unknown angular velocities of individual links.

2.3.3. Limited velocity relationships

Various limited velocity relationships may be evaluated for the part of the mechanism model considered, and two such relationships are demonstrated here. The first of these relates the upper and lower wishbone spin velocities, i.e.

$$\dot{\phi} = f(\dot{\psi})$$

The velocity of P_3 via $\vec{6,3}$ is

$$\overline{V}_3 = \overline{W}_A \times (\overline{r}_3 - \overline{r}_6)$$

$$= \dot{\psi}\,\overline{\lambda}_{6,7} \times (\overline{r}_3 - \overline{r}_6)$$

And the velocity of P_2 via $\vec{8,2}$ is

$$\overline{V}_2 = \overline{W}_C \times (\overline{r}_2 - \overline{r}_8)$$

$$= \dot{\phi}\,\overline{\lambda}_{8,9} \times (\overline{r}_2 - \overline{r}_8)$$

Applying the constraint equation (2.22) to P_2 and P_3

$$\overline{\lambda}_{3,2} \circ \overline{V}_3 = \overline{\lambda}_{3,2} \circ \overline{V}_2$$

$$\overline{\lambda}_{3,2} \circ [\dot{\psi}\,\overline{\lambda}_{6,7} \times (\overline{r}_3 - \overline{r}_6)] = \overline{\lambda}_{3,2} \circ [\dot{\phi}\,\overline{\lambda}_{8,9} \times (\overline{r}_2 - \overline{r}_8)]$$

Expanding and re-arranging yields

$$\dot{\phi} = \left[\frac{L_{8,9}\ (G7)}{L_{6,7}\ (G8)}\right]\dot{\psi} \qquad (2.30)$$

where

$$G7 = (G1)\ (x_2 - x_3) + (G2)\ (y_2 - y_3) + (G3)\ (z_2 - z_3) \qquad (2.31(a))$$

$$G8 = (G4)\ (x_2 - x_3) + (G5)\ (y_2 - y_3) + (G6)\ (z_2 - z_3) \qquad (2.31(b))$$

The second of the relationships may be expressed as

$$\overline{W}_B, \dot{\phi} = f\ (\dot{s}, \dot{\psi})$$

The velocity of P_4 via $\vec{6,3}$ and $\vec{3,4}$ is

$$\overline{V}_4 = \left[(\overline{W}_A \times (\overline{r}_3 - \overline{r}_6)\right] + \left[\overline{W}_B \times (\overline{r}_4 - \overline{r}_3)\right]$$

And the velocity of P_5 as a direct function of a degree-of-freedom variable is

$$\overline{V}_5 = \dot{s}\ \overline{\lambda}_{18,19}$$

Applying the constraint equation (2.22) to the two spherical pair centres at P_4 and P_5

$$\overline{\lambda}_{4,5} \circ \overline{V}_4 = \overline{\lambda}_{4,5} \circ \overline{V}_5$$

$$\therefore\ \overline{\lambda}_{4,5} \circ \left[\{\overline{W}_A \times (\overline{r}_3 - \overline{r}_6)\} + \{\overline{W}_B \times (\overline{r}_4 - \overline{r}_3)\}\right]$$

$$= \overline{\lambda}_{4,5} \circ \left[\dot{s}\ \overline{\lambda}_{18,19}\right] \qquad (2.32)$$

Equation (2.24) may be resolved into three component scalar equations, and together with equation (2.32) used to evaluate the required relationships; substituting $\overline{W}_A = \dot{\psi}\ \overline{\lambda}_{6,7}$ and $\overline{W}_C = \dot{\phi}\ \overline{\lambda}_{8,9}$, expanding, re-arranging, simplifying, and putting into matrix format yields the matrix equation (2.33). Further geometric functions are defined by

$$G9 = (x_{19}-x_{18})\ (x_5-x_4)+(y_{19}-y_{18})\ (y_5-y_4)+(z_{19}-z_{18})\ (z_5-z_4) \qquad (2.34(a))$$

$$G10 = -(z_4-z_3)\ (y_5-y_4) + (y_4-y_3)\ (z_5-z_4) \qquad (2.34(b))$$

$$G11 = (z_4-z_3)\ (x_5-x_4) - (x_4-x_3)\ (z_5-z_4) \qquad (2.34(c))$$

$$G12 = -(y_4-y_3)\ (x_5-x_4) + (x_4-x_3)\ (y_5-y_4) \qquad (2.34(d))$$

$$G13 = (G1)\ (x_5-x_4) + (G2)\ (y_5-y_4) + (G3)\ (z_5-z_4) \qquad (2.34(e))$$

2.3.4. General acceleration relationships

All required acceleration relationships may be obtained by differentiating the relevant velocity equations, and in the general case, equations (2.24), (2.25), and (2.26) may be differentiated to yield

$$[\bar{\alpha}_A \times (\bar{r}_3 - \bar{r}_6)] + [\bar{W}_A \times (\bar{V}_3 - \bar{V}_6)]$$

$$+ [\bar{\alpha}_B \times (\bar{r}_2 - \bar{r}_3)] + [\bar{W}_B \times (\bar{V}_2 - \bar{V}_3)]$$

$$= [\bar{\alpha} \times (\bar{r}_2 - \bar{r}_8)] + [\bar{W}_C \times (\bar{V}_2 - \bar{V}_8)] \qquad (2.35)$$

$$[\bar{\alpha}_A \times (\bar{r}_3 - \bar{r}_6)] + [\bar{W}_A \times (\bar{V}_3 - \bar{V}_6)]$$

$$+ [\bar{\alpha}_B \times (\bar{r}_4 - \bar{r}_3)] + [\bar{W}_B \times (\bar{V}_4 - \bar{V}_3)]$$

$$+ [\bar{\alpha}_D \times (\bar{r}_5 - \bar{r}_4)] + [\bar{W}_D \times (\bar{V}_5 - \bar{V}_4)] = \ddot{s}\,\bar{\lambda}_{18,19} + \dot{s}\,\dot{\bar{\lambda}}_{18,19} \qquad (2.36)$$

$$\bar{\alpha}_D \circ \bar{\lambda}_{4,5} + \bar{W}_D \circ \dot{\bar{\lambda}}_{4,5} = \ddot{\theta} \qquad (2.37)$$

P_6, P_8, P_{18}, and P_{19} are stationary with respect to the frame of reference

$$\therefore \quad \bar{V}_6 = \bar{V}_8 = \bar{V}_{18} = \bar{V}_{19} = \bar{0} \qquad (2.38(a))$$

$$\therefore \quad \dot{\bar{\lambda}}_{18,19} = \frac{d}{dt}\left[(\bar{r}_{19} - \bar{r}_{18})/L_{18,19}\right]$$

$$= \bar{0} \qquad (2.38(b))$$

Also

$$\bar{\alpha}_A = \frac{d}{dt}\left[\dot{\psi}\,\bar{\lambda}_{6,7}\right]$$

$$= \ddot{\psi}\,\bar{\lambda}_{6,7} \qquad (2.38(c))$$

Similarly

$$\bar{\alpha}_C = \ddot{\phi}\,\bar{\lambda}_{8,9} \qquad (2.38(d))$$

The vector equations (2.35) and (2.36) may each be resolved into their respective component scalar equations and together with equation (2.37) form a sufficient set of equations to evaluate the required acceleration relationships. Substituting the simplifying expressions (2.38) into these equations, expanding, re-arranging, simplifying, and putting into matrix format, results in the matrix equation (2.39). The matrix [B] in this equation is defined by equation (2.40), and the various velocity dependent functions (H) are defined in the set of equations (2.41). A3X, A3Y, and A3Z are the components of the acceleration vector of P_3, and may be obtained by applying equation (2.21), i.e.

$$\bar{A}_3 = \bar{A}_6 + [\bar{\alpha}_A \times (\bar{r}_3 - \bar{r}_6)] + [\bar{W}_A \times (\bar{V}_3 - \bar{V}_6)]$$

Substituting

$$\bar{A}_6 = \bar{V}_6 = \bar{0}$$

$$\bar{W}_A = \dot{\psi}\,\bar{\lambda}_{6,7} \text{ and } \bar{\alpha}_A = \ddot{\psi}\,\bar{\lambda}_{6,7}$$

expanding, re-arranging, and resolving into its three components yields

$$A3X = \left(\frac{G1}{L_{6,7}}\right)\ddot{\psi} + \left(\frac{\dot{\psi}}{L_{6,7}}\right)^2[(y_7 - y_6)\ (G3) - (z_7 - z_6)\ (G2)] \qquad (2.42(a))$$

$$A3Y = \left(\frac{G2}{L_{6,7}}\right)\ddot{\psi} + \left(\frac{\dot{\psi}}{L_{6,7}}\right)^2[(z_7 - z_6)\ (G1) - (x_7 - x_6)\ (G3)] \qquad (2.42(b))$$

$$A3Z = \left(\frac{G3}{L_{6,7}}\right)\ddot{\psi} + \left(\frac{\dot{\psi}}{L_{6,7}}\right)^2[(x_7 - x_6)\ (G2) - (y_7 - y_6)\ (G1)] \qquad (2.42(c))$$

Finally, it may be noted that a point of simplification may be made upon more detailed examination of equation (2.37), i.e.

$$\bar{\alpha}_D \circ \bar{\lambda}_{4,5} + \bar{W}_D \circ \dot{\bar{\lambda}}_{4,5} = \ddot{\theta}$$

Now

$$\bar{\lambda}_{4,5} = (\bar{r}_5 - \bar{r}_4)/L_{4,5}$$

$$\therefore \quad \dot{\bar{\lambda}}_{4,5} = (\bar{V}_5 - \bar{V}_4)/L_{4,5}$$

Substituting

$$\bar{V}_5 = \bar{V}_4 + [\bar{W}_D \times (\bar{r}_5 - \bar{r}_4)]$$

$$\dot{\bar{\lambda}}_{4,5} = [\bar{W}_D \times (\bar{r}_5 - \bar{r}_4)]/L_{4,5}$$

$$\therefore \quad \bar{W}_D \circ \dot{\bar{\lambda}}_{4,5} = \bar{W}_D \circ \left[\frac{1}{L_{4,5}}\{\bar{W}_D \times (\bar{r}_5 - \bar{r}_4)\}\right] \qquad (2.43)$$

Mixed triple products of vectors are invariant under circular permutations, and using this property, equation (2.43) becomes

$$\bar{W}_D \circ \dot{\bar{\lambda}}_{4,5} = \frac{1}{L_{4,5}}(\bar{r}_5 - \bar{r}_4) \circ (\bar{W}_D \times \bar{W}_D)$$

$$= 0 \qquad (2.44)$$

Equation (2.37) thus reduces to

$$\bar{\alpha}_D \circ \bar{\lambda}_{4,5} = \ddot{\theta} \qquad (2.45)$$

And also, because of this, the velocity dependent function (H7) may be seen to be equal to zero.

2.3.5. Limited acceleration relationships

The angular accelerations of the upper and lower wishbone links may be related by applying equation (2.23) to points P_2 and P_3, thus

$$\dot{\overline{\lambda}}_{3,2} o(\overline{V}_3 - \overline{V}_2) + \overline{\lambda}_{3,2} o(\overline{A}_3 - \overline{A}_2) = 0$$

substituting

$$\overline{V}_2 = \dot{\phi}\ \overline{\lambda}_{8,9} \times (\overline{r}_2 - \overline{r}_8)$$

$$\overline{A}_2 = [\ddot{\phi}\ \overline{\lambda}_{8,9} \times (\overline{r}_2 - \overline{r}_8)] + [\dot{\phi}\ \overline{\lambda}_{8,9} \times \overline{V}_2]$$

$$\overline{V}_3 = \dot{\psi}\ \overline{\lambda}_{6,7} \times (\overline{r}_3 - \overline{r}_6)$$

expanding and re-arranging, this becomes

$$\ddot{\phi}[G4 + H4)\ (x_2-x_3) + (G5 + H5)\ (y_2-y_3) + (G6 + H6)(z_2-z_3)]$$

$$= L_{8,9}\Big[A3X\ (x_2-x_3) + A3Y\ (y_2-y_3) + A3Z(z_2-z_3)$$

$$- \left\{\left(\frac{G4}{L_{8,9}}\right)\dot{\phi} - \left(\frac{G1}{L_{6,7}}\right)\dot{\psi}\right\}^2$$

$$- \left\{\left(\frac{G5}{L_{8,9}}\right)\dot{\phi} - \left(\frac{G2}{L_{6,7}}\right)\dot{\psi}\right\}^2$$

$$- \left\{\left(\frac{G6}{L_{8,9}}\right)\dot{\phi} - \left(\frac{G3}{L_{6,7}}\right)\dot{\psi}\right\}^2\Big] \qquad (2.46)$$

where the components of $\overline{A}_3$ are given in equation (2.42), and geometry (G) and velocity (H) dependent functions are as previously defined.

The second of the limited acceleration relationships, as with the second of the limited velocity relationships, avoids consideration of the coupler (link-D). Differentiating equations (2.24) and (2.32) yields

$$\left[\overline{\alpha}_A \times (\overline{r}_3 - \overline{r}_6)\right] + \left[\overline{W}_A \times (\overline{V}_3 - \overline{V}_6)\right]$$

$$+ \left[\overline{\alpha}_B \times (\overline{r}_2 - \overline{r}_3)\right] + \left[\overline{W}_B \times (\overline{V}_2 - \overline{V}_3)\right]$$

$$= \left[\overline{\alpha}_C \times (\overline{r}_2 - \overline{r}_8)\right] + \left[\overline{W}_C \times (\overline{V}_2 - \overline{V}_8)\right] \qquad (2.47)$$

$$\dot{\overline{\lambda}}_{4,5} o\left[\{\overline{W}_A \times (\overline{r}_3 - \overline{r}_6)\} + \{\overline{W}_B \times (\overline{r}_4 - \overline{r}_3)\}\right]$$

$$+ \overline{\lambda}_{4,5} o\Big[\{\overline{\alpha}_A \times (\overline{r}_3 - \overline{r}_6)\} + \{\overline{W}_A \times (\overline{V}_3 - \overline{V}_6)\}$$

$$+ \{\overline{\alpha}_B \times (\overline{r}_4 - \overline{r}_3) + \{\overline{W}_B \times (\overline{V}_4 - \overline{V}_3)\}\Big]$$

$$= \bar{\lambda}_{4,5} \circ \left[\{\dot{s}\ \dot{\bar{\lambda}}_{18,19}\} + \{\ddot{s}\ \bar{\lambda}_{18,19}\} \right]$$

$$+ \dot{\bar{\lambda}}_{4,5} \circ \left[\dot{s}\ \bar{\lambda}_{18,19} \right] \qquad (2.48)$$

Equation (2.47) may be resolved into three component equations and together with equation (2.48), upon substitution of equations (2.38), expanding, re-arranging, and simplifying may be put into matrix format; see matrix equation (2.49). Two further velocity dependent functions are defined in this process and these are

$$H14 = (H11)\ (x_5 - x_4) + (H12)\ (y_5 - y_4) + (H13)\ (z_5 - z_4) \qquad (2.50(a))$$

$$H15 = \left[\frac{\dot{s}}{L_{18,19}} (x_{19}-x_{18}) - (V4X) \right]^2 + \left[\frac{\dot{s}}{L_{18,19}} (y_{19}-y_{18}) - (V4Y) \right]^2$$

$$+ \left[\frac{\dot{s}}{L_{18,19}} (z_{19}-z_{18}) - (V4Z) \right]^2 \qquad (2.50(b))$$

2.3.6 Wheel kinematics

The wheel (link-F) has the freedom to rotate about an axis fixed in the stub axle (link-B). The direction of this spin axis is defined by the unit vector $\bar{\lambda}_{1,12}$. With the wheel spin velocity (W) defined to be positive in the direction shown in Fig.11, the angular velocity of the wheel relative to the axle may be written as

$$\bar{W}_R = W\ \bar{\lambda}_{1,12}$$

And by definition

$$\bar{W}_R = \bar{W}_F - \bar{W}_B$$

$$\therefore \quad \bar{W}_F = \bar{W}_B + W\ \bar{\lambda}_{1,12} \qquad (2.51)$$

The angular acceleration may be obtained by differentiating equation (2.51) to yield

$$\bar{\alpha}_F = \bar{\alpha}_B + \dot{W}\ \bar{\lambda}_{1,12} + W\ \dot{\bar{\lambda}}_{1,12} \qquad (2.52)$$

2.3.7. Velocity and acceleration of an arbitrary point

The velocity and acceleration of a point P_Q is given, where P_Q is in turn considered rigidly attached to each of the links.

Link-A

$$\bar{V}_Q = \left[\dot{\psi}\ \bar{\lambda}_{6,7} \times (\bar{r}_Q - \bar{r}_6) \right]$$

$$\bar{A}_Q = \left[\ddot{\psi}\ \bar{\lambda}_{6,7} \times (\bar{r}_Q - \bar{r}_6) \right] + \left[\dot{\psi}\ \bar{\lambda}_{6,7} \times \bar{V}_Q \right]$$

Link-B

$$\bar{V}_Q = \bar{V}_3 + \left[\bar{W}_B \times (\bar{r}_Q - \bar{r}_3)\right]$$
$$\bar{A}_Q = \bar{A}_3 + \left[\bar{\alpha}_B \times (\bar{r}_Q - \bar{r}_3)\right] + \left[\bar{W}_B \times (\bar{V}_Q - \bar{V}_3)\right]$$

Where P_3 may be considered as part of link-A, and $\bar{V}_3$ and $\bar{A}_3$ evaluated accordingly.

Link-C

$$\bar{V}_Q = \left[\dot{\phi}\, \bar{\lambda}_{8,9} \times (\bar{r}_Q - \bar{r}_8)\right]$$
$$\bar{A}_Q = \left[\ddot{\phi}\, \bar{\lambda}_{8,9} \times (\bar{r}_Q - \bar{r}_8)\right] + \left[\dot{\phi}\, \bar{\lambda}_{8,9} \times \bar{V}_Q\right]$$

Link-D

$$\bar{V}_Q = \bar{V}_4 + \left[\bar{W}_D \times (\bar{r}_Q - \bar{r}_4)\right]$$
$$\bar{A}_Q = \bar{A}_4 + \left[\bar{\alpha}_D \times (\bar{r}_Q - \bar{r}_4)\right] + \left[\bar{W}_D \times (\bar{V}_Q - \bar{V}_4)\right]$$

Where P_4 may be considered as part of link-B and $\bar{V}_4$ and $\bar{A}_4$ evaluated accordingly.

Link-E

$$\bar{V}_Q = \dot{s}\, \bar{\lambda}_{18,19}$$
$$\bar{A}_Q = \ddot{s}\, \bar{\lambda}_{18,19}$$

Link-F

$$\bar{V}_Q = \bar{V}_{12} + \left[\bar{W}_F \times (\bar{r}_Q - \bar{r}_{12})\right]$$
$$\bar{A}_Q = \bar{A}_{12} + \left[\bar{\alpha}_F \times (\bar{r}_Q - \bar{r}_{12})\right] + \left[\bar{W}_F \times (\bar{V}_Q - \bar{V}_{12})\right]$$

Where P_{12} may be considered as part of link-B, and $\bar{V}_{12}$ and $\bar{A}_{12}$ evaluated accordingly.

2.4. DYNAMIC ANALYSIS

2.4.1. Transformation of vectors between orthogonal axis sets

Letting the unit vectors along the co-ordinate axes in two orthogonal axis sets be ($\underline{i}$, $\underline{j}$, $\underline{k}$) and ($\underline{e}_x$, $\underline{e}_y$, $\underline{e}_z$) respectively, then, these may be related by

$$\underline{e}_x = T_{11}\,\underline{i} + T_{12}\underline{j} + T_{13}\underline{k} \qquad (2.53(a))$$
$$\underline{e}_y = T_{21}\,\underline{i} + T_{22}\underline{j} + T_{23}\underline{k} \qquad (2.53(b))$$
$$\underline{e}_z = T_{31}\,\underline{i} + T_{32}\underline{j} + T_{33}\underline{k} \qquad (2.53(c))$$

This may be denoted in matrix format by

$$\begin{bmatrix} \underline{e}_x \\ \underline{e}_y \\ \underline{e}_z \end{bmatrix} = \begin{bmatrix} \\ T \\ \\ \end{bmatrix} \begin{bmatrix} \underline{i} \\ \underline{j} \\ \underline{k} \end{bmatrix}$$

Where the matrix

$$\begin{bmatrix} \\ T \\ \\ \end{bmatrix} = \begin{bmatrix} T_{11} & T_{12} & T_{13} \\ T_{21} & T_{22} & T_{23} \\ T_{31} & T_{32} & T_{33} \end{bmatrix} \qquad (2.54)$$

Given that a vector ($\bar{r}$) has components (a, b, c) and (A,B,C) respectively, as seen in these two frames, that is

$$\bar{r} = a\,\underline{i} + b\,\underline{j} + c\,\underline{k} \qquad (2.55(a))$$

$$\bar{r} = A\,\underline{e}_x + B\,\underline{e}_y + C\,\underline{e}_z \qquad (2.55(b))$$

then it is required that the relationship between (a, b, c) and (A, B,C) be found.

Firstly, given that a, b, and c are known:

$$A = \bar{r} \circ \underline{e}_x$$

substituting equation (2.53(a)) for $\underline{e}_x$, and equation (2.55(a)) for $\underline{r}$

$$A = (a\,\underline{i} + b\,\underline{j} + c\,\underline{k}) \circ (T_{11}\,\underline{i} + T_{12}\,\underline{j} + T_{13}\,\underline{k})$$

$$= a\,T_{11} + b\,T_{12} + c\,T_{13}$$

Similarly

$$B = a\,T_{21} + b\,T_{22} + c\,T_{23}$$

$$C = a\,T_{31} + b\,T_{32} + c\,T_{33}$$

Putting these equations in matrix format

$$\begin{bmatrix} A \\ B \\ C \end{bmatrix} = \begin{bmatrix} \\ T \\ \\ \end{bmatrix} \begin{bmatrix} a \\ b \\ c \end{bmatrix} \qquad (2.56)$$

Alternatively, if A, B, and C are known:

using the equation set (2.53)

$$A\,\underline{e}_x = A\,(T_{11}\,\underline{i} + T_{12}\,\underline{j} + T_{13}\,\underline{k})$$

$$B\,\underline{e}_y = B\,(T_{21}\,\underline{i} + T_{22}\,\underline{j} + T_{23}\,\underline{k})$$

$$C\,\underline{e}_z = C\,(T_{31}\,\underline{i} + T_{32}\,\underline{j} + T_{33}\,\underline{k})$$

Adding these three equations

$$\begin{aligned} A\,\underline{e}_x + B\,\underline{e}_y + C\,\underline{e}_z &= (A\,T_{11} + B\,T_{21} + C\,T_{31})\,\underline{i} \\ &\quad + (A\,T_{12} + B\,T_{22} + C\,T_{32})\,\underline{j} \\ &\quad + (A\,T_{13} + B\,T_{23} + C\,T_{33})\,\underline{k} \\ &= \overline{r} \end{aligned}$$

And comparison with equation (2.55(a)) shows that

$$\begin{bmatrix} a \\ b \\ c \end{bmatrix} = \begin{bmatrix} \\ T' \\ \\ \end{bmatrix} \begin{bmatrix} A \\ B \\ C \end{bmatrix} \qquad (2.57)$$

where $[T']$ is the transpose of $[T]$. If the inverse of the transformation matrix $[T]$ were denoted by $[T^{-1}]$, then it would follow directly from equation (2.56) that

$$\begin{bmatrix} a \\ b \\ c \end{bmatrix} = \begin{bmatrix} \\ T^{-1} \\ \\ \end{bmatrix} \begin{bmatrix} A \\ B \\ C \end{bmatrix}$$

and comparison of this with equation (2.57) reveals a well known aspect of orthogonal transformations: that of the equivalence of the inverse and transpose of the transformation matrix.

2.4.2. Equations of motion for a rigid body

The equations of motion for a rigid body in 3-dimensional space may be considered in two distinct parts: one dealing with the translational motion and the other with the rotational motion of the body. Having decided on using a Newtonian vector mechanics formulation, then considering the free body diagram of a body, the following equations (taken from Beer and Johnston (36))may be applied:

$$\sum \overline{F} = m\,\overline{A}_G \qquad (2.58)$$

$$\sum (\overline{M})_G = (\dot{\overline{H}}_G)_{GX'Y'Z'} \qquad (2.59)$$

where, referring to Fig.12,

OXYZ is an inertial frame of reference, the frame GX'Y'Z' is attached

to the centre of the body and remains parallel to the inertial frame, and Gxyz is fixed in the body.
And

m = mass of the body

$\sum \bar{F}$ = sum of forces acting on the body

$\sum (\bar{M})_G$ = sum of moments about the centre of mass, G.

$\bar{A}_G$ = acceleration of G relative to OXYZ

$\bar{H}_G$ = angular momentum of the body about G relative to the frame GX'Y'Z'

$(\dot{\bar{H}}_G)_{GX'Y'Z'}$ = rate of change of $\bar{H}_G$ with respect to the frame GX'Y'Z'

Equation (2.58) referring to the translational motion of the body may be applied directly, but a more convenient form of the equation (2.59) concerned with the rotational dynamics of the body will be derived.

Referring to Fig.13, if S_1 and S_2 are two orthogonal frames of reference, and the angular velocity of the frame S_1 relative to S_2 is $\bar{\Omega}$, then it can be shown that the rate of change of a vector $\bar{a}$ as seen by observers in each of the frames may be related by:

$$\left(\frac{d\bar{a}}{dt}\right)_{S_2} = \left(\frac{d\bar{a}}{dt}\right)_{S_1} + (\bar{\Omega} \times \bar{a}) \qquad (2.60)$$

Now the angular momentum vector $(\bar{H}_G)$ in equation (2.59) is obtained by transforming the angular velocity of the body $(\bar{W})$ using the inertia tensor of the body. In evaluating $(\dot{\bar{H}}_G)_{GX'Y'Z}$, it is clear that as the orientation of the body changes, so in general would the inertia tensor, providing a problem of analysis in trying to determine this change. However, this difficulty may be avoided by applying the principle stated in equation (2.60) to equation (2.59), which becomes

$$\sum(\bar{M})_G = (\dot{\bar{H}}_G)_{Gxyz} + (\bar{W} \times \bar{H}_G) \qquad (2.61)$$

where

$(\dot{\bar{H}}_G)_{Gxyz}$ = rate of change of $\bar{H}_G$ with respect to the frame Gxyz

$\bar{W}$ = angular velocity of the body and therefore also of frame G_{xyz} relative to OXYZ or GX'Y'Z'

It will be seen that this avoids any need to evaluate rates of change of inertia tensor, and this is an important advantage of employing body fixed axes in dynamic analyses of rigid bodies.

The unit vectors along the co-ordinate axes of frames OXYZ and Gxyz are $(\underline{i}, \underline{j}, \underline{k})$ and $(\underline{e}_x, \underline{e}_y, \underline{e}_z)$ respectively, and the components of a vector $(\bar{V})$ in each of the frames is denoted by

$$\bar{V} = (VX)\,\underline{i} + (VY)\,\underline{j} + (VZ)\,\underline{k}$$

$$= (V_x)\,\underline{e}_x + (V_y)\,\underline{e}_y + (V_z).\underline{e}_z$$

And the transformation matrix [T] relating the two sets of unit vectors is known, where

$$\begin{bmatrix} \underline{e}_x \\ \underline{e}_y \\ \underline{e}_z \end{bmatrix} = \begin{bmatrix} \quad T \quad \end{bmatrix} \begin{bmatrix} \underline{i} \\ \underline{j} \\ \underline{k} \end{bmatrix}$$

For simplicity of notation, the angular momentum vector is hence referred to as $\overline{H}$, where it is understood to be determined about the centre of mass (G). The angular velocity vector

$$\begin{aligned} \overline{W} &= (WX)\ \underline{i} + (WY)\ \underline{j} + (WZ)\ \underline{k} \\ &= (W_x)\ \underline{e}_x + (W_y)\ \underline{e}_y + (W_z)\ \underline{e}_z \end{aligned} \tag{2.62}$$

The angular momentum vector

$$\begin{aligned} \overline{H} &= (HX)\ \underline{i} + (HY)\ \underline{j} + (HZ)\ \underline{k} \\ &= (H_x)\ \underline{e}_x + (H_y)\ \underline{e}_y + (H_z)\ \underline{e}_z \end{aligned}$$

And the components may readily be related by the transformation matrix [T]. Given that the inertia tensor of the body relative to the body fixed axes is [I], then the components of $\overline{H}$ in this axis set are given in the matrix equation

$$\begin{bmatrix} H_x \\ H_y \\ H_z \end{bmatrix} = \begin{bmatrix} \quad I \quad \end{bmatrix} \begin{bmatrix} W_x \\ W_y \\ W_z \end{bmatrix}$$

$$= \begin{bmatrix} \quad I \quad \end{bmatrix} \begin{bmatrix} \quad T \quad \end{bmatrix} \begin{bmatrix} WX \\ WY \\ WZ \end{bmatrix} \tag{2.63}$$

$$\begin{bmatrix} HX \\ HY \\ HZ \end{bmatrix} = \begin{bmatrix} \quad T' \quad \end{bmatrix} \begin{bmatrix} H_x \\ H_y \\ H_z \end{bmatrix}$$

$$\therefore \quad \begin{bmatrix} HX \\ HY \\ HZ \end{bmatrix} = \begin{bmatrix} \quad T' \quad \end{bmatrix} \begin{bmatrix} \quad I \quad \end{bmatrix} \begin{bmatrix} \quad T \quad \end{bmatrix} \begin{bmatrix} WX \\ WY \\ WZ \end{bmatrix} \tag{2.64}$$

The rate of change of $\overline{H}$ seen by an observer in the body fixed frame

$$\left(\frac{d\overline{H}}{dt}\right)_{Gxyz} = \dot{H}_x \underline{e}_x + \dot{H}_y \underline{e}_y + \dot{H}_z \underline{e}_z \qquad (2.65)$$

and since the inertia tensor is constant in this frame,

$$\begin{bmatrix} \dot{H}_x \\ \dot{H}_y \\ \dot{H}_z \end{bmatrix} = \begin{bmatrix} \\ I \\ \\ \end{bmatrix} \begin{bmatrix} \dot{W}_x \\ \dot{W}_y \\ \dot{W}_z \end{bmatrix}$$

The vector $(\dot{\overline{H}})_{Gxyz}$ may be transformed into the frame GX'Y'Z', and its components obtained from the matrix equation

$$\begin{bmatrix} [(\dot{\overline{H}})_{Gxyz}]o \ \underline{i} \\ [(\dot{\overline{H}})_{Gxyz}]o \ \underline{j} \\ [(\dot{\overline{H}})_{Gxyz}]o \ \underline{k} \end{bmatrix} = \begin{bmatrix} \\ T' \\ \\ \end{bmatrix} \begin{bmatrix} \dot{H}_x \\ \dot{H}_y \\ \dot{H}_z \end{bmatrix}$$

$$= \begin{bmatrix} \\ T' \\ \\ \end{bmatrix} \begin{bmatrix} \\ I \\ \\ \end{bmatrix} \begin{bmatrix} \dot{W}_x \\ \dot{W}_y \\ \dot{W}_z \end{bmatrix} \qquad (2.66)$$

Applying the principle stated in equation (2.60) to the angular velocity vector

$$\left(\frac{d\overline{W}}{dt}\right)_{GX'Y'Z'} = \left(\frac{d\overline{W}}{dt}\right)_{Gxyz} + (\overline{W} \times \overline{W})$$

$$= \left(\frac{d\overline{W}}{dt}\right)_{Gxyz}$$

Equation (2.62) may therefore be differentiated to yield the angular acceleration vector

$$\overline{\alpha} = (\dot{WX})\ \underline{i} + (\dot{WY})\ \underline{j} + (\dot{WZ})\ \underline{k}$$

$$= (\dot{W}_x)\ \underline{e}_x + (\dot{W}_y)\ \underline{e}_y + (\dot{W}_z)\ \underline{e}_z$$

where

$$\begin{bmatrix} \dot{W}_x \\ \dot{W}_y \\ \dot{W}_z \end{bmatrix} = \begin{bmatrix} \\ T \\ \\ \end{bmatrix} \begin{bmatrix} \dot{WX} \\ \dot{WY} \\ \dot{WZ} \end{bmatrix} \qquad (2.67)$$

And substituting this into equation (2.66) yields

$$\begin{bmatrix} [(\dot{\bar{H}})_{Gxyz}]o\ \underline{i} \\ [(\dot{\bar{H}})_{Gxyz}]o\ \underline{j} \\ [(\dot{\bar{H}})_{Gxyz}]o\ \underline{k} \end{bmatrix} = \begin{bmatrix} \\ T' \\ \\ \end{bmatrix} \begin{bmatrix} \\ I \\ \\ \end{bmatrix} \begin{bmatrix} \\ T \\ \\ \end{bmatrix} \begin{bmatrix} \dot{WX} \\ \dot{WY} \\ \dot{WZ} \end{bmatrix} \qquad (2.68)$$

Defining the angular velocity matrix by

$$\begin{bmatrix} \\ W \\ \\ \end{bmatrix} = \begin{bmatrix} 0 & -WZ & WY \\ WZ & 0 & -WX \\ -WY & WX & 0 \end{bmatrix} \qquad (2.69)$$

It can be shown,(see for instance, Suh and Radcliffe (37)),that a vector product operation may be replaced by a matrix multiplication operation; the components of $(\bar{W} \times \bar{H})$ may thus be obtained from the matrix equation

$$\begin{bmatrix} (\bar{W} \times \bar{H})o\ \underline{i} \\ (\bar{W} \times \bar{H})o\ \underline{j} \\ (\bar{W} \times \bar{H})o\ \underline{k} \end{bmatrix} = \begin{bmatrix} \\ W \\ \\ \end{bmatrix} \begin{bmatrix} HX \\ HY \\ HZ \end{bmatrix}$$

And substituting equation (2.64)

$$\begin{bmatrix} (\bar{W} \times \bar{H})o\ \underline{i} \\ (\bar{W} \times \bar{H})o\ \underline{j} \\ (\bar{W} \times \bar{H})o\ \underline{k} \end{bmatrix} = \begin{bmatrix} \\ W \\ \\ \end{bmatrix} \begin{bmatrix} \\ T' \\ \\ \end{bmatrix} \begin{bmatrix} \\ I \\ \\ \end{bmatrix} \begin{bmatrix} \\ T \\ \\ \end{bmatrix} \begin{bmatrix} WX \\ WY \\ WX \end{bmatrix} \qquad (2.70)$$

Resolving vector equation (2.61) along the unit vectors $\underline{i}$, $\underline{j}$, and $\underline{k}$, using equations (2.68) and (2.70) and putting into matrix format yields

$$\begin{bmatrix} [\Sigma(M)_G]o\ \underline{i} \\ [\Sigma(M)_G]o\ \underline{j} \\ [\Sigma(M)_G]o\ \underline{k} \end{bmatrix} = \begin{bmatrix} \\ T' \\ \\ \end{bmatrix} \begin{bmatrix} \\ I \\ \\ \end{bmatrix} \begin{bmatrix} \\ T \\ \\ \end{bmatrix} \begin{bmatrix} \dot{WX} \\ \dot{WY} \\ \dot{WZ} \end{bmatrix}$$

$$+ \begin{bmatrix} \\ W \\ \\ \end{bmatrix} \begin{bmatrix} \\ T' \\ \\ \end{bmatrix} \begin{bmatrix} \\ I \\ \\ \end{bmatrix} \begin{bmatrix} \\ T \\ \\ \end{bmatrix} \begin{bmatrix} WX \\ WY \\ WZ \end{bmatrix} \qquad (2.71)$$

And this is the required form of the equations concerned with the rotational dynamics of rigid bodies; a desirable feature of the matrix equation (2.71) is that all components of the angular acceleration vector are those seen in the inertial frame, and it will be seen that this enables the kinematic equations of section (2.3) to be used directly and simultaneously with the dynamics equations.

2.4.3. Equations of motion for a constrained rigid body

Two cases are considered: the first is of a body constrained to move in a given rectilinear direction, and the second is of a body constrained to rotate about a given axis. The model in each case has only one degree of freedom.

The translational equation of motion for the first model may be obtained by resolving equation (2.58) along the axis of possible motion.

$$\bar{\lambda}o\ (\Sigma\bar{F}) = \bar{\lambda}o\ (m.\bar{A}_G) \qquad (2.72)$$

where $\bar{\lambda}$ is a unit vector along this axis.

The rotational motion of the second model may be analysed by use of the equation

$$I.\ddot{\beta} = [\Sigma(\bar{M})_Q]o\ \bar{\lambda} \qquad (2.73)$$

where

I = moment of inertia of the body about the axis of rotation.

$\bar{\lambda}$ = unit vector along axis of rotation .

$\ddot{\beta}$ = angular acceleration of body about the axis of rotation, and defined such that $\bar{W} = \dot{\beta}\ \bar{\lambda}$, which indicates the sense of β

$\Sigma(M)_Q$ = sum of moments about a point P_Q on the axis

2.4.4. Model equations

Fig. 14 illustrates the mechanism model disconnected in part and showing internal forces and moments at points considered common to any two links; gravitational forces, and forces and moments due to interaction with sub-systems are also shown. It may be seen that the law of action and reaction has been inherently applied in the process of assigning internal force and moment vectors on each part of a joint connecting any two links; the various equations of motion may then be applied to each of the links.

A point to note in referring to the model is that the moment vector $\bar{M}_{12}$ by virtue of the nature of frictionless revolute joints, must be contained within a plane perpendicular to the spin axis, and therefore in general can only have two orthogonal components. The following constraint equation on this moment vector may be applied:

$$\bar{M}_{12}\ o\bar{\lambda}_{1,12} = 0 \qquad (2.74)$$

Finally, in referring to the link equations, it may be noted that the expressions for the accelerations of the link mass centres may be derived simply from comparison with the equations of section (2.3.7), and the forces and moments obtained from inspection of the free body diagrams of the individual links shown in Fig.14.

Link-A

Applying equation (2.73):

$$I_{6,7}\ddot{\psi} = [\Sigma(\bar{M})_6] \circ \bar{\lambda}_{6,7}$$

$$= \bar{\lambda}_{6,7} \circ \left[\{(\bar{r}_{G/A} - \bar{r}_6) \times m_A\, g\, \underline{k}\} + \{(\bar{r}_3 - \bar{r}_6) \times -\bar{F}_3\}\right]$$

$$\therefore I_{6,7}\ddot{\psi} + \bar{\lambda}_{6,7} \circ \left[\bar{r}_3 - \bar{r}_6) \times \bar{F}_3\right] = \bar{\lambda}_{6,7} \circ \left[(\bar{r}_{G/A} - \bar{r}_6) \times m_A\, g\, \underline{k}\right] \quad (2.75)$$

Link-B

Applying equation (2.58):

$$\Sigma\bar{F} = m_B\, \bar{A}_{G/B}$$

where

$$\Sigma\bar{F} = \bar{F}_2 + \bar{F}_3 + \bar{F}_4 + \bar{F}_{12} + m_B\, g\, \underline{k}$$

$$\bar{A}_{G/B} = \bar{A}_3 + [\bar{\alpha}_B \times (\bar{r}_{G/B} - \bar{r}_3)] + [\bar{W}_B \times (\bar{V}_{G/B} - \bar{V}_3)]$$

$$= \ddot{\psi}\,[\bar{\lambda}_{6,7} \times (\bar{r}_3 - \bar{r}_6)] + \dot{\psi}[\bar{\lambda}_{6,7} \times \bar{V}_3]$$

$$+ [\bar{\alpha}_B \times (\bar{r}_{G/B} - \bar{r}_3)] + [\bar{W}_B \times (\bar{V}_{G/B} - \bar{V}_3)]$$

$$\therefore \frac{1}{m_B}\,[\bar{F}_2 + \bar{F}_3 + \bar{F}_4 + \bar{F}_{12}] - \ddot{\psi}[\bar{\lambda}_{6,7} \times (\bar{r}_3 - \bar{r}_6)]$$

$$- [\bar{\alpha}_B \times (\bar{r}_{G/B} - \bar{r}_3)] = \dot{\psi}[\bar{\lambda}_{6,7} \times \bar{V}_3] - g\, \underline{k}$$

$$+ [\bar{W}_B \times (\bar{V}_{G/B} - \bar{V}_3)] \quad (2.76)$$

Applying equation (2.71):

$$\begin{bmatrix} [\Sigma(\bar{M})_{G/B}] \circ \underline{i} \\ [\Sigma(\bar{M})_{G/B}] \circ \underline{j} \\ [\Sigma(\bar{M})_{G/B}] \circ \underline{k} \end{bmatrix} = \begin{bmatrix} \\ T'_B \\ \\ \end{bmatrix} \begin{bmatrix} \\ I_B \\ \\ \end{bmatrix} \begin{bmatrix} \\ T_B \\ \\ \end{bmatrix} \begin{bmatrix} \alpha BX \\ \alpha BY \\ \alpha BZ \end{bmatrix}$$

$$+ \begin{bmatrix} W \end{bmatrix} \begin{bmatrix} T'_B \end{bmatrix} \begin{bmatrix} I_B \end{bmatrix} \begin{bmatrix} T_B \end{bmatrix} \begin{bmatrix} WBX \\ WBY \\ WBZ \end{bmatrix} \qquad (2.77)$$

where

$$\Sigma(\bar{M})_{G/B} = [(\bar{r}_2 - \bar{r}_{G/B}) \times \bar{F}_2] + [(\bar{r}_3 - \bar{r}_{G/B}) \times \bar{F}_3]$$

$$+ [(\bar{r}_4 - \bar{r}_{G/B}) \times \bar{F}_4] + [(\bar{r}_{12} - \bar{r}_{G/B}) \times \bar{F}_{12}] + \bar{M}_{12}$$

Link-C

Applying equation (2.73):

$$I_{8,9}\ddot{\phi} = [\Sigma(\bar{M})_8] \circ \bar{\lambda}_{8,9}$$

$$= \bar{\lambda}_{8,9} \circ \left[\{(\bar{r}_{G/C} - \bar{r}_8) \times m_c\, g\, \underline{k}\} + \{(\bar{r}_2 - \bar{r}_8) \times -\bar{F}_2\}\right.$$

$$\left. + \{(\bar{r}_{10} - \bar{r}_8) \times \bar{F}_{10}\} + \{(\bar{r}_{11} - \bar{r}_8) \times \bar{F}_{11}\}\right]$$

$$\therefore I_{8,9}\ddot{\phi} + \bar{\lambda}_{8,9} \circ [(\bar{r}_2 - \bar{r}_8) \times \bar{F}_2]$$

$$= \bar{\lambda}_{8,9} \circ [(\bar{r}_{10} - \bar{r}_8) \times \bar{F}_{10}] + \bar{\lambda}_{8,9} \circ [(\bar{r}_{11} - \bar{r}_8) \times \bar{F}_{11}]$$

$$+ \bar{\lambda}_{8,9} \circ [(\bar{r}_{G/C} - \bar{r}_8) \times m_c\, g\, \underline{k}] \qquad (2.78)$$

Link-D

Applying equation (2.58):

$$\Sigma\bar{F} = m_D\, \bar{A}_{G/D}$$

where

$$\Sigma\bar{F} = -\bar{F}_4 - \bar{F}_5 + m_D\, g\, \underline{k}$$

$$\bar{A}_{G/D} = \ddot{s}\, \bar{\lambda}_{18,19} + [\bar{\alpha}_D \times (\bar{r}_{G/D} - \bar{r}_5)] + [\bar{W}_D \times (\bar{V}_{G/D} - \bar{V}_5)]$$

$$\therefore \ddot{s}\, \bar{\lambda}_{18,19} + [\bar{\alpha}_D \times (\bar{r}_{G/D} - \bar{r}_5)] + \frac{1}{m_D}[\bar{F}_4 + \bar{F}_5]$$

$$= g\, \underline{k} - [\bar{W}_D \times (\bar{V}_{G/D} - \bar{V}_5)] \qquad (2.79)$$

Applying equation (2.71):

$$\begin{bmatrix} [\Sigma(\bar{M})_{G/D}]\circ \underline{i} \\ [\Sigma(M)_{G/D}]\circ \underline{j} \\ [\Sigma(M)_{G/D}]\circ \underline{k} \end{bmatrix} = \begin{bmatrix} \\ T'_D \\ \\ \end{bmatrix} \begin{bmatrix} \\ I_D \\ \\ \end{bmatrix} \begin{bmatrix} \\ T_D \\ \\ \end{bmatrix} \begin{bmatrix} \alpha DX \\ \alpha DY \\ \alpha DZ \end{bmatrix}$$

$$+ \begin{bmatrix} \\ W_D \\ \\ \end{bmatrix} \begin{bmatrix} \\ T'_D \\ \\ \end{bmatrix} \begin{bmatrix} \\ I_D \\ \\ \end{bmatrix} \begin{bmatrix} \\ T_D \\ \\ \end{bmatrix} \begin{bmatrix} WDX \\ WDY \\ WDZ \end{bmatrix} \qquad (2.80)$$

where

$$\Sigma(\bar{M})_{G/D} = \left[(\bar{r}_4 - \bar{r}_{G/D}) \times -\bar{F}_4\right] + \left[(\bar{r}_5 - \bar{r}_{G/D}) \times -\bar{F}_5\right]$$

Link-E

Applying equation (2.72):

$$\bar{\lambda}_{18,19} \circ \left[\Sigma\bar{F}\right] = \bar{\lambda}_{18,19} \circ \left[m_E \bar{A}_{G/E} \right]$$

where

$$\Sigma\bar{F} = \bar{F}_{20} + \bar{F}_5 + m_E g \underline{k}$$

$$\bar{A}_{G/E} = \ddot{s}\, \bar{\lambda}_{18,19}$$

And the component of the force transmitted to the rack by the steering gear pinion along the direction of freedom is F_p, where

$$F_p = \bar{\lambda}_{18,19} \circ \bar{F}_{20}$$

$$\therefore m_E \ddot{s} - \bar{\lambda}_{18,19} \circ \bar{F}_5 - F_p = \bar{\lambda}_{18,19} \circ (m_E g \underline{k}) \qquad (2.81)$$

Link-F

Applying equation (2.58):

$$\Sigma\bar{F} = m_F \bar{A}_{G/F}$$

where

$$\Sigma\overline{F} = \overline{F}_T - \overline{F}_{12} + m_F\, g\, \underline{k}$$

$$\overline{A}_{G/F} = \overline{A}_{12} + \left[\overline{\alpha}_F \times (\overline{r}_{G/F} - \overline{r}_{12})\right] + \left[\overline{W}_F \times (\overline{V}_{G/F} - \overline{V}_{12})\right]$$

$$= \ddot{\psi}\left[\overline{\lambda}_{6,7} \times (\overline{r}_3 - \overline{r}_6)\right] + \dot{\psi}\left[\overline{\lambda}_{6,7} \times \overline{V}_3\right] + \left[\overline{\alpha}_B \times (\overline{r}_{12} - \overline{r}_3)\right]$$

$$+ \left[\overline{W}_B \times (\overline{V}_{12} - \overline{V}_3)\right] + \left[\overline{\alpha}_F \times (\overline{r}_{G/F} - \overline{r}_{12})\right]$$

$$+ \left[\overline{W}_F \times (\overline{V}_{G/F} - \overline{V}_{12})\right]$$

$$\therefore \ddot{\psi}\left[\overline{\lambda}_{6,7} \times (\overline{r}_3 - \overline{r}_6)\right] + \left[\overline{\alpha}_B \times (\overline{r}_{12} - \overline{r}_3)\right] + \frac{1}{m_F}\overline{F}_{12}$$

$$+ \left[\overline{\alpha}_F \times (\overline{r}_{G/F} - \overline{r}_{12})\right] = \frac{1}{m_F}\overline{F}_T + g\,\underline{k} - \dot{\psi}\left[\overline{\lambda}_{6,7} \times \overline{V}_3\right]$$

$$- \left[\overline{W}_B \times (\overline{V}_{12} - \overline{V}_3)\right] - \left[\overline{W}_F \times (\overline{V}_{G/F} - \overline{V}_{12})\right] \qquad (2.82)$$

Applying equation (2.71):

$$\begin{bmatrix} [\Sigma(\overline{M})_{G/F}]o\ \underline{i} \\ [\Sigma(M)_{G/F}]o\ \underline{j} \\ [\Sigma(M)_{G/F}]o\ \underline{k} \end{bmatrix} = \begin{bmatrix} \\ T'_F \\ \\ \end{bmatrix}\begin{bmatrix} \\ I_F \\ \\ \end{bmatrix}\begin{bmatrix} \\ T_F \\ \\ \end{bmatrix}\begin{bmatrix} \alpha FX \\ \alpha FY \\ \alpha FZ \end{bmatrix}$$

$$+ \begin{bmatrix} \\ W_F \\ \\ \end{bmatrix}\begin{bmatrix} \\ T'_F \\ \\ \end{bmatrix}\begin{bmatrix} \\ I_F \\ \\ \end{bmatrix}\begin{bmatrix} \\ T_F \\ \\ \end{bmatrix}\begin{bmatrix} WFX \\ WFY \\ WFZ \end{bmatrix} \qquad (2.83)$$

where

$$\Sigma(\overline{M})_{G/F} = \overline{M}_T - \overline{M}_{12} + \left[(\overline{r}_{13} - \overline{r}_{G/F}) \times \overline{F}_T\right]$$

$$\left[(\overline{r}_{12} - \overline{r}_{G/F}) \times -\overline{F}_{12}\right]$$

2.5. A FEW COMMENTS

The various equations derived in this chapter together with the sub-system equations will be seen to form a sufficient set for the computer simulation of the system model, and this is described in Chapter 5. Once all equations are put into their required final forms, it is seen that components of vectors referred to are those seen in the frame OXYZ. In general, when referred to a frame of reference, a vector may have three components, and in the case, such as for $\overline{M}_{12}$, where the vector must be in a particular plane, a constraint equation of the type (2.74) may be applied. An alternative to this would be to select a planar axis set in the plane of the constrained vector and only therefore assign two component variables to the vector as seen in this planar axis set. A method of selection of such an axis set is given in Appendix D. This may also be useful in kinematic analyses of mechanisms with redundant degrees of freedom, and this is demonstrated in Appendix E, which contains an analysis of the familiar RSSR mechanism.

Some of the methods used here have been further applied to a different suspension and steering mechanism model and this is included in Appendix F. The model is that of a system commonly found in commercial vehicles, and a simple static force and kinematic analysis of this mechanism is demonstrated.

$$
\begin{bmatrix} \\ \\ \\ \\ A \\ \\ \\ \\ \\ \\ \end{bmatrix}
\begin{bmatrix} WBX \\ \\ WBY \\ \\ WBZ \\ \\ \dot{\phi} \\ \\ WDX \\ \\ WDY \\ \\ WDZ \\ \\ \end{bmatrix}
=
\begin{bmatrix} -\left(\frac{G1}{L_{6,7}}\right)\dot{\psi} & & \\ & & \\ -\left(\frac{G2}{L_{6,7}}\right)\dot{\psi} & & \\ & & \\ -\left(\frac{G3}{L_{6,7}}\right)\dot{\psi} & & \\ & & \\ -\left(\frac{G1}{L_{6,7}}\right)\dot{\psi} & + & \left(\frac{x_{19}-x_{18}}{L_{18,19}}\right)\dot{s} \\ & & \\ -\left(\frac{G2}{L_{6,7}}\right)\dot{\psi} & + & \left(\frac{y_{19}-y_{18}}{L_{18,19}}\right)\dot{s} \\ & & \\ -\left(\frac{G3}{L_{6,7}}\right)\dot{\psi} & + & \left(\frac{z_{19}-z_{18}}{L_{18,19}}\right)\dot{s} \\ & & \\ (L_{4,5})\,\dot{\theta} & & \\ & & \end{bmatrix}
$$

(2.27)

$$
\begin{bmatrix} \\ \\ \\ \\ \\ \\ \\ \\ \end{bmatrix} A \begin{bmatrix} \\ \\ \\ \\ \\ \\ \\ \\ \end{bmatrix} = \begin{bmatrix} 0 & (z_2 - z_3) & -(y_2 - y_3) & -\left(\frac{G4}{L_{8,9}}\right) & 0 & 0 & 0 \\ -(z_2 - z_3) & 0 & (x_2 - x_3) & -\left(\frac{G5}{L_{8,9}}\right) & 0 & 0 & 0 \\ (y_2 - y_3) & -(x_2 - x_3) & 0 & -\left(\frac{G6}{L_{8,9}}\right) & 0 & 0 & 0 \\ 0 & (z_4 - z_3) & -(y_4 - y_3) & 0 & 0 & (z_5 - z_4) & -(y_5 - y_4) \\ -(z_4 - z_3) & 0 & (x_4 - x_3) & 0 & -(z_5 - z_4) & 0 & (x_5 - x_4) \\ (y_4 - y_3) & -(x_4 - x_3) & 0 & 0 & (y_5 - y_4) & -(x_5 - x_4) & 0 \\ 0 & 0 & 0 & 0 & (x_5 - x_4) & (y_5 - y_4) & (z_5 - z_4) \end{bmatrix}
$$

(2.28)

$$G1 = (y_7 - y_6)(z_3 - z_6) - (z_7 - z_6)(y_3 - y_6)$$

$$G2 = (z_7 - z_6)(x_3 - x_6) - (x_7 - x_6)(z_3 - z_6)$$

$$G3 = (x_7 - x_6)(y_3 - y_6) - (y_7 - y_6)(x_3 - x_6)$$

$$G4 = (y_9 - y_8)(z_2 - z_8) - (z_9 - z_8)(y_2 - y_8)$$

$$G5 = (z_9 - z_8)(x_2 - x_8) - (x_9 - x_8)(z_2 - z_8)$$

$$G6 = (x_9 - x_8)(y_2 - y_8) - (y_9 - y_8)(x_2 - x_8)$$

(2.29)

$$\begin{bmatrix} 0 & (z_2 - z_3) & -(y_2 - y_3) & -\left(\frac{G4}{L_{8,9}}\right) \\ -(z_2 - z_3) & 0 & (x_2 - x_3) & -\left(\frac{G5}{L_{8,9}}\right) \\ (y_2 - y_3) & -(x_2 - x_3) & 0 & -\left(\frac{G6}{L_{8,9}}\right) \\ G10 & G11 & G12 & 0 \end{bmatrix} \begin{bmatrix} WBX \\ WBY \\ WBZ \\ \dot{\phi} \end{bmatrix} = \begin{bmatrix} -\left(\frac{G1}{L_{6,7}}\right)\dot{\psi} \\ -\left(\frac{G2}{L_{6,7}}\right)\dot{\psi} \\ -\left(\frac{G3}{L_{6,7}}\right)\dot{\psi} \\ -\left(\frac{G13}{L_{6,7}}\right) + \left(\frac{G9}{L_{18,19}}\right)\dot{s} \end{bmatrix}$$

(2.33)

$$
\begin{bmatrix} \\ \\ \\ \\ B \\ \\ \\ \\ \\ \end{bmatrix}
\begin{bmatrix} \alpha BX \\ \alpha BY \\ \alpha BZ \\ \ddot{\phi} \\ \alpha DX \\ \alpha DY \\ \alpha DZ \end{bmatrix}
=
\begin{bmatrix}
\{ \ (H4) - (H1) - (A3X) \ \} \\
\{ \ (H5) - (H2) - (A3Y) \ \} \\
\{ \ (H6) - (H3) - (A3Z) \ \} \\
\left\{ \left(\frac{x_{19} - x_{18}}{L_{18,19}} \right) \ddot{s} - (H8) - (A3X) - (H11) \right\} \\
\left\{ \left(\frac{y_{19} - y_{18}}{L_{18,19}} \right) \ddot{s} - (H9) - (A3Y) - (H12) \right\} \\
\left\{ \left(\frac{z_{19} - z_{18}}{L_{18,19}} \right) \ddot{s} - (H10) - (A3Z) - (H13) \right\} \\
\{ \ (L_{4,5}) \ \ddot{\theta} - (H7) \ \}
\end{bmatrix}
$$

(2.39)

$$
\begin{bmatrix} \\ \\ \\ \\ \\ \\ \\ \\ \end{bmatrix}
B
\begin{bmatrix} \\ \\ \\ \\ \\ \\ \\ \\ \end{bmatrix}
=
\begin{bmatrix}
0 & (z_2 - z_3) & -(y_2 - y_3) & -\left(\frac{G4}{L_{8,9}}\right) & 0 & 0 & 0 \\
-(z_2 - z_3) & 0 & (x_2 - x_3) & -\left(\frac{G5}{L_{8,9}}\right) & 0 & 0 & 0 \\
(y_2 - y_3) & -(x_2 - x_3) & 0 & -\left(\frac{G6}{L_{8,9}}\right) & 0 & 0 & 0 \\
0 & (z_4 - z_3) & -(y_4 - y_3) & 0 & 0 & (z_5 - z_4) & -(y_5 - y_4) \\
-(z_4 - z_3) & 0 & (x_4 - x_3) & 0 & -(z_5 - z_4) & 0 & (x_5 - x_4) \\
(y_4 - y_3) & -(x_4 - x_3) & 0 & 0 & (y_5 - y_4) & -(x_5 - x_4) & 0 \\
0 & 0 & 0 & 0 & (x_5 - x_4) & (y_5 - y_4) & (z_5 - z_4)
\end{bmatrix}
$$

(2.40)

$$
\begin{aligned}
H1 &= (WBY)\ (V2Z - V3Z) - (WBZ)\ (V2Y - V3Y) \\
H2 &= (WBZ)\ (V2X - V3X) - (WBX)\ (V2Z - V3Z) \\
H3 &= (WBX)\ (V2Y - V3Y) - (WBY)\ (V2X - V3X) \\
H4 &= (WCY)\ (V2Z) - (WCZ)\ (V2Y) \\
H5 &= (WCZ)\ (V2X) - (WCX)\ (V2Z) \\
H6 &= (WCX)\ (V2Y) - (WCY)\ (V2X) \\
H7 &= (WDX)\ (V5X-V4X) + (WDY)\ (V5Y-V4Y) + (WDZ)\ (V5Z-V4Z) \\
H8 &= (WDY)\ (V5Z-V4Z) - (WDZ)\ (V5Y-V4Y) \\
H9 &= (WDZ)\ (V5X-V4X) - (WDX)\ (V5Y-V4Z) \\
H10 &= (WDX)\ (V5Y-V4Y) - (WDY)\ (V5X-V4X) \\
H11 &= (WBY)\ (V4Z-V3Z) - (WBZ)\ (V4Y-V3Y) \\
H12 &= (WBZ)\ (V4X-V3X) - (WBX)\ (V4Z-V3Z) \\
H13 &= (WBX)\ (V4Y-V3Y) - (WBY)\ (V4X-V3X)
\end{aligned}
$$

(2.41)

$$
\begin{bmatrix}
0 & (z_2 - z_3) & -(y_2 - y_3) & -\left(\frac{G4}{L_{8,9}}\right) \\
-(z_2 - z_3) & 0 & (x_2 - x_3) & -\left(\frac{G5}{L_{8,9}}\right) \\
(y_2 - y_3) & -(x_2 - x_3) & 0 & -\left(\frac{G6}{L_{8,9}}\right) \\
G10 & G11 & G12 & 0
\end{bmatrix}
\begin{bmatrix}
\alpha BX \\ \alpha BY \\ \alpha BZ \\ \ddot{\phi}
\end{bmatrix}
=
\begin{bmatrix}
\{ (H4) - (H1) - (A3X) \} \\
\{ (H5) - (H2) - (A3Y) \} \\
\{ (H6) - (H3) - (A3Z) \} \\
\{ \left(\frac{G9}{L_{18,19}}\right) \ddot{s} + (H15) - (H14) \\
\quad + (x_5 - x_4)(A3X) + (y_5 - y_4)(A3Y) \\
\quad + (z_5 - z_4)(A3Z) \}
\end{bmatrix}
$$

(2.49)

CHAPTER 3 A MATHEMATICAL DESCRIPTION OF SUB-SYSTEM MECHANICS

SUMMARY

Models for the tyre, main spring, shock absorber, and steering gear sub-systems are described. A mathematical description of the way in which these models interact with the main mechanism model is then subsequently presented.

3.1. INTRODUCTION

The four sub-systems considered to complement the main suspension and steering mechanism model described in Chapter 2 are the tyre, main spring, shock absorber, and steering gear from the steering pinion up to and including the handwheel. The purpose of this chapter is to present a mathematical description of the way in which these sub-systems interact with the main mechanism model.

Inspection of the physical suspension and steering system indicates that the main spring, shock absorber, and steering gear sub-systems may be modelled using lumped parameter models with the inertial, elastic, and damping properties of the models being determined empirically. The models actually adopted for these three sub-systems are shown in Fig.15 and may be seen to be uni-directional in nature and considered to be terminated at single points at each end. The tyre component may not, however, be so readily modelled. Any realistic analytical model would need to be 3-dimensional in nature with distributed mechanical properties, and the mathematical formulation of this type of model would clearly be a very difficult task. Similarly, because of the complex interaction between the tyre and ground surface for spatial motions of the wheel, the formulation of a generalized empirical model would also present problems. For these reasons, tyre models are, in general, restricted to considering only specific aspects of tyre behaviour. Two types of empirically based tyre models are sometimes employed in steering and suspension vibration studies and these are considered here. The essential difference in approach between the two types of models is that while the first considers only the mechanical (elastic) properties of the tyre, the second type of model combines this with considerations of the slip angle and attitude angle concepts (utilized in the study of tyre mechanics) to formulate a simple model capable of providing a transient tyre response simulation. A model from each of these types has been investigated. The first model, (tyre model 1), employs a translational spring which is perpendicular to the ground and acting between the centre of the wheel and the ground surface, and a torsional spring providing a self-aligning torque (acting perpendicular to the ground plane) which is a function of the steer angle of the wheel. The second model, (tyre model 2), also employs a translational spring to provide a vertical reaction force in the same manner, but differs from the first model in that it provides a description of the generation of a lateral force as well as a self-aligning torque for certain motions of the wheel relative to the ground. The development of a lateral force and a self-aligning torque in this second model is based on the well known straight tangent tyre model which considers the deflected equatorial line of the tyre to be a straight line with no slippage occurring within the tyre contact patch.

The two tyre models differ only in their treatment of the steering response of the tyre, the vertical response being identical between models and uncoupled to the steering response within each of the models. The steady state frequency response of the two models to steering inputs has been compared with experimental response data for the limited conditions of zero camber and centre point steering. And on the basis of these results and knowledge of the simplicity with which each of the models may be incorporated within the main mechanism

model, tyre model 1 was selected to complete the suspension and steering model. The analysis of the steering response of the tyre model 2 (under these limited conditions) is however briefly outlined here for completeness, and a comparison of experimental and theoretical frequency response data is presented in Chapter 6. Ellis (12) is referred to for a full account of this model and a more complete discussion of tyre mechanics in general as both the approach and nomenclature used in describing tyre behaviour in this thesis is largely taken from that work.

3.2. TYRE MECHANICS

3.2.1. Wheel orientation

The road wheel is modelled as a perfectly symmetric circular disc which is constrained to rotate about an axis passing through its geometric centre in a perpendicular manner to the disc plane. The axis of rotation is fixed in the stub axle. The orientation of the road wheel relative to the ground plane and vehicle may be defined by the steer angle (δ) and camber angle (ϕ'). And, referring to the mechanism model, this orientation may be seen to be dependent only on the upper wishbone link position (ψ) and steering rack position (s).

A right-handed wheel axis set ($12X_WY_WZ_W$) may be defined by specifying the unit vectors along the axes in this frame. Referring to Fig.16, the unit vectors $\underline{\lambda}_{TX}$,$\underline{\lambda}_{TY}$ and $\underline{\lambda}_{TZ}$ are defined such that $\underline{\lambda}_{TZ}$ is perpendicular to the ground plane and pointing into the ground, $\underline{\lambda}_{TX}$ is parallel to the line of intersection between the ground plane and wheel plane and pointing forwards along the line of possible wheel travel, and $\underline{\lambda}_{TY}$ is defined so as to complete the unit vector axis set. The ground plane is parallel to the xy-plane,

$$\therefore \quad \underline{\lambda}_{TZ} = \underline{k} \tag{3.1}$$

$\underline{\lambda}_{TX}$ is perpendicular to the spin axis of the wheel and to any perpendicular line to the ground, and may therefore be found from the equation

$$\underline{\lambda}_{TX} = \frac{(\underline{\lambda}_{TZ} \times \overline{\lambda}_{1,12})}{|\underline{\lambda}_{TZ} \times \overline{\lambda}_{1,12}|} \tag{3.2}$$

and $\underline{\lambda}_{TY}$ completes the required triad of unit vectors and is given by

$$\underline{\lambda}_{TY} = \underline{\lambda}_{TZ} \times \underline{\lambda}_{TX} \tag{3.3}$$

The steer angle (δ) is defined as the angle between the vectors $\underline{i}$ and $\underline{\lambda}_{TX}$ and, with the sense defined positive in the direction shown in Fig.16, is given by

$$\delta = \tan^{-1}\left(\frac{\underline{\lambda}_{TX} \circ \underline{j}}{\underline{\lambda}_{TX} \circ \underline{i}}\right) \tag{3.4}$$

The wheel camber angle (ϕ') is the angle by which the wheel needs to be rotated about the line along $\underline{\lambda}_{TX}$ to bring the wheel plane perpendicular to the ground plane, and evaluating the unit vector ($\bar{e}$) perpendicular to $\bar{\lambda}_{1,12}$ and $\underline{\lambda}_{TX}$ from

$$\bar{e} = \bar{\lambda}_{1,12} \times \underline{\lambda}_{TX} \tag{3.5}$$

then the wheel camber angle is the angle between $\bar{e}$ and $\underline{\lambda}_{TZ}$ and is defined by

$$\phi' = - \tan^{-1} \left(\frac{\bar{e} \circ \underline{\lambda}_{TY}}{\bar{e} \circ \underline{\lambda}_{TZ}} \right) \tag{3.6}$$

3.2.2. Tyre model 1

The tyre force vector ($\bar{F}_T$) is given by

$$\bar{F}_T = \bar{F}_{DC} - k_{TZ} (z_{12} - z_{DC}) \underline{k} \tag{3.7}$$

where

$\bar{F}_{DC}$ is the static tyre force,

z_{DC} is the z co-ordinate value of the position vector of P_{12} at the mechanism position when $\bar{F}_T = \bar{F}_{DC}$,

z_{12} is the z co-ordinate of P_{12}, and

k_{TZ} is the vertical stiffness of the tyre

The moment vector ($\bar{M}_T$) is given by

$$\bar{M}_T = -k_{T\theta} \delta \underline{k} \tag{3.8}$$

where

$K_{T\theta}$ is the torsional stiffness of the tyre.

And the steady state frequency response of this model to steering inputs may be evaluated directly from equation (3.8) upon substitution of $\delta = \hat{\delta} \sin wt$.

3.2.3. Tyre model 2

The tyre model considered is shown in Fig.17. The wheel is steered about an axis perpendicular to the ground and passing through the centre of the wheel; this axis intersects the ground plane at point P. The position of the centre of the tyre contact patch is located by point Q, and this centre may be distorted laterally by an amount y_T from P when a lateral tyre force (FTY) is present. P moves with a speed U along a line parallel to the X-axis, and the velocities of P and Q may therefore be expressed as

$$\bar{V}_P = U \underline{i} \quad , \text{ and}$$

$$\bar{V}_Q = U \underline{i} + \dot{y}_T \underline{\lambda}_{TY}$$

The tyre slip angle (θ_s) is the angle between the velocity vectors $\bar{V}_Q$ and $\bar{V}_P$ and is given by

$$\theta_s = \tan^{-1}\left(\frac{\dot{y}_T \cos\delta}{U - \dot{y}_T \sin\delta}\right)$$

and for small angles, this expression may be approximated to

$$\theta_s = \dot{y}_T / U$$

The attitude angle (α) is defined by

$$\alpha = \delta - \theta_s$$

$$= \delta - \dot{y}_T/U \qquad (3.9)$$

and this is the angle between the wheel centre line and the velocity vector $\bar{V}_Q$. The lateral force is considered a function of both the lateral distortion of the tyre and the attitude angle, and this may be expressed as

$$FTY = k_{TY}\, y_T$$

$$= C\,\alpha \qquad (3.10)$$

where

C is commonly known as the cornering stiffness and is equal to the rate of change of lateral force with respect to the attitude angle, and

k_{TY} is the lateral stiffness of the tyre.

$\therefore\ k_{TY}\, y_T = C\,\alpha$

Substituting equation (3.9) for α and re-arranging yields the first order differential equation

$$\dot{y}_T + U\,\lambda\, y_T = U\,\delta \qquad (3.11)$$

where

$$\lambda = k_{TY}/C$$

The (steering) frequency response of this model may now be examined by substituting $\delta = \hat{\delta}\ \sin wt$ into equation (3.11), and evaluating the steady state solution for y_T, which is

$$y_T = \left(\frac{U^2\,\lambda\,\hat{\delta}}{w^2 + U^2\lambda^2}\right)\sin wt - \left(\frac{U\,w\,\hat{\delta}}{w^2+U^2\lambda^2}\right)\cos wt \qquad (3.12)$$

The lateral force response to a sinusoidal steering input may then be evaluated from equation (3.10).

The self-aligning torque (MTZ) is also related to the attitude angle by

$$MTZ = N.\alpha \qquad (3.13)$$

where

N is the rate of change of the aligning torque with respect to the attitude angle.

From equation (3.10)

$$\alpha = (k_{TY}\ y_T)/C$$

and this may be substituted into equation (3.13) to yield

$$MTZ = (N\ k_{TY}\ y_T)/C \qquad (3.14)$$

Equation (3.12) may now be substituted into equation (3.14) to yield the steady state self-aligning torque response of the tyre to sinusoidal steering inputs.

3.3. MAIN SPRING MECHANICS

The main spring is modelled as a single elastic element which is connected to the sub-frame and link-C by spherical joints. The spring force is given by

$$\bar{F}_s = \left[F_{SDC} + k_s \left(|\bar{r}_{10} - \bar{r}_{16}| - \ell_{REF}\right)\right] \bar{\lambda}_{16,10}$$

where

k_s is the spring stiffness,

ℓ_{REF} is the distance between points P_{10} and P_{16} at the reference position of link-C, and

F_{SDC} is the constant spring force level at this reference position.

The force on link-C at P_{10} (due to interaction with the spring) is equal in magnitude but opposite in direction to the force vector $\bar{F}_s$ and is therefore given by

$$\bar{F}_{10} = \left[F_{SDC} + k_s \left(|\bar{r}_{10} - \bar{r}_{16}| - \ell_{REF}\right)\right] \bar{\lambda}_{10,16} \qquad (3.15)$$

3.4. SHOCK ABSORBER MECHANICS

The shock absorber sub-system is modelled as a single viscous damping element which is connected to the sub-frame and link-C by spherical joints. The damper force is given by

$$\overline{F}_D = c\ (\overline{V}_{11} \circ \overline{\lambda}_{17,11})\ \overline{\lambda}_{17,11}$$

where

c is the coefficient of viscous damping.

The force on link-C at P_{11} (due to interaction with the damper) is equal in magnitude but opposite in direction to the force vector $\overline{F}_D$ and is therefore given by

$$\overline{F}_{11} = c\ (\overline{V}_{11} \circ \overline{\lambda}_{17,11})\ \overline{\lambda}_{11,17} \qquad (3.16)$$

3.5. STEERING GEAR MECHANICS

The steering gear model is constrained to rotational motion about an axis fixed in the frame OXYZ, and consists of two elements (representing the steering pinion and handwheel components) which have inertial properties and are inter-connected by torsional spring and damper elements arranged in parallel. The pinion is kinematically geared to the steering rack, and it is therefore clear that the handwheel rotational motion provides only one further degree of freedom to the suspension and steering system model produced when this sub-system is coupled to the (four degree-of-freedom) main mechanism model described in Chapter 2.

Referring to the sub-system model shown in Fig 15, the equations of motion for the handwheel and pinion may be written as

$$I_H\ \ddot{\theta}_H = -k_H(\theta_H - \theta_P) - c_H\ (\dot{\theta}_H - \dot{\theta}_P)$$

and

$$I_p\ \ddot{\theta}_P = k_H\ (\theta_H - \theta_P) + c_H(\dot{\theta}_H - \dot{\theta}_P) - R_P\ F_p$$

where

$\dot{\theta}_H$ is the spin velocity of the handwheel,

$\dot{\theta}_P$ is the spin velocity of the pinion,

I_H is the moment of inertia of the handwheel about the axis of rotation,

I_P is the moment of inertia of the pinion about the axis of rotation,

k_H is the rotational stiffness of the steering column,

c_H is the rotational viscous damping coefficient of the steering column, and

R_P is the effective radius of the pinion gear.

The pinion angle of rotation and rack movement may be kinematically related by the expression

$$s = R_p \theta_p$$

and also on differentiation

$$s = R_p \dot{\theta}_p \quad \text{and} \quad \ddot{s} = R_p \ddot{\theta}_p$$

And these kinematic relationships may now be used in the handweel and pinion equations to eliminate variables θ_p, $\dot{\theta}_p$, and $\ddot{\theta}_p$, resulting in the equations

$$I_H \ddot{\theta}_H = -k_H (\theta_H - s/R_p) - c_H(\dot{\theta}_H - \dot{s}/R_p) \tag{3.17}$$

and

$$I_p \ddot{s}/R_p = k_H(\theta_H - s/R_p) + c_H (\dot{\theta}_H - \dot{s}/R_p) - R_p F_p \tag{3.18}$$

Equation (3.18) may then be substituted into the steering rack equation (2.81) to eliminate F_p and, on re-arranging, the rack equation of motion now becomes

$$\left(m_E + I_p/R^2_p\right) \ddot{s} - \bar{\lambda}_{18,19} \circ \bar{F}_5 = \bar{\lambda}_{18,19} \circ (m_E . g . \underline{k}) + \frac{k_H}{R_p} (\theta_H - s/R_p) + \frac{c_H}{R_p} (\dot{\theta}_H - \dot{s}/R_p) \tag{3.19}$$

CHAPTER 4 EXPERIMENTAL WORK

SUMMARY

A description is given of the experimental work undertaken to provide response data that may be used to compare with theoretical simulation results. The theoretical models employed require knowledge of certain parameter values before any simulation work may be done, and a description of the tests performed to determine these values, together with component properties in general, is also included.

4.1. INTRODUCTION

Most of the experimental work performed falls into two categories. The first deals with the evaluation of response data from a physical system under specific test conditions, and this is done to provide a comparison with the response data obtained from the computer simulation of theoretical models. The second deals with the evaluation of model parameter values (pertaining to the physical system under test) required as input data for the simulation program prior to computer execution. In addition to these two main areas of work, some experimental work designed to investigate component properties in general has been undertaken, and this is also reported here. The task of evaluating model parameter values is clearly related to the broader area of work concerned with the examination of component properties in general, and the presentation of work reflects this fact. The evaluation and use of frequency response functions demonstrates this relationship very well and it will be seen that these functions not only provide a description of the system properties (within a given test frequency bandwidth) but may be further analysed to yield estimates of model parameter values. These functions also serve to provide a measure of the suitability of assumed parametric models over a range of dynamic forcing conditions.

Test requirements for road wheel rotation were satisfied by use of a rolling drum rig in which the tyres are loaded onto the outside surface of two five foot diameter drums which are driven by an electric motor. The electric motor is coupled to the drums by means of an eddy current coupler (which provides the means of speed control), and a mechanical gearbox. The two drums may be regarded as a single unit having a common axis of rotation which is driven from a belt and pulley arrangement between this axis and the gearbox. There are two main advantages of use here of this type of rig over a suspension and steering test apparatus travelling on a road. Firstly that unwanted vibrations due to interaction between the tyres and unmeasured ground irregularities are likely to be of a lower magnitude and certainly of a more deterministic nature, and secondly that the test rig and instrumentation requirements are simpler with the experiment being stationary. The curvature of the drums do not in themselves present a particular problem to the experiments performed except in so far as not all the tyre parameters were evaluated while the tyre was loaded on the drums but on a nominally flat surface. There is therefore a margin of error in some of the parameter values used in the simulation work because of this. The static vertical stiffness of the tyre has however been measured both on the drums and on a flat bed test rig and this does provide some information concerning the effects of drum curvature.

Response data has been collected for three separate types of tests performed using the drum rig. These tests were designed to determine the steering frequency response of the tyre, the steady state oscillatory response of the suspension and steering system to an out of balance wheel, and the transient response of the suspension and steering system to an impulsive force input on the tyre. Results from these tests and some corresponding simulation results are presented in Chapter 6. The tests involved in the determination of model parameter values are to a certain extent less confined to take a particular form, and several different approaches may be employed to estimate a particular parameter,

each yielding a different value for the simple reason that the physical component does not behave in exactly the same manner as predicted by the theoretical model. The ability to experiment with the various approaches is therefore useful not only in providing estimates for the various parameters but also in assessing component properties generally, and it is considered that the use of a digital computer to process data in tests of this kind is essential. A data processing system has been developed for this purpose. The computer employed in the simulation work, the Cromemco System Three, has been enhanced by the addition of a data acquisition card enabling the machine to sample up to eight channels of analogue signals at discrete intervals of time and store this information within the digital computer for subsequent processing. The software necessary for the processing of data required as part of the various tests has been developed and,as with the simulation related programming work, is described in Chapter 5.

4.2. MEASUREMENT OF COMPONENT PROPERTIES

4.2.1. Tyre

Tests on the tyre component were designed to measure the static stiffnesses of the non-rolling tyre, and the steady state lateral force and self-aligning torque to attitude angle relationships of the rolling tyre. The two test rigs necessary for these measurements were operational within a research contract being carried out at Cranfield, and full use of these was made; a full description of these rigs may be found in reference (38).

Estimates of the vertical, lateral, and torsional stiffnesses of the tyre are evaluated under the three conditions schematically illustrated in Fig.18. In all these three test conditions the wheel is fixed in space and the tyre is loaded at the contact patch with a flat plate. The flat plate is supported via a load cell on an air bearing pad, and this in turn is supported by a pivoted body which may be so rotated to enable the tyre to be loaded in a near vertical manner. The mechanical arrangement on the air bearing permits either lateral motion of the bearing or rotational motion of the bearing about an axis through the wheel centre and perpendicular to the flat plate. Measurements of the possible air bearing movements together with the loads applied in each mode of operation under static conditions enable the determination of the required stiffness parameters. The force versus deflection characteristic of the tyre (at various tyre pressures) under a vertical loading condition is shown in Fig 19, and this relationship may be seen to be near linear for vertical loads exceeding 2.5kN. Fig 20 illustrates the variation of the vertical and lateral stiffnesses with tyre pressure when these parameters are determined within linear loading conditions. Some estimates of the torsional stiffness of the tyre are obtainable from the test rig although these are subject to variations of typically $\pm$ 30% from the sample mean. This large variability in the measurement of the torsional stiffness is due primarily to the effects of friction within the mechanical arrangement in this low loading condition (in which only relatively small forces are exerted to induce the required rotational movements).

The test rig employed for the measurement of the properties of the rolling

tyre is schematically outlined in Fig 21. The test rig consists of a trolley with a single beam axle and wheels which are steered in opposing directions by an electro-hydraulic actuator; the steering being so arranged as to minimise the net lateral force on the trolley as the two tyres are steered. A piezoelectric based load cell designed specifically for the task of measuring tyre forces was manufactured by Kistler (Instruments AG) and this was installed on the stub axle. The load cell provided measurement of the effective force vector and moment vector acting at a reference point in the load cell necessary to balance the forces acting between the wheel and stub axle. The steer angle is measured by a rotary potentiometer positioned on the beam axle and geared to the king pin. The vertical tyre force is largely dependent on the trolley weight and this was varied by the addition of concrete blocks. The trolley is fixed in position over the drum rig, and aligned so that there is a condition of zero steer angle and, when the wheels rotate, zero attitude angle. The measurements required are for steady state conditions, and in these cases it is apparent from the definition of the attitude angle that the steer and attitude angles are equivalent.

The test procedure is to oscillate the wheels about the straight ahead position in a sinusoidal manner and record the measured steer angle, and force and moment vector variables. The peak steer angle was limited in tests to approximately 2^{o} and this ensured that the lateral force and self-aligning torque variation with respect to the steer angle was linear. The frequency of oscillation is adjusted with respect to the rolling speed of the tyre so as to ensure that a quasi-static condition of measurement exists, that is that the force and moment variables measured at any given instantaneous steer angle approximate very closely to those measured under the steady state condition of zero steer velocity at the same steer angle. Typically, at a rolling speed of 20 m.p.h., the frequency of oscillation may be 0.1 Hz. These tests were repeated at various tyre vertical loads and tyre rolling speeds, and a linear regression analysis was performed in each case to determine the required tyre parameter value. Examination of Fig 22 shows that the variation of cornering stiffness ($dF_Y/d\alpha$) and self-aligning torque coefficient($dM_Z/d\alpha$) with respect to rolling speed is small and apparently arbitrary. And, as the measurements are subject to statistical error (with the data in general being more scattered at higher rolling speeds), the observed variation (of typically less than 7% from the sample mean) of these parameters with speed is not considered to be significant. The variation of the cornering stiffness and self-aligning torque coefficient with respect to the tyre vertical force is shown in Figs 23 and 24 respectively.

The static vertical stiffness of the non-rolling tyre on the curved surface of a drum was also determined by using the trolley rig described. The vertical tyre force was incrementally increased by increasing the trolley weight (by the addition of concrete blocks), and the vertical tyre force and vertical wheel deflection were measured. The force being measured by the Kistler load cell, and the deflection being measured by a dial test indicator fixed by a magnetic base onto the drum and monitoring the movement of a fixed point on the wheel. This measurement was performed only at a tyre pressure of 34 p.s.i., and the calculated stiffness was found to be about 28% lower than that

calculated using the flat bed tyre stiffness test rig. As with previous vertical stiffness measurements however, apart from the initial loading condition, the force to deflection relationship was found to be linear. The variation of the stiffness around the circumference of the tyre could be readily examined using the test arrangement described and this was also done. Four equispaced points around the circumference of the tyre were arbitrarily selected and marked, and with the tyre being loaded against the drum surface at one of these points, the vertical stiffness was evaluated. The tyre was then unloaded, rotated and the procedure repeated in turn for the other loading positions located by the points. The peak variation of the tyre stiffness from the sample mean was found to be approximately 5%.

4.2.2. Main spring and shock absorber

An existing test rig was modified to facilitate the testing of the main spring and shock absorber units. The modification was the addition of a test frame over an electro-hydraulic actuator unit enabling the test items to be fixed at one end and excited by the actuator at the other end. The test frame, with the shock absorber in place, is shown in Fig. 25, and the complete test rig together with the computing system used in this work is shown in Fig. 26. The main spring may be secured in place with the same fixtures. A strain-gauged load cell is located between the top of the test item and the top securing plate, and this measures the force (F) along the direction of motion of the actuator which is also along the main spring/shock absorber centre line. A rectilinear potentiometer is attached between the top plate and the top of the actuator, and this measures the relative displacement (X) across either of the test items. For the purposes of calculating parameter values from the various tests, the top plate is considered to be stationary, and this is a good approximation since the measured acceleration levels on this plate are found to be less than 1% of the corresponding measured acceleration levels of the actuator under all dynamic testing conditions for the two test items.

The main spring force to deflection relationship measured under static conditions is shown in Fig.27 and this may be seen to be linear away from the initial loading position of the spring; the static stiffness within the linear loading region is given by the gradient of the line drawn through the relevant data points. A description of the dynamic behaviour of the main spring may be obtained from evaluation of the frequency response function between the force (F) and displacement (X) variables, and the modulus of this function is shown in Fig.28. The test procedure employed in the determination of this function is to use bandlimited (1-20Hz) random noise as the actuator input control signal and monitor the ensuing spring behaviour by measuring the relevant force and displacement variables; the dynamic motions are limited to the linear regions of (static) response by maintaining a preset compression on the spring during the test. The force and displacement signals are digitised and then processed to yield estimates of the required function; a discussion of the data processing involved in this is provided in Chapter 5. The convergence of the modulus of the dynamic stiffness function to the static stiffness value of the spring is of course expected and may be seen from the figure, and this is a limited but useful check on the accuracy of the evaluated function.

The shock absorber, unlike the main spring, exhibits a significant degree of non-linearity in its behaviour and this may be seen from inspection of the force (F) and displacement (X) signals plotted in Fig.29. This plot corresponds to a test condition in which a near triangular displacement waveform is input into the shock absorber unit by the actuator. The force signal of a linear viscous damper model in this condition would be rectangular in shape, and although the actual force signal does have the presence of such a rectangular waveform, there is also the apparent superposition of a random waveform on this. The properties of the rubber bushes to be found on these units (acting between each of the absorber sliding parts and the points of connection to the test rig) may be expected to contribute to the complexity of the shock absorber behaviour. The relatively high static stiffnesses of the bushes, see Fig.30, suggests however that the bushes are unlikely to significantly affect the shock absorber behaviour at lower frequencies of vibration.

A single viscous damper element is the assumed model for the shock absorber, and the coefficient of viscous damping for this model and shock absorber properties in general have been evaluated using three different test and data analysis procedures. The first of these methods uses a triangular displacement input waveform, and evaluates a mean coefficient of viscous damping. For a triangular waveform of period T seconds, the mean coefficient of viscous damping calculated over a time span of one period is given by

$$c = \frac{1}{T|\dot{X}|} \int_0^T |F(t)| \, dt \qquad (4.1)$$

where $|\dot{X}|$ is the mean absolute value of the velocity across the shock absorber and is given approximately by the near constant positive gradient of the displacement signal, and $|F(t)|$ is the magnitude of the instantaneous force at time t. The mean coefficient of viscous damping evaluated using an equivalent discretised form of equation (4.1) is found to be dependent on the velocity across the shock absorber as shown in Fig.31; the velocity being varied by changing both the peak displacement value and the frequency of excitation of the actuator, but ensuring that the displacement waveform remains triangular in form under all test conditions. The damping coefficient may be seen to vary significantly only at the lower velocities. This may be explained if one considers the total measured force to be essentially composed of a velocity dependent force and a frictional force of near constant magnitude, so that as the relative velocity across the shock absorber decreases the velocity dependent viscous damping force also decreases and forms a decreasing percentage of the total force, thereby producing the effect shown when the coefficient is calculated as described. This model of shock absorber behaviour is reinforced by force measurements under static conditions which confirm the action of this type of frictional force. The second approach employed in determining the coefficient of viscous damping provides a description of the variation of the coefficient over the different parts of a cyclic motion input by the actuator. The actuator control signal used is sinusoidal; the resulting displacement and force signals measured being sinusoidal in nature but visibly distorted in shape. The force and displacement signals are digitised over several cycles of excitation, with approximately 250 data points covering each cycle. A quadratic curve is fitted to data

around a given reference data point, the displacement expression is differentiated to yield an equation for the velocity and, on using the equations to calculate the force and velocity values at this point, a coefficient of damping is then evaluated as the force to velocity ratio. The procedure is repeated for different reference data points selected over several cycles of data; the results obtained from following this procedure are shown in Fig.32. The force and velocity values used in the damper calculations may be considered as well smoothed estimates of these variables around the reference point times as the data used in each of the curve fits covers approximately one quarter of the main signal component wavelength. Attention has been restricted here to considering damper values calculated when the relative velocity across the shock absorber has exceeded 150 m.m./s, thereby reducing the influence of the non-velocity dependent forces apparent from the first test procedure. The third test procedure adopted for the shock absorber is similar to that used for the investigation of the dynamic behaviour of the main spring. Bandlimited (1-20 Hz) random noise is used as the actuator control signal, and the force (F) and displacement (X) data measured as the actuator system and test item respond to this input are processed to yield estimates of the frequency response function between the measured variables. The modulus of this particular function may then be weighted by the angular frequency and the modulus of the response function between force and velocity, (the modulus of a mechanical impedance function) thus obtained, see Fig.33. The function shown may be considered to illustrate the variation of the damping properties of the shock absorber with respect to frequency. The modulus of the impedance function evaluated is found to be dependent on levels of excitation and the effect of roughly doubling the force and displacement mean square levels within each frequency band is also shown in the figure. Finally, it may be noted that in all tests conducted on the shock absorber, the dependency of behaviour on the temperature has been apparent; the results shown here are from tests performed during which the outside case temperature of the shock absorber unit remained between 20^{o}C and 25^{o}C. The variation of the damping coefficient with temperature has been investigated, and a 10% drop in the value of this parameter has been measured for an increase of temperature from 20^{o}C to 40^{o}C.

4.2.3. Steering column

The steering column stiffness was calculated from measurements taken from a torque transducer and a rotary potentiometer at the handwheel. The handwheel is rotated to full lock position and then forced by hand into further rotational movement thereby twisting the steering column; the rack effectively remaining stationary under this test condition. The ratio of the torque applied (from the full lock position) to the subsequent rotational movement of the handwheel yields a value for the static rotational stiffness of the steering column.

4.2.4. Inertial properties of components

The desire to determine the suspension and steering component masses, and moments and products of inertia (referred to in the inertial tensors defined about body fixed axes) could only be partially satisfied. Although a spring force balance could be used to determine the masses of the various components, the moment and product of inertia values

could not be so readily evaluated. The larger of the moment of inertia values about certain of the axes through the components could however be measured using the Trifilar method and this was done whenever possible. The upper and lower wishbone links were constrained to rotate about their normal axes of rotation, and set into motion like simple pendulums, and the moments of inertia about these axes determined from measurements of the periods of oscillation. The remaining inertial properties were estimated from knowledge of the geometry of the bodies.

4.3. RESPONSE DATA EVALUATION

4.3.1. Tyre steering frequency response

The test rig employed in the evaluation of the properties of the rolling tyre (and previously described) was also used in determining the lateral force and self-aligning torque frequency response of the rolling tyre to steering inputs. The tyres are loaded onto the drums in exactly the same manner as before and, with the drums driven at a constant velocity, a near sinusoidal steering input is applied to the wheels about the straight ahead position. The peak steer angle is again limited to approximately 2^{o}. The results from Fourier analyses of the measured data series are then used to determine the force/moment to steer magnitude and phase relationships at the frequency of excitation. This process is repeated for various steering input frequencies and the frequency response functions are mapped out over the required frequency range. It may be noted that Fourier analysis is made necessary only by the inability of the actuator system to input a clean sinusoidal steer waveform, thereby requiring the analysis to estimate signal component magnitudes and phases at the excitation frequency.

4.3.2. Steady state oscillations of the suspension and steering system

A test frame was designed and built around a suspension and steering system of the double wishbone and rack and pinion type and, with the tyres loaded centrally over the drums, was fixed rigidly in place as shown in Fig.34. Rectilinear potentiometers were used to measure distances between points on the wishbones to reference points on the stationary test frame, and under virtually zero load conditions on the links, the outputs from these instruments were calibrated against the angular displacements of the wishbone links. A further rectilinear potentiometer was also attached between the steering rack and rack housing, and a number of piezoelectric accelerometers were used to measure the motions of points around the suspension and steering system. The transducers used were required to monitor relatively small movements, and it was necessary to amplify the various output signals from the transducers in order to utilize the full dynamic range of the signal recording device. And because of the limited dynamic range of the amplifiers employed, the usually large direct current (DC) outputs from the rectilinear potentiometers were removed prior to amplification; this was done by summing the signals with equal magnitude negative DC voltages from external sources. The piezoelectric accelerometers have an inherent low frequency cut-off characteristic and are well suited to measurements of small oscillations, and were used in conjunction with standard charge amplifiers. During tests, the output from the amplifiers was stored on magnetic tape and at a

later stage the data was digitised and processed using a digital computer.

The experiment involved bolting a mass onto one of the wheels making it out of balance, as shown in Fig.35 and rotating the drums at a constant speed. With the tyre rolling, vibrations of the suspension and steering components were readily induced, and measurements were recorded when a near steady state condition of vibration was attained. The mass added to the wheel was selected so that the vibrations observed were predominantly at the frequency corresponding to the angular rotational frequency of the wheel. The probable level of vibration induced by the presence of the unbalancing mass was assessed by repeating the experiment with a balanced wheel and comparing results. The experiment was also repeated several times using different tyre pressure settings to provide data under varying test conditions.

4.3.3. Transient response

The suspension and steering system and associated test apparatus described in the previous section were also employed in the determination of the transient response of the system to an impulsive input. The test entailed applying a vertical blow to the tyre with a hammer instrumented with a piezoelectric force transducer. The essential difference within the test set-up was that chocks were used to make sure that the drums remained stationary during the measurement period, and of course that the measured force was also recorded.

CHAPTER 5 COMPUTING WORK

SUMMARY

A description of the computational aspects of the various simulation programs developed within this work is presented, and reference is made to flow charts which illustrate the arrangement and structure of these computer programs. Data analysis programs are also reviewed, and a brief description of the digital computer employed is included.

5.1. INTRODUCTION

A microprocessor based digital computer, the Cromemco System Three, was employed in both the simulation and data analysis work. This machine is essentially a 'desk-top personal computer' and in the particular version used came with~ 64 kilobytes of directly addressable memory and four 8" floppy disc drives, with each disc having a storage capacity of ~494 kilobytes. The computer programs are written in Fortran, and are restricted in size by the ~ 44 kilobytes of machine memory available to the user, the remainder being taken up by the Cromemco Disc Operating System (CDOS) and the Link loader. In cases where this memory was insufficient, programs have been chained using the disc as an intermediate store for information. Permanent record of computer output may be obtained from a line printer and digital plotter inter-connected to the machine.

Three sets of simulation programs have been developed in this work and these essentially cover the position, kinematic, and dynamic analyses of the suspension and steering system model. The input data required by the programs are the rectangular co-ordinates of the labelled points in the system at a given reference position of the mechanism, and the inertial, elastic, and damping parameter values of the various suspension and steering components. The parameter values were determined from experiment as described in Chapter 4, while the rectangular co-ordinates were determined from measurements on engineering drawings of the suspension and steering system which were supplied by the manufacturer. Flow charts for the main programs and subroutines are presented to enable understanding of the various calculation procedures, while others which are either similar in structure to those given or may be found in standard software libraries are referred to in tables only by name and function description; the vector and matrix subroutines are for example given in Tables 5.1 and 5.2 respectively.

5.2. SIMULATION WORK

5.2.1. Position analysis

The program POSITION enables the complete suspension and steering mechanism model to be displaced from a known reference position by an amount equal to the degree-of-freedom displacement-component values ψ and s input by the user. And because of the possible dual solution in the intersection of three spheres routine called by this program, the total displacement is achieved incrementally using the minimum distance criterion described in Chapter 2 to select the appropriate set of co-ordinates at each step. The flow chart for the position program is shown in Fig.36. Either of the subroutines SPHERE or SPHERC correspondingly yielding an exact or iteratively converging solution to the problem of three spheres may be used, and flow charts for these subroutines are shown in Figs 37-39. The procedure for evaluating the road wheel orientation is outlined in Fig.40.

5.2.2. Kinematic analysis

Three self-contained programs have been written in which the kinematic velocity relationships are used to drive all or parts of the mechanism model from one position to another. The procedure involves inputing values for the degree-of-freedom velocity-component variables, and solving the kinematic equations for the angular velocities of the links. The rectilinear velocities of points in the mechanism may then be evaluated and integrated over a small time interval using Euler's method to obtain incremental displacements of points. This procedure is then repeated until the required position has been reached. KINEM1 displaces the lower wishbone link in relation to displacements of the upper wishbone link, using equation (2.30) to relate angular spin velocities ϕ and ψ. KINEM2 displaces both the lower wishbone link and stub axle given upper wishbone link and steering rack motions, using matrix equation (2.33) at each step prior to integration to solve for $\overline{W}_B$ and $\dot{\phi}$ as a function of $\dot{\psi}$ and s. And KINEM3 employs the full velocity relationships given in matrix equation (2.27) to displace the complete mechanism. Flow charts for these programs are given in Figs. 41-43.

5.2.3. Dynamic analysis

The numerical procedure employed to simulate the dynamic response of the model to known inputs is common among this type of inherently non-linear initial-value problem. The first stage of the procedure involves solving a set of differential and constraint equations simultaneously to yield instantaneous values for the acceleration variables. Then, given that velocity and displacement values are known at that instant, these may be used with the acceleration values to estimate the velocity and displacement values after a short interval of time, the time step of integration. All variable values in the equations are then accordingly up-dated, and this process repeated for a given simulation run-time. The dynamics program set developed for this work also incorporates a position and kinematic analysis at the beginning of the simulation enabling the mechanism to be displaced from the known reference position to the designated initial condition position, and also enabling firstly the angular velocities of the links and subsequently the rectilinear velocities of all labelled points in the model to be evaluated given the initial condition degree-of-freedom velocity-component values. The kinematic analysis is essentially required to ensure that the initial condition motions of all links are compatible with the physical constraints of the system and therefore that the mechanism will retain its integrity during the subsequent integration steps. The complete dynamics simulation is achieved by executing a set of programs which are chained together, running under the CDOS software as shown in Fig.44. The separation into several programs is required to limit individual program memory requirements thus enabling them to be loaded into the machine. While running this set of programs, files on the discs are used to store intermediate simulation results and to keep loop counts, as information in memory is lost each time a different program is loaded. Flow charts for some of the dynamics simulation programs and subroutines are shown in Figs 45-55, while the remainder are described in Tables 5.3, 5.4, and 5.5.

The kinematic constraint equations (2.35), (2.36), (2.45), and (2.52), the equation of constraint (2.74) on the internal moment vector $\bar{M}_{12}$, and the equations of motion (2.75) - (2.80), (2.82), (2.83), (3.17), and (3.19) are re-arranged and put into the matrix format

$$\left[\text{DMAT}\right] \quad \left[\text{OPMAT}\right] \quad = \quad \left[\text{IPMAT}\right] \qquad (5.1)$$

where

$$\left[\text{OPMAT'}\right] = \left[\begin{array}{ccccc} \ddot{\psi} & \ddot{\phi} & \ddot{\theta} & \dot{w} & \alpha BX \\ \alpha BZ & \alpha DX & \alpha DY & \alpha DZ & \alpha FX \\ \alpha FY & \alpha FZ & F2X & F2Y & F2Z \\ F3X & F3Y & F3Z & F4X & F4Y \\ F4Z & F5X & F5Y & F5Z & F12X \\ F12Y & F12Z & M12X & M12Y & \\ M12Z & \ddot{s} & \ddot{\theta}_H & & \end{array}\right],$$

$\left[\text{DMAT}\right]$ is a (33 x 33) matrix which contains information about the position of the mechanism and the inertial properties of the links, and

$\left[\text{IPMAT}\right]$ is a (33 x 1) matrix which contains information about the position of the mechanism, velocities, and inputs to the model.

The spring and damper reaction forces are evaluated from equations (3.15) and (3.16) respectively; the tyre moment response is obtained from equation (3.8), while the force response of the tyre given in equation (3.7) is modified to

$$\bar{F}_T = \bar{F}_{DC} - k_{TZ} (z_{12} - z_{DC}) \underline{k} + \bar{F}_E$$

where $\bar{F}_E$ is an external force artificially input by the user to excite the system.

The simulation begins by running the program INCOND which sets up the initial condition positions and velocities, and proceeds with program DYNAM which evaluates the various expressions and coefficients of variables in the model equations thereby effectively setting up the matrix equation (5.1). Program INVERT inverts the matrix [DMAT] and passes control back to DYNAM, which then proceeds to evaluate matrix [OPMAT]. Here, a fourth-order Runge-Kutta method is used to integrate the acceleration variables, upon which the process is repeated as described earlier. Noting that the elements of the matrix [DMAT] are functions only of the co-ordinates of various points in the model

and inertial properties of links which are fixed, then it is apparent that for small movements of the mechanism model this matrix may be regarded as being time invariant. In these instances, the inversion needs only to be performed once, thereby significantly reducing the computer run-time for a given simulation; this may be considered to effect a partial linearisation of the geometric aspects of the model.

An important aspect of this work is that the equations employed in the simulation are formulated numerically in the computer directly from the equations given, eliminating the need for further manipulation of equations in order to obtain matrix equation (5.1) explicitly, and this is useful because it presents a very efficient way of formulating models of this and greater complexity. This numerical formulation is effected in two stages. Firstly by employing a set of subroutines that evaluate expressions and the coefficients of unknown variables within expressions which are common in form within the equations. And secondly by using the PIPMAT and PDMAT sets of subroutines to input the results of calculations from the first stage into the appropriate locations in the machine thereby numerically constituting the matrix equation (5.1). The functions of the various subroutines used within the first stage may be summarised as follows:

1) TMAT

Given three reference points (P_I, P_J, P_K) which are associated with a link but are not co-linear, a link body fixed axis set is defined by the unit vectors along the axes, i.e.

$$\underline{e}_x = (\bar{r}_J - \bar{r}_I)/\ |\bar{r}_J - \bar{r}_I|$$

$$\underline{e}_y = \underline{e}_x \times \left[(\bar{r}_K - \bar{r}_I)/\ |\bar{r}_K - \bar{r}_I|\ \right]$$

$$\underline{e}_z = \underline{e}_x \times \underline{e}_y$$

Then TMAT evaluates the transformation matrix $[T]$ between this body fixed frame and the inertial frame of reference so that

$$\begin{bmatrix} \underline{e}_x \\ \underline{e}_y \\ \underline{e}_z \end{bmatrix} = \begin{bmatrix} \\ T \\ \\ \end{bmatrix} \begin{bmatrix} \underline{i} \\ \underline{j} \\ \underline{k} \end{bmatrix}$$

2) TFORM

Evaluates the matrices $[T1]$ and $[T2]$ which may be used in the rotational equations of motion, where

$$[T1] = [T'][I][T]$$

and

$$[\,T2\,] \;=\; [\,W\,]\,[\,T'\,]\,[\,I\,]\,[\,T\,]\begin{bmatrix} WX \\ WY \\ WZ \end{bmatrix}$$

3) MOMENT

Given an expression of the form

$$\overline{M}_J \;=\; (\overline{r}_I - \overline{r}_J) \times \overline{F}_I$$

the matrix [RMOM] is evaluated so that

$$\begin{bmatrix} MJX \\ MJY \\ MJZ \end{bmatrix} = \begin{bmatrix} \\ RMOM \\ \\ \end{bmatrix} \begin{bmatrix} FIX \\ FIY \\ FIZ \end{bmatrix}$$

4) RESMOM

Evaluates the array [RM] so that

$$\overline{\lambda}\, o\left[\,(\overline{r}_I - \overline{r}_J) \times \overline{F}_I\right] \;=\; RM(1).\,FIX + RM(2).\,FIY + RM(3).\,FIZ$$

5) RMGRAV

Evaluates expressions of the form

$$\overline{\lambda}\, o\left[(\overline{r}_I - \overline{r}_J) \times mg.\underline{k}\right]$$

5.3. DATA ANALYSIS WORK

Time series data analysis is covered by the two main programs SCAN and FRF, with a number of associated subroutines written to enable graphical output to be obtained on a visual display unit and digital plotter. The flow charts for these programs and subroutines are shown in Figs. 56-61; the main program flow charts only illustrate the overall structure of the programs concerned, since a description of the computational aspects of the various time series analyses may be found in many references. SCAN is the generalised program enabling data capture, storage, and processing of the kind indicated by its flow chart, whereas FRF is specifically intended for the evaluation of frequency response functions. The Fourier coefficients required in frequency analysis work are calculated using the algorithm given by Newland (39), while the general procedures and recommendations outlined by Bendat (40) are followed in determining frequency response functions.

VECTOR SUBROUTINES	
VECADD	Addition
VECSUB	Subtraction
VECDOT	Scalar/dot product
VECPLY	Vector/cross product
VECMAG	Magnitude
VECUNI	Unit vector
VECCAL	Calibration/scaling
VECEQU	Equivalence
VECZER	Zero vector
VECMAT	Conversion to matrix format

TABLE 5.1

MATRIX SUBROUTINES	
MATADD	Addition
MATSUB	Subtraction
MATPLY	Multiplication
MATPOS	Transposition
MATINV	Inversion
MATEQU	Equivalence
MATZER	Zero matrix
MATUNI	Identity matrix
MATCAL	Calibration/scaling
MATCRT	Zero column/row search

TABLE 5.2

PIPMAT SUBROUTINES	
IPVEC	Defines three elements of matrix IPMAT from components of a vector.
IPELEM	Defines three elements of matrix IPMAT from matrix T2.

TABLE 5.3

PDMAT SUBROUTINES	
IFORCE	Inputs coefficients of unknown internal forces (for the translational equations of motion) into matrix DMAT.
MM	Inputs coefficients of unknown internal forces (for the rotational equations of motion) into matrix DMAT.
ROTAA	Inputs coefficients of angular acceleration vector (from matrix T1) into matrix DMAT.
AAXRR	Evaluates coefficients of angular acceleration vector ($\bar{\alpha}$) from expressions of the form $[\bar{\alpha} \times (\bar{r}_I - \bar{r}_J)]$, and inputs into matrix DMAT.

TABLE 5.4

OTHER SUBROUTINES	
RSUB	Evaluates displacement vector between two points.
VSUB	Evaluates relative velocity vector between two
	points
VECVEL	Velocity vector equivalenced to velocity matrix.
VVMAT	Velocity matrix equivalenced to velocity vector.
LENGTH	Calculates distance between two points.
EQUIV	Equates elements of the angular velocity array
	with corresponding variables in the output
	vector array [Y]
LINVEL	Evaluates velocities of various points in the
	mechanism.
KINVEL	Evaluates angular velocities of all links
	from the degree-of-freedom velocity-component
	values.
POSN	Evaluates position vectors of various points in
	the mechanism from the degree-of-freedom dis-
	placement values s and ψ.

TABLE 5.5.

CHAPTER 6 RESULTS

SUMMARY

Simulated responses of the theoretical models are presented, and where available, experimental data is provided for comparison. Theoretical results are generally shown to compare well with both measured results and those expected from physical considerations of simplified models of the system.

6.1. POSITION ANALYSIS

The program POSITION has been executed in several different modes to yield information about the road wheel orientation with respect to the degree-of-freedom variables ψ and s, and the results from these computer runs are shown in Figs. 62 - 67. The different runs correspond to conditions in which one of the variables ψ or s is held constant, while the other is varied and the changing steer and camber angles are evaluated. The two plots of δ versus s and ϕ' versus ψ have been checked with measurements taken from engineering drawings of the suspension and steering system. One measure of the degree of non-linearity of the mechanism kinematics may be obtained from examination of the variation of $d\psi/d\phi$ with respect to the wishbone orientation defined by angle ψ, and a plot of this relationship is shown in Fig.68. For small displacements of less than 1^o from the mechanism reference position ($\psi = 0^o$), $d\psi/d\phi$ effectively remains constant at 1.44; the maximum variation of $d\psi/d\phi$ being $\sim$10% when considering the total range of link displacements.

The kinematic programs have also been executed, and the co-ordinates of points at various link positions have been printed out for comparison. The results from all programs have been found to agree with one another.

6.2. TYRE FREQUENCY RESPONSE

The lateral force and self-aligning torque steering frequency response data for the tyre is shown in Figs.69 - 74. These illustrate the steady state force and moment responses of the tyre to sinusoidal steering inputs. The magnitudes of the respective frequency response functions have been normalized by dividing with the limiting function magnitudes as the frequency approaches zero; the functions are plotted as functions of road wheel oscillations per metre rolled, as is customary with this type of rolling tyre response data. The theoretical results shown are those predicted by tyre model 2; tyre model 1 only producing a self-aligning torque response, and this being a constant of unit magnitude. The effect of varying the tyre parameter λ by $\pm$ 20% is illustrated.

6.3. EXPERIMENTAL AND THEORETICAL DYNAMICS

6.3.1. Steady state response

A comparison of experimental and theoretical simulation results obtained for the case of an unbalancing mass of 0.3 kg at a radius of 0.143m from the wheel spin axis is shown in Figs 75 - 77; the tyre pressure being set at 34 psi for these tests. And the results for the same test performed with a balanced wheel are shown in Figs 78 - 80. The results from similar tests at a tyre pressure of 26 psi are shown in Figs 81 and 82. It is noted that although the general instrumentation noise levels were low, some noticeable noise was output by the amplifiers used, and in fact the signal waveform shown in Fig.80 is essentially due to this.

6.3.2. Transient response

After the force applied to the tyre in the transient system test has been removed, the system may be considered to be in free motion. The theoretical free motion or transient response of the model is evaluated by letting the upper wishbone link have an initial condition spin velocity which is calculated from the measured displacement trace at a point in time when the force signal (shown in Fig.83) has decayed to zero. The results from this simulation may then be compared to the measured response data; the results for the two tyre pressures of 34 psi and 26 psi are respectively shown in Figs. 84 and 85. The small shift in the theoretical angular displacement levels apparent near the end of the simulation run-time is due to the inexact estimation of $\overline{F}_{DC}$ and F_{SDC} needed to balance the effects of gravitational forces.

6.4. FURTHER DYNAMICS SIMULATION RESULTS

The validity of the simulation of the dynamics of the suspension and steering system may also be assessed by examining simulation results in relation to physical considerations of the system mechanics; this is especially true of the near vertical motions of the wheel which may be considered uncoupled to the steering motions of the mechanism to yield a linear one degree-of-freedom model whose behaviour is well known. The results from the simulation of the dynamics of the model are shown in Figs 86 - 96, and unless otherwise stated the models used have the same geometry and parameter values as the reference suspension and steering system model and are simulated with $\overline{F}_{DC}$ and F_{SDC} equal to zero, zero initial condition velocities, and a time step of integration of 0.002 seconds. The upper wishbone link angle ψ is the output variable generally monitored.

The response of the suspension from a zero velocity initial condition acting under the action of gravitational forces is shown in Fig. 86, and this illustrates the expected underdamped response of the system from a non-equilibrium starting position; there is virtually no change in response for w = 0 rad/s and w = 100 rad/s and this is because of the small camber changes with wishbone link movements occurring with this particular mechanism geometry. And the effect of varying the upper wishbone link axis position, so that $d\psi/d\phi$ (at $\psi = 0$) increases from 1.44 to 2.71 with a correspondingly increased variation of camber angle with respect to ψ, is shown in Fig.87.

Figs 88 - 90 show the variation of internal forces at points P_2 and P_3; the steady state magnitudes are found to agree with results from a static force analysis of the mechanism. The main vertical dynamic load path in the mechanism may be expected to be through the lower wishbone link and this is indeed the case as demonstrated by the plots of the force components F2Z and F3Z. The force at P_5 along the line of action of the steering rack is shown in Fig.91. The effects of varying the coefficient of viscous damping (c) and vertical tyre stiffness (k_{TZ}) on the reference model are shown in Figs. 92 and 93. In both cases, the peak amplitudes, frequencies of oscillation, decay rates, and asymtotically reached equilibrium positions check with those expected from physical considerations.

Halving the time step of integration for the reference model with no damping may be seen from Fig.94 to have virtually no effect. The small

drift in the trace is thought to be due to numerical inaccuracies in the simulation process; this type of drift may be expected to be less acute for realistic models with damping. The ability of the simulation process to retain the integrity of the mechanism is demonstrated in Fig.95 where the kinematic relationship $d\psi/d\phi$ evaluated during the dynamics simulation of the reference model is shown to agree with the results from purely kinematic considerations. The function is evaluated from $\dot{\psi}/\dot{\phi}$ at the higher spin velocities of the lower link in order to ensure the numerical accuracy of the calculation.

Finally, the response of the reference model to a sinusoidal vertical force input at the wheel is investigated, and the results from this are shown in Fig.96. The peak magnitude of the force is 100N, and the peak angular displacement ($\hat{\psi}$) is read from the time series simulation results of ψ after a steady state oscillation is achieved. This result is again totally compatible with physical considerations and with the previous set of results pertaining to the simulation of the reference model.

CHAPTER 7 DISCUSSION

SUMMARY

Some general comments regarding the simulation of the position, kinematics, and dynamics of the suspension and steering mechanism model are made. The theoretical and experimental results are reviewed, and possible reasons for differences described.

It is clear from the position analysis that for a well defined mechanism model there is no significant computational difficulty in calculating displacements of the model from a known reference position. The requirement that any displacement be performed in stages is due to the possible dual solution of the three spheres routine as previously explained, and presents no real problem since the position program has a high computational efficiency, typically only taking a few seconds to run. Although no general assessment may be readily made of the number of increments necessary for a given displacement, ten steps have been normally used here for movements covering the whole range of displacements possible with no false selection of co-ordinates occurring. Similarly, no computational difficulties have arisen in solving the various sets of equations employed in the kinematics programs, although when considering the equations (2.27) , (2.30), and (2.33) it is conceivable that under certain co-ordinate conditions these may not be solved. It may be readily shown with simpler 4-bar linkage mechanisms, that similar types of kinematic equations become indeterminate at positions in which any two of the movable interconnected links form a straight line. And this may be expected from physical considerations of such a mechanism in this configuration since one of these two links may be given an arbitrary velocity while the third movable link velocity is zero. It may be expected that the kinematic equations derived for the suspension and steering system mechanism model in this work will also be indeterminate for positions in which no unique velocity relationship is expected for similar reasons. It is interesting to note that the matrices which may be inverted as a first step in determining the link velocity relationships are identical to the corresponding matrices resulting from the acceleration relationships. This may be seen from examination of matrix [A] from equation (2.27) and matrix [B] from equation (2.39), and matrix equations (2.33) and (2.49), and is to be expected since the possible reasons for the velocity relationships to be indeterminate are equally applicable to the acceleration relationships.

The time step of integration used in the execution of the kinematic programs is completely user definable, and not surprisingly, with generally increased accuracy resulting from decreasing the time step for a given simulation. The cumulative errors involved in the simulation process and subsequently the gradually increasing loss of integrity of the mechanism may be checked by comparing the link lengths during the simulation with the true values. The time steps used within this study have been chosen in relation to the degree-of-freedom velocities so that about one hundred steps are taken to displace the mechanism from one limiting position to another. The maximum time step of integration that may be used in the dynamics simulation is limited (from a stability point of view) by the minimum period of oscillation of the model under free motion. Again, as with the kinematic simulations, decreasing the step size generally results in improved accuracy although the high computing time requirements in this case makes judicious choice of the step size very important. The simulation results shown in this thesis have mainly been obtained using a time step of 0.002 seconds, giving approximately 30 steps in any one cycle of the highest frequency of natural oscillation for the model; typically, a given simulation using this step would require several hours of computer time to run.

A point to note about the dynamics simulation is that the starting initial condition position of the mechanism model is coincident with the equilibrium position only if the static forces $\bar{F}_{DC}$ and F_{SDC} on the tyre and main spring respectively exactly balance the action of the gravitational forces on the mechanism under static conditions. And because this balance is dependent on the geometry of the mechanism model, an iterative procedure is used to estimate these forces. The procedure is to estimate values for $\bar{F}_{DC}$ and F_{SDC}, execute the dynamics set of programs and, on examining link movements, revise estimates for the next computer run until the steady state position reached is sufficiently close to that required.

The theoretical results of the steady state tests with an out of balance wheel show good correlation with the experimental data when allowance is made for the data taken from the balanced wheel test. The experimentally measured response with the balanced wheel is essentially due to what may be regarded as the unmeasured inputs to the system, these are the tyre irregularities, drum surface irregularities, non-symmetric geometric aspects of the wheel such as out of round and wobble, and also the possibly true unknown amount of out of balance in the wheel. The main frequency of forced vibration of the suspension and steering system in these tests is approximately 8 Hz, and this is directly controlled by the drum speed. This frequency and additional mass causing wheel unbalance were chosen so that measured vibration levels were predominantly at the frequency corresponding to the rotational frequency of the wheel, at the same time ensuring that no major longitudinal vibration of the wheel was induced thereby requiring the inclusion of bush flexibility of the lower link in the model. The theoretical and experimental transient response data does not compare as favourably as the steady state data, as may be seen from the relevant figures. And this is not entirely surprising, since the multi-body model adopted in this work with simple model representations for the sub-systems and in particular for the tyre may be expected to simulate more closely the low frequency responses of the system. Finally, it may be noted that although accelerometers were used in the steady state and transient test measurements, and that these were useful in demonstrating the mechanistic behaviour of the system in showing the relationship between $\ddot{\psi}$ and $\ddot{\phi}$ during the tests, attempts to numerically double integrate the signals to yield displacements were not successful. The resulting displacement plots consistently showed a divergence from known equilibrium positions.

CHAPTER 8 CONCLUSIONS AND SUGGESTIONS FOR FURTHER WORK

SUMMARY

The conclusions that may be drawn from this work are described, and a line of development for future work is suggested.

The work presented in this thesis has shown the modelling of a double wishbone/rack and pinion suspension and steering system as a multi-body system with spatial kinematics. Vector and matrix methods are well suited to analysing the 3-dimensional mechanics of models of this type. And a position, kinematics, and dynamics analysis using these methods has been demonstrated, and the ability to digitally simulate the complex spatial motions of the steered wheels proven. The usefulness of the non-linear dynamics simulation is limited by the large computing time requirement. A comparison of theoretical and experimental dynamics results indicates the applicability of the theoretical models at low frequencies of vibration.

A useful progression of this work would be to use the non-linear simulation programs developed to provide data from which linear models may be synthesized, thus resulting in a more efficient simulation of the vibrational behaviour of suspension and steering systems. Modern data analysis techniques may be used to provide more accurate models for the sub-systems. It may also be useful to incorporate the more realistic string type tyre models into the analysis.

APPENDIX A

REFERENCES

(1) WALDRON, P.,
"Spatial Mechanisms: a survey",
I.Mech.E., One-day discussion on Mechanisms, 1971.

(2) STAPH, H.E.,
"Kinematic Analysis of Space Mechanisms by Vectors",
Transactions of The Seventh Conference on Mechanisms,
Purdue University, 1962.

(3) CHACE, M.A.,
"Mechanisms Analysis by Vector Mathematics",
Transactions of The Seventh Conference on Mechanisms,
Purdue University, 1962.

(4) ELLIS, J.R.,
"Transfer functions for linkage mechanisms",
S.A.S. Report, Cranfield Institute of Technology, 1973.

(5) TIMM, R.F. & ELLIS, J. R.,
"The use of digital simulation languages in mechanism study",
Oklahoma State University, Mechanisms Conference, 1969.

(6) TIMM, R.F., LARSON, C.S., & NAGAMATSU, B.H.,
"The computer modelling of 'large' mechanical systems - dynamic and kinematic analysis",
I.Mech.E., Conference on Mechanisms, 1972.

(7) BEGG, W.S.,
"The dynamic behaviour of the spatial R.S.S.R. four-bar mechanism",
Ph.D. Thesis, Cranfield Institute of Technology, 1974.

(8) SHETH, P.N., & UICKER, J.J.,
"IMP (Integrated Mechanisms Program), a computer-aided design analysis system for mechanisms and linkage",
Transactions of the A.S.M.E., Journal of Engineering for Industry, May 1972.

(9) UICKER, J.J.,
"Dynamic behaviour of spatial linkages",
Transactions of the A.S.M.E., Journal of Engincering for Industry, February 1969.

(10) LIVERMORE, D.F.,
"The determination of equilibrium configurations of spring-restrained mechanisms using (4x4) matrix methods",
Transactions of the A.S.M.E., Journal of Engineering for Industry, February 1967.

(11) HELLER, R., TUTEN, J.M., KADALA, P.S. & LAW, E.H.,
"Analog and digital computer simulation of coulomb friction",
Report No. FRA/ORD-78/07 , Federal Railroad Administration,
Washington DC, December 1977.

(12) ELLIS, J.R.,
"Vehicle Dynamics",
S.A.S. Notes, Cranfield Institute of Technology.

(13) DORGHAM, M.A.,
"The non-linear vibration of the steered wheels of road vehicles",
Ph.D. Thesis, Cranfield Institute of Technology, 1976.

(14) HALES, F.D.,
"A theoretical analysis of the lateral properties of suspension systems",
Proc. I.Mech.E., Vol. 179, Part 2A,
No.2, 1964-65.

(15) ELLIS, J.R.,
"A study of suspension mechanisms",
A.S.A.E. Report No. 5, Cranfield Institute of Technology,
October 1969.

(16) BUTLER, D.M.
"Suspension Analysis",
M.Sc. Thesis, Cranfield Institute of Technology, 1970.

(17) GOUGH, V.E., BARSON, C.W., HUTCHINSON, J.C. & JAMES, D.H.
"Tyre and vehicle vibration",
Proc. I.Mech.E., Vol.179, Part 2A, No.7, 1964-65.

(18) LA BARRE, R.P. & MILLS, B.,
"An investigation into the dynamic stability of steering systems",
Proc. I.Mech.E., Vol.183, Part 2A, No.6, 1968-69.

(19) PODGORSKI, W.A.
"The wheel shimmy problem: its relation to longitudinal tire forces, vehicle motions, and normal load oscillations",
Ph.D. Thesis, Cornell University, 1974.

(20) DÖDLBACHER, G.
"Mathematical investigation to reduce steering wheel 'shimmy' ",
I.A.V.S.D. Extensive Summaries, Vehicle System Dynamics, 1979.

(21) HARDENBERG, J.F., EWINS, J. & GROOTENHUIS, P,
"Suspension design to reduce internal road noise",
FISITA, XIVth Congress, London 1972.

(22) SCHIELEN, W.O.
"Dynamical analysis of suspension systems",
Proc. 5th V.S.D., 2nd I.U.T.A.M., 1977.

(23) MORMAN, K.N.
"Non-linear model formulation forthe static and dynamic analyses of front suspensions",
S.A.E. Paper No. 770052, 1977.

(24) ORLANDEA, N. & CHACE, M.A.,
"Simulation of a vehicle suspension with the ADAMS computer program",
S.A.E. Paper No. 770053, 1977.

(25) CLARK, S.K.,
"Mechanics of Pneumatic Tires",
National Bureau of Standards Monograph 122,
Washington DC 20243, November 1971.

(26) OVERTON, J.A., MILLS, B. & ASHLEY, C.,
"The vertical response characteristics of the non-rolling tyre",
Proc. I.Mech.E., Vol.184, Part 2A, No.2, 1969-70.

(27) ROGERS, L.C. & BREWER, H.K.,
"Synthesis of tire equations for use in shimmy and other dynamic studies",
Journal of Aircraft, Vol.8, No.9, September 1971.

(28) PACEJKA, H.B.,
"Tyre factors and front wheel vibrations",
One-day industrial conference on vehicle dynamics,
The Open University, May 1978.

(29) SHARP, R.S. & JONES, C.J.,
"A Comparison of Tyre Representations in a Simple Wheel Shimmy Problem",
Vehicle System Dynamics, 9, 1980.

(30) CAPTAIN, K.M., BOGHANI, A.B. & WORMLEY, D.N.
"Analytical Tire Models for Dynamic Vehicle Simulation",
Vehicle System Dynamics, 8, 1979

(31) POTTS, G.R., & CSORA, T.T.,
"Tire vibration studies - the state of the art",
Paper presented in the Akron Rubber Group Winter Meeting, January 1974.

(32) POTTS, G.R., BELL, C.A., CHAREK, L.T. & ROY, T.K.,
"Tire Vibrations",
Tire Science and Technology, TSTCA, Vol.5, No.4, November 1977.

(33) PARS, L.A.,
"A treatise on Analytical Dynamics",
Heinemann Educational Books Ltd, 1965.

(34) PAUL, B.,
"Kinematics and dynamics of planar machinery",
Prentice-Hall, 1979.

(35) CAPILDEO, R.,
"Vector algebra and mechanics",
Addison-Wesley Publishing Company, 1968.

(36) BEER, F.P. & JOHNSTON, E.R.,
"Vector Mechanics for Engineers",
McGraw-Hill International Book Company, 1972.

(37) SUH, C.J. & RADCLIFFE, C.W.,
"Kinematics and Mechanisms Design",
John Wiley & Sons, 1978.

(38) Vehicle Safety Research,
Transport & Road Research Laboratory Reports (1977-1980),
S.A.S., Cranfield Institute of Technology.

(39) NEWLAND, D.E.,
"An introduction to random vibrations and spectral analysis",
Longman Group Limited, 1975.

(40) BENDAT, J.S.,
"Signal analysis applications for random vibration and acoustic problems",
Conference at The Open University, 1981.

APPENDIX B

Additional complexities in the basic rack and pinion/double wishbone mechanism model

While retaining the mechanistic characteristics of the system, some extensions to the basic model may be made, and these include modelling the effects of damping in the steering part of the mechanism, backlash, bush flexibility, and anti-roll bars, and the method of inclusion of most of these is clear. The inclusion of bush flexibility provides the biggest increase in complexity to the model and for this reason is described further. The lower wishbone link is quite commonly incorporated with flexible bushes at points of attachment to the vehicle body, and this is used as an example here, see Fig.B1. Ignoring the effective moments due to elastic restraining forces at points P_8 and P_9, then for small displacements of P_8 and P_9, the resulting forces $\overline{F}_8$ and $\overline{F}_9$ may be linearly related to the displacements.

The bush flexibility introduces a further five degrees of freedom to the mechanism model; the only constraint on link-C being that P_2 remains a fixed distance away from P_3. Six equations pertaining to this link may be formulated for use in a dynamics simulation of the complete mechanism, and these are the full rigid body equations (2.58) and (2.71). And kinematic constraint equations are modified to include all possible motions of link-C.

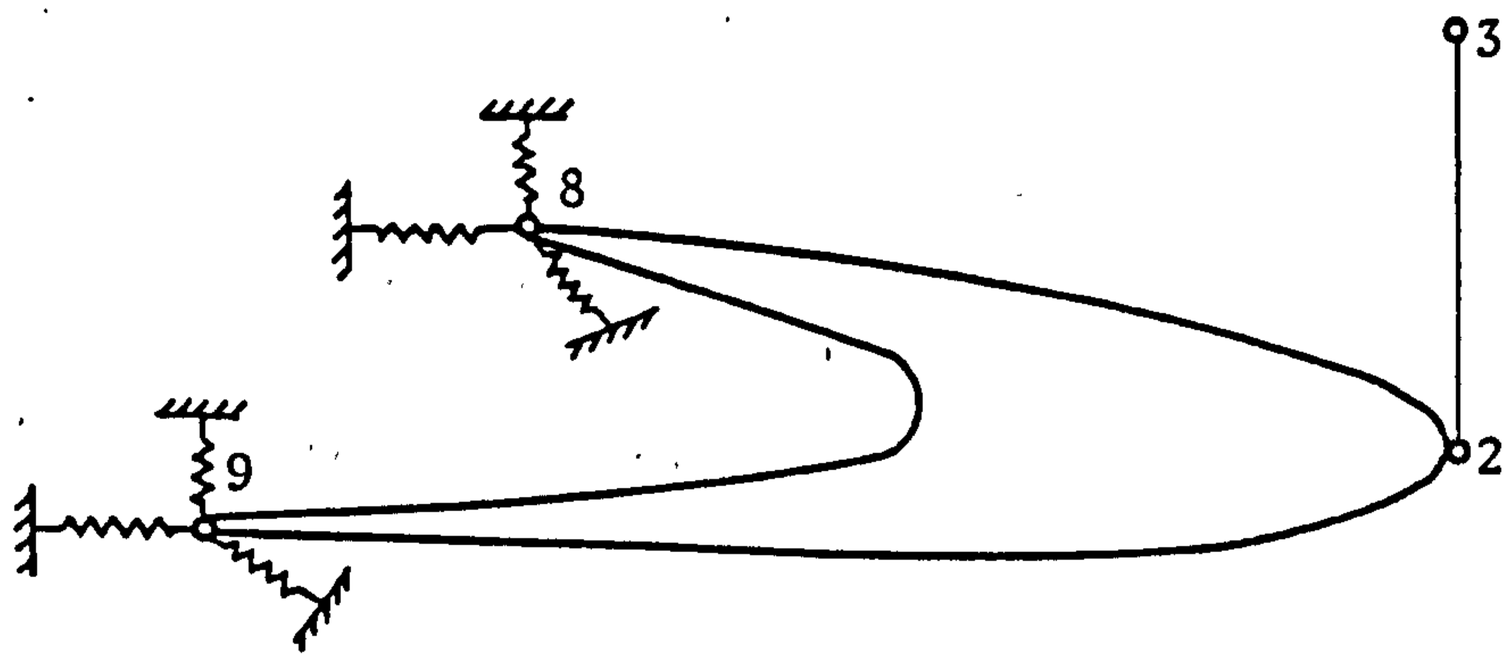
8
9
3
2

(a)

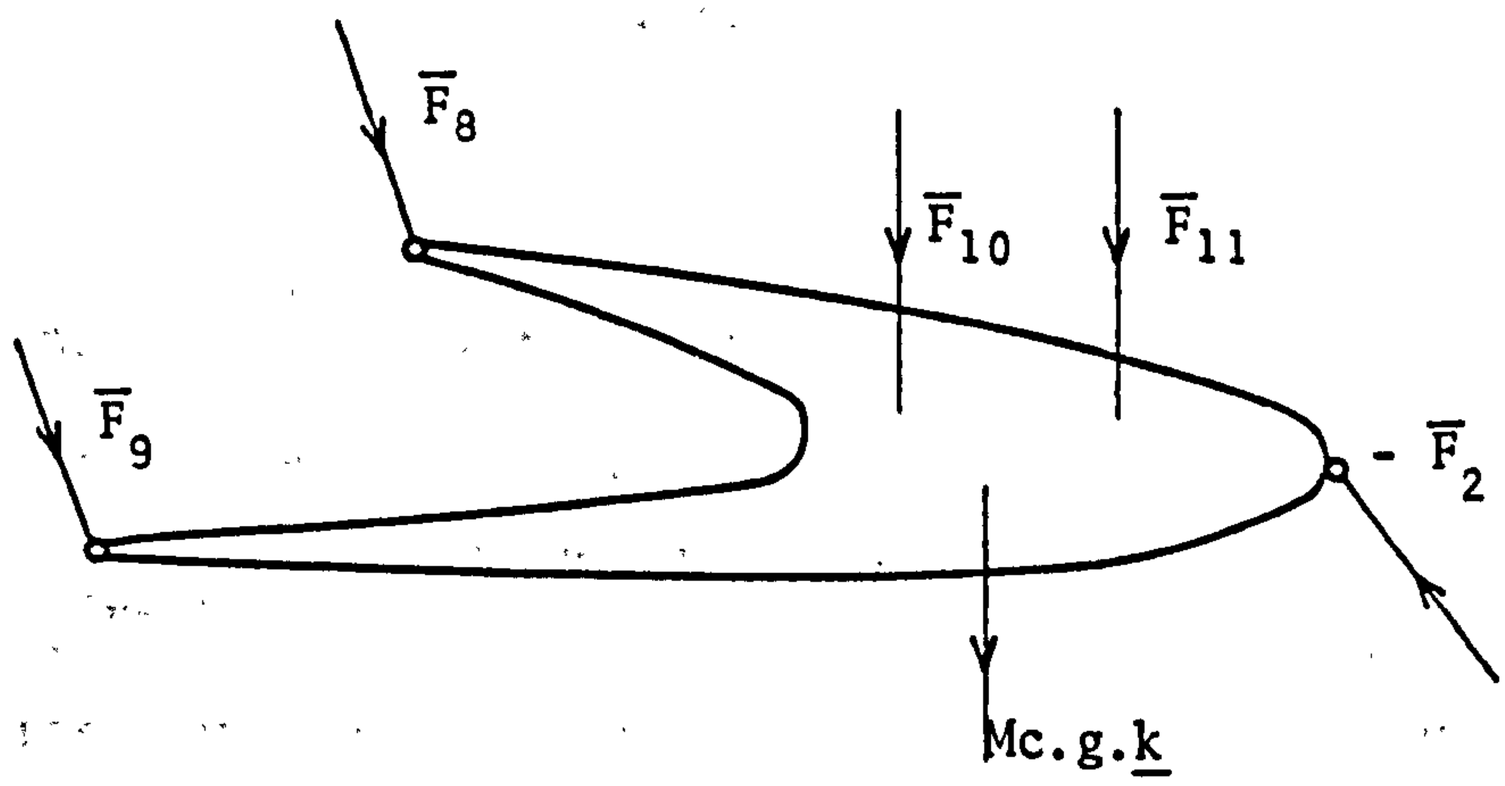
$\overline{F}_8$
$\overline{F}_{10}$
$\overline{F}_{11}$
$\overline{F}_9$
$-\overline{F}_2$
Mc.g.k

(b)

Fig. B1

APPENDIX C

Iterative solution to the intersection of three spheres

The problem may be re-stated as follows: given three fixed reference points $P_1(x_1, y_1, z_1,)$, $P_2(x_2,y_2,z_2)$, and $P_3(x_3,y_3,z_3)$ and their respective distances L_1, L_2, and L_3 to a point P in space, then it is required that the co-ordinates of P(x,y,z) be found. An iterative numerical solution may be attempted using the Newton-Raphson algorithm given that an initial estimate of the required position is available; the three constraint equations are of the form:

$$(x-x_i)^2 + (y-y_i)^2 + (z-z_i)^2 = L_i^2$$

for i = 1,2,3. Letting

$$f_i(x,y,z) = (x-x_i)^2 + (y-y_i)^2 + (z-z_i)^2 - L_i^2$$

for i = 1,2,3, then for an incorrect estimate (x,y,z), $f_i(x,y,z) \neq 0$ for i = 1,2,3. In the neighbourhood of an arbitrary point $(x^{(r)}, y^{(r)}, z^{(r)})$, these equations may be approximated by the linear terms of a Taylor series, -

$$f_i\left[x^{(r+1)}, y^{(r+1)}, z^{(r+1)}\right] \simeq f_i^{(r)} + \left[\frac{\partial f_i}{\partial x}\right]^{(r)} \Delta x + \left[\frac{\partial f_i}{\partial y}\right]^{(r)} .\Delta y + \left[\frac{\partial f_i}{\partial z}\right]^{(r)} .\Delta z$$

where

$f_i^{(r)}$ and $\left[\frac{\partial f_i}{\partial \varepsilon}\right]^{(r)}$ (with ε = x,y,z) represent the functions f_i and their partial derivatives evaluated at point $\left[x^{(r)}, y^{(r)}, z^{(r)}\right]$. If an estimate is initially made and the Taylor series equations $f_i\left[x^{(r+1)}, y^{(r+1)}, z^{(r+1)}\right]$, i = 1,2,3 are equated to zero, then a set of three simultaneous equations will result, the solution of which will yield values for Δx, Δy, and Δz such that a new estimate of x,y,z will be

$$x^{(r+1)} = x^{(r)} + \Delta x$$

$$y^{(r+1)} = y^{(r)} + \Delta y$$

$$z^{(r+1)} = z^{(r)} + \Delta_z$$

In matrix format

$$\left[f^{(r+1)}\right] \simeq \left[f^{(r)}\right] + \left[J^{(r)}\right]\left[\Delta\varepsilon\right] = \left[0\right]$$

$$\therefore \quad \left[\Delta\varepsilon\right] = -\left[J^{(r)}\right]^{-1}\left[f^{(r)}\right]$$

where $\left[\Delta\varepsilon\right]' = \begin{bmatrix}\Delta x\\ \Delta y\\ \Delta z\end{bmatrix}$ are the corrections to the values of $x^{(r)}, y^{(r)}, z^{(r)}$;

$$\left[f^{(r)}\right] = \begin{bmatrix} f_1^{(r)}\\ f_2^{(r)}\\ f_3^{(r)}\end{bmatrix}$$

are the residuals and give a measure of the error involved in each function having used $x^{(r)}, y^{(r)}, z^{(r)}$ as an estimate; the Jacobian matrix [J] is evaluated at $(x^{(r)}, y^{(r)}, z^{(r)})$, and is

$$[J] = \begin{bmatrix} \frac{\partial f_1}{\partial x} & \frac{\partial f_1}{\partial y} & \frac{\partial f_1}{\partial z}\\ \frac{\partial f_2}{\partial x} & \frac{\partial f_2}{\partial y} & \frac{\partial f_2}{\partial z}\\ \frac{\partial f_3}{\partial x} & \frac{\partial f_3}{\partial y} & \frac{\partial f_3}{\partial z}\end{bmatrix}$$

And the partial derivatives are

$$\frac{\partial f_i}{\partial x} = 2(x-x_i)$$

$$\frac{\partial f_i}{\partial y} = 2(y-y_i)$$

$$\frac{\partial f_i}{\partial z} = 2(z-z_i)$$

for i = 1,2,3.

The procedure outlined may be seen to depend on the ability to evaluate the inverse of the Jacobian matrix, and the condition that this may not be possible may be investigated by setting the determinant of this matrix to zero; the determinant |J| is given by

$$|J| = \frac{\partial f_1}{\partial x}\left[\frac{\partial f_2}{\partial y}\frac{\partial f_3}{\partial z} - \frac{\partial f_2}{\partial z}\frac{\partial f_3}{\partial y}\right] - \frac{\partial f_1}{\partial y}\left[\frac{\partial f_2}{\partial x}\frac{\partial f_3}{\partial z} - \frac{\partial f_2}{\partial z}\frac{\partial f_3}{\partial x}\right] + \frac{\partial f_1}{\partial z}\left[\frac{\partial f_2}{\partial x}\frac{\partial f_3}{\partial y} - \frac{\partial f_2}{\partial y}\frac{\partial f_3}{\partial x}\right]$$

Substituting for the partial derivatives, and setting the determinant to zero

$$2(x-x_1)\left[2(y-y_2)\ 2(z-z_3)\ -2(z-z_2)\ 2(y-y_3)\right]$$
$$-2(y-y_1)\left[2(x-x_2)\ 2(z-z_3)\ -2(z-z_2)\ 2(x-x_3)\right]$$
$$+2(z-z_1)\left[2(x-x_2)\ 2(y-y_3)\ -2(y-y_2)\ 2(x-x_3)\right] = 0$$

Expanding, simplifying, and re-arranging

$$x\left[y_2z_3 - y_3z_2 - y_1z_3 + y_1z_2 + y_3z_1 - y_2z_1\right]$$
$$+ y\left[x_1z_3 - x_1z_2 - x_2z_3 + x_3z_2 + x_2z_1 - x_3z_1\right]$$
$$+ z\left[x_1y_2 - x_1y_3 - x_2y_1 + x_3y_1 + x_2y_3 - y_2x_3\right]$$

$$+\left[x_1y_3z_2 - x_1y_2z_3 + x_2y_1z_3 - x_3y_1z_2 - x_2y_3z_1 + x_3y_2z_1\right] = 0$$

and since the co-ordinates of P(x,y,z) may be arbitrarily selected with only a change in the lengths L_1, L_2, and L_3, then it follows that for this expression to be generally true, the coefficients of x,y, and z must all be equal to zero.

It was found that the condition that the three reference points P_1, P_2, and P_3 all lie on a straight line presented difficulties in attempts at an analytical solution to this problem, and this condition is equivalent to

$$(\overline{r}_2 - \overline{r}_1) \times (\overline{r}_3 - \overline{r}_1) = \overline{0}$$

And expanding this and comparing with the coefficients of x, y, and z here reveals that this is equivalent to having a zero determinant and therefore it is to be expected that this iterative approach will also fail when this geometric condition exists.

APPENDIX D

Selection of two mutually orthogonal unit vectors perpendicular to a known space vector

Letting

$$\bar{\lambda} = \lambda_x \underline{i} + \lambda_y \underline{j} + \lambda_z \underline{k}$$

be a known unit vector in a given orthogonal frame of reference, then it is required that two mutually orthogonal unit vectors ($\bar{\lambda}_1$, $\bar{\lambda}_2$) perpendicular to $\bar{\lambda}$ be evaluated. It is clear that having evaluated one of these, the other may then be evaluated from the vector product of the two known unit vectors. It is also clear from physical consideration of the problem that a unique solution does not exist, and that some selection procedure needs to be adopted.

Without any loss of generality, the base of the unit vectors may be taken to be at the origin of the frame of reference; see Fig. D1. The point P(x,y,z) is located at the tip of the vector $\bar{\lambda}_1$, and its locus is shown to be a circle in the plane containing $\bar{\lambda}_1$ and $\bar{\lambda}_2$ and centred at the origin with unit radius. The two conditions on $\bar{\lambda}_1$ are

$$| \bar{\lambda}_1 | = 1$$

$$\bar{\lambda}_1 \circ \bar{\lambda} = 0$$

The co-ordinates of the point P are, by definition, equivalent to the direction cosines of the vector $\bar{\lambda}_1$

$$\therefore \quad \bar{\lambda}_1 = x \underline{i} + y \underline{j} + z \underline{k}$$

Substituting for $\bar{\lambda}$ and $\bar{\lambda}_1$, the two constraint equations become

$$x^2 + y^2 + z^2 = 1 \qquad \text{(D1)}$$

$$x \lambda_x + y \lambda_y + z \lambda_z = 0 \qquad \text{(D2)}$$

From equation (D2), provided $\lambda_z \neq 0$

$$z = -x \left(\frac{\lambda x}{\lambda_z}\right) - y \left(\frac{\lambda y}{\lambda_z}\right) \qquad \text{(D3)}$$

$$\therefore \quad z^2 = x^2 \left(\frac{\lambda x}{\lambda_z}\right)^2 + 2\, x.y \left(\frac{\lambda x}{\lambda_z}\right)\left(\frac{\lambda y}{\lambda_z}\right) + y^2 \left(\frac{\lambda y}{\lambda_z}\right)^2$$

Substituting this into equation (D1), and re-arranging

$$Ax^2 + Cy\, x + (B\, y^2 - 1) = 0$$

where

$$A = 1 + \left(\frac{\lambda x}{\lambda_z}\right)^2$$

$$B = 1 + \left(\frac{\lambda y}{\lambda_z}\right)^2$$

$$C = 2 \left(\frac{\lambda x}{\lambda_z}\right) \left(\frac{\lambda y}{\lambda_z}\right)$$

$$\therefore \quad x = -\left(\frac{C}{2A}\right) y \pm \sqrt{[D\, y^2 + \frac{1}{A}]} \qquad \text{(D4)}$$

where

$$D = \left(\frac{C}{2A}\right)^2 - \left(\frac{B}{A}\right)$$

A selection procedure for $\bar{\lambda}_1$ may now be implemented by differentiating x with respect to y, and equating this to zero. This process simply maximizes or minimizes x with respect to y. Differentiating equation (D4) and equating to zero.

$$\frac{dx}{dy} = -\left(\frac{C}{2A}\right) \pm \frac{1}{2} [Dy^2 + \frac{1}{A}]^{-\frac{1}{2}} . 2Dy$$

$$= 0$$

$$\therefore \quad \pm Dy = \left(\frac{C}{2A}\right) \sqrt{[Dy^2 + \frac{1}{A}]}$$

$$\therefore \quad y^2 = \frac{\frac{1}{A} \left(\frac{C}{2A}\right)^2}{D \left[D - \left(\frac{C}{2A}\right)^2\right]}$$

$$= \frac{\frac{1}{A} \left(\frac{C}{2A}\right)^2}{D \left(\frac{-B}{A}\right)}$$

$$\therefore \quad y = \pm \left(\frac{C}{2A}\right) \sqrt{\left(\frac{-1}{DB}\right)} \qquad \text{(D5)}$$

Either positive or negative value may be taken for y, and equations (D4) and then (D3) may then be used to obtain corresponding values for x and z.

It may be noted that under certain conditions $\bar{\lambda}_1$ may be selected immediately, and these are that

if $\lambda_x = 0$ then let $\bar{\lambda}_1 = \underline{i}$

if $\lambda_y = 0$ then let $\bar{\lambda}_1 = \underline{j}$

if $\lambda_z = 0$ then let $\bar{\lambda}_1 = \underline{k}$

and if any two of these conditions exist, then either of the possible choices will be acceptable.

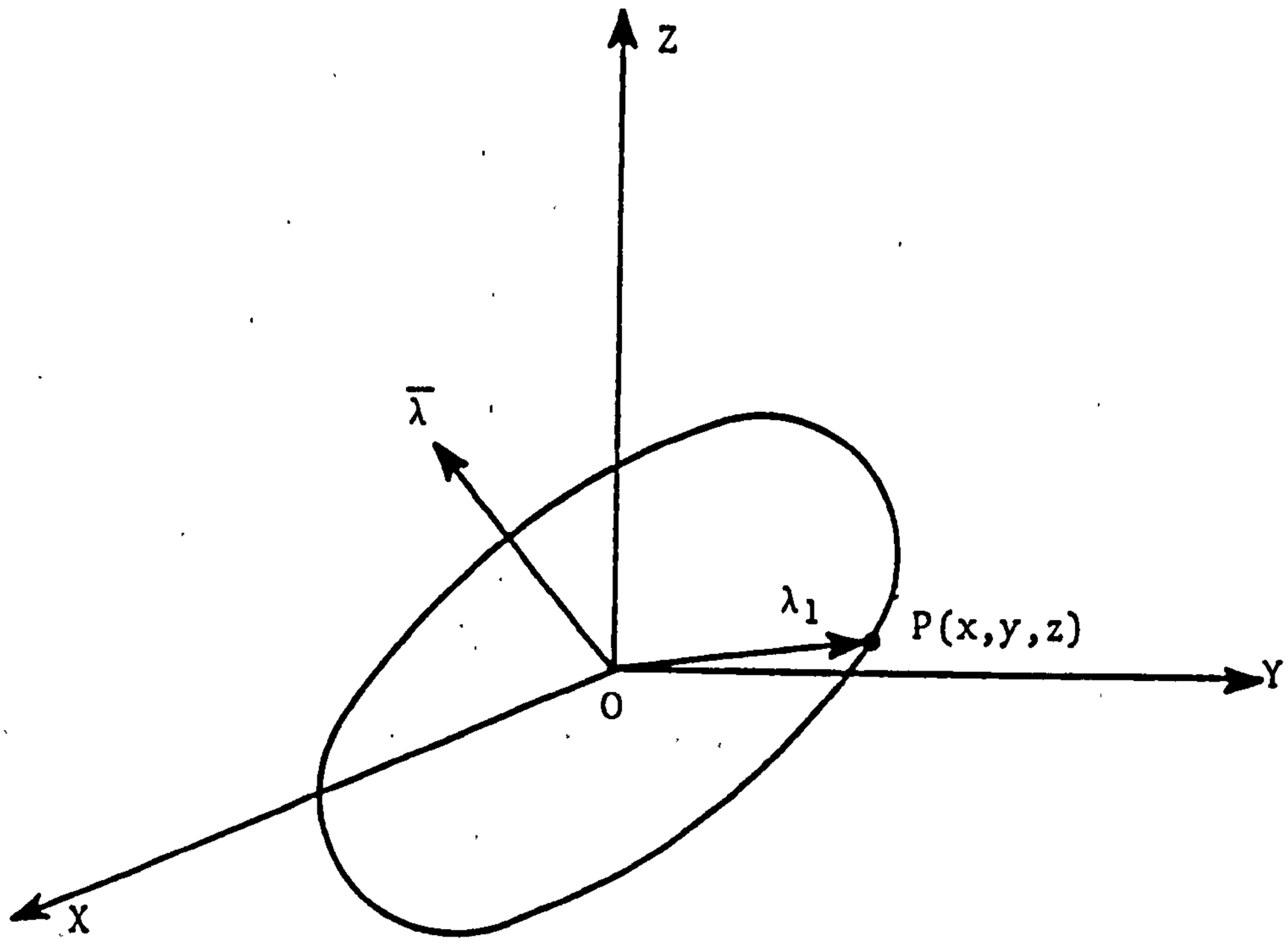

Fig.D1

APPENDIX E

Kinematic analysis of a RSSR mechanism

The mechanism has two degrees of freedom and, referring to Fig. E1, it can be seen that $\dot{\psi}$ and $\dot{\delta}$ may be considered as the degree-of-freedom motion variables with all other link velocities related to these two velocity-components. $\bar{\lambda}_1$ and $\bar{\lambda}_2$ are two mutually orthogonal unit vectors which are perpendicular to $\bar{\lambda}_{4,3}$ and may be evaluated using the procedure developed in Appendix D.

The general velocity relationships may be obtained by evaluating and equating the velocity of P_4 obtained via the two different kinematic routes possible, and also employing a constraint equation on $\bar{W}_B$ which allows for the freedom $\dot{\delta}$. The angular velocities of links A and C may be immediately seen to be

$$\bar{W}_A = \dot{\psi}\,\bar{\lambda}_{1,2} \quad \text{and} \quad \bar{W}_C = \dot{\phi}\,\bar{\lambda}_{5,6}$$

The velocity of P_4 via $\vec{1,3}$ and $\vec{3,4}$ is

$$\bar{V}_4 = [\dot{\psi}\,\bar{\lambda}_{1,2} \times (\bar{r}_3 - \bar{r}_1)] + [\bar{W}_B \times (\bar{r}_4 - \bar{r}_3)] \qquad \text{(E1)}$$

And via $\vec{5,4}$

$$\bar{V}_4 = [\dot{\phi}\,\bar{\lambda}_{5,6} \times (\bar{r}_4 - \bar{r}_5)] \qquad \text{(E2)}$$

Equating these two expressions, and re-arranging

$$[\dot{\phi}.\bar{\lambda}_{5,6} \times (\bar{r}_4 - \bar{r}_5)] - [\bar{W}_B \times (\bar{r}_4 - \bar{r}_3)] = [\dot{\psi}.\bar{\lambda}_{1,2} \times (\bar{r}_3 - \bar{r}_1)] \qquad \text{(E3)}$$

And allowing for the freedom of rotation of link-B about the axis through P_3 and P_4

$$\bar{W}_B \circ \bar{\lambda}_{4,3} = \dot{\delta} \qquad \text{(E4)}$$

Equations (E3) and (E4) may be used to evaluate $\dot{\phi}$ and $\bar{W}_B$ as a function of $\dot{\psi}$ and $\dot{\delta}$.

An alternative to this formulation is possible if the angular velocity of link-B is put in the form:

$$\bar{W}_B = \dot{\delta}.\bar{\lambda}_{4,3} + W_1.\bar{\lambda}_1 + W_2\bar{\lambda}_2 \qquad \text{(E5)}$$

Substituting this into equation (1)

$$\bar{V}_4 = [\dot{\psi}.\bar{\lambda}_{1,2} \times (\bar{r}_3 - \bar{r}_1)] + [(\dot{\delta}.\bar{\lambda}_{4,3} + W_1\bar{\lambda}_1 + W_2\,\bar{\lambda}_2) \times (\bar{r}_4 - \bar{r}_3)]$$

and since

$$\dot{\delta}.\,\bar{\lambda}_{4,3} \times (\bar{r}_4 - \bar{r}_3) = \bar{0}$$

this may be simplified to yield

$$\bar{V}_4 = \dot{\psi}[\bar{\lambda}_{1,2} \times (\bar{r}_3-\bar{r}_1)] + W_1[\bar{\lambda}_1 \times (\bar{r}_4-\bar{r}_3)] + W_2\ [\bar{\lambda}_2 \times (\bar{r}_4-\bar{r}_3)] \quad \text{(E6)}$$

Equations (E6) and (E2) may then be equated, and solved to evaluate $\dot{\phi}$, W_1, and W_2 as a function of $\dot{\psi}$ and $\dot{\delta}$.

Finally, the ratio of the spin velocities of links A and C may be evaluated by making use of the equivalent displacement constraint equation, i.e.

$$\bar{V}_3 \circ \bar{\lambda}_{4,3} = \bar{V}_4 \circ \bar{\lambda}_{4,3}$$

$$\therefore [\dot{\psi}\ \bar{\lambda}_{1,2} \times (\bar{r}_3 - \bar{r}_1)] \circ \bar{\lambda}_{4,3} = [\dot{\phi}\ \bar{\lambda}_{5,6} \times (\bar{r}_4 - \bar{r}_5)] \circ \bar{\lambda}_{4,3}$$

$$\therefore \left(\frac{\dot{\phi}}{\dot{\psi}}\right) = \frac{[\bar{\lambda}_{1,2} \times (\bar{r}_3 - \bar{r}_1)] \circ \bar{\lambda}_{4,3}}{[\bar{\lambda}_{5,6} \times (\bar{r}_4 - \bar{r}_5)] \circ \bar{\lambda}_{4,3}} \quad \text{(E7)}$$

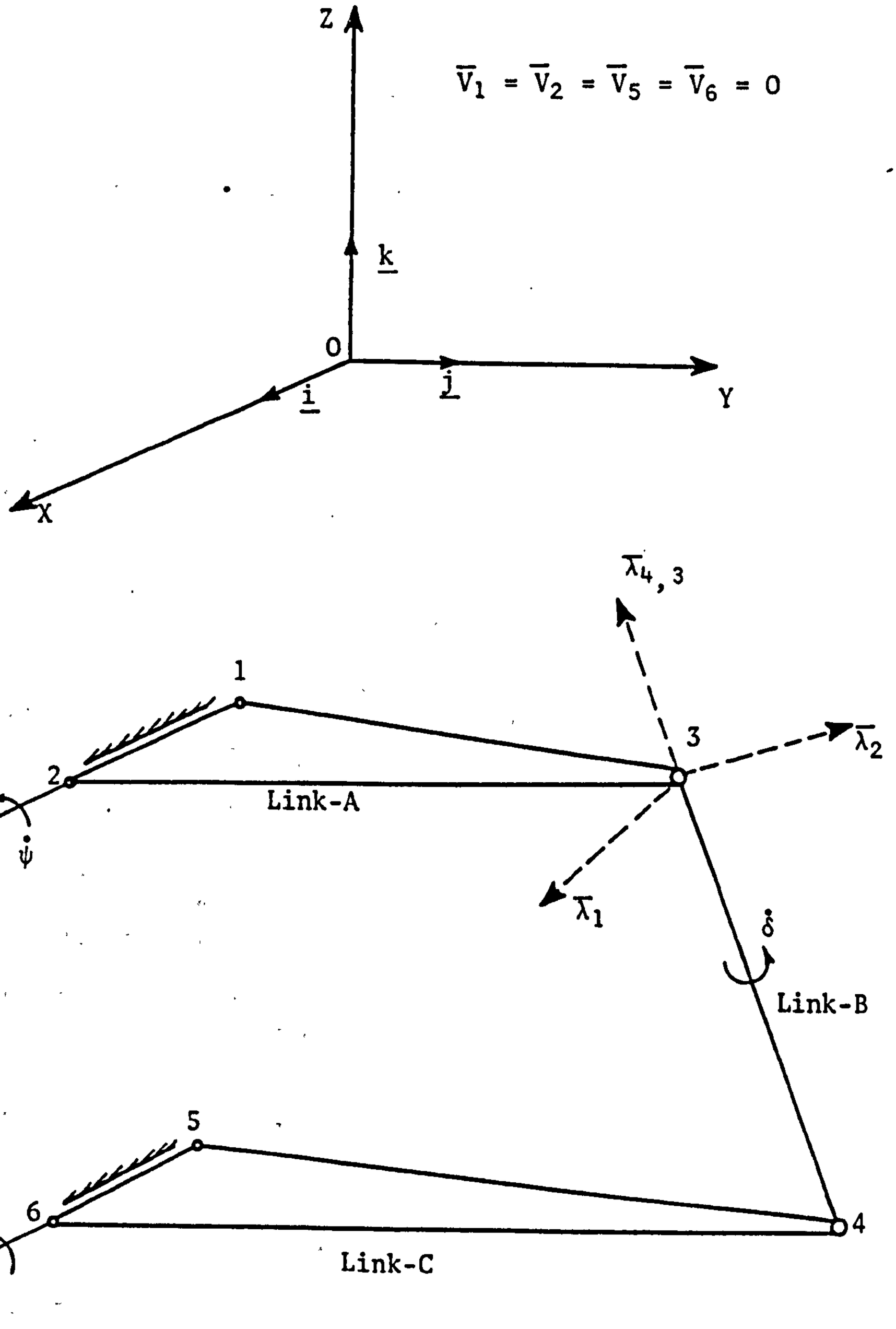
Z
$\bar{V}_1 = \bar{V}_2 = \bar{V}_5 = \bar{V}_6 = 0$
k
O
i
j
Y
X
$\bar{\lambda}_{4,3}$
1
2
3
$\bar{\lambda}_2$
Link-A
$\dot{\psi}$
$\bar{\lambda}_1$
$\dot{\delta}$
Link-B
5
6
4
Link-C
ϕ

Fig. E1

APPENDIX F

Analysis of a typical commercial vehicle suspension and steering system model.

This note is concerned with the demonstration of a static force analysis and a kinematic analysis applied to a beam axle suspension with steering achieved by the rotation of a steering drop arm connected to the stub axle via a ball jointed drag link. A schematic diagram of the system is shown in Fig. F1, with the essential points in the system numbered 1 through 7, and the links labelled using the letters A through D. The links in the model are rigid, and inter-connected with frictionless revolute and spherical joints.

All vectors are referred to a right-handed frame of reference fixed in the vehicle. And, for brevity, the analyses are performed only for one side of the vehicle front end; the extension to both sides being direct and simple.

1) Static force analysis

A free body diagram of each link in the system is given in Fig. F2, showing the forces and moments taken to be acting on each link. An external force and moment vector is the 'input' at point P_6, and this is balanced by an external torque (T) on the steering drop arm. Gravitational forces have been ignored. It may be seen that the law of action and reaction has been inherently applied in the process of assigning internal force and moment vectors on each part of a joint connecting any two links; a force and moment balance equation may then be formulated for each link.

The unit vector along the axis of rotation of the drop arm is denoted by $\bar{\lambda}_R$, and the unit vector along the king pin axis is $\bar{\lambda}_K$. In Fig.F2 $\bar{F}(n)$ implies that the force vector may in general be taken to have n orthogonal components, and similarly for $\bar{M}(n)$. The restriction on spherical joints is that they transmit no moment, and on revolute joints that the moment along the axis of possible rotation be zero. Other notation used includes

$\Sigma(\bar{M})_A$ = sum of moments about point P_A

$\bar{\lambda}_R = (\lambda RX)\,\underline{i} + (\lambda RY)\,\underline{j} + (\lambda RZ)\,\underline{k}$

$\bar{\lambda}_K = (\lambda KX)\,\underline{i} + (\lambda KY)\,\underline{j} + (\lambda KZ)\,\underline{k}$

$\bar{F}_I = (FIX)\,\underline{i} + (FIY)\,\underline{j} + (FIZ)\,\underline{k}$

$\bar{M}_I = (MIX)\,\underline{i} + (MIY)\,\underline{j} + (MIZ)\,\underline{k}$

The link equations may now be formulated.

Link-A

The force equation is $\Sigma\bar{F} = \bar{0}$,

$\therefore \quad \bar{F}_1 + \bar{F}_2 = \bar{0}$ (F1)

The moment equation is $\Sigma\bar{M} = 0$, taking moments about point P_1

$$\bar{M}_1 + \bar{M}_s + [(\bar{r}_2 - \bar{r}_1) \times \bar{F}_2] = \bar{0} \qquad (F2)$$

Resolving moments about the axis of possible rotation, and substituting for $\bar{M}_s = T\,\bar{\lambda}_R$

$$\bar{\lambda}_R o \bar{M}_1 + \bar{\lambda}_R o (T\,\bar{\lambda}_R) + \bar{\lambda}_R o\,[(\bar{r}_2 - \bar{r}_1) \times \bar{F}_2] = 0$$

and making use of the fact that $\bar{\lambda}_R o\,\bar{M}_1 = 0$ this becomes

$$T + \bar{\lambda}_R o\,[(\bar{r}_2 - \bar{r}_1) \times \bar{F}_2] = 0 \qquad (F3)$$

Expanding, and re-arranging yields

$$\begin{aligned} T + &(F2X)\,[(\lambda RY)\,(z_2 - z_1) - (\lambda RZ)\,(y_2 - y_1)] \\ + &(F2Y)\,[(\lambda RZ)\,(x_2 - x_1) - (\lambda RX)\,(z_2 - z_1)] \\ + &(F2Z)\,[(\lambda RX)\,(y_2 - y_1) - (\lambda RY)\,(x_2 - x_1)] = 0 \end{aligned} \qquad (F4)$$

Link-B

$$\Sigma\bar{F} = \bar{0}$$

$$\therefore \quad -\bar{F}_2 - \bar{F}_3 = 0 \qquad (F5)$$

$$\Sigma(\bar{M})_2 = (\bar{r}_3 - \bar{r}_2) \times (-\bar{F}_3)$$

$$= \bar{0} \qquad (F6)$$

Now

$$|\Sigma(\bar{M})_2| = |\bar{r}_3 - \bar{r}_2|\,|\bar{F}_3|\,\sin\theta$$

$|\bar{r}_3 - \bar{r}_2| \neq 0$, and for $|\bar{F}_3| \neq 0$

$\Rightarrow \quad \sin\theta = 0$

$\therefore \quad \theta = 0, \pm\pi, \pm 2\pi, \ldots\ldots$

$(\bar{r}_3 - \bar{r}_2)$ and $\bar{F}_3$ are therefore collinear, and $\bar{F}_3$ may be expressed in the form

$$\bar{F}_3 = \hat{F}_3\,\bar{\lambda}_{3,2}$$

$$= \left(\frac{x_2 - x_3}{L_{2,3}}\right)\hat{F}_3\,\underline{i} + \left(\frac{y_2 - y_3}{L_{2,3}}\right)\hat{F}_3\,\underline{j} + \left(\frac{z_2 - z_3}{L_{2,3}}\right)\hat{F}_3\,\underline{k} \qquad (F7)$$

and

if $\hat{F}_3 > 0 \Rightarrow$ link 2,3 is in tension

if $\hat{F}_3 < 0 \Rightarrow$ link 2,3 is in compression

Link-C

The forces in the steering system may be evaluated by taking moments about the king pin axis,

$$[\Sigma(\overline{M})_4] \circ \overline{\lambda}_K = [\overline{M}_4 + \overline{M}_5 + \{(\overline{r}_5 - \overline{r}_4) \times \overline{F}_5\} + \{(\overline{r}_3 - \overline{r}_4) \times \overline{F}_3\} + \overline{M} + \{(\overline{r}_6 - \overline{r}_4) \times \overline{F}\}] \circ \overline{\lambda}_K$$

$$= 0 \qquad \text{(F8)}$$

$$\overline{\lambda}_K \circ [\overline{M}_4 + \overline{M}_5] = 0$$

and since $\overline{\lambda}_K \equiv \overline{\lambda}_{4,5}$, then $\overline{\lambda}_K \circ [(\overline{r}_5 - \overline{r}_4) \times \overline{F}_5] = 0$

Thus, equation (F8) reduces to

$$\overline{\lambda}_K \circ [(\overline{r}_3 - \overline{r}_4) \times \overline{F}_3] = -\overline{\lambda}_K \circ \overline{M} - \overline{\lambda}_K \circ [(\overline{r}_6 - \overline{r}_4) \times \overline{F}] \qquad \text{(F9)}$$

Letting the external force and moment vector at P_6

$$\overline{F} = (FX)\,\underline{i} + (FY)\,\underline{j} + (FZ)\,\underline{k}$$

$$\overline{M} = (MX)\,\underline{i} + (MY)\,\underline{j} + (MZ)\,\underline{k}$$

And using the fact that

$$\overline{S} \circ (\overline{P} \times \overline{Q}) = \begin{vmatrix} S_x & S_y & S_z \\ P_x & P_y & P_z \\ Q_x & Q_y & Q_z \end{vmatrix}$$

equation (F9) may be expanded to yield

$$F3X\,[\lambda KY\,(z_3 - z_4) - \lambda KZ\,(y_3 - y_4)]$$
$$+ F3Y\,[\lambda KZ\,(x_3 - x_4) - \lambda KX\,(z_3 - z_4)]$$
$$+ F3Z\,[\lambda KX\,(y_3 - y_4) - \lambda KY\,(x_3 - x_4)]$$

$$= -[\lambda KX\,(MX) + \lambda KY\,(MY) + \lambda KZ\,(MZ)]$$
$$+ FX\,[\lambda KZ\,(y_6 - y_4) - \lambda KY\,(z_6 - z_4)]$$
$$+ FY\,[\lambda KX\,(z_6 - z_4) - \lambda KZ\,(x_6 - x_4)]$$
$$+ FZ\,[\lambda KY\,(x_6 - x_4) - \lambda KX\,(y_6 - y_4)] \qquad \text{(F10)}$$

From equation (F7)

$$F3X = \left(\frac{x_2-x_3}{L_{2,3}}\right)\hat{F}_3 \quad ; \quad F3Y = \left(\frac{y_2-y_3}{L_{2,3}}\right)\hat{F}_3 \quad ; \quad F3Z = \left(\frac{z_2-z_3}{L_{2,3}}\right)\hat{F}_3$$

and substitution of these into equation (F10) will enable a solution for $\hat{F}_3$ and hence $\bar{F}_3$ to be made. From equation (F5), $\bar{F}_2 = -\bar{F}_3$, and substituting this into equation (F4) yields a solution for T.

Considering the support reaction forces and moments, $\bar{F}_1$ and $\bar{M}_1$ may be evaluated by employing equations (F1) and (F2) respectively. There are more restraints on link-C than necessary to maintain equilibrium, and the forces and moments on this body are therefore statically indeterminant. However, employing the force equation yields

$$\bar{F}_4 + \bar{F}_5 = -\bar{F}_3 - \bar{F}$$

and this may be useful in looking at forces transmitted to the suspension joints and the front axle.

2) Kinematic analysis

Considering the mechanism model shown in Fig. F3, it is apparent that the system has eight degrees of freedom, the steering part of the mechanism has two ($\dot{\theta}$,$\dot{\phi}$) and the axle has six (V7X, V7Y, V7Z, WDX, WDY, WDZ). It should then be possible to evaluate all the linear and angular velocities of the mechanism links as a function of these degree-of-freedom velocity-components.

Referring to Fig. F3, the angular velocity of link-C relative to link-D is given by

$$\bar{W}_C - \bar{W}_D = \dot{\psi}\,\bar{\lambda}_{5,4}$$

$$\therefore \quad \bar{W}_C = \bar{W}_D + \dot{\psi}\,\bar{\lambda}_{5,4} \qquad \text{(F11)}$$

and the angular velocity of link-A is

$$\bar{W}_A = \dot{\theta}\,\bar{\lambda}_R$$

Point P_1 is stationary in the frame of reference i.e. $\bar{V}_1 = \bar{0}$

$$\therefore \quad \bar{V}_2 = \bar{V}_1 + [\bar{W}_A \times (\bar{r}_2-\bar{r}_1)]$$

$$= \dot{\theta}\,\bar{\lambda}_R \times (\bar{r}_2 - \bar{r}_1) \qquad \text{(F12)}$$

And the velocity of P_3 via $\vec{1,2}$ and $\vec{2,3}$ is therefore

$$\bar{V}_3 = \bar{V}_2 + [\bar{W}_B \times (\bar{r}_3 - \bar{r}_2)]$$

$$= [\dot{\theta}\,\bar{\lambda}_R \times (\bar{r}_2 - \bar{r}_1)] + [\bar{W}_B \times (\bar{r}_3 - \bar{r}_2)] \qquad \text{(F13)}$$

The velocity of P_3 via $\vec{7,4}$ and $\vec{4,3}$ is

$$\bar{V}_3 = \bar{V}_7 + [\bar{W}_D \times (\bar{r}_4 - \bar{r}_7)] + [\bar{W}_C \times (\bar{r}_3 - \bar{r}_4)]$$

and substituting for $\bar{W}_C$ from equation (F11) and simplifying, this becomes

$$\bar{V}_3 = \bar{V}_7 + [\bar{W}_D \times (\bar{r}_3 - \bar{r}_7)] + [\dot{\psi}\ \bar{\lambda}_{5,4} \times (\bar{r}_3 - \bar{r}_4)] \qquad (F14)$$

Equations (F13) and (F14) may now be equated and re-arranged to yield

$$[\bar{W}_B \times (\bar{r}_3 - \bar{r}_2)] - [\dot{\psi}\ \bar{\lambda}_{5,4} \times (\bar{r}_3 - \bar{r}_4)]$$

$$= \bar{V}_7 + [\bar{W}_D \times (\bar{r}_3 - \bar{r}_7)] - [\dot{\theta}\ \bar{\lambda}_R \times (\bar{r}_2 - \bar{r}_1)] \qquad (F15)$$

The spin velocity of link-B about the axis through P_2 and P_3 may be taken account of by the equation

$$\bar{W}_B \circ \bar{\lambda}_{3,2} = \dot{\phi} \qquad (F16)$$

and equations (F15) and (F16) should now be sufficient to solve for $(\bar{W}_B, \dot{\psi})$ given the inputs $(\bar{V}_7, \bar{W}_D, \dot{\theta}, \dot{\phi})$. Resolving equation (F15) into its three components, and putting these with equation (F16) into matrix format results in the matrix equation (F17), and this is in a form suitable for numerical computation of the required kinematic relationships.

Alternatively, if information about the coupler (link-B) is not required directly, then an analysis may be made by employing the equivalent displacement constraint equation between points P_2 and P_3, i.e.

$$\bar{\lambda}_{2,3} \circ \bar{V}_2 = \bar{\lambda}_{2,3} \circ \bar{V}_3$$

and substituting for $\bar{V}_2$ from equation (F12) and for $\bar{V}_3$ from equation (F14), this becomes

$$\bar{\lambda}_{2,3} \circ [\dot{\theta}\ \bar{\lambda}_R \times (\bar{r}_2 - \bar{r}_1)] = \bar{\lambda}_{2,3} \circ [\dot{\psi}\ \bar{\lambda}_{5,4} \times (\bar{r}_3 - \bar{r}_4)]$$

$$+ \bar{\lambda}_{2,3} \circ [\bar{V}_7 + \{\bar{W}_D \times (\bar{r}_3 - \bar{r}_7)\}]$$

$$\therefore \dot{\psi} = \left[\frac{\bar{\lambda}_{2,3} \circ \{\dot{\theta}\ \bar{\lambda}_R \times (\bar{r}_2 - \bar{r}_1)\} - \bar{\lambda}_{2,3} \circ \{\bar{V}_7 + [\bar{W}_D \times (\bar{r}_3 - \bar{r}_7)]\}}{\bar{\lambda}_{2,3} \circ \{\bar{\lambda}_{5,4} \times (\bar{r}_3 - \bar{r}_4)\}} \right] \qquad (F18)$$

And for no axle motion, the following speed ratio for the steering system results, -

$$\begin{pmatrix} \dot{\psi} \\ \dot{\theta} \end{pmatrix} = \left[\frac{\bar{\lambda}_{2,3} \circ \{\bar{\lambda}_R \times (\bar{r}_2 - \bar{r}_1)\}}{\bar{\lambda}_{2,3} \circ \{\bar{\lambda}_{5,4} \times (\bar{r}_3 - \bar{r}_4)\}} \right] \qquad (F19)$$

$$
\begin{bmatrix}
0 & (z_3-z_2) & -(y_3-y_2) & -\{\lambda 54Y(z_3-z_4) \\ & & & -\lambda 54Z\ (y_3-y_4)\} \\
(z_3-z_2) & 0 & -(x_3-x_2) & -\{\lambda 54X\ (z_3-z_4) \\ & & & -\lambda 54Z\ (x_3-x_4) \\
(y_3-y_2) & -(x_3-x_2) & 0 & -\{\lambda 54X\ (y_3-y_4) \\ & & & -\lambda 54Y\ (x_3-x_4)\} \\
\left(\frac{x_2-x_3}{L_{2,3}}\right) & \left(\frac{y_2-y_3}{L_{2,3}}\right) & \left(\frac{z_2-z_3}{L_{2,3}}\right) & 0
\end{bmatrix}
\begin{bmatrix} WBX \\ WBY \\ WBZ \\ \dot{\psi} \end{bmatrix}
=
\begin{bmatrix}
\{V7X + WDY\ (z_3-z_7) - WDZ\ (y_3-y_7)\} \\
-\dot{\theta}\{\lambda RY(z_2-z_1) - \lambda RZ\ (y_2-y_1)\} \\
\{-V7Y + WDX\ (z_3-z_7) - WDZ(x_3-x_7)\} \\
-\dot{\theta}\{\lambda RX\ (z_2-z_1) - \lambda RZ\ (x_2-x_1)\} \\
\{V7Z + WDX\ (y_3-y_7) - WDY\ (x_3-x_7)\} \\
-\dot{\theta}\{\lambda RX\ (y_2-y_1) - \lambda RY\ (x_2-x_1)\} \\
\dot{\phi}
\end{bmatrix}
$$

(F17)

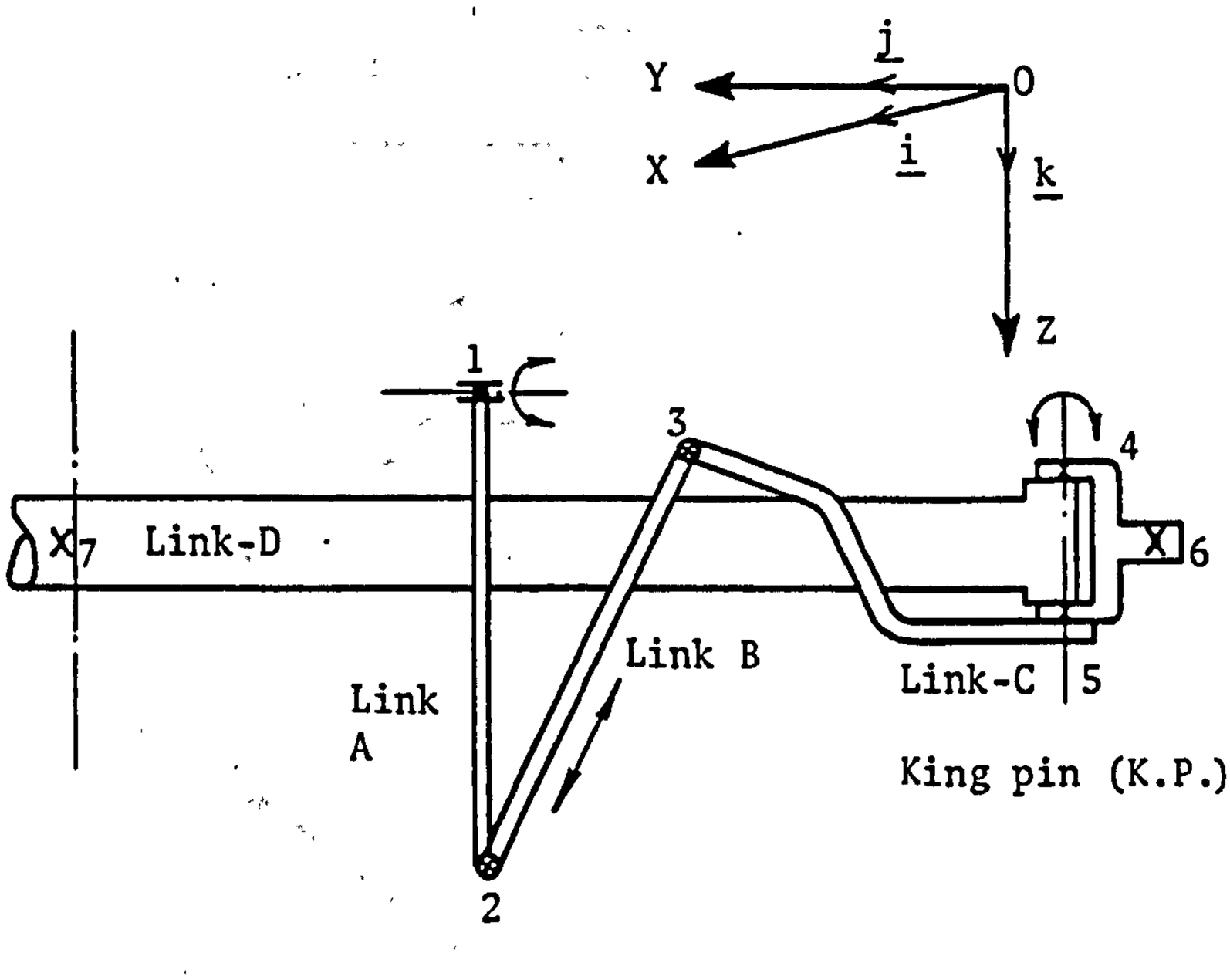

Fig. F1

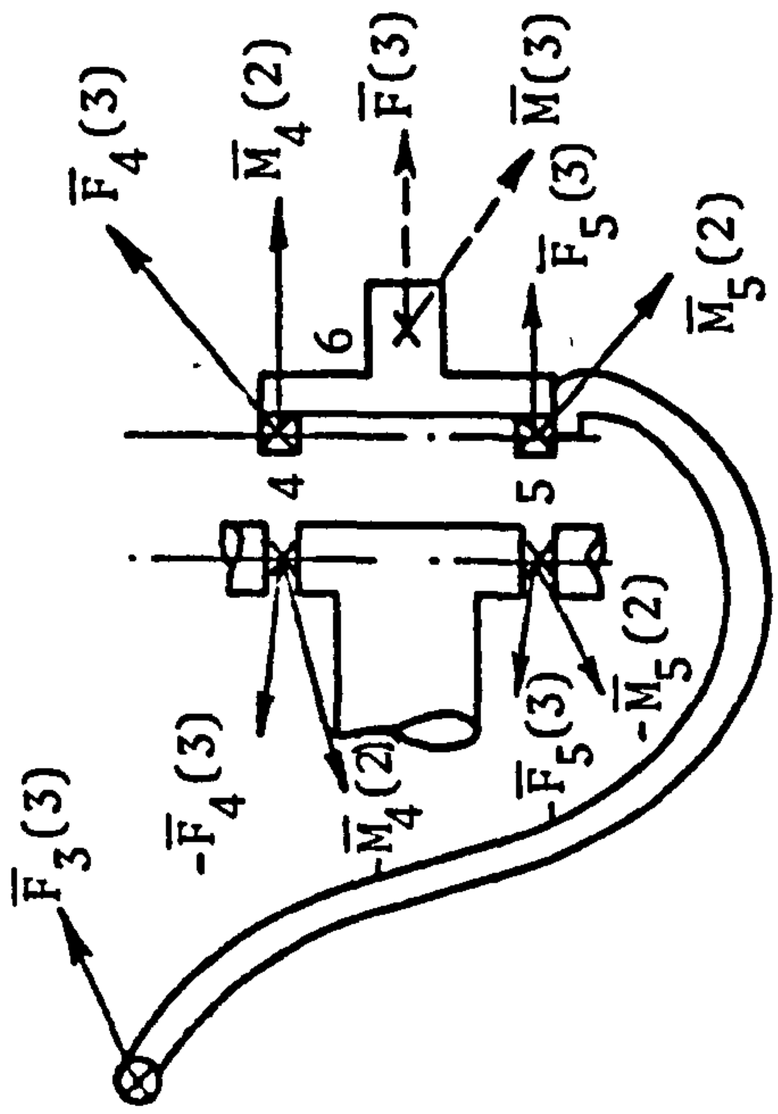

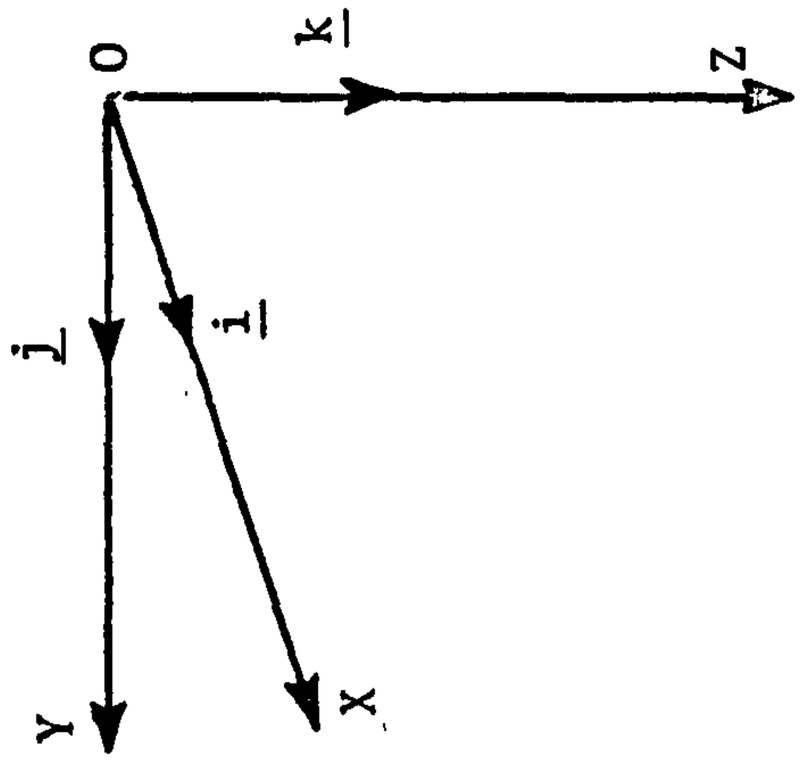

F2

i, j, k unit vectors

$\bar{M}_s$ at point 1, and $\bar{F}/\bar{M}$ at point 6

are active (or external to whole system) forces/moments

Fig.

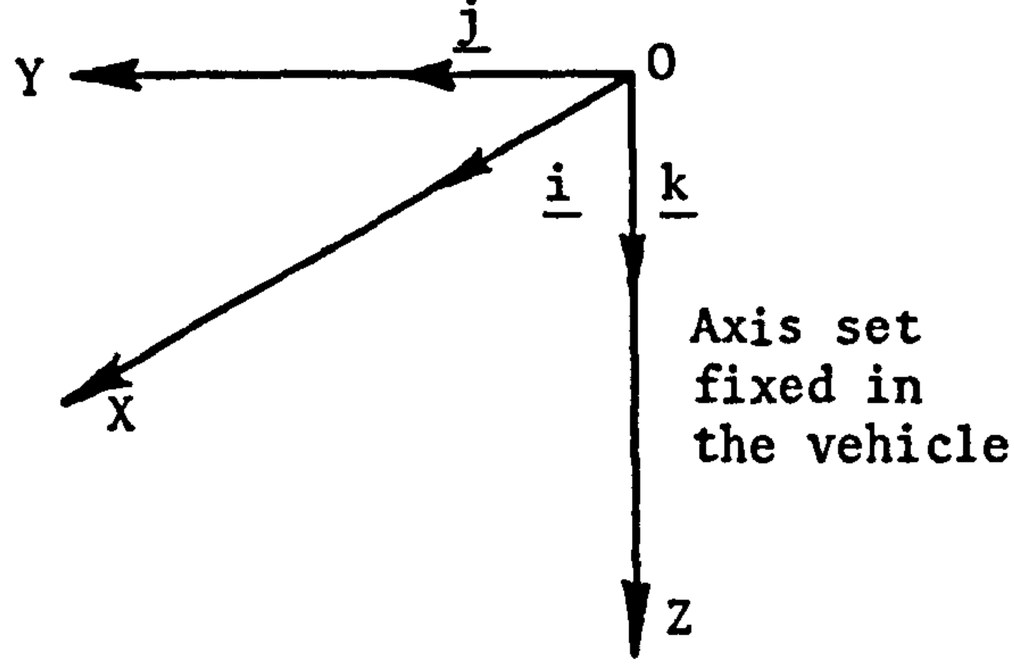

Velocity of point P_I, $\bar{V}_I$ = VIX.$\underline{i}$ + VIY.$\underline{j}$ + VIZ.$\underline{k}$

Angular Velocity of link-N, $\bar{W}_N$ = WNX.$\underline{i}$ + WNY.$\underline{j}$ + WNZ.$\underline{k}$

$\bar{W}_A = \dot{\theta}.\lambda_R$

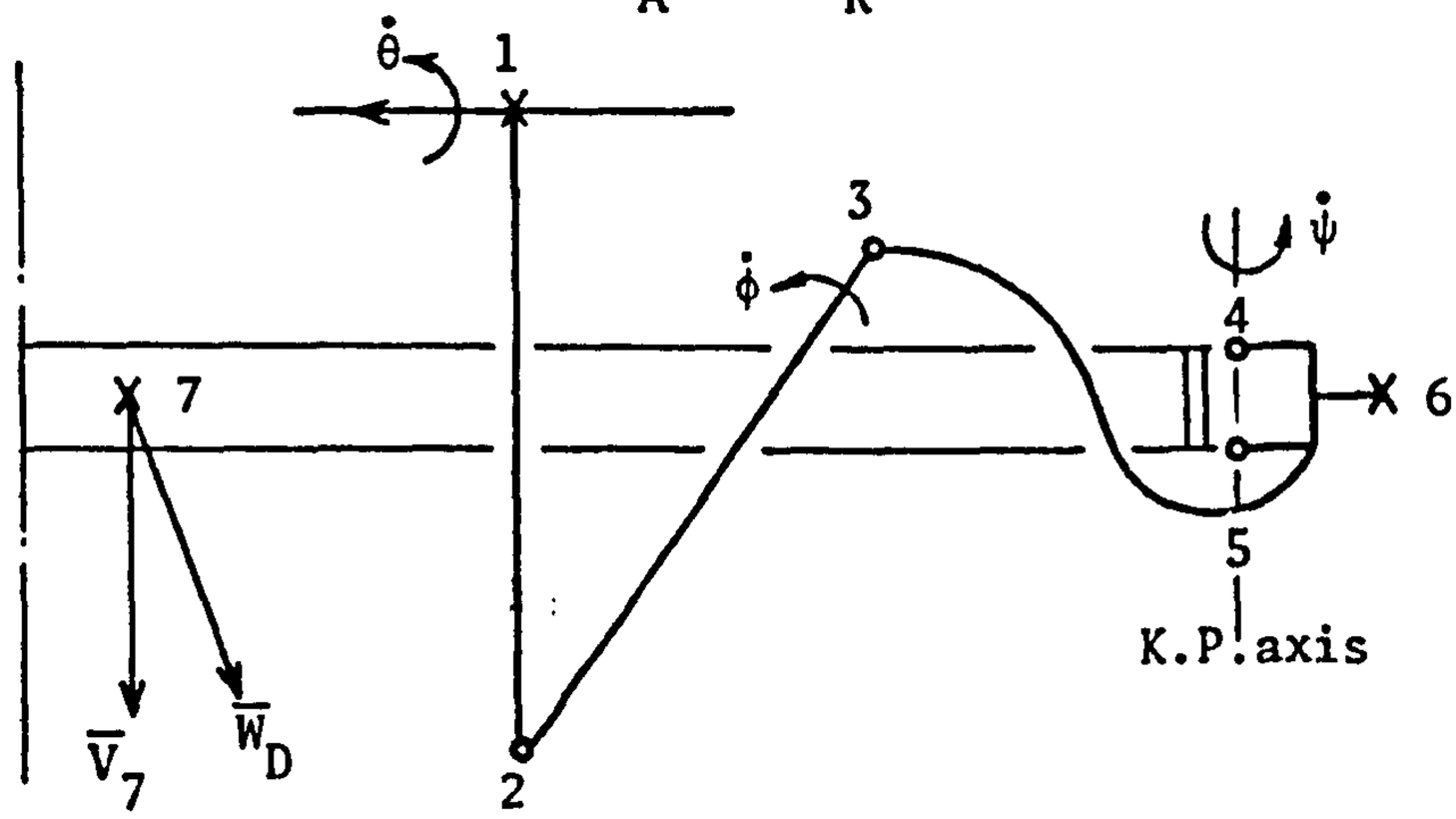

Fig. F3

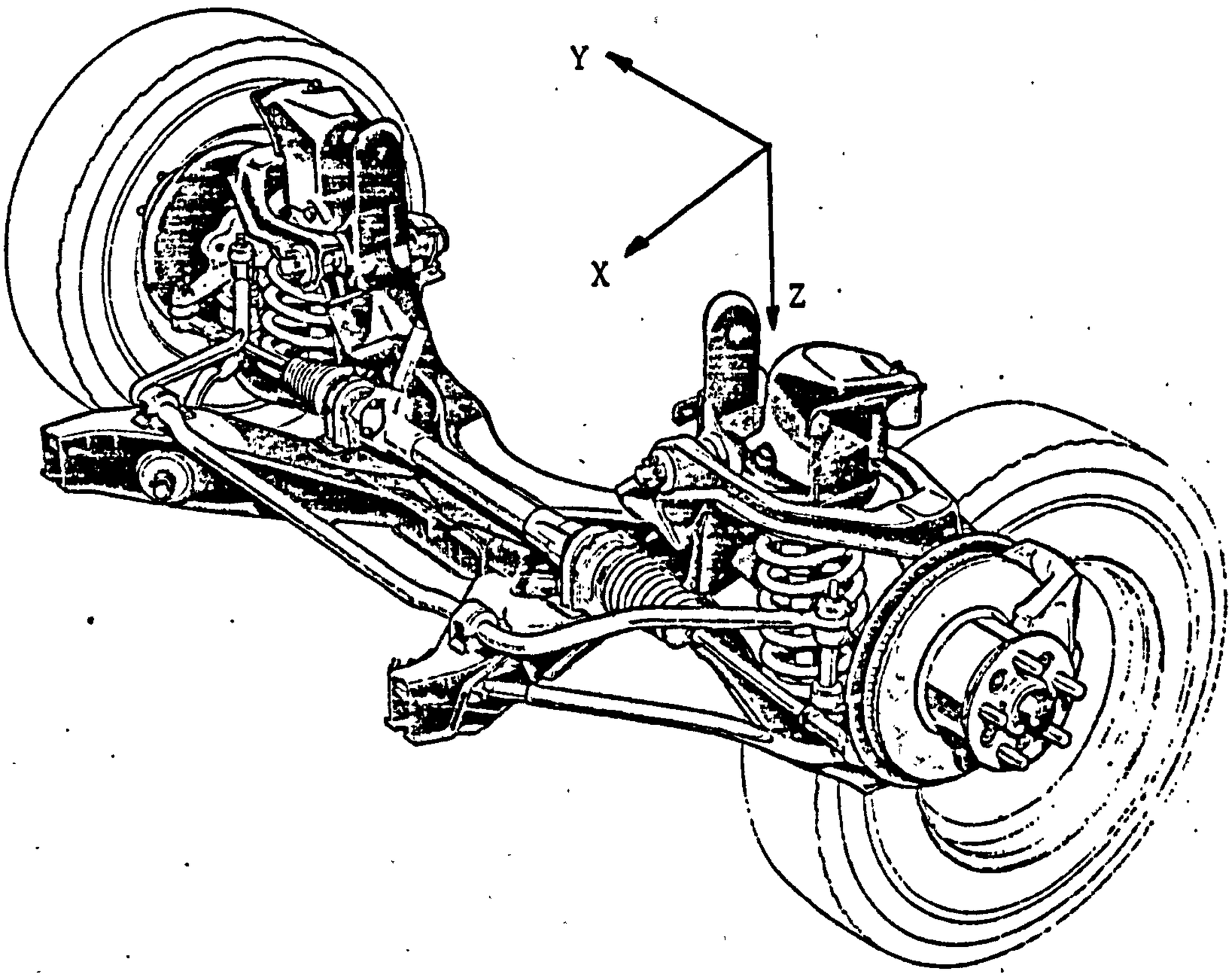

Fig. 1

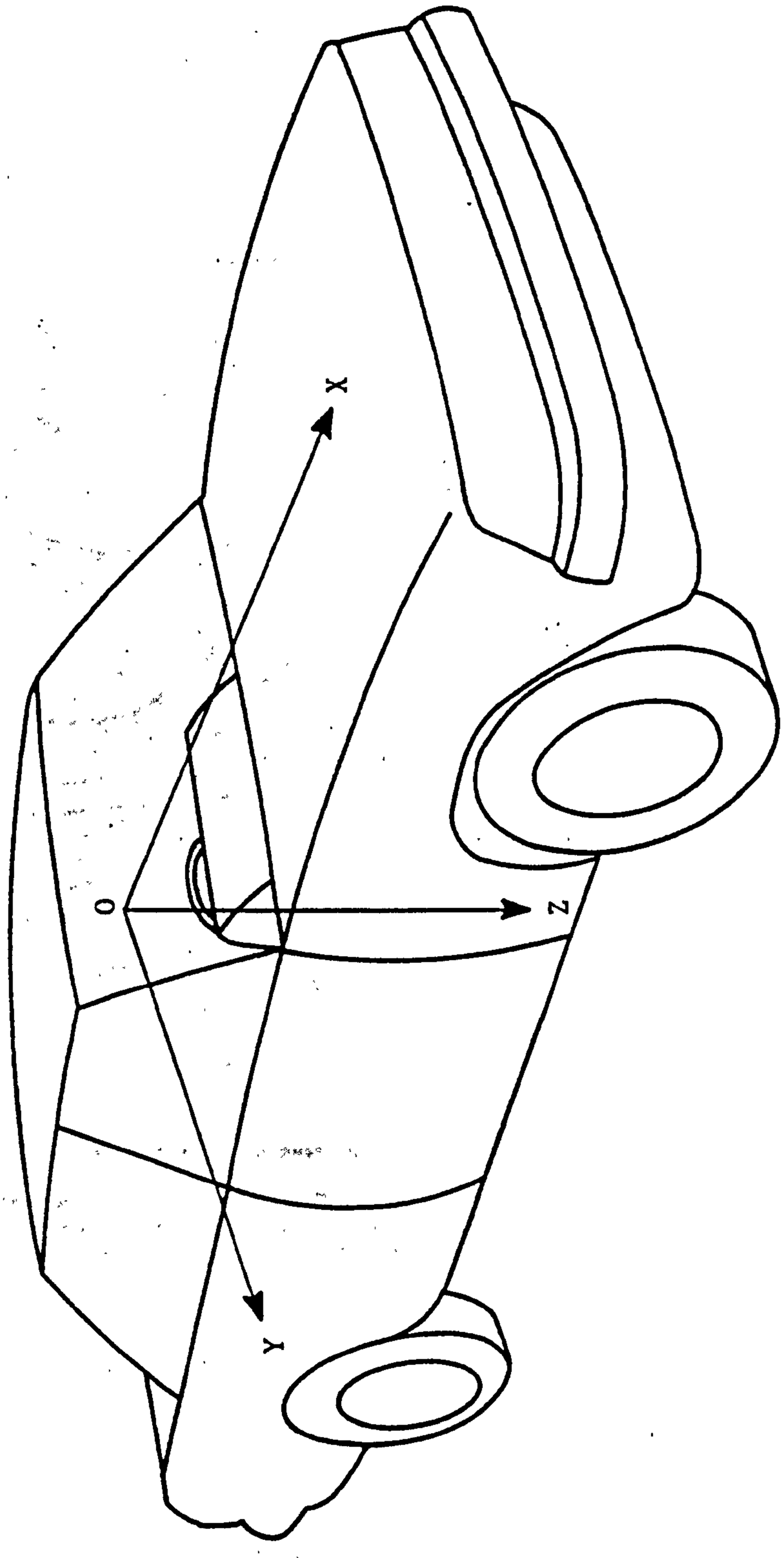

Fig. 2

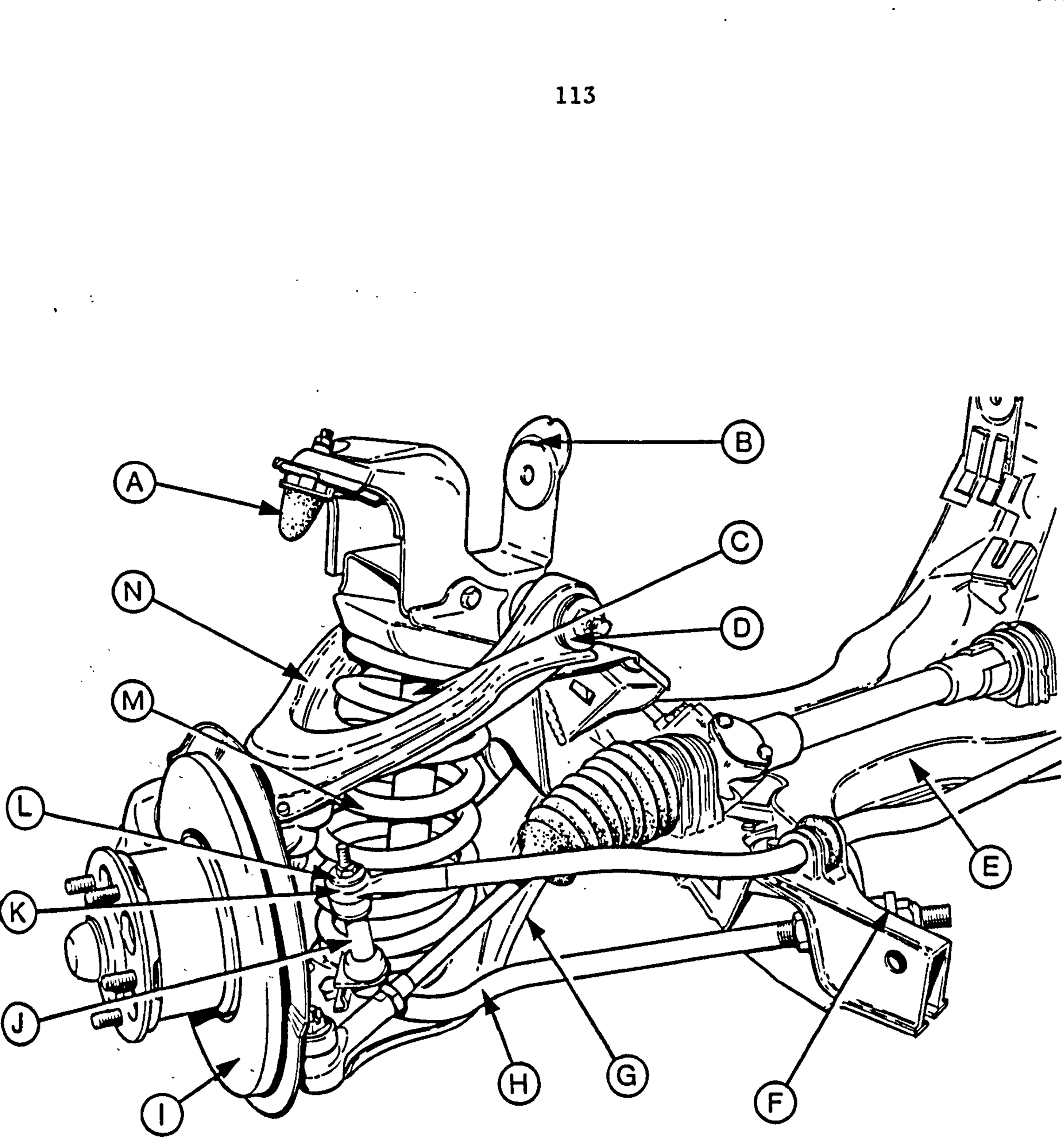

Front suspension assembly

A Bump rubber
B Body to subframe mount
C Shock absorber
D Upper pivot bolt
E Subframe
F Tie-bar front mounting
G Lower swinging arm
H Tie-bar
I Disc/hub assembly
J Connecting link
K Stabiliser bar
L Bush
M Coil spring
N Upper swinging arm

Fig. 3

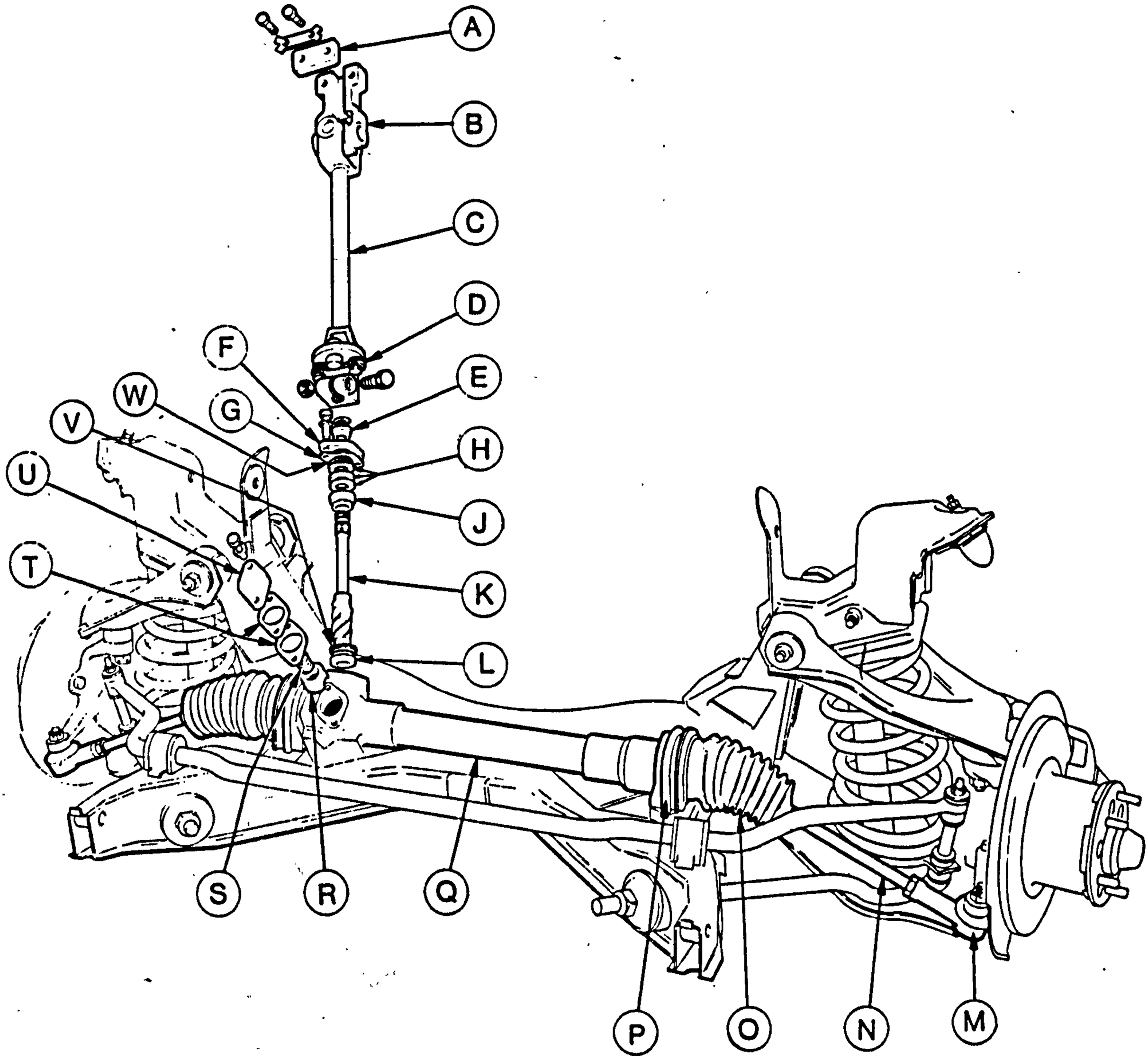

Rack and pinion steering gear manual steering

A Lock bar
B Universal joint
C Steering lower shaft
D Flexible coupling
E Seal
F Cover plate
G Gasket
H Shims
J Pinion upper bearing
K Pinion
L Pinion lower bearing
M Track-rod end
N Track-rod
O Rubber gaiter
P Mounting U-clamp
Q Rack housing
R Slipper
S Preload spring
T Shims
U Cover plate
V Spacer
W Spacer

Fig. 4

LINK DESCRIPTION

A Upper wishbone

B Stub axle

C Lower wishbone

D Track rod/coupler

E Rack

F Disc and wheel

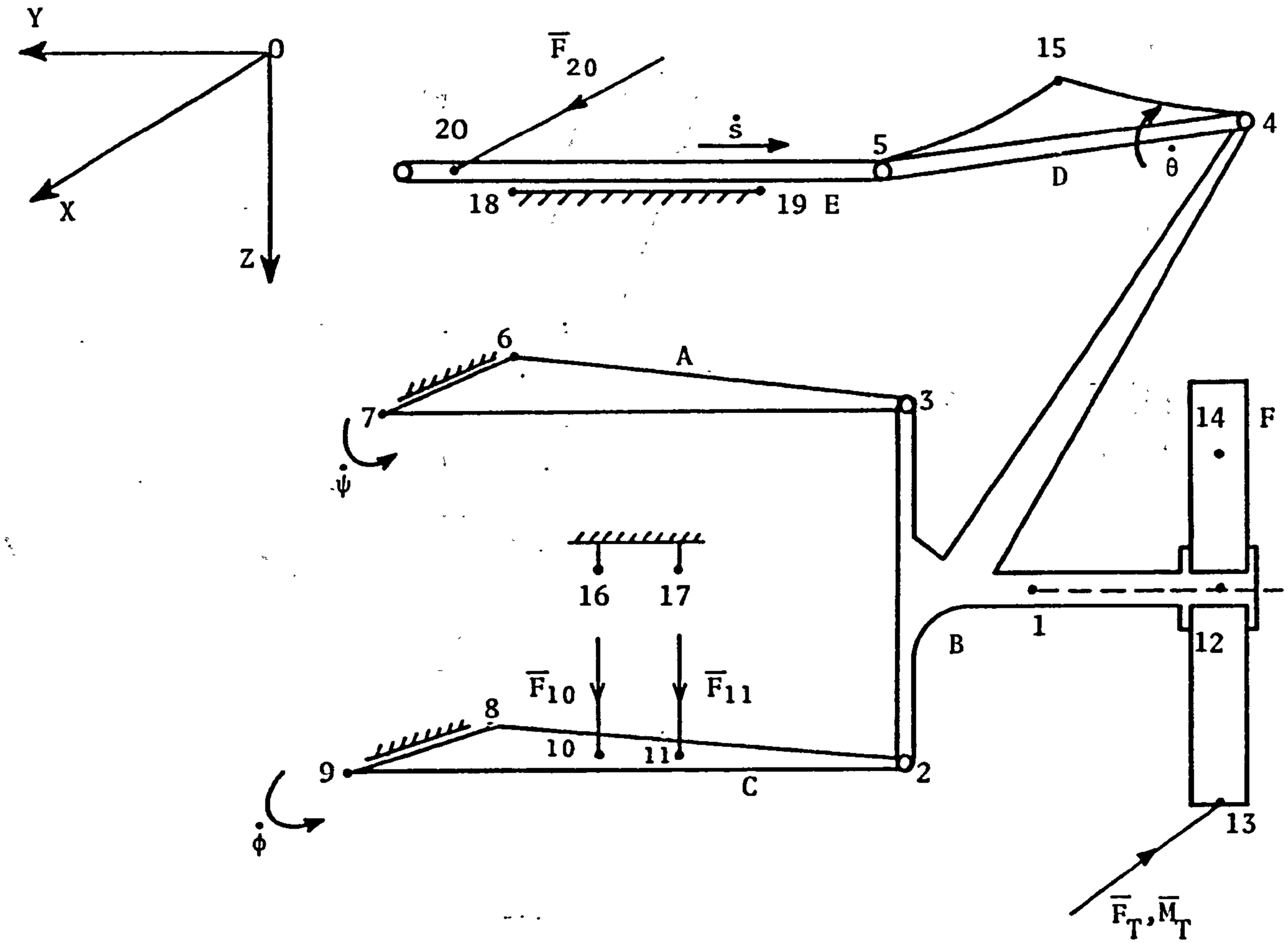

Fig. 5

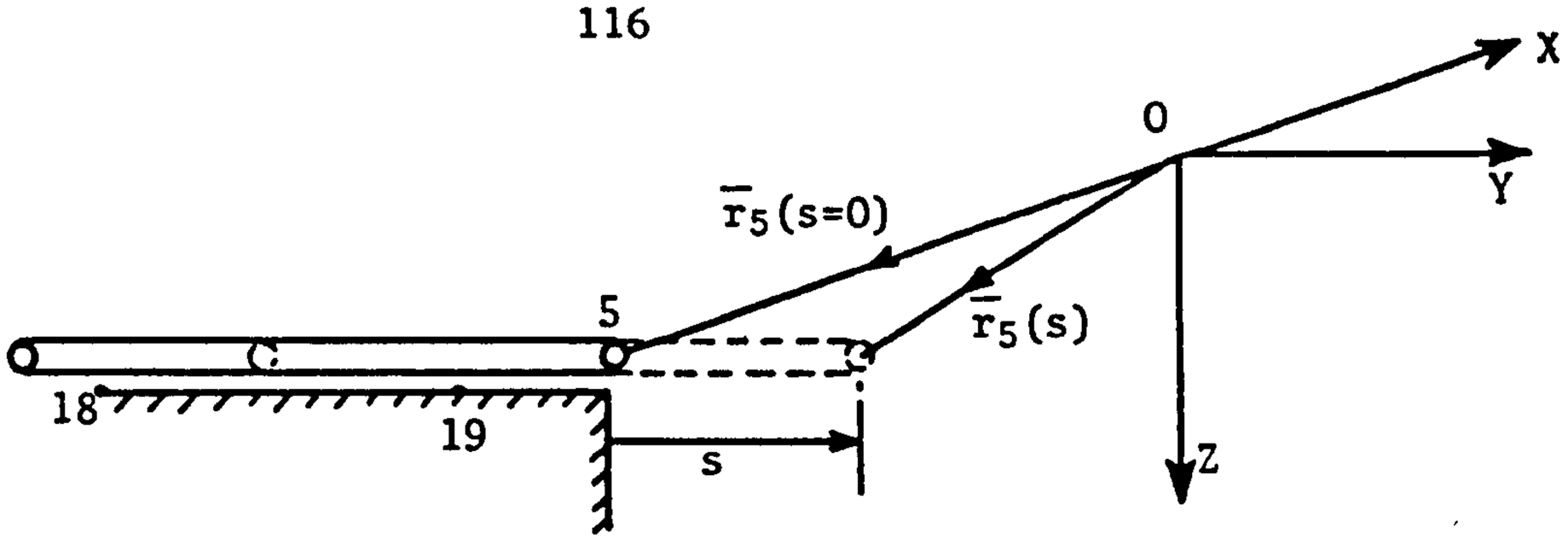
X
0
Y
$\bar{r}_5(s=0)$
$\bar{r}_5(s)$
5
18
19
s
Z

(a)

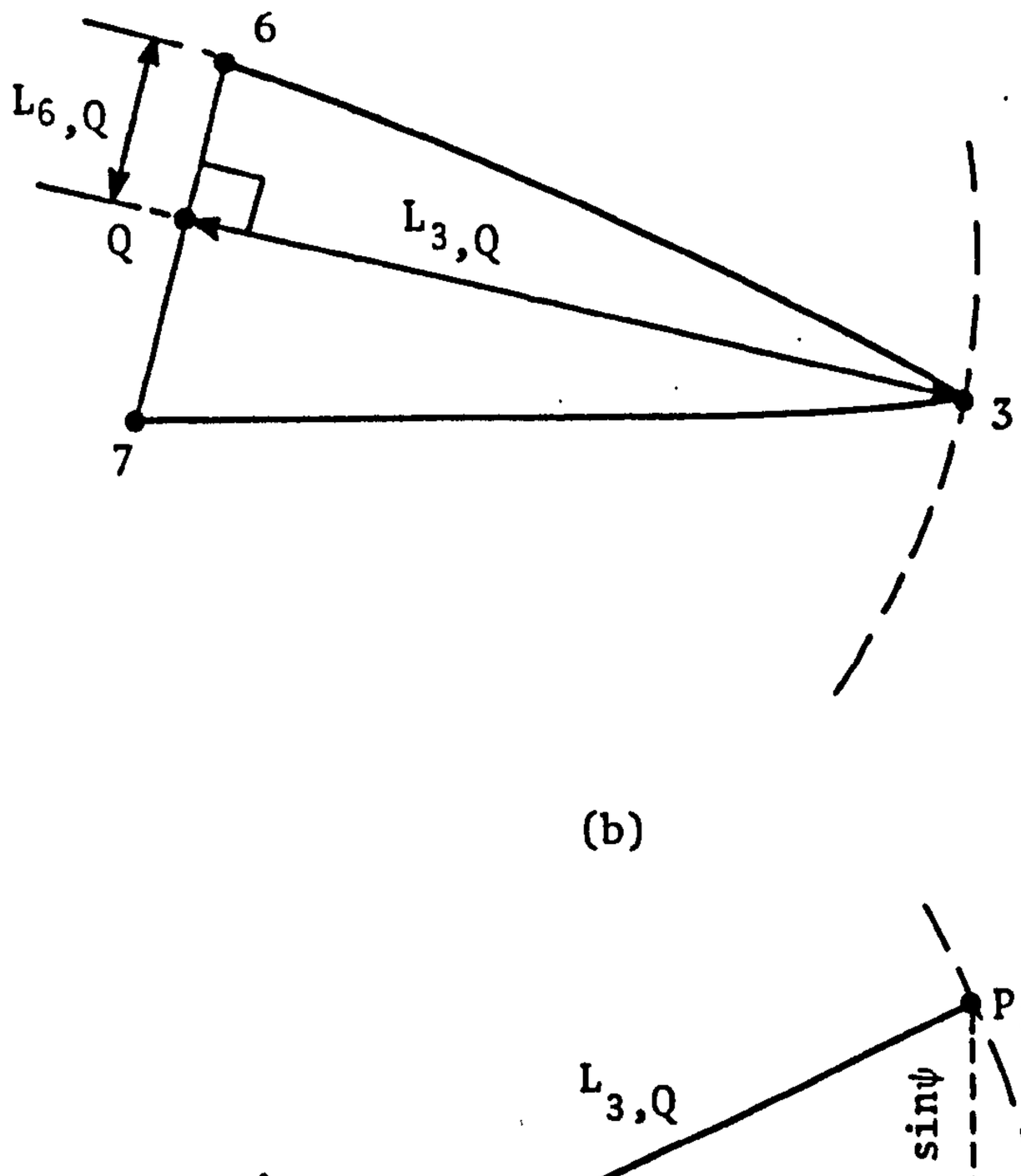
6
$L_{6,Q}$
Q
$L_{3,Q}$
3
7

(b)

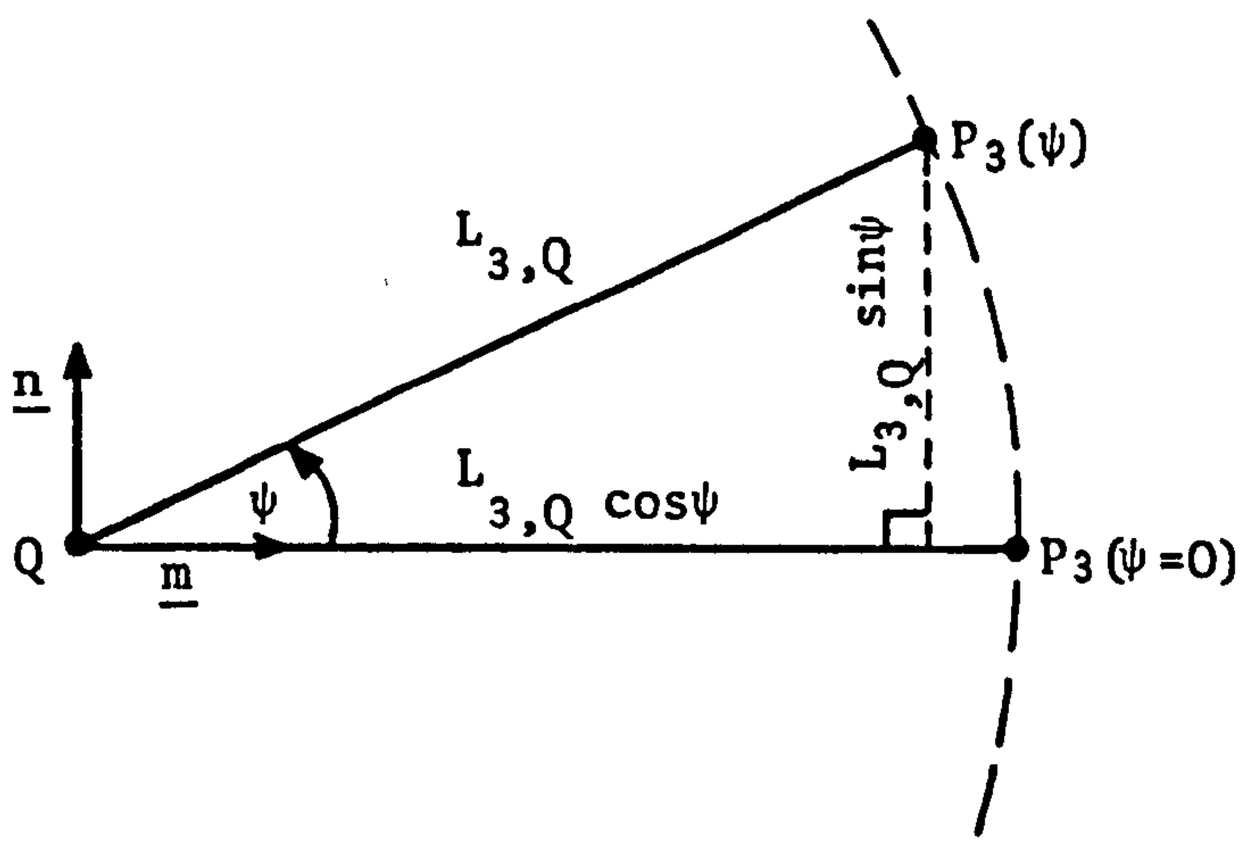
$P_3(\psi)$
$L_{3,Q}$
$L_{3,Q}\sin\psi$
n
ψ
$L_{3,Q}\cos\psi$
Q
m
$P_3(\psi=0)$

(c)

Fig. 6

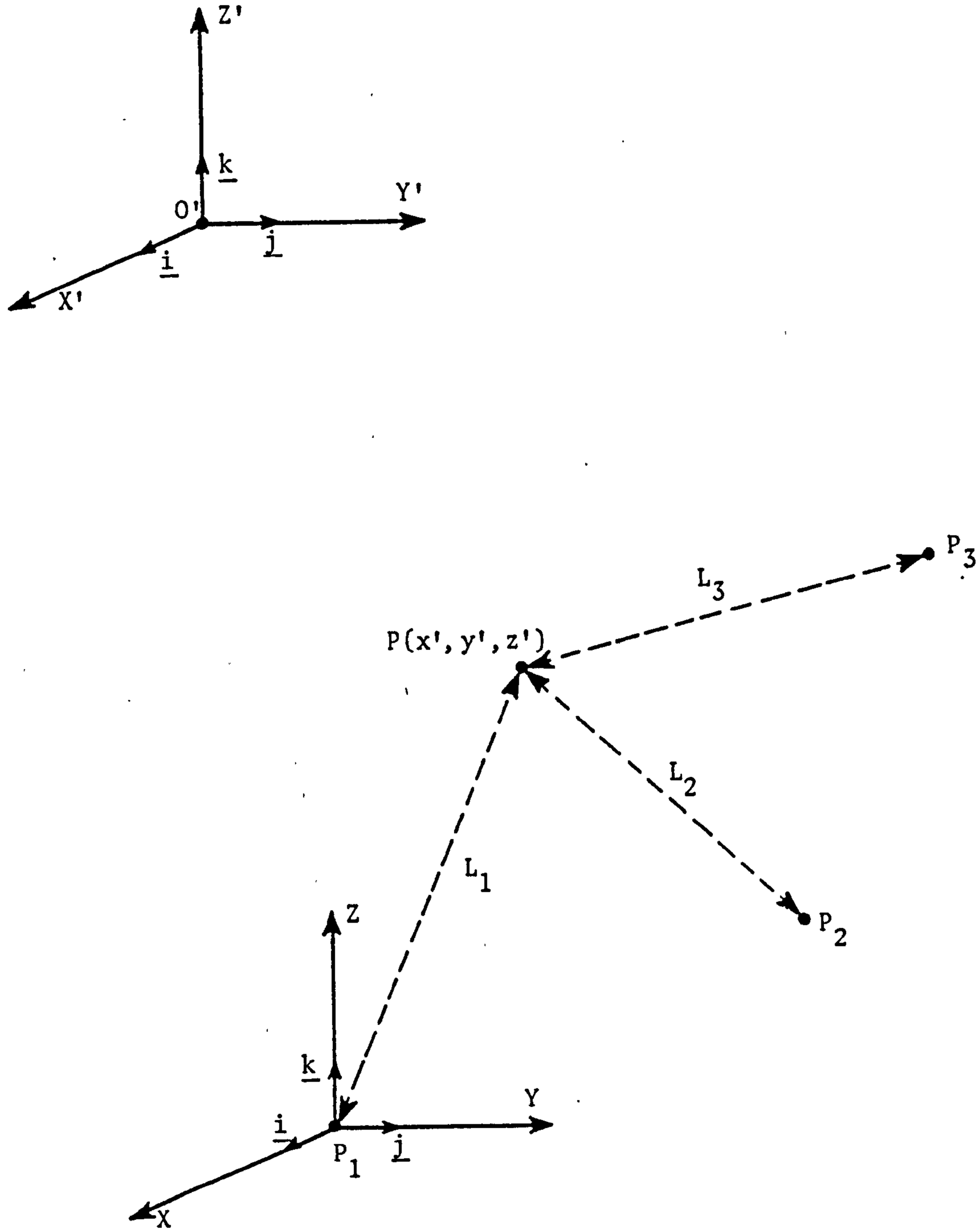

Fig. 7

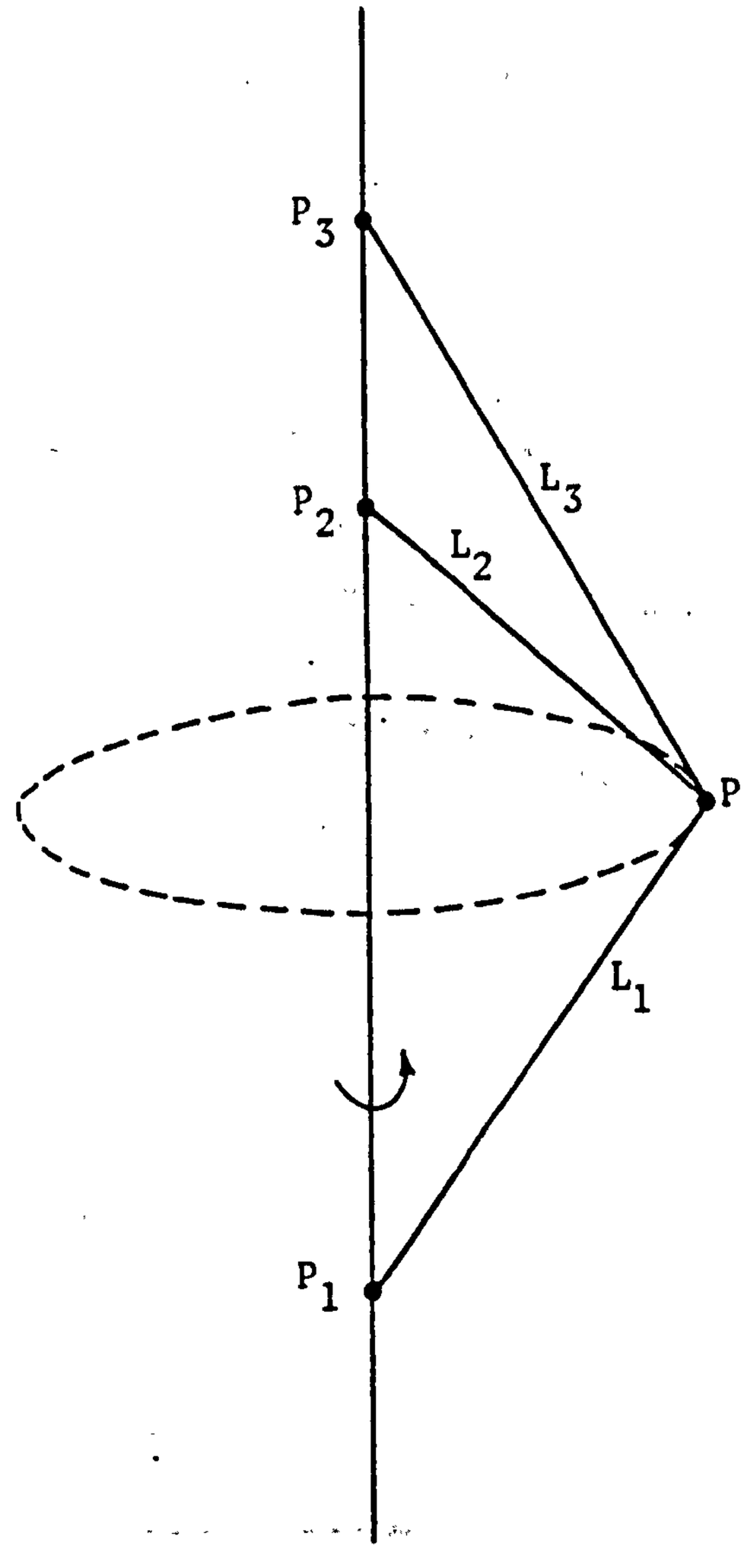

Fig. 8

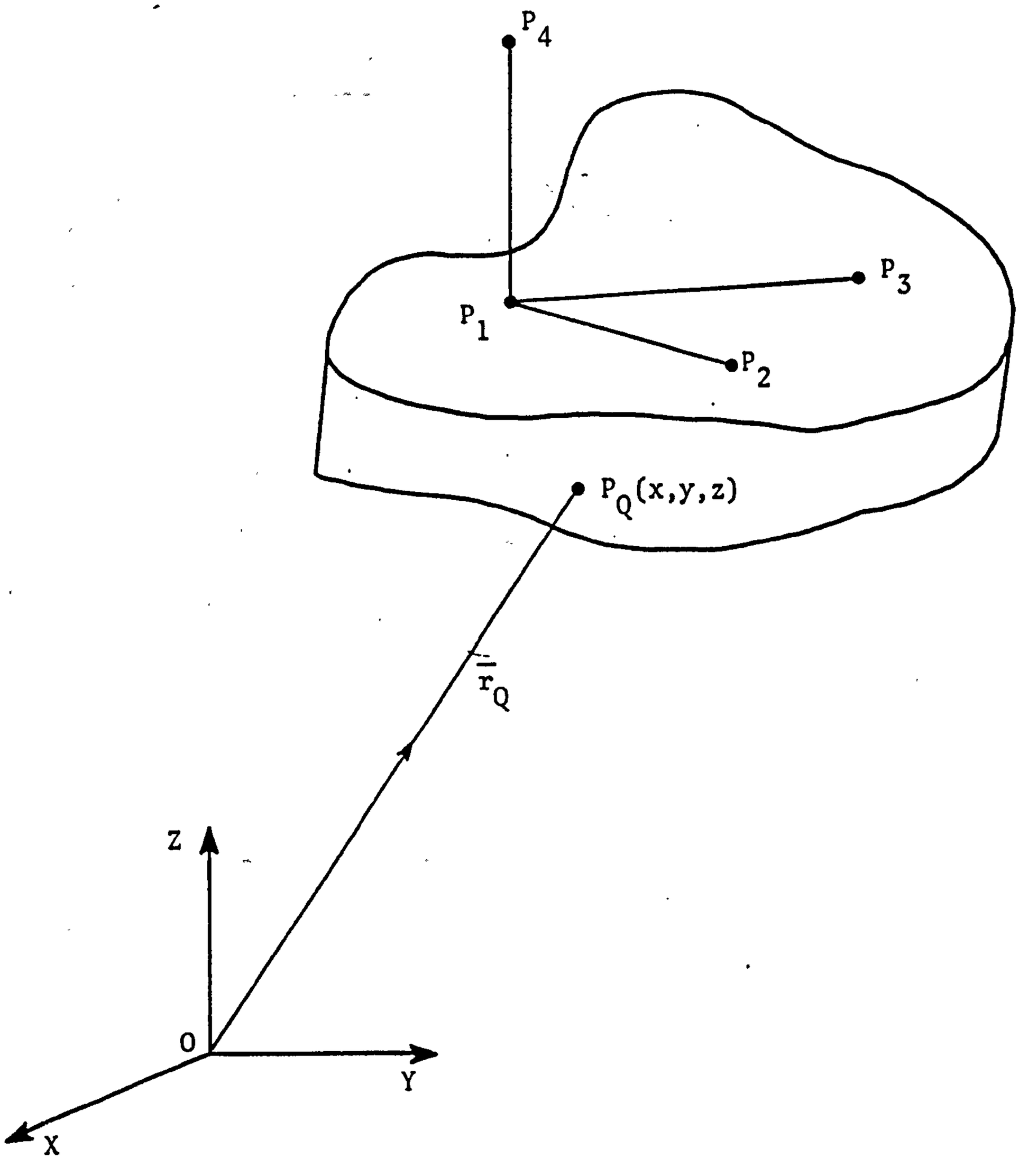

Fig. 9

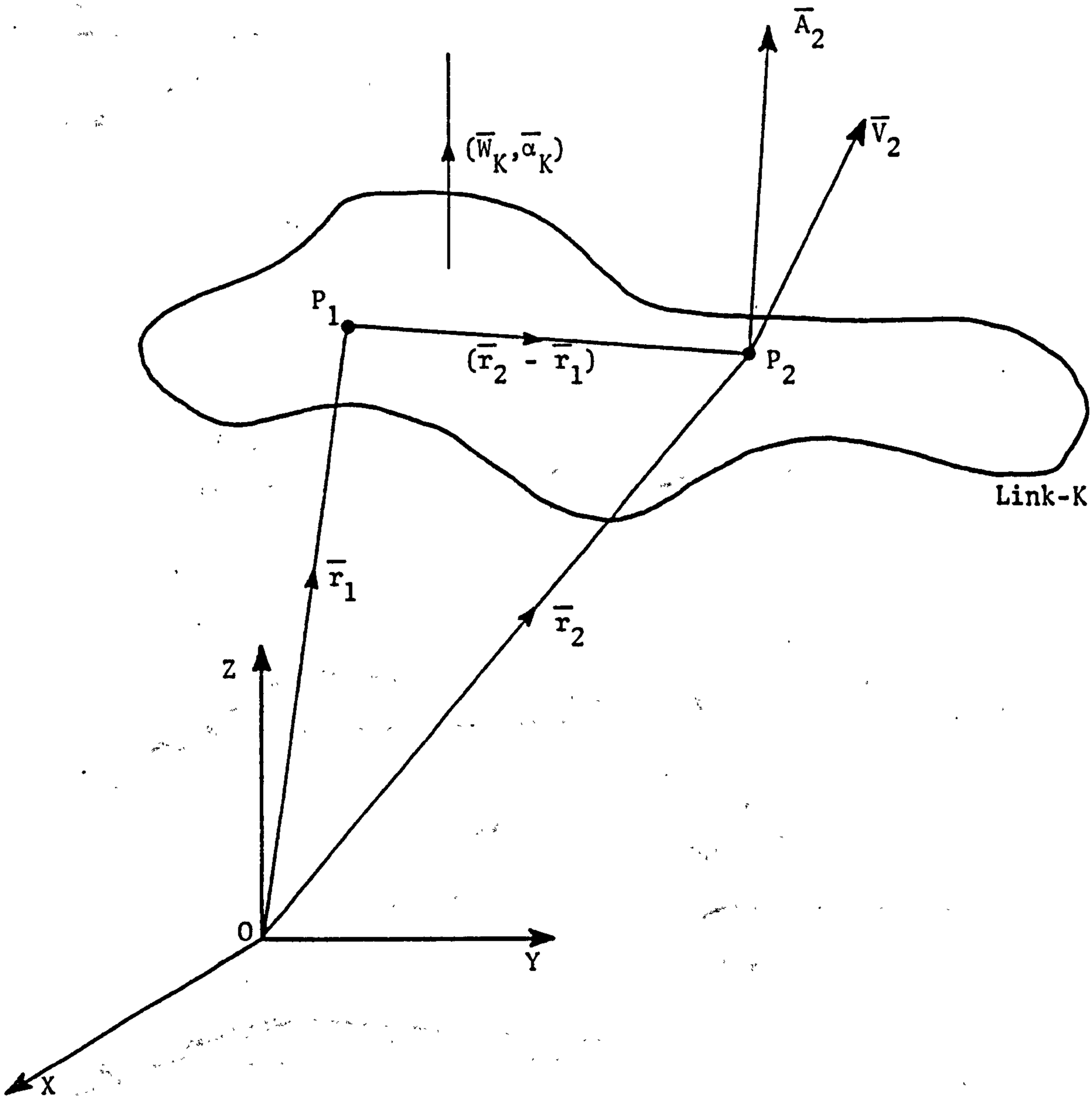
$\overline{A}_2$
$(\overline{W}_K, \overline{\alpha}_K)$
$\overline{V}_2$
P_1
$(\overline{r}_2 - \overline{r}_1)$
P_2
Link-K
$\overline{r}_1$
$\overline{r}_2$
Z
O
Y
X

Fig. 10

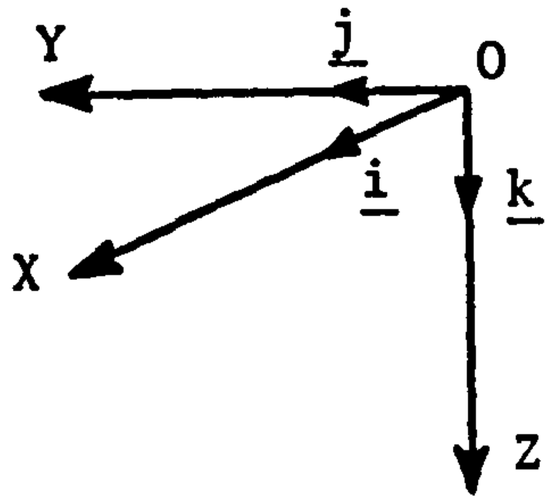
Y
j
O
i
k
X
Z

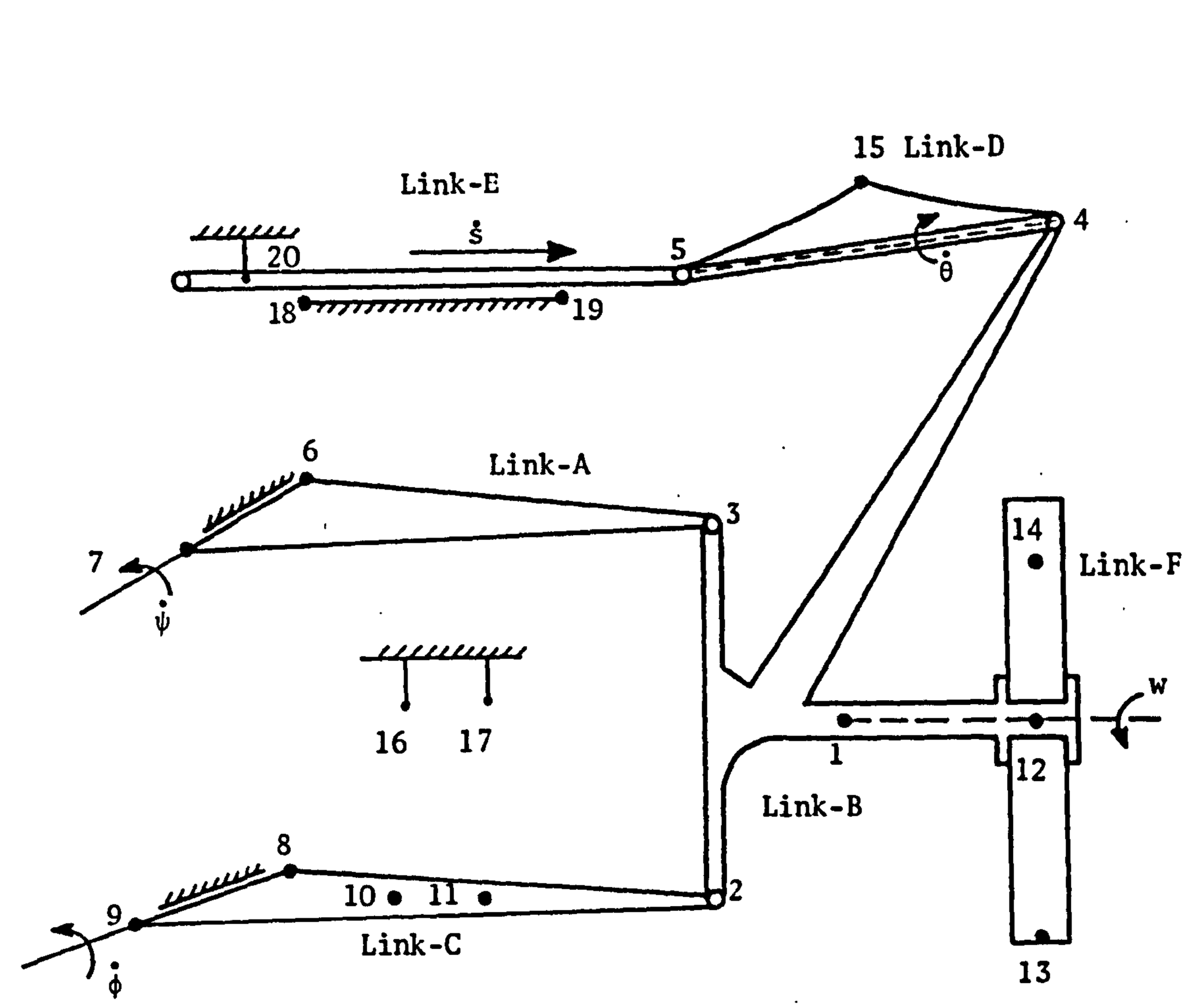
15 Link-D
Link-E
ṡ
20
5
4
θ̇
18
19
6
Link-A
3
7
ψ̇
14
Link-F
16
17
w
1
12
Link-B
8
10
11
2
9
Link-C
φ̇
13

Fig. 11

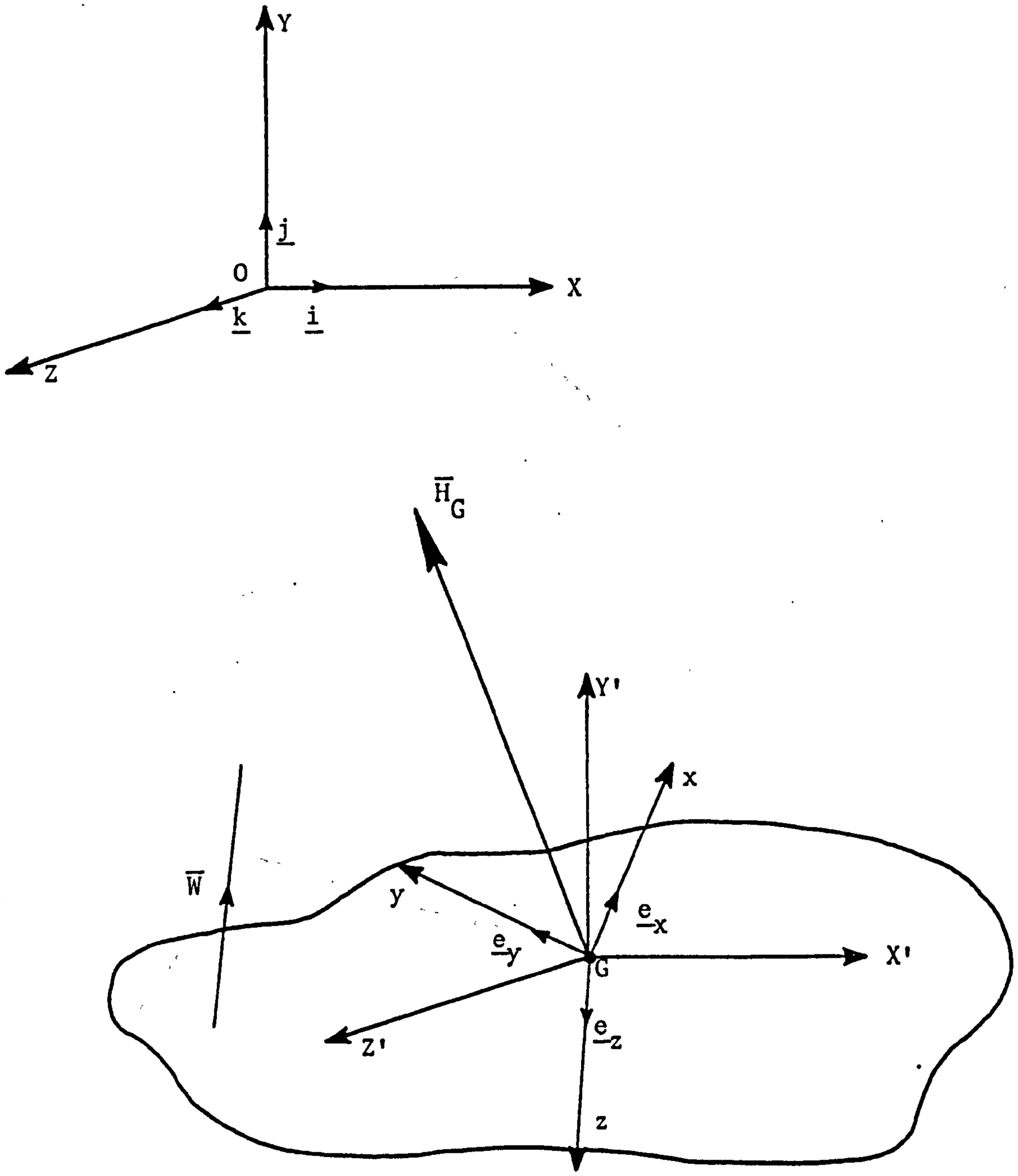
Y
j
O
X
k
i
Z
$\overline{H}_G$
Y'
x
$\overline{W}$
y
$\underline{e}_x$
$\underline{e}_y$
G
X'
Z'
$\underline{e}_z$
z

Fig.12

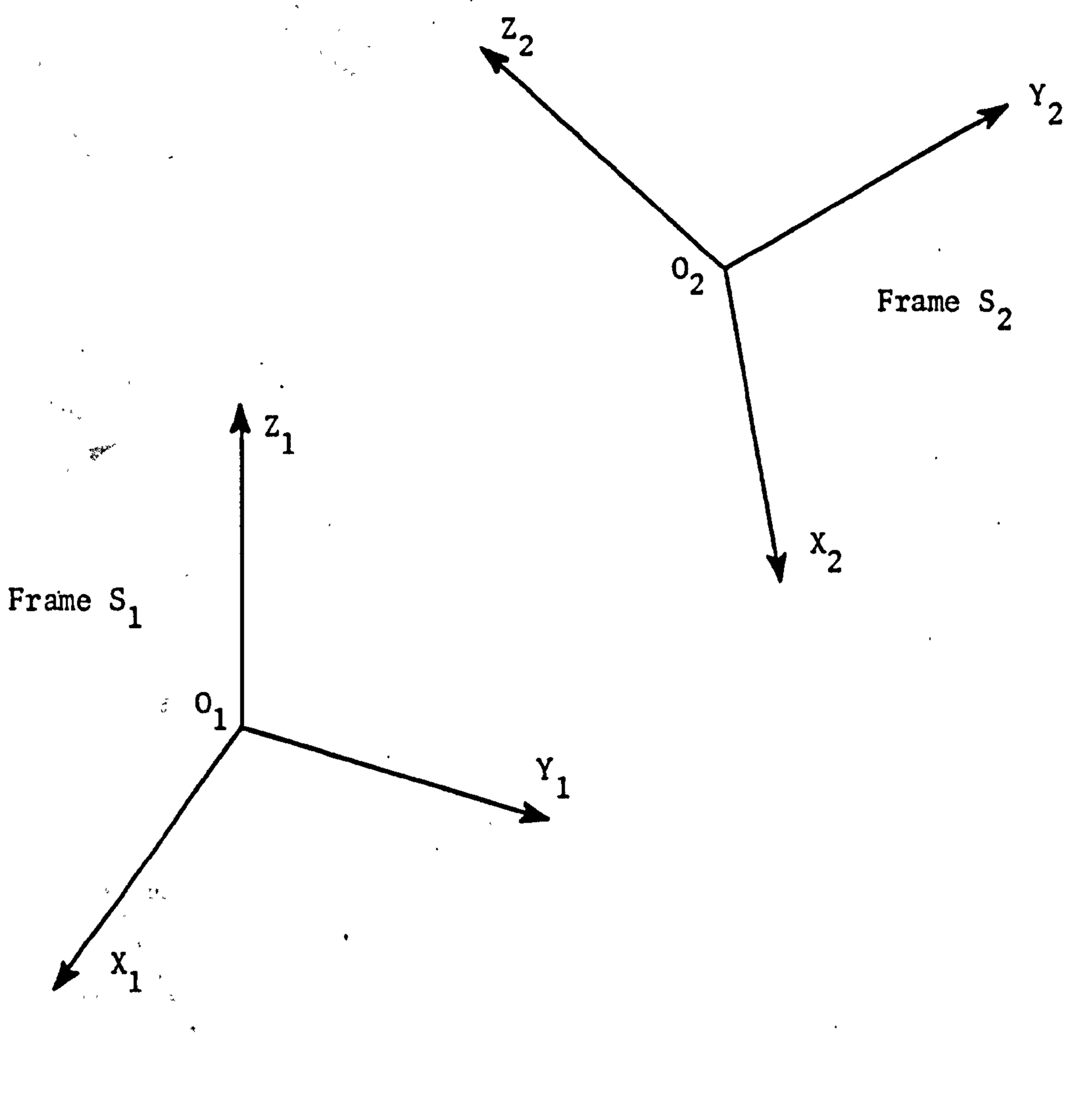

Fig. 13

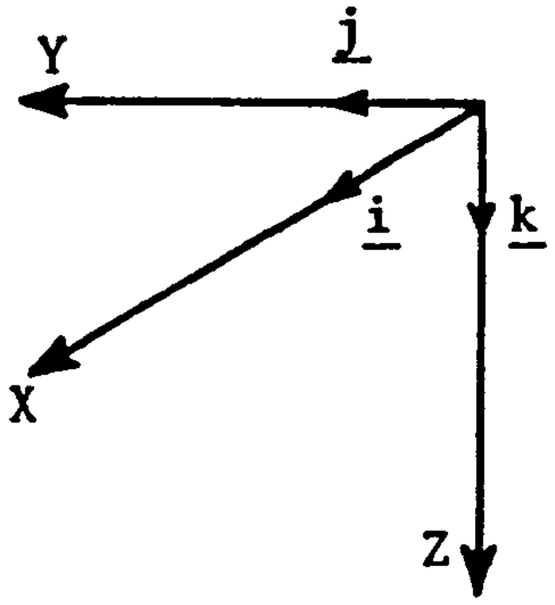
Y
j
i
k
X
Z

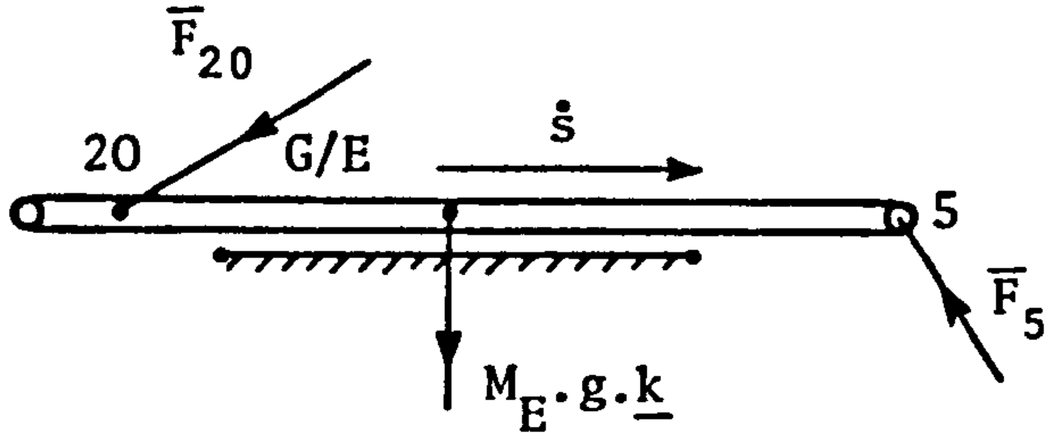
$\overline{F}_{20}$
20
G/E
ṡ
5
$\overline{F}_5$
$M_E \cdot g \cdot \underline{k}$

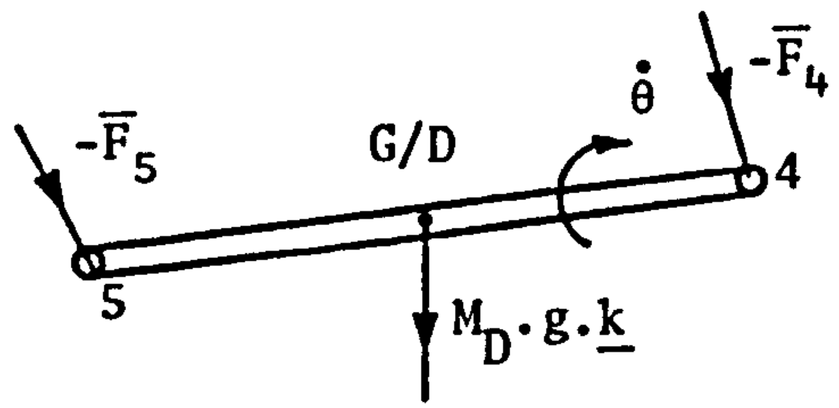
$-\overline{F}_5$
G/D
θ̇
$-\overline{F}_4$
4
5
$M_D \cdot g \cdot \underline{k}$

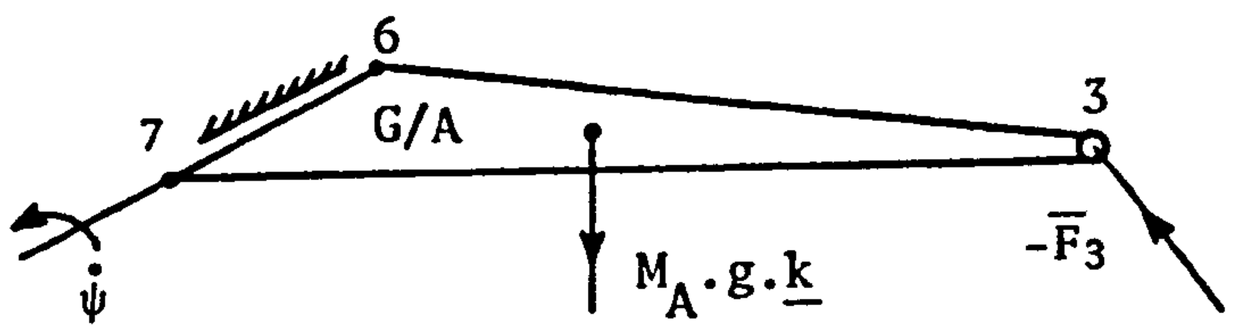
6
7
G/A
3
$\dot{\psi}$
$M_A \cdot g \cdot \underline{k}$
$-\overline{F}_3$

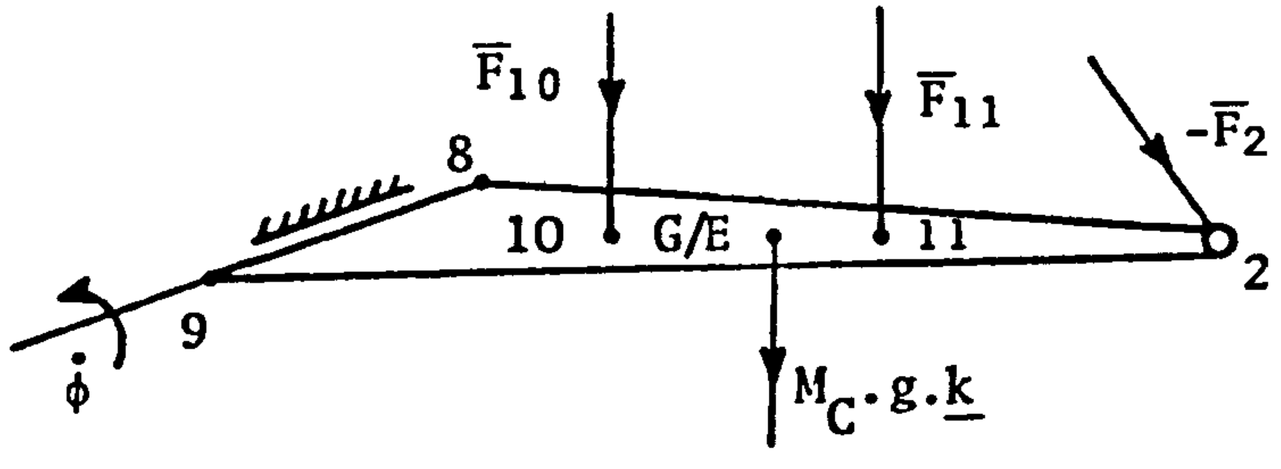
$\overline{F}_{10}$
$\overline{F}_{11}$
$-\overline{F}_2$
8
10
G/E
11
2
9
$\dot{\phi}$
$M_C \cdot g \cdot \underline{k}$

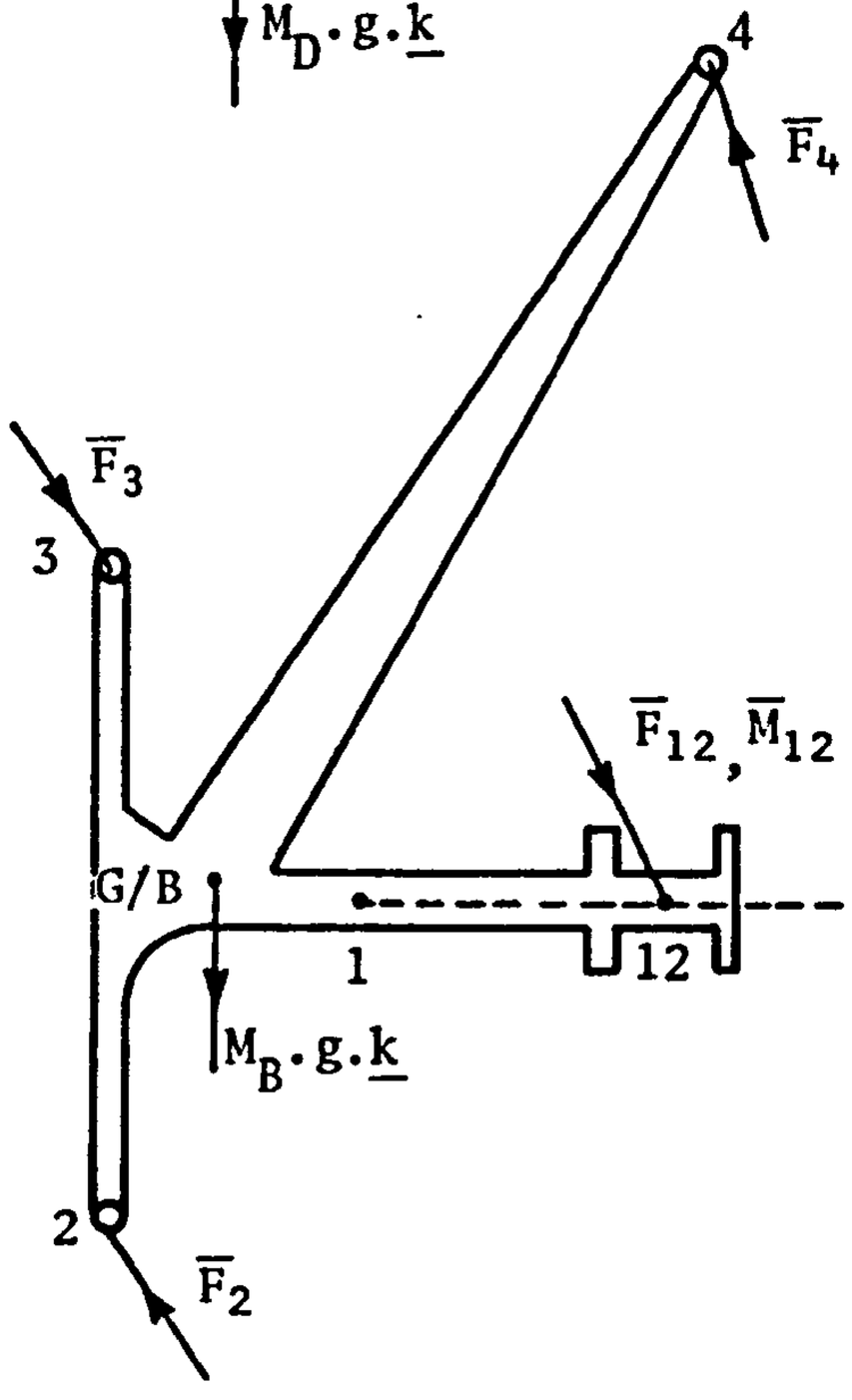
4
$\overline{F}_4$
$\overline{F}_3$
3
$\overline{F}_{12}, \overline{M}_{12}$
G/B
1
12
$M_B \cdot g \cdot \underline{k}$
2
$\overline{F}_2$

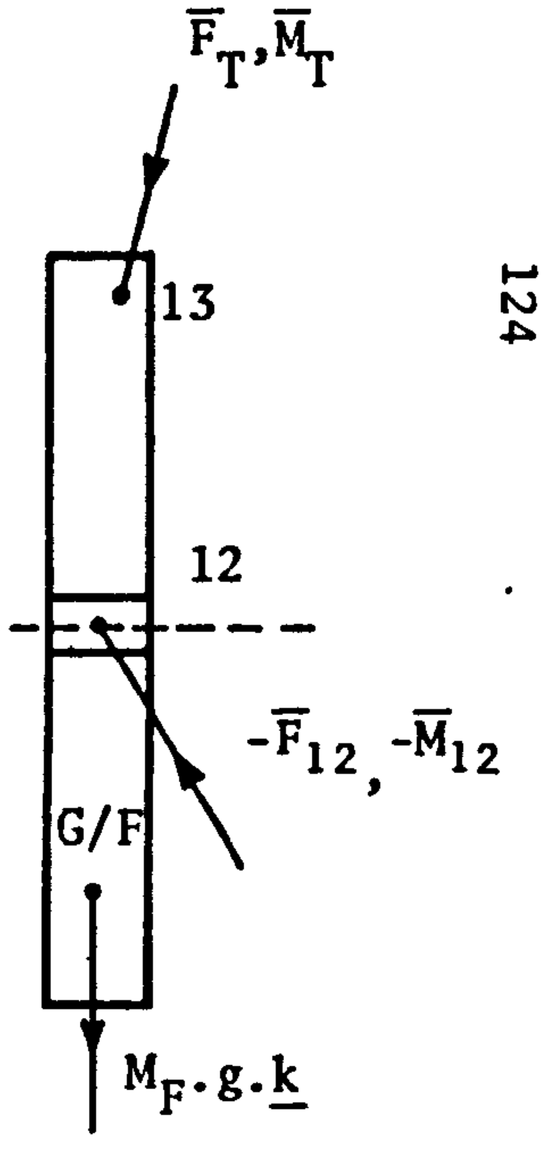
$\overline{F}_T, \overline{M}_T$
13
12
$-\overline{F}_{12}, -\overline{M}_{12}$
G/F
$M_F \cdot g \cdot \underline{k}$

Fig. 14

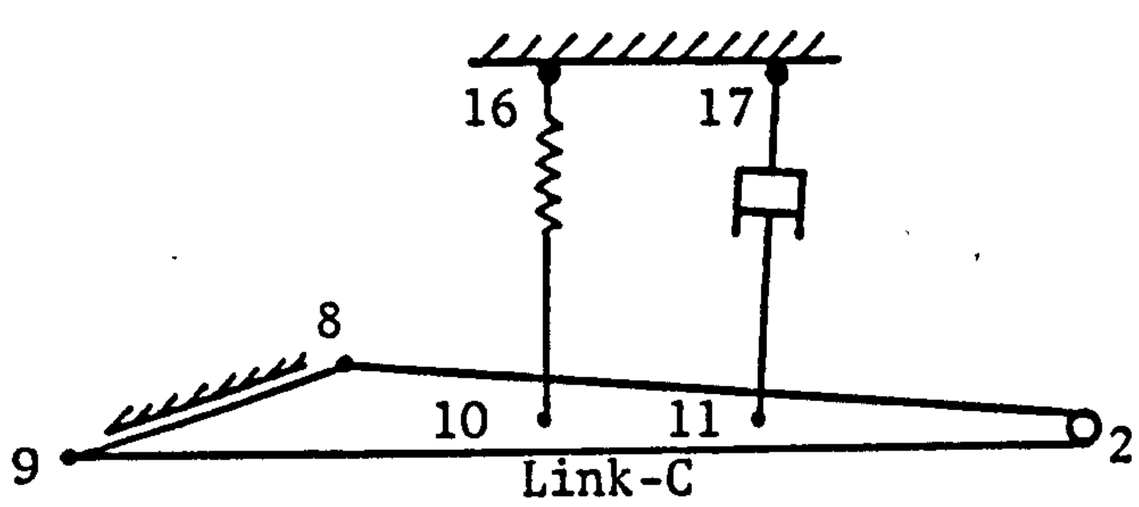

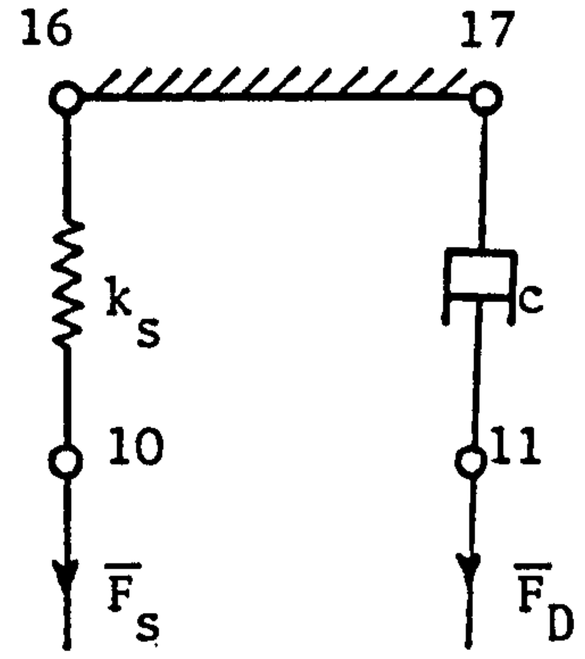

(a)

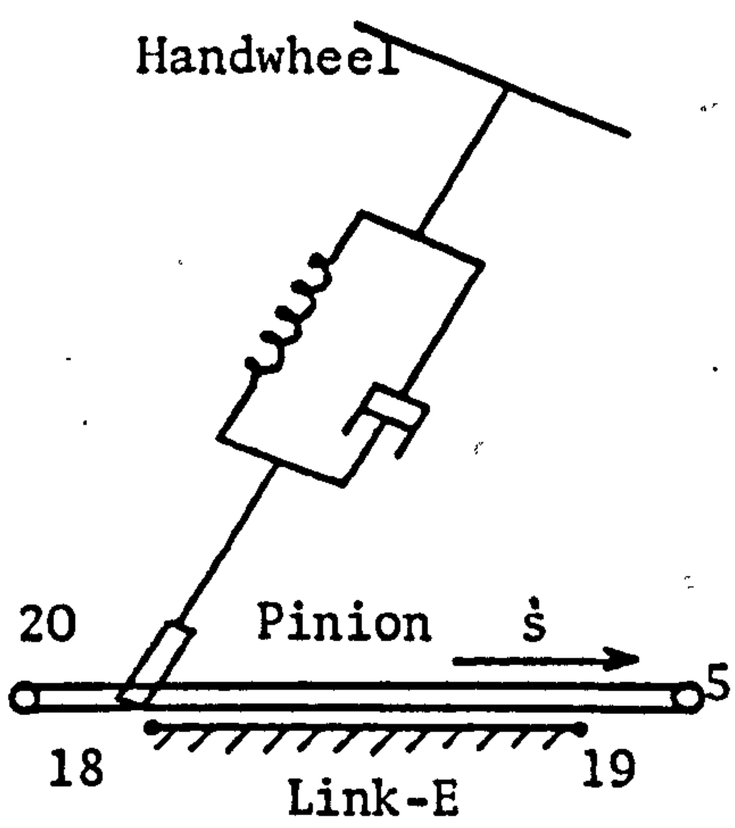

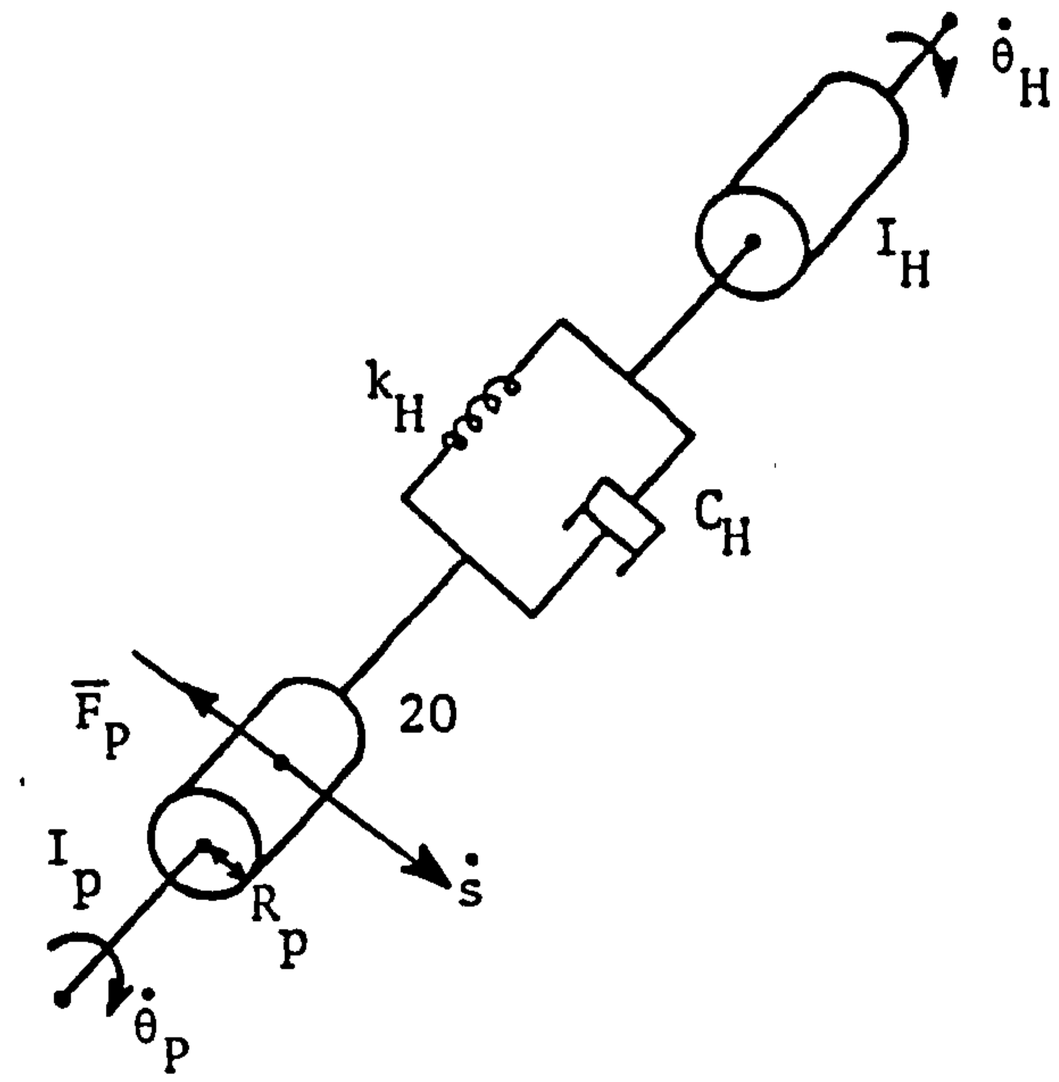

(b)

Fig.15 Models of (a) the main spring and shock absorber and (b) steering gear

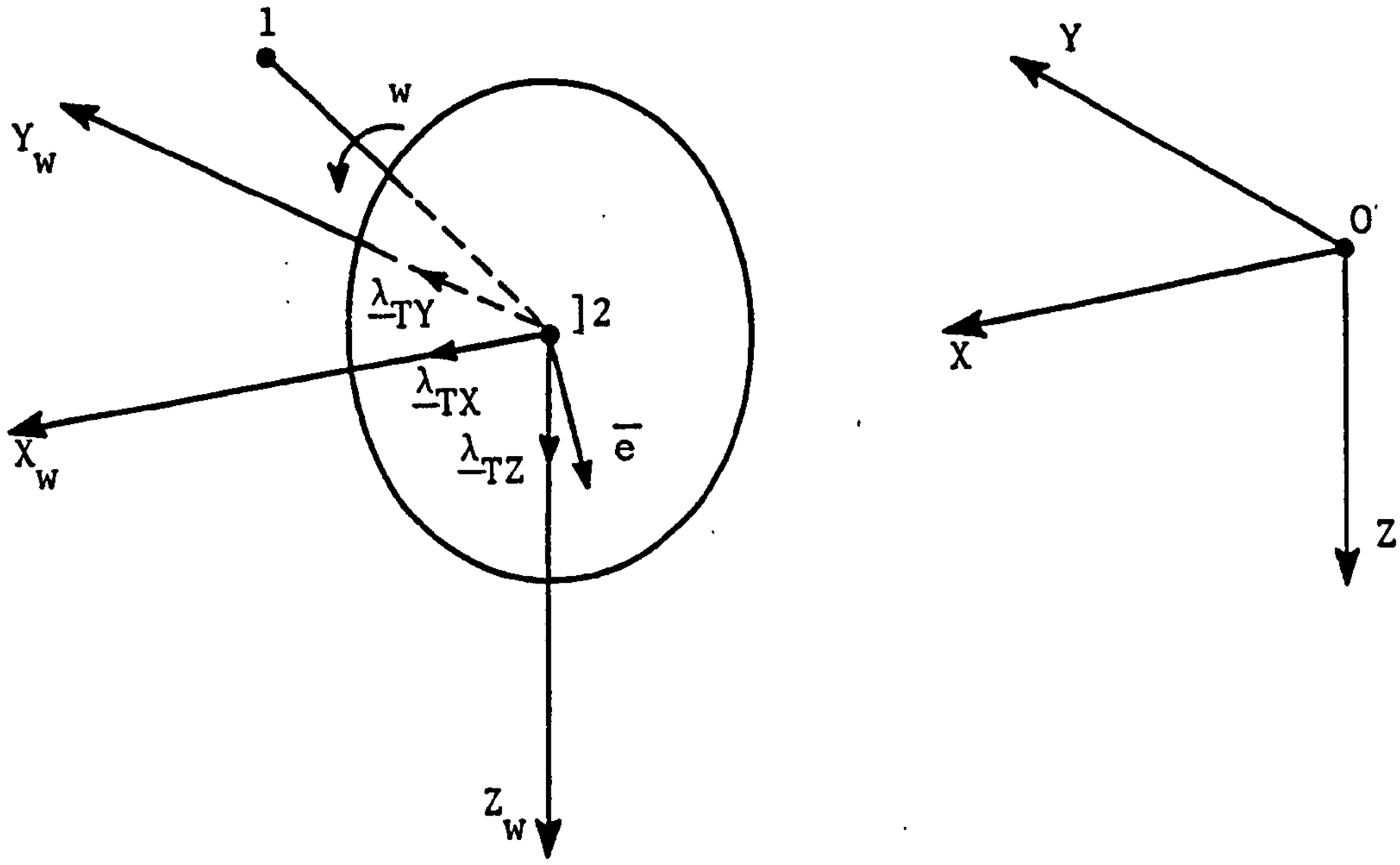

(a)

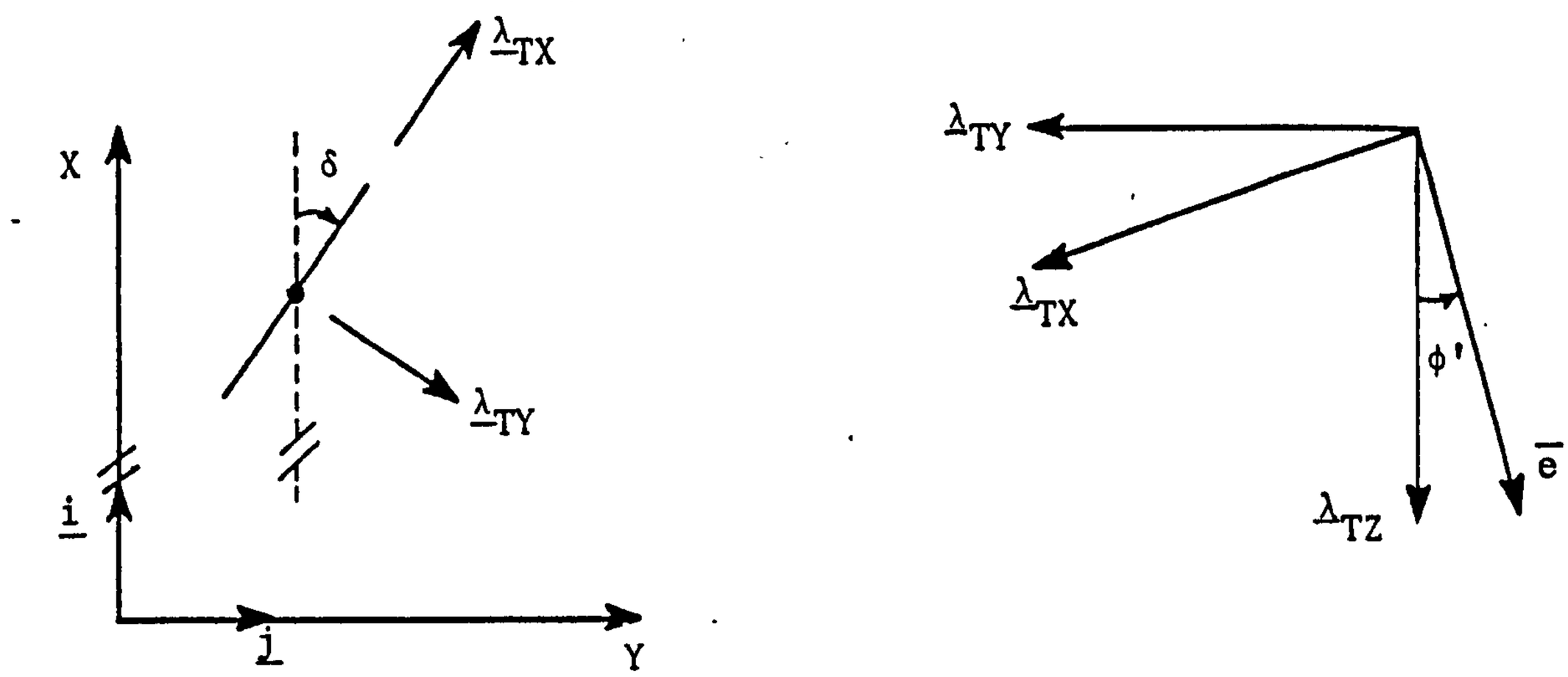

(b)

Fig.16 Schematic diagram of a) wheel model, and
b) wheel geometry

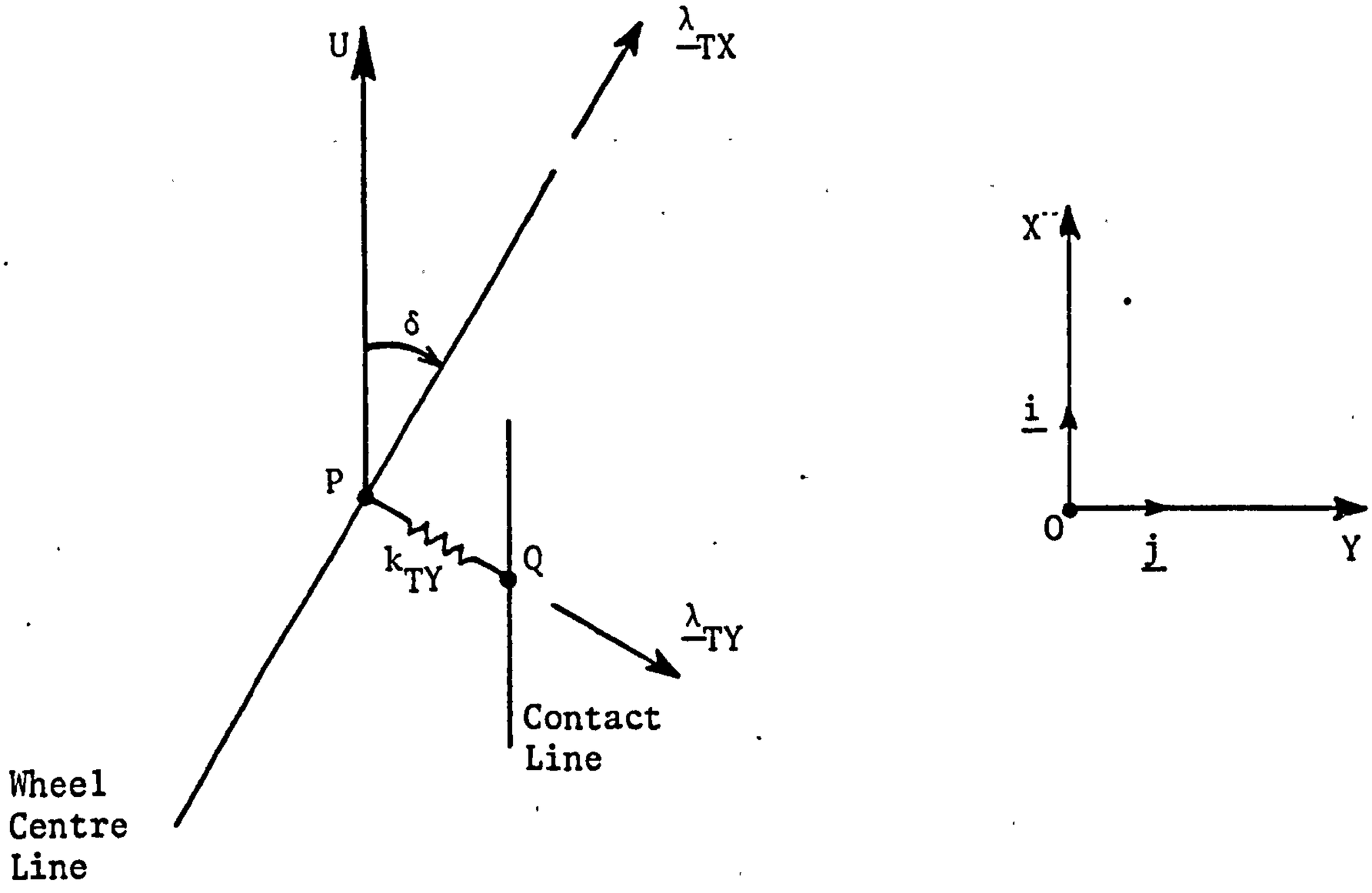

(a)

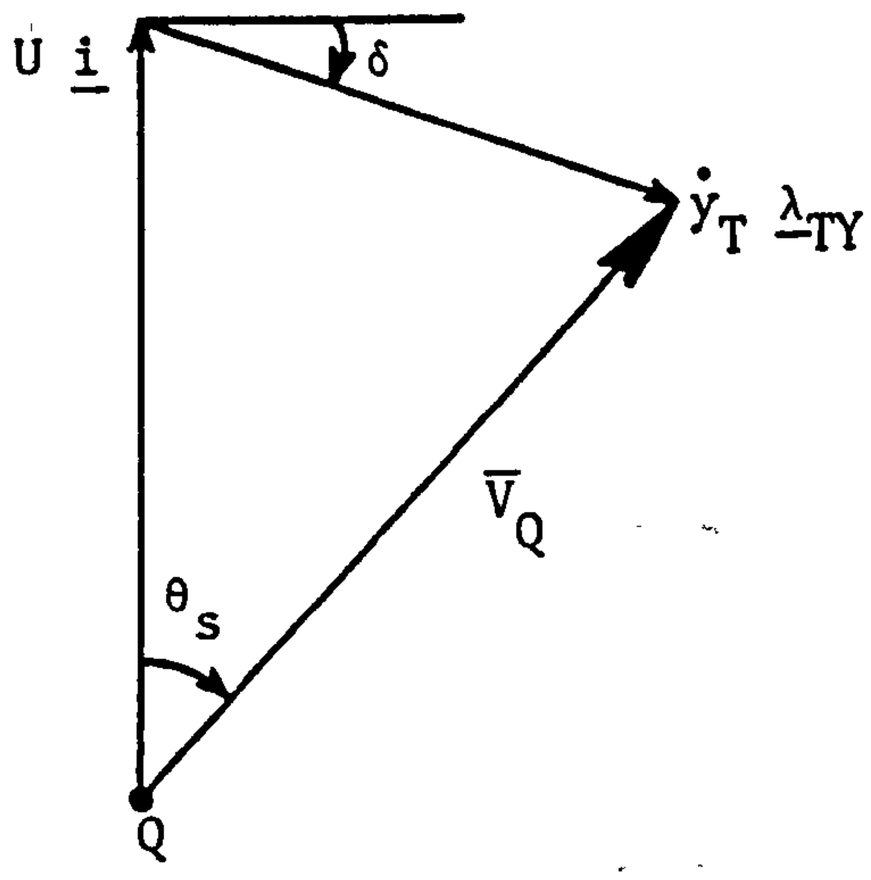

(b)

Fig.17 a) model diagram of tyre model 2 and
b) velocity diagram for point Q

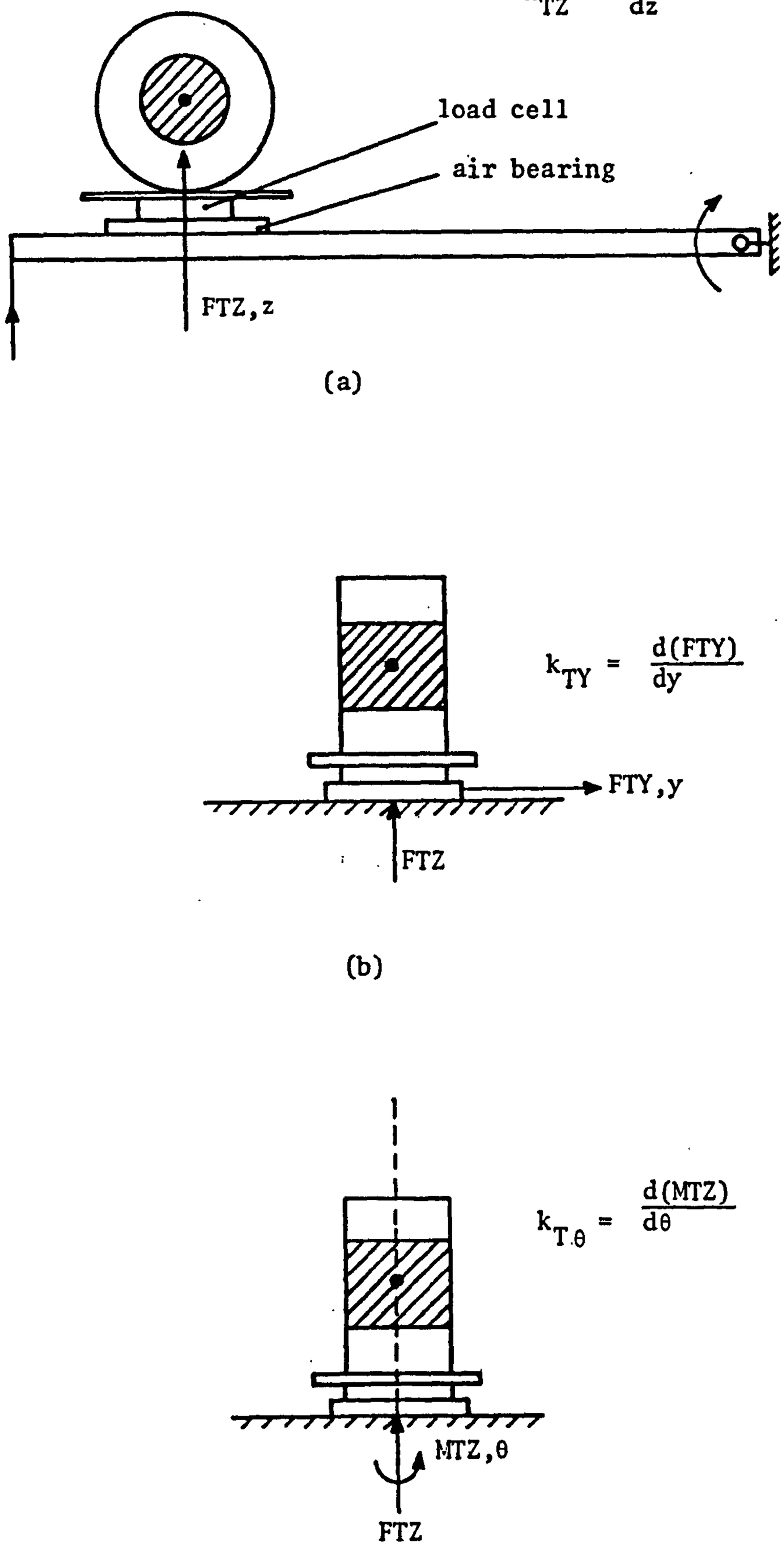

Fig.18 Schematic illustration of tests to evaluate a) vertical, b) lateral, and c) torsional static stiffnesses of tyre.

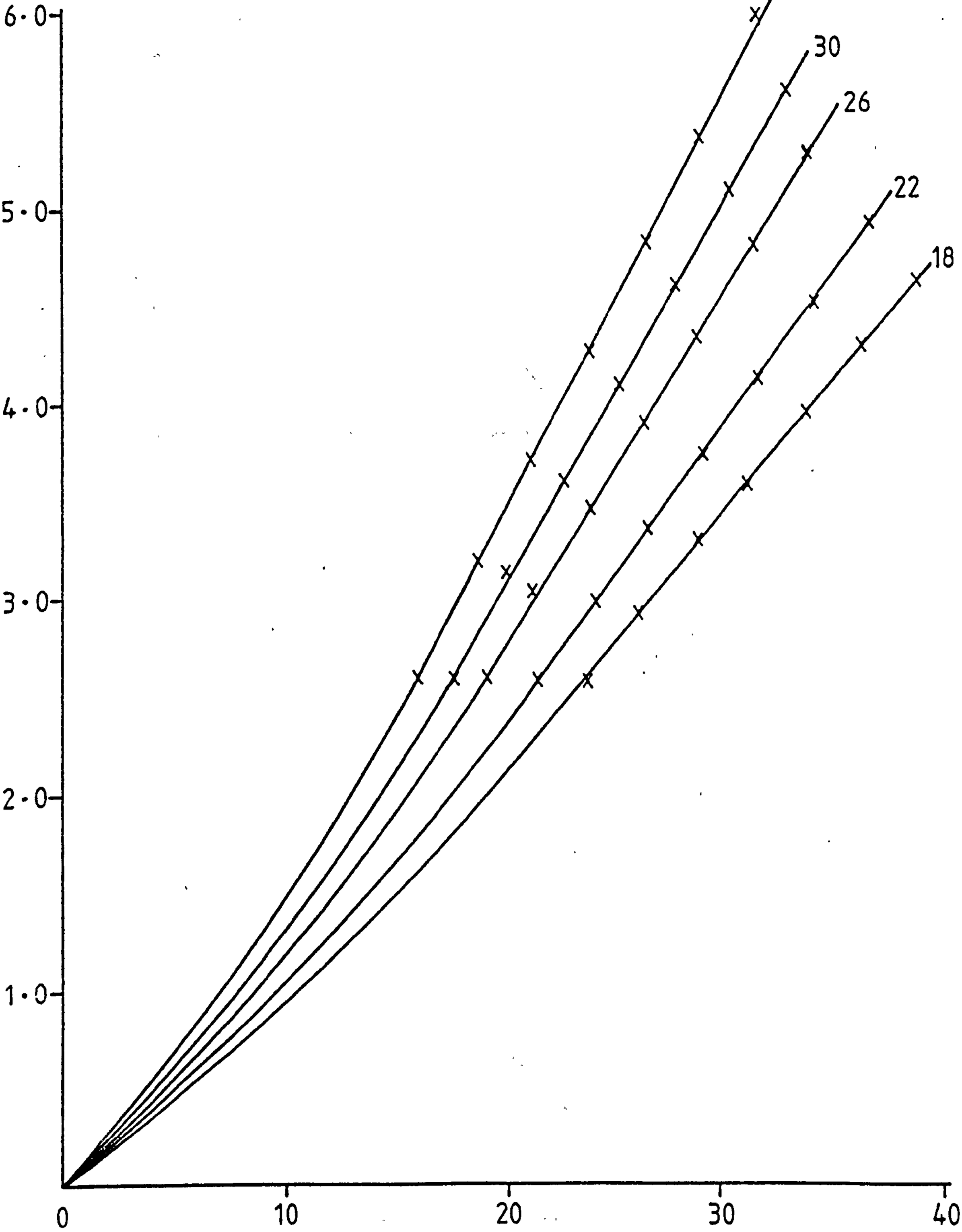

VERTICAL FORCE VERSUS DEFLECTION CHARACTERISTIC OF NON-ROLLING TYRE

Fig. 19

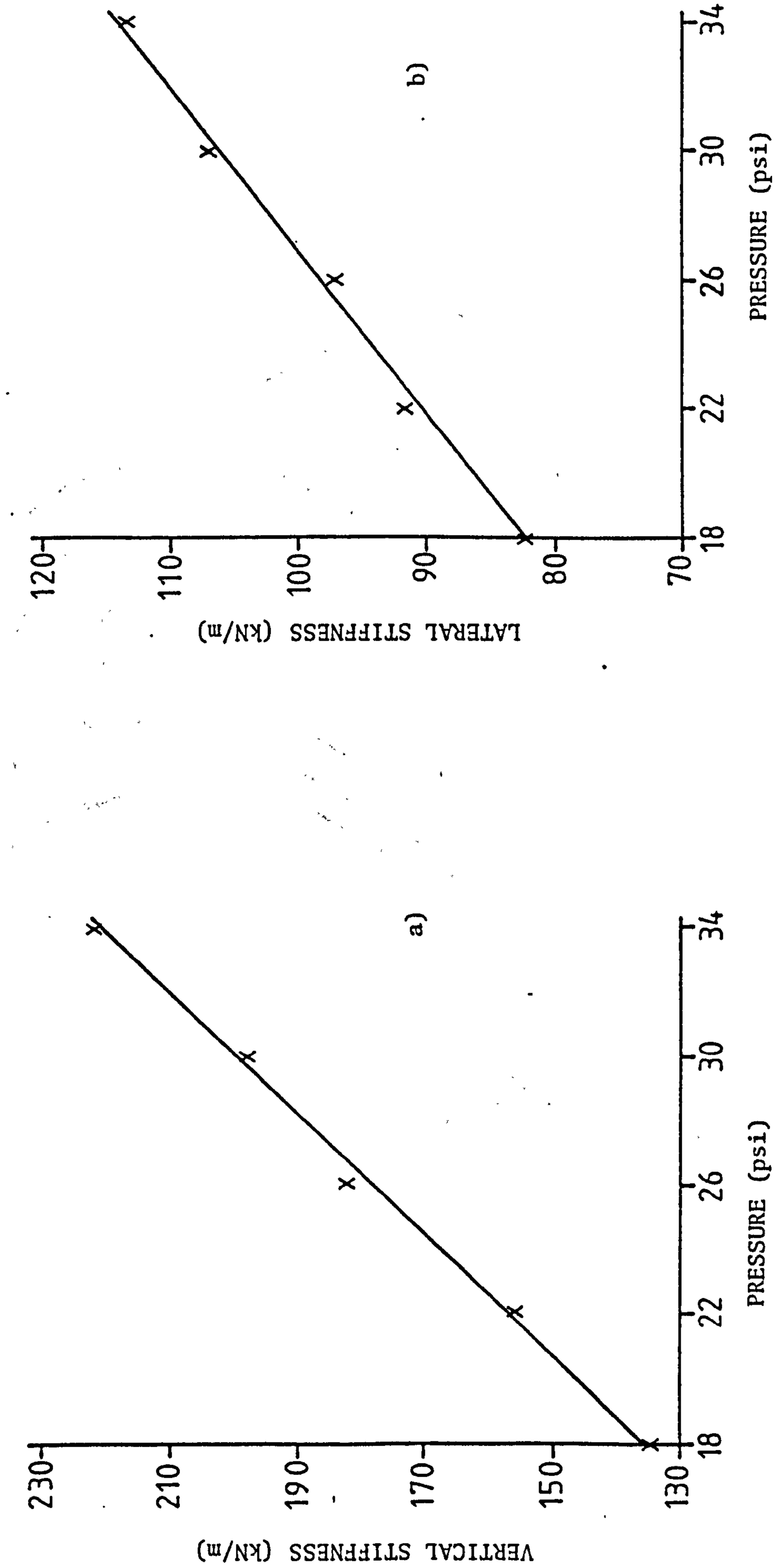

NON-ROLLING TYRE STIFFNESS AS A FUNCTION OF PRESSURE; F_z > 2.5 kN

Fig.20

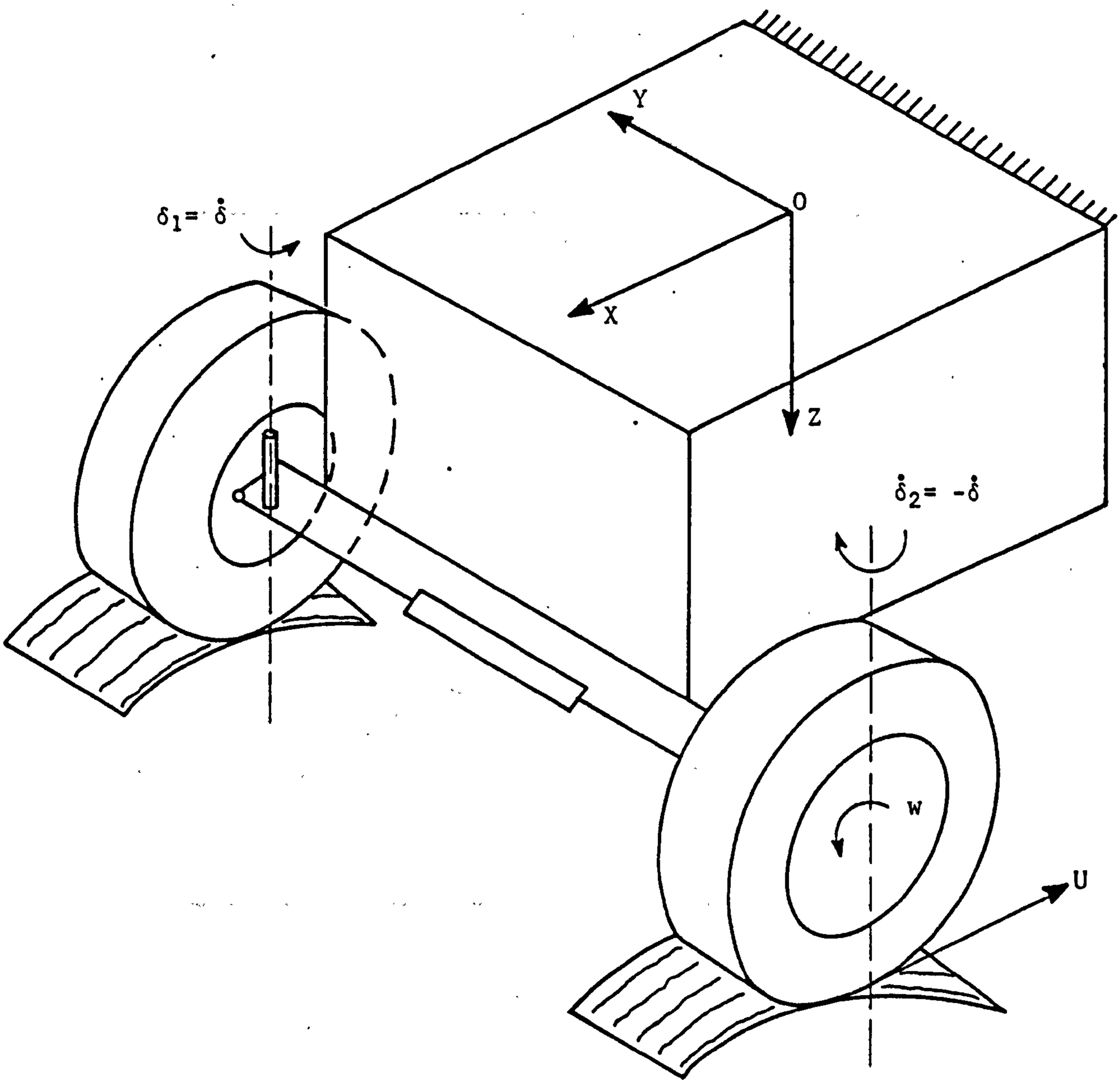

Fig.21

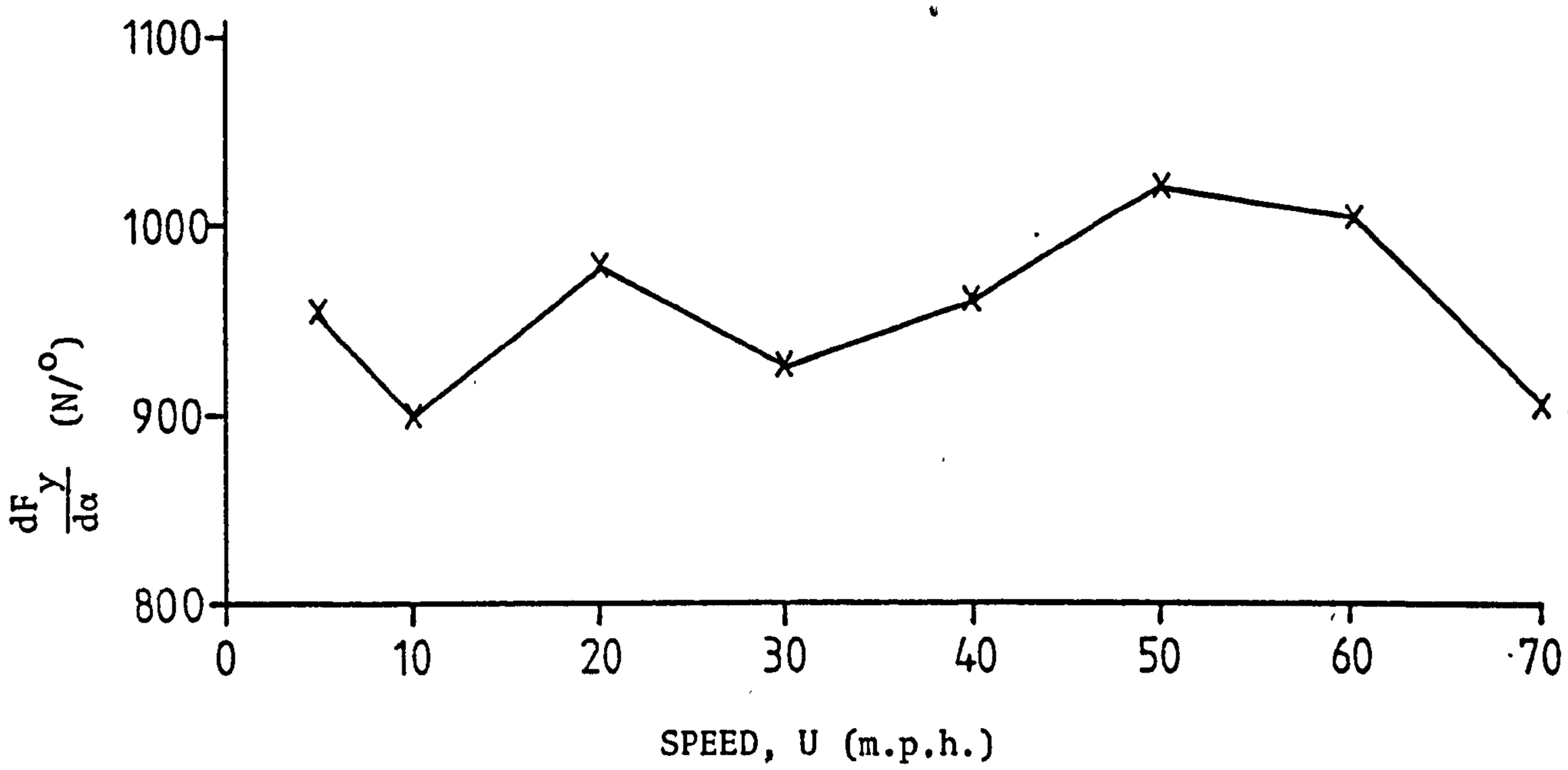

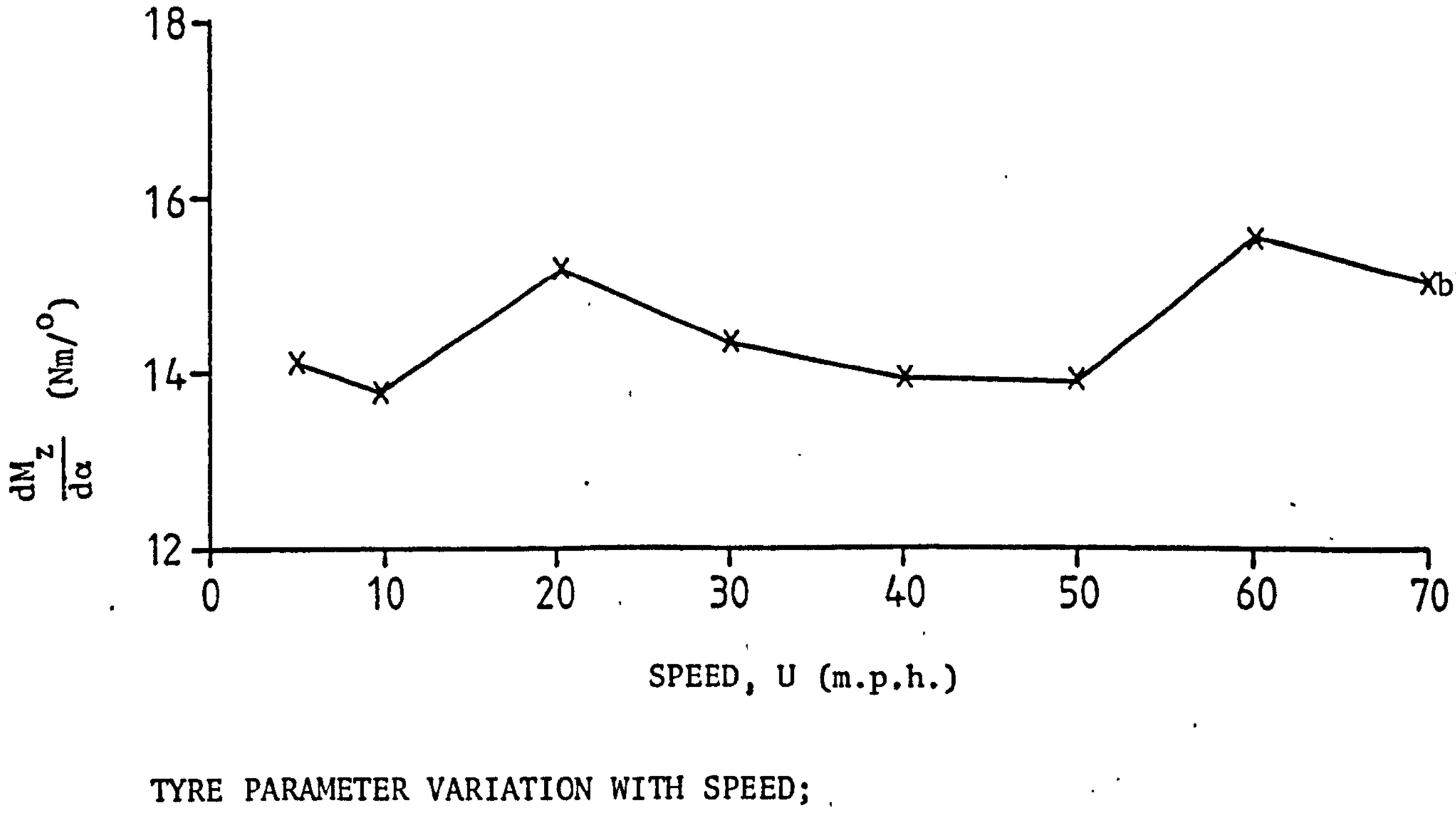

TYRE PARAMETER VARIATION WITH SPEED;

a) Cornering stiffness $\left(\frac{dF_y}{d\alpha}\right)$,

b) Self aligning torque coefficient $\left(\frac{dM_z}{d\alpha}\right)$,

$\left[p = 34 \text{ psi}, \quad F_z = 3.77 \text{ kN}\right]$

Fig.22

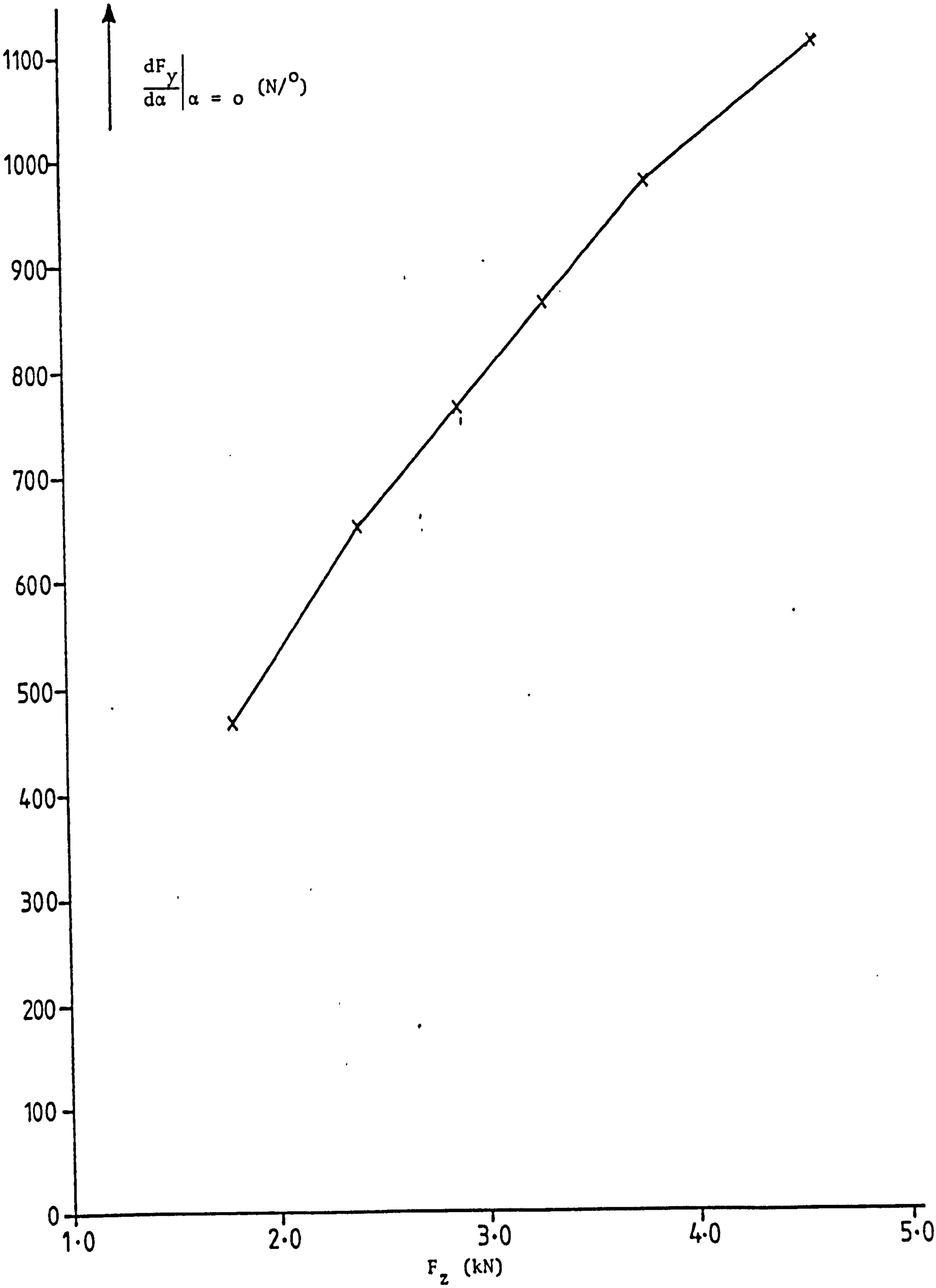

CORNERING STIFFNESS $\left(\frac{dF_y}{d\alpha}\right)$ OF TYRE AS A FUNCTION OF THE VERTICAL FORCE (F_z), U = 5 m.p.h., p = 34 p.s.i.

Fig. 23

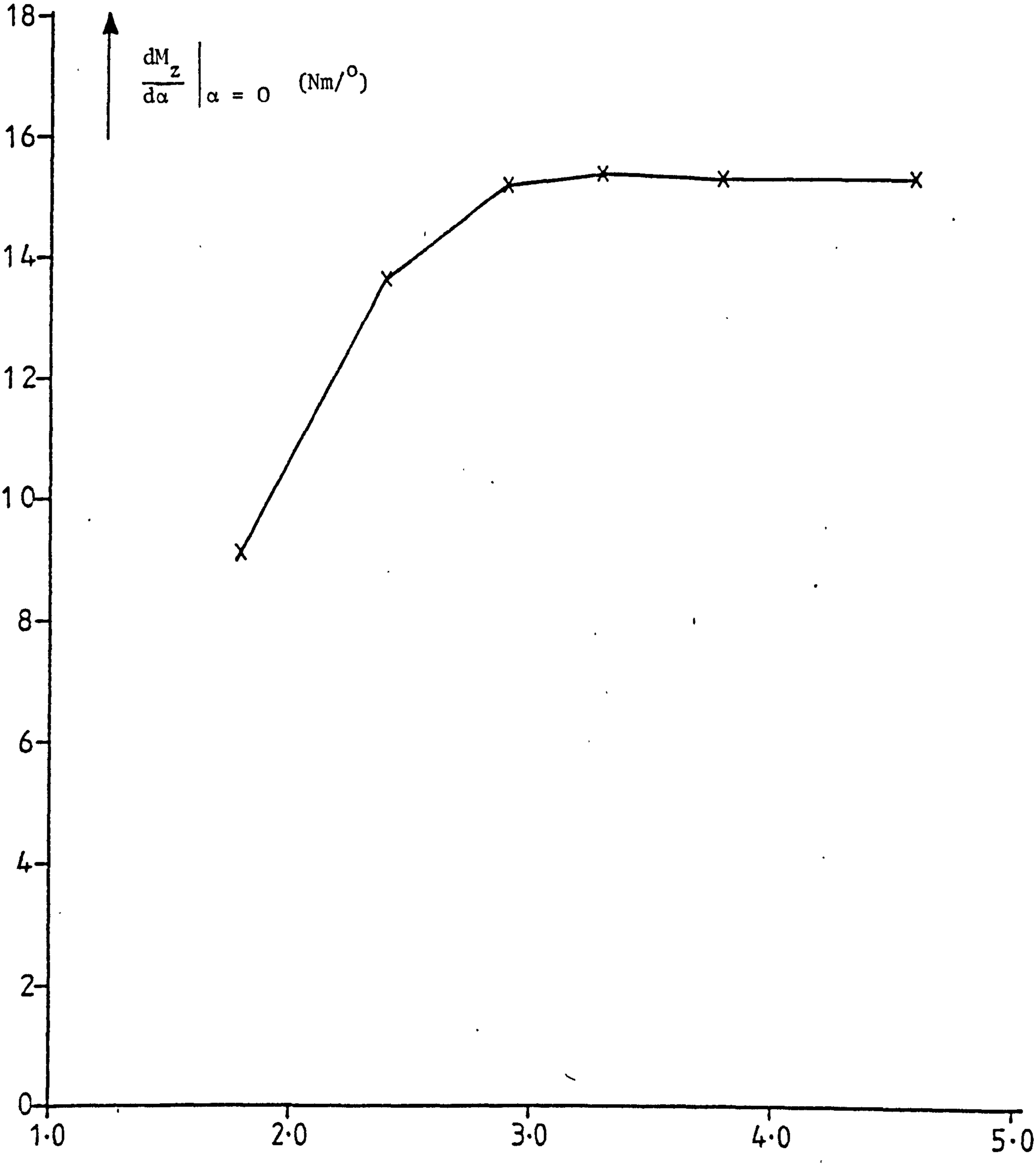

SELF ALIGNING TORQUE COEFFICIENT $\left(\frac{dM_z}{d\alpha}\right)$ OF TYRE AS A FUNCTION OF THE VERTICAL FORCE (F_z); U = 5 m.p.h., p = 34 psi.

Fig.24

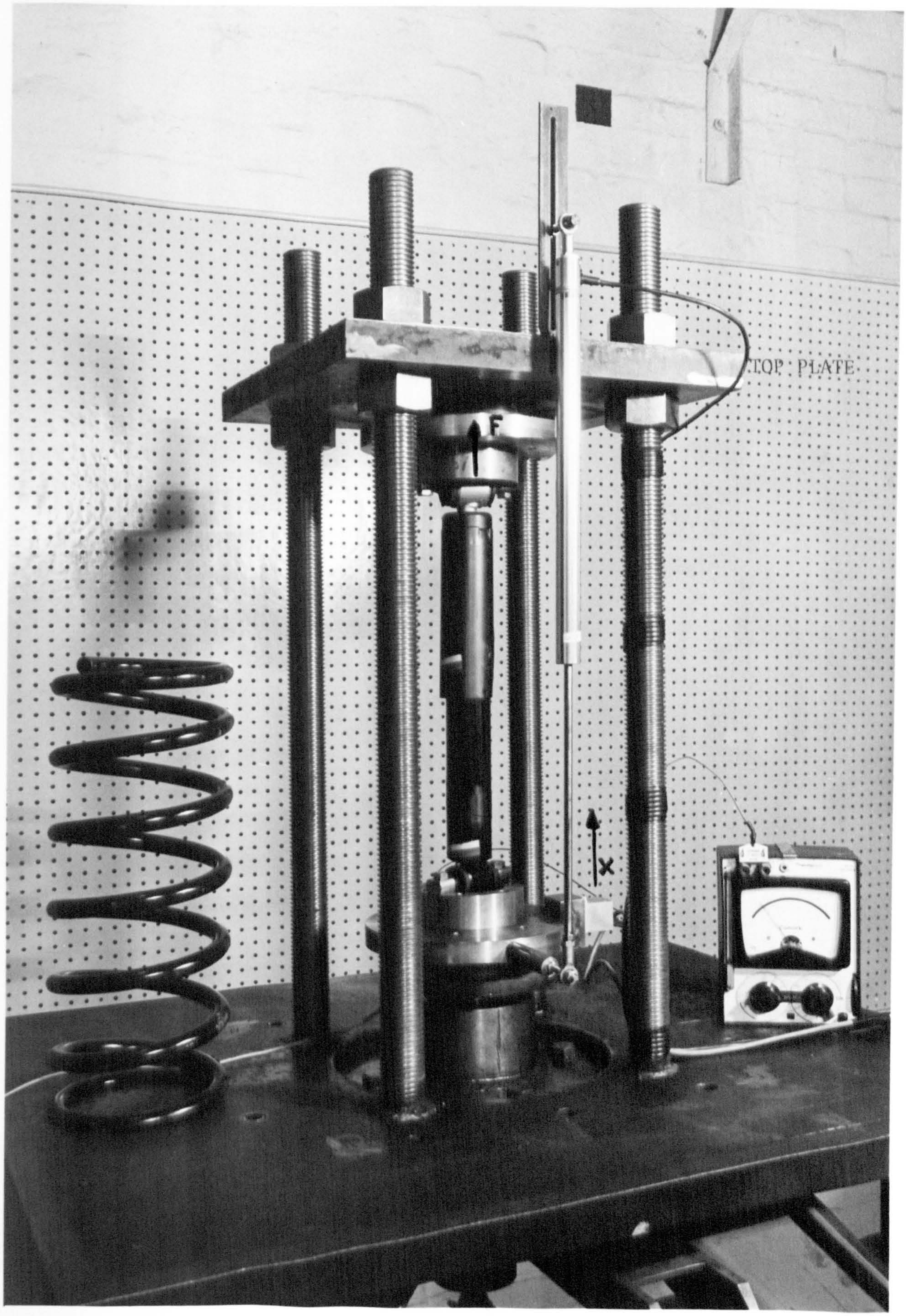

Fig. 25

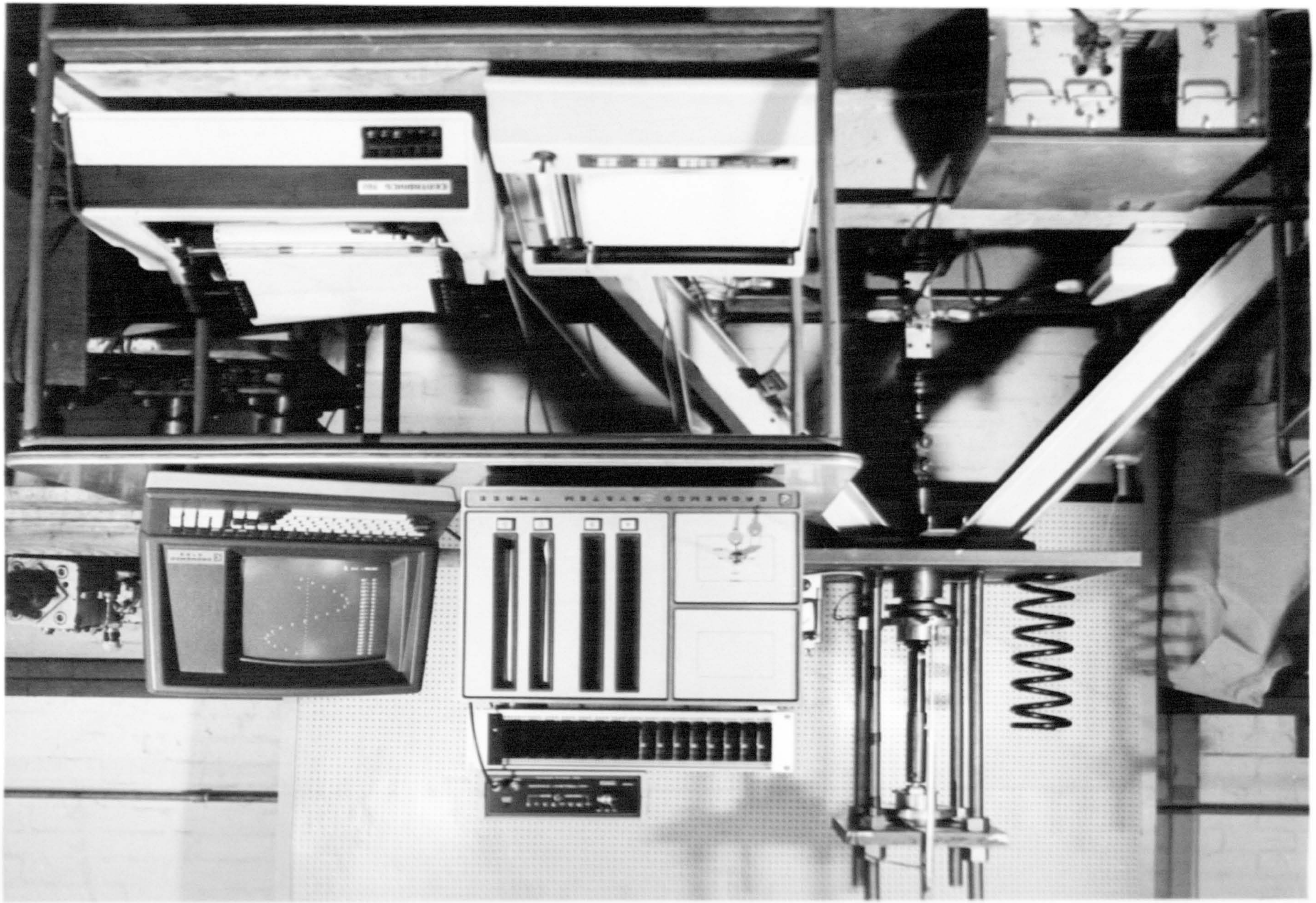

Fig. 26

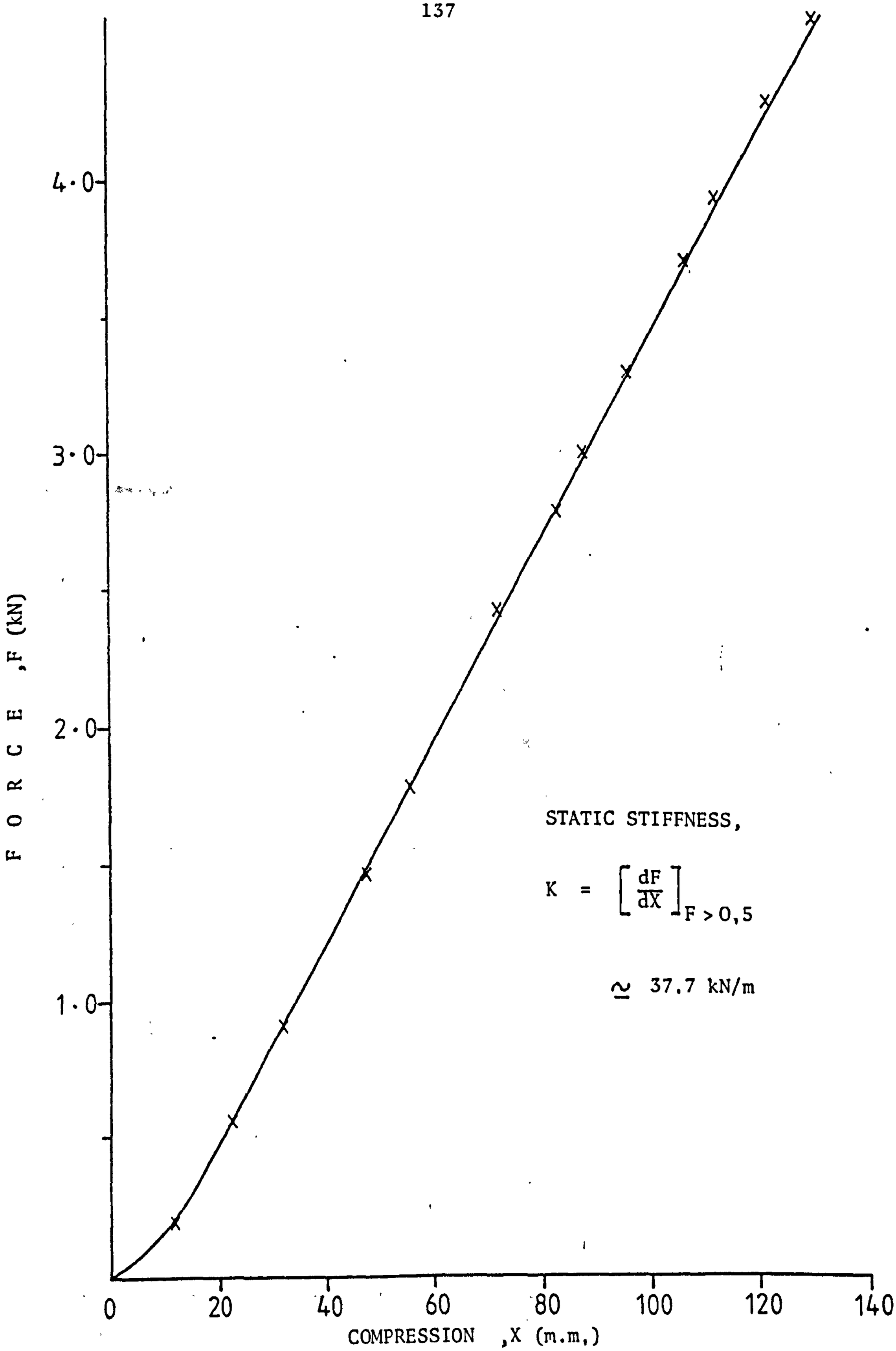

STATIC FORCE VERSUS COMPRESSION CHARACTERISTIC OF MAIN SPRING

Fig.27

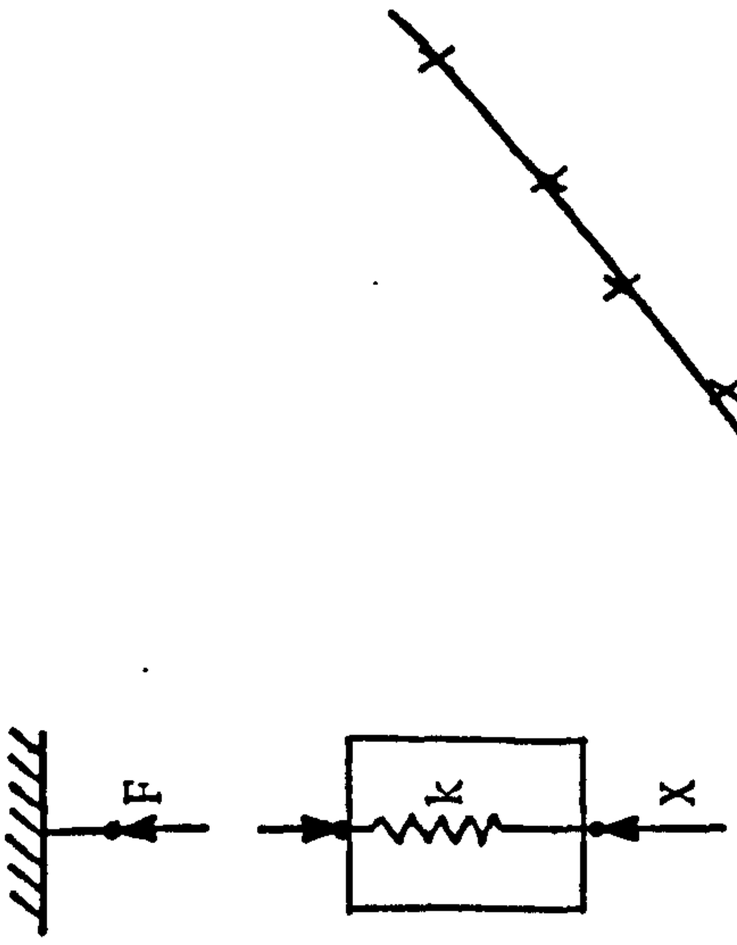

$\hat{\gamma}^2(f) > 0.99$

Δf = 0.78125 Hz

n = 100

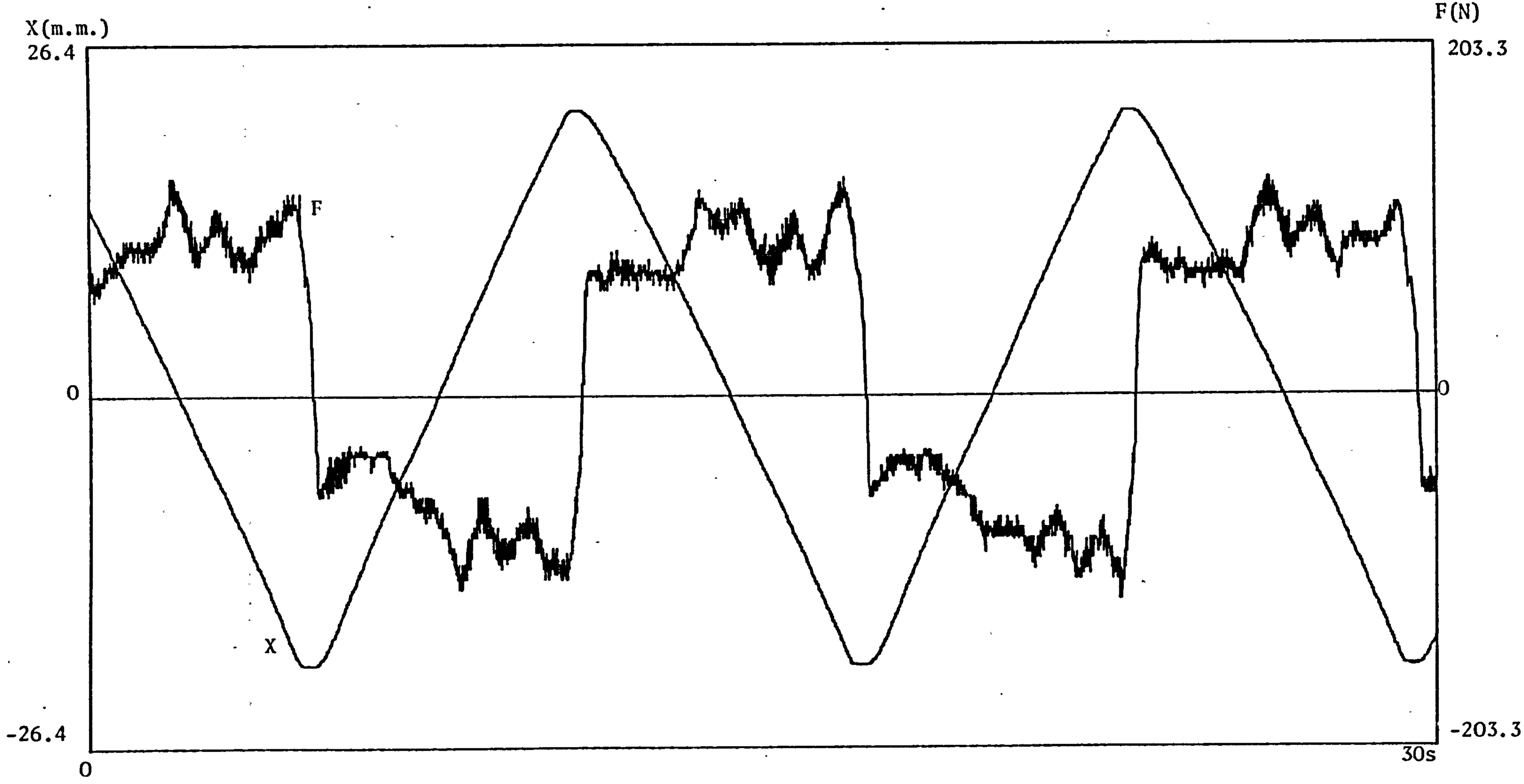

Fig. 29

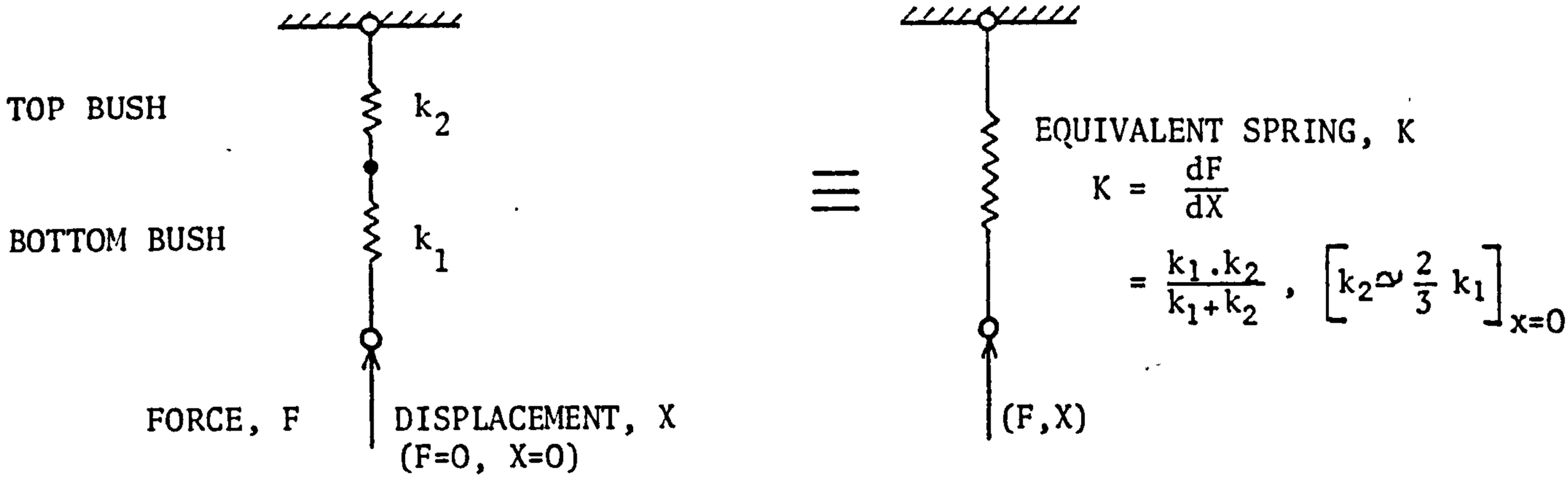

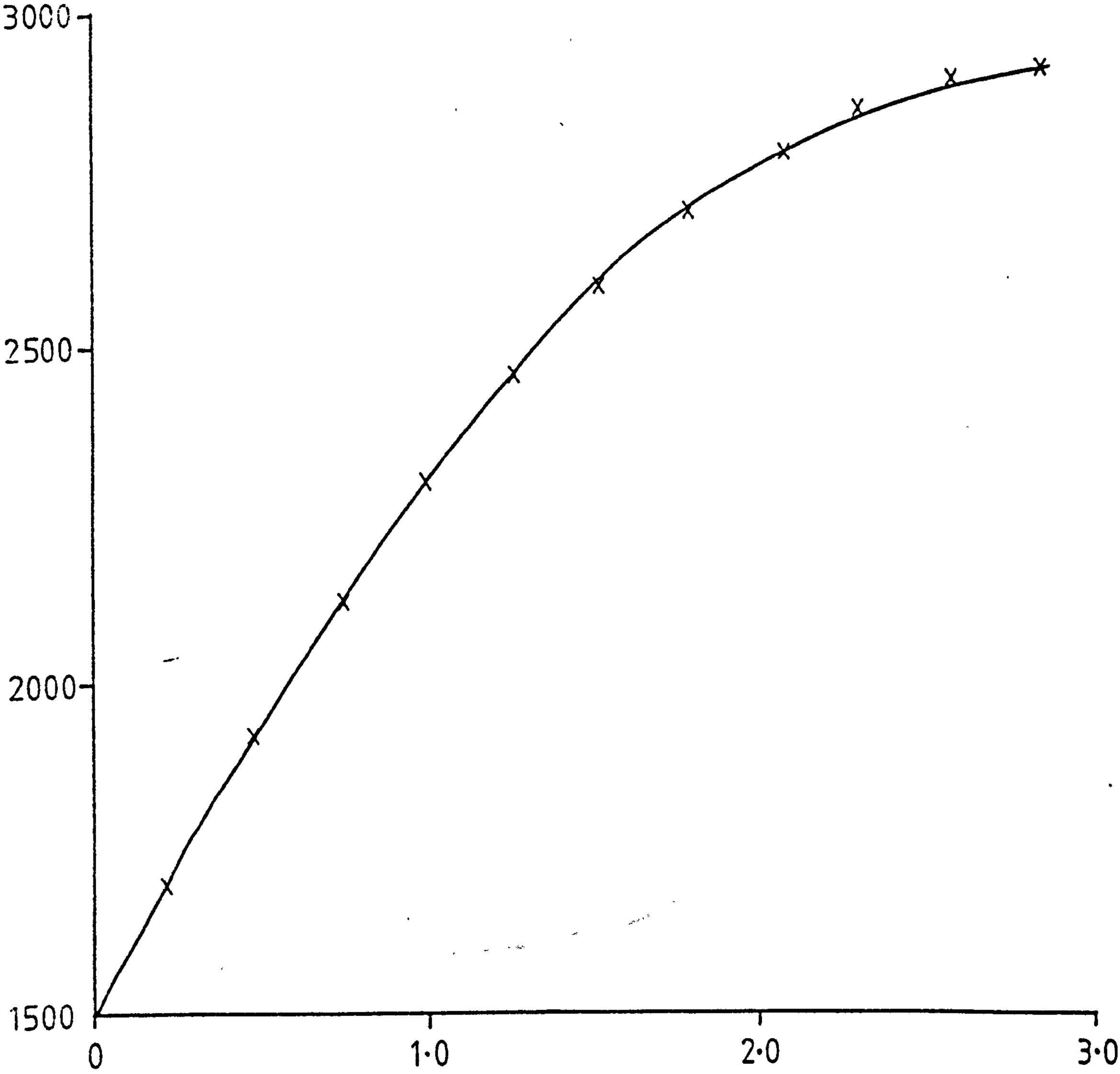

DAMPER BUSH STIFFNESS AS A FUNCTION OF BUSH COMPRESSION

Fig.30

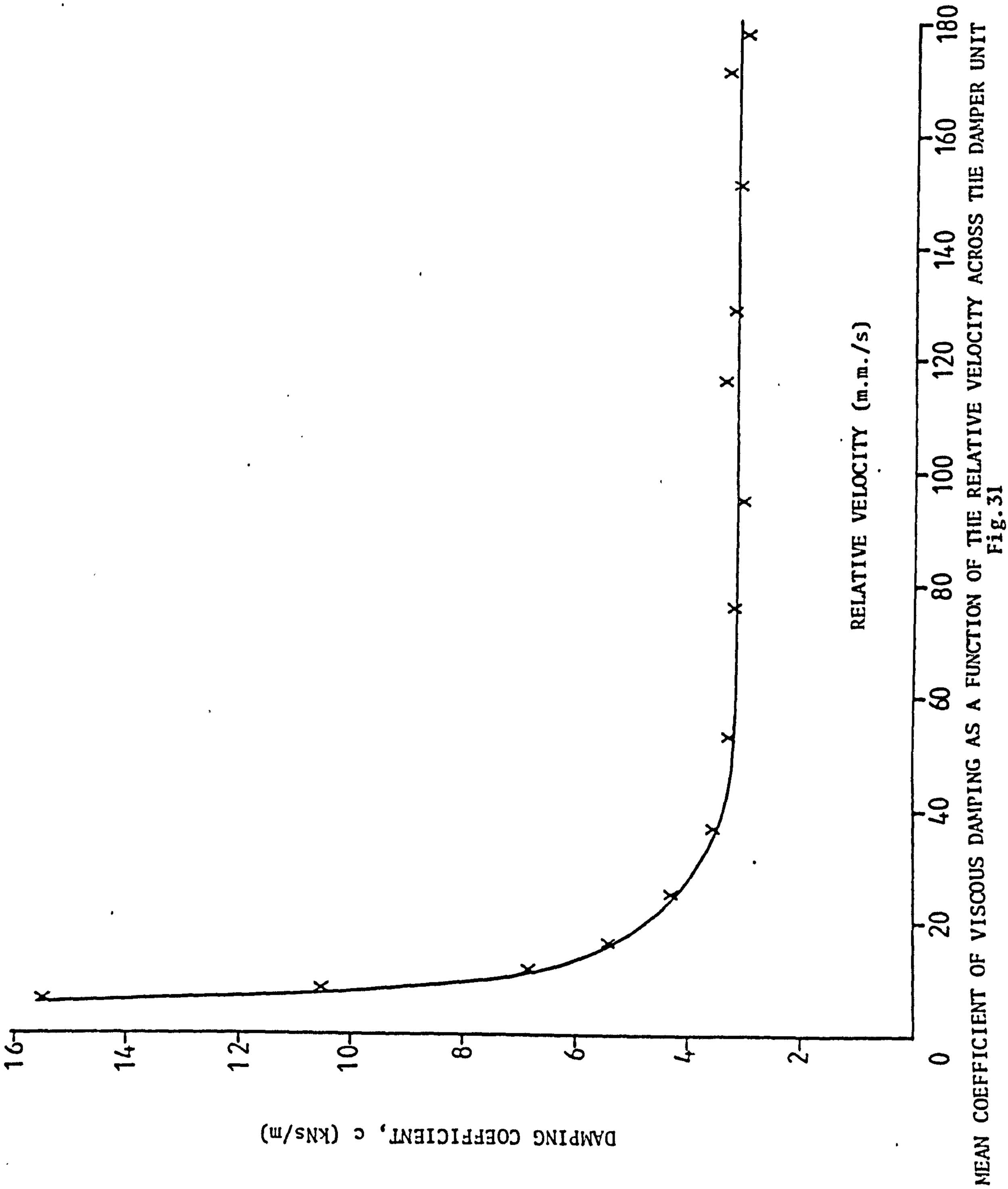
MEAN COEFFICIENT OF VISCOUS DAMPING AS A FUNCTION OF THE RELATIVE VELOCITY ACROSS TIE DAMPER UNIT
RELATIVE VELOCITY (m.m./s)
DAMPING COEFFICIENT, c (kNs/m)
0
20
40
60
80
100
120
140
160
180
2
4
6
8
10
12
14
16

Fig.31

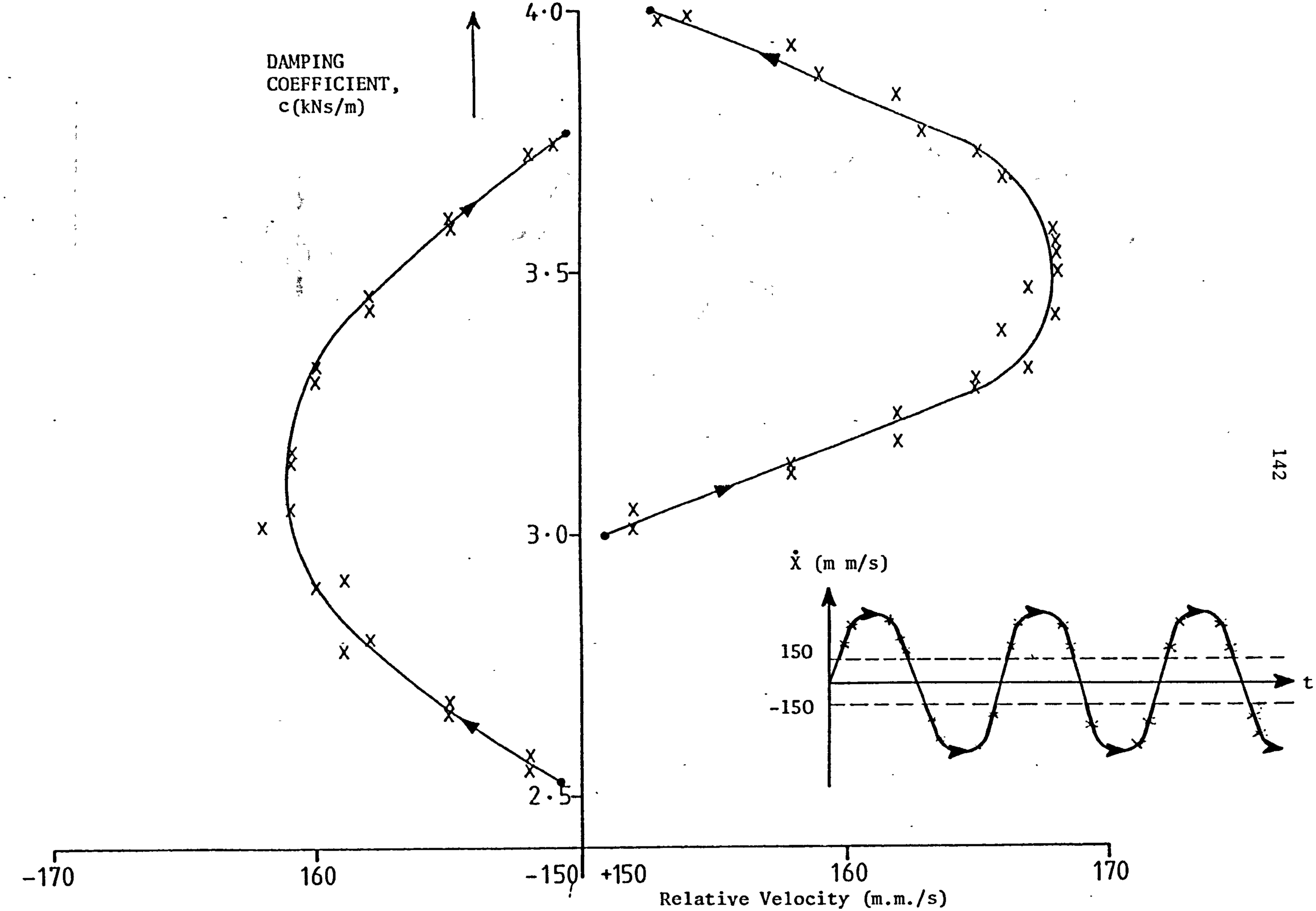

COEFFICIENT OF VISCOUS DAMPING VERSUS RELATIVE VELOCITY ACROSS DAMPER UNIT; c EVALUATED OVER SEVERAL CYCLES OF DATA

Fig.32

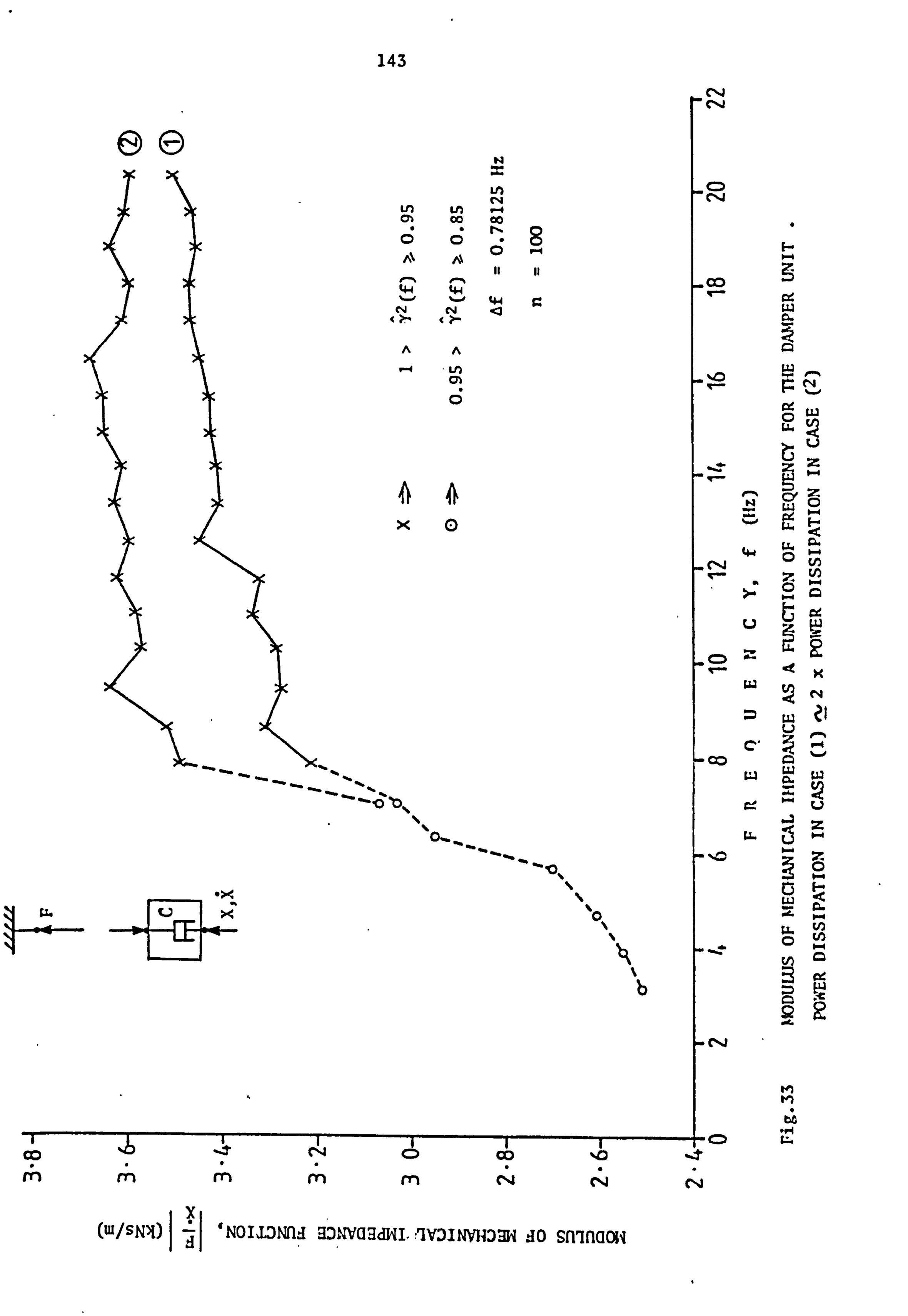
MODULUS OF MECHANICAL IMPEDANCE AS A FUNCTION OF FREQUENCY FOR THE DAMPER UNIT .
POWER DISSIPATION IN CASE (1) ≃ 2 x POWER DISSIPATION IN CASE (2)
FREQUENCY, f (Hz)
MODULUS OF MECHANICAL IMPEDANCE FUNCTION, |F/Ẋ| (kNs/m)
1 > γ̂²(f) ≥ 0.95
0.95 > γ̂²(f) ≥ 0.85
Δf = 0.78125 Hz
n = 100
F
C
X,Ẋ
①
②

Fig.33

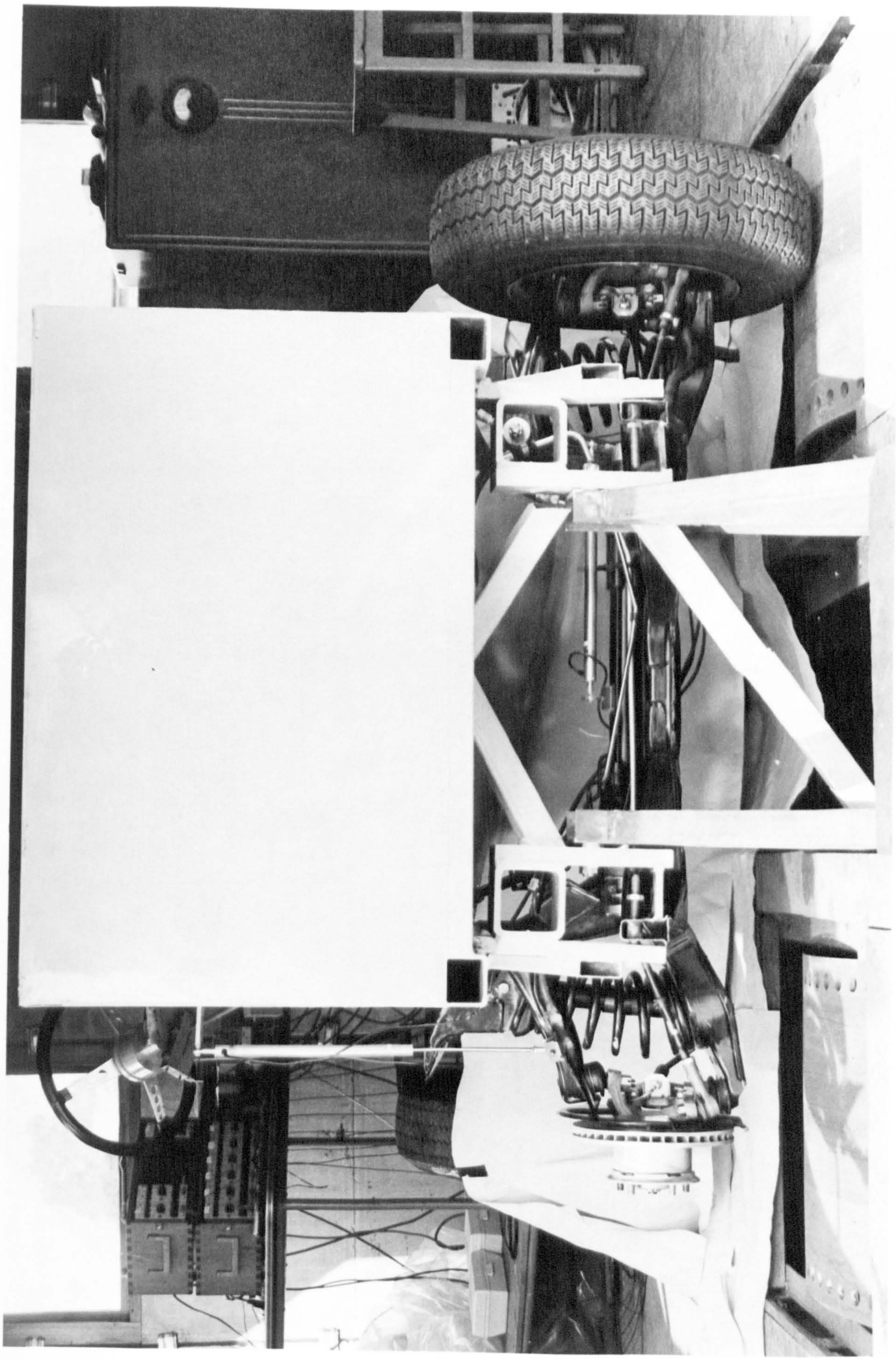

Fig. 34

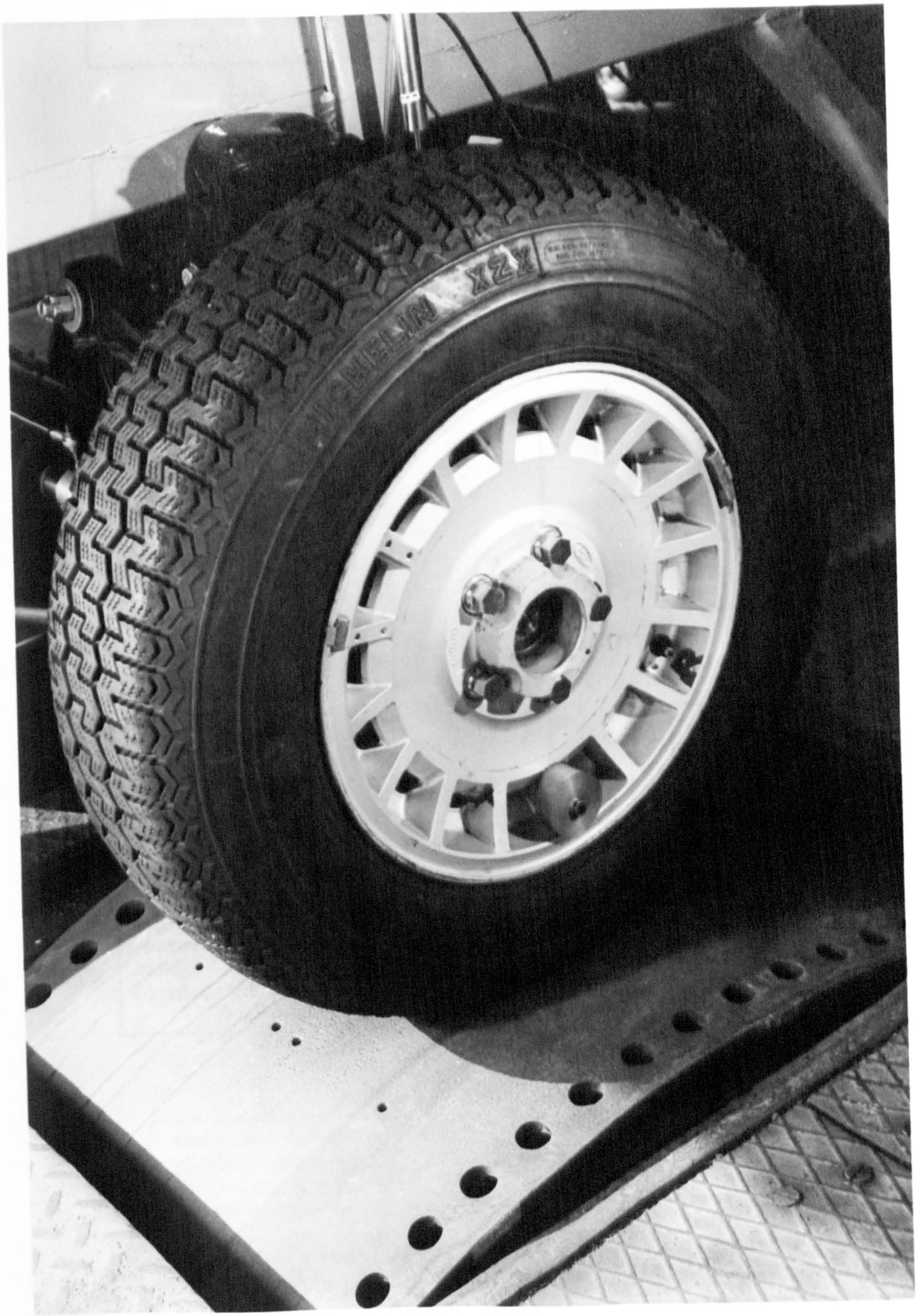

Fig. 35

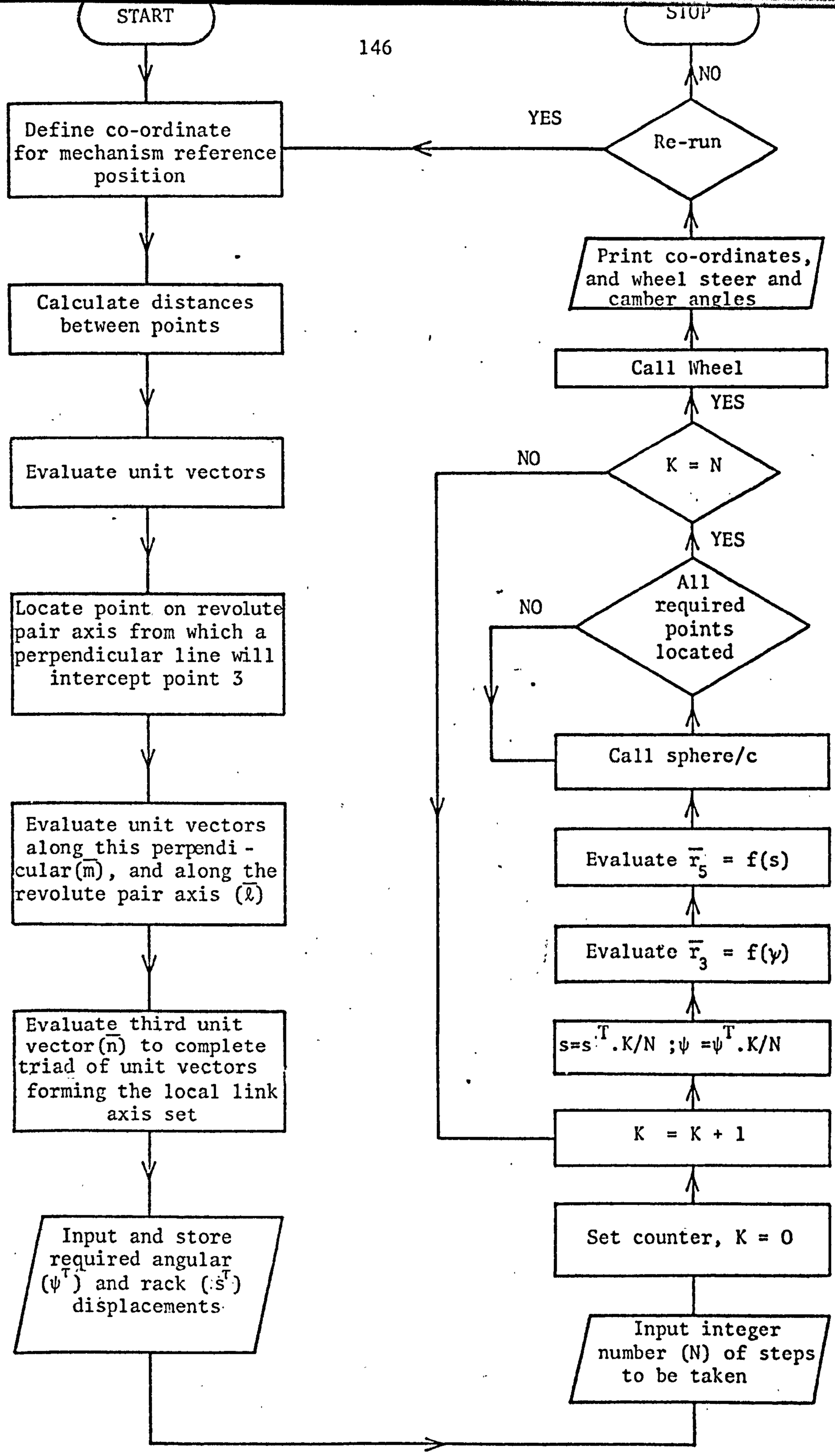

Fig.36 Flow chart for program POSITION

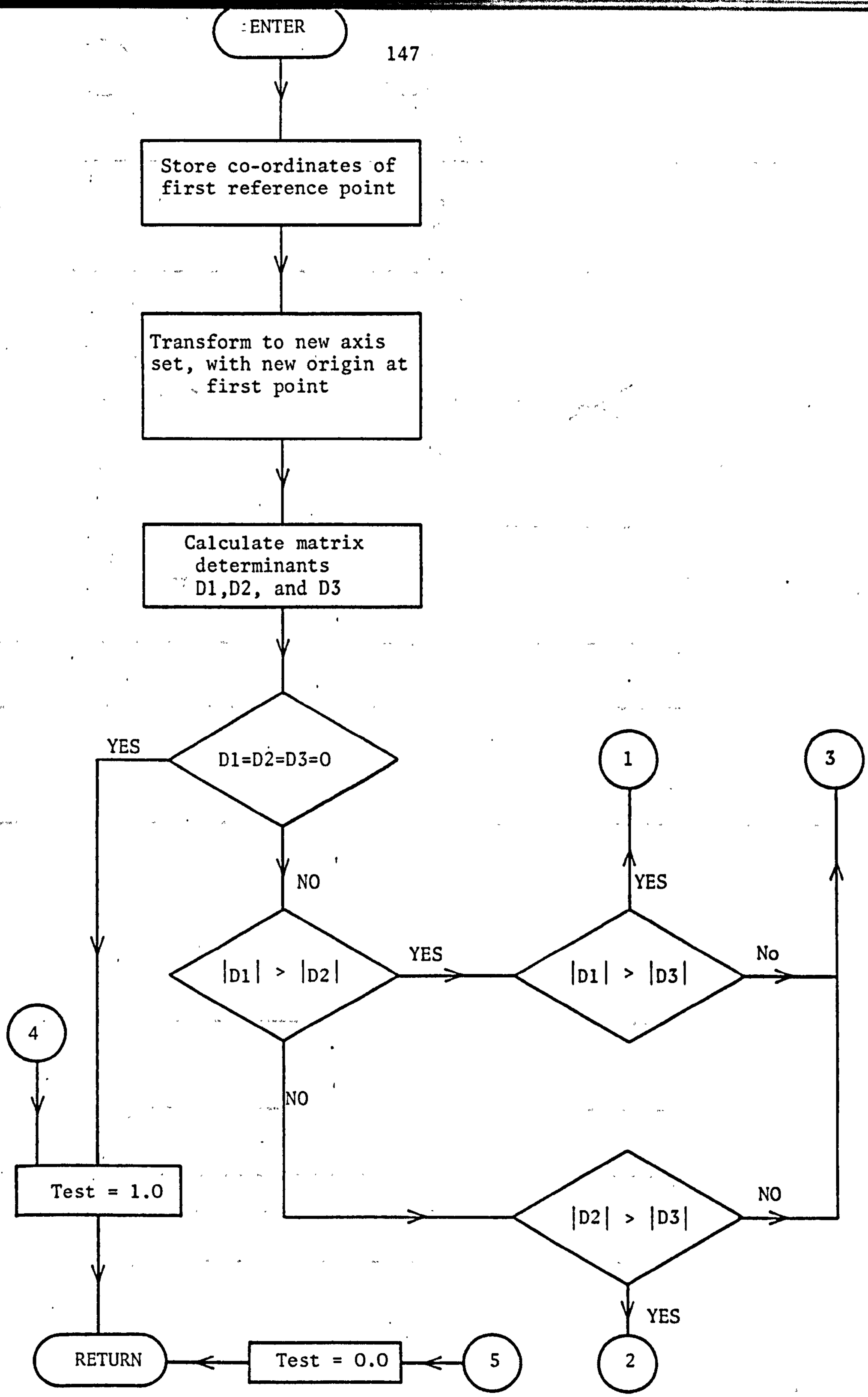

Fig.37 Flow chart for subroutine SPHERE

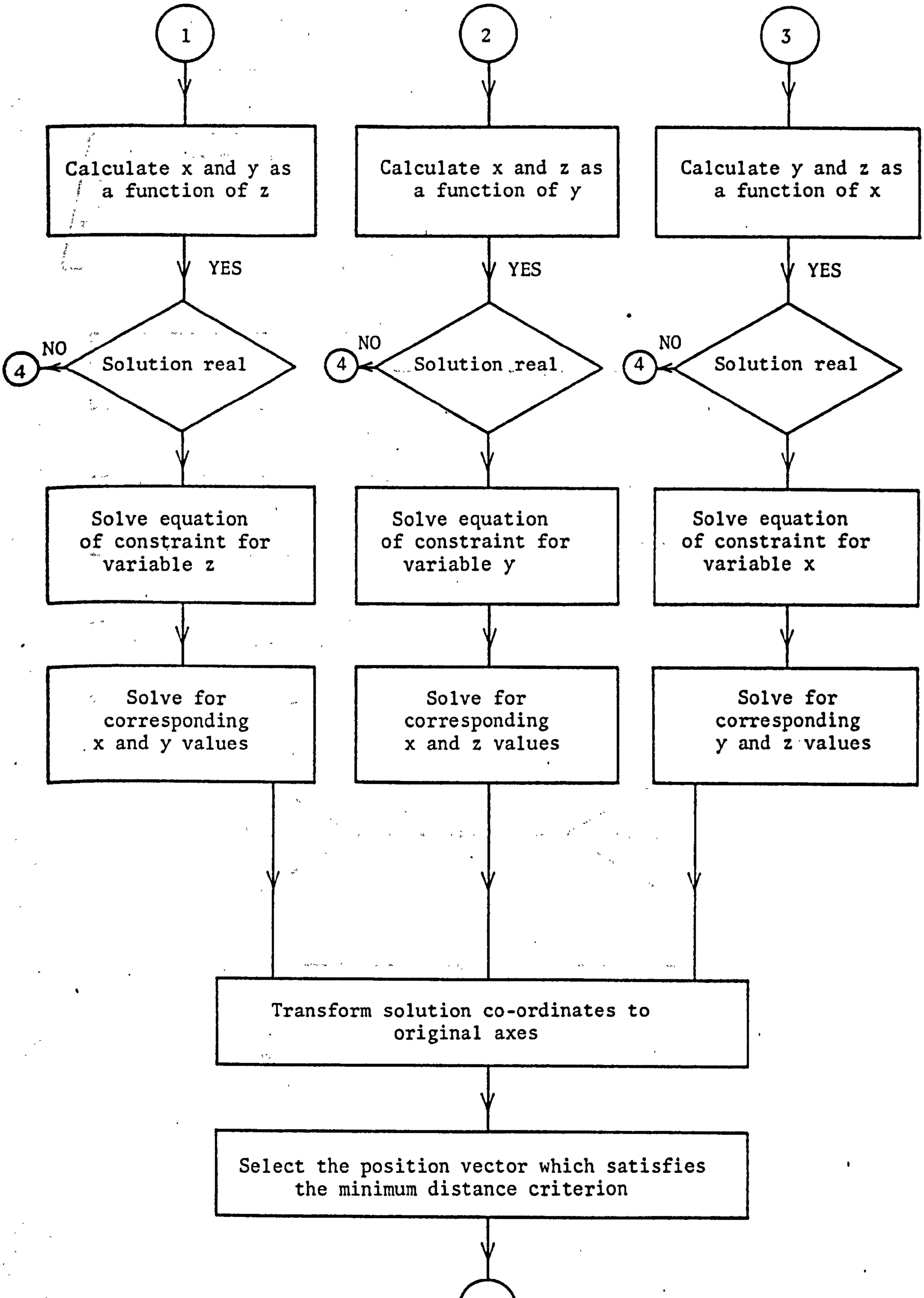

Fig. 38 Flow chart for subroutine SPHERE

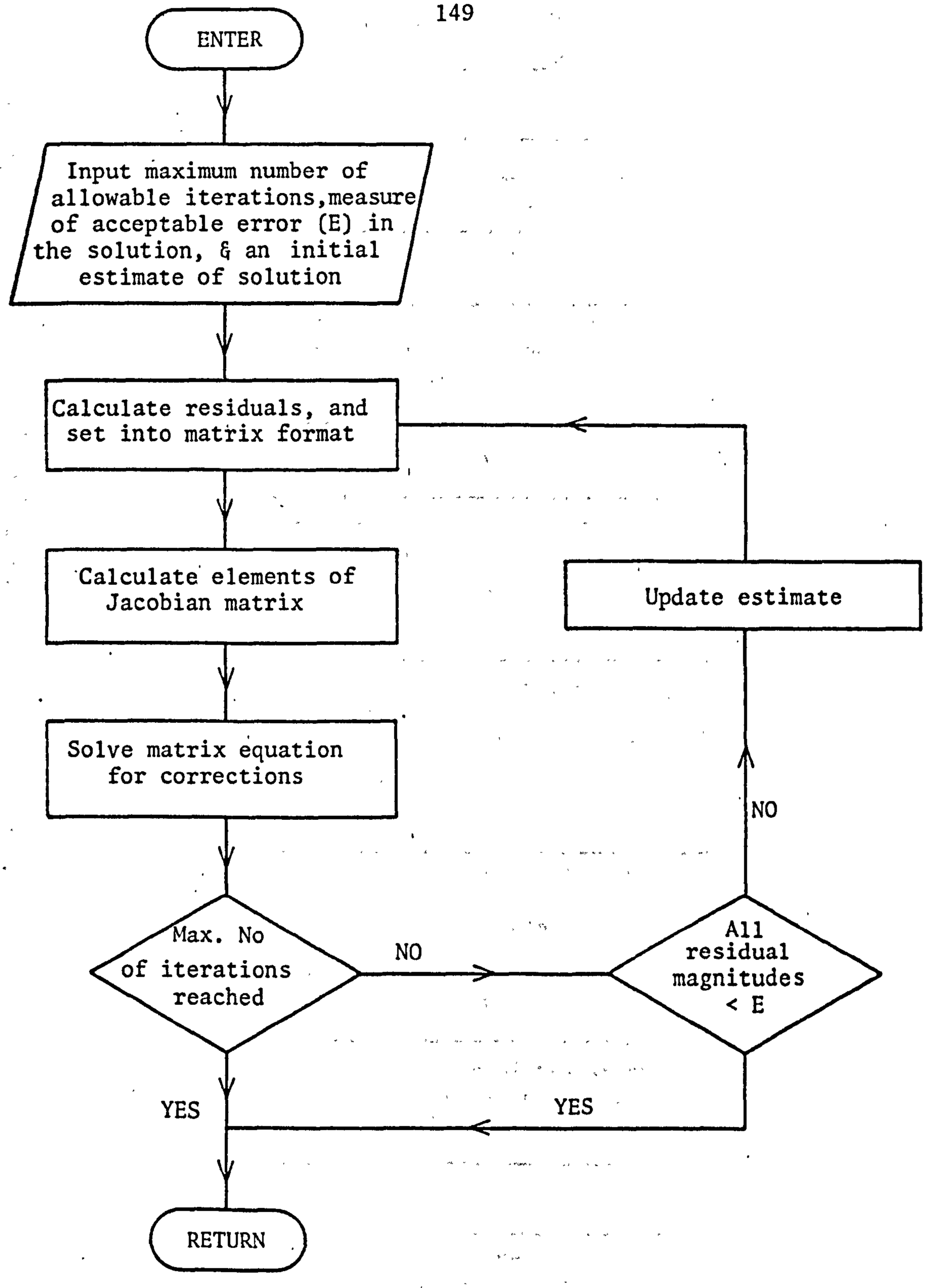

Fig.39. Flow chart for subroutine SPHERC

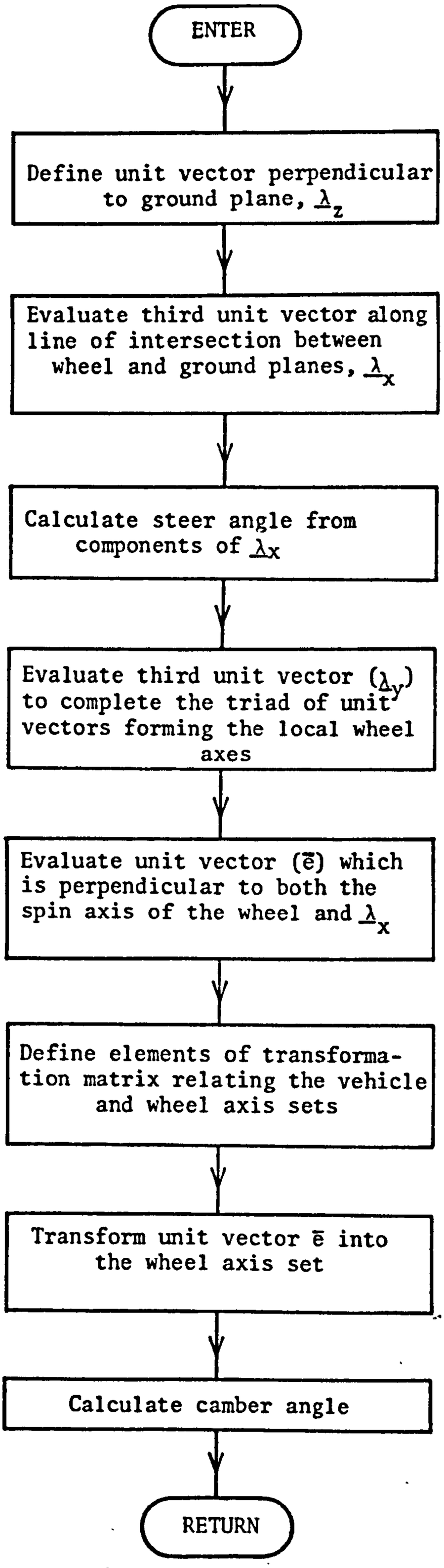

Fig.40. Flow chart for subroutine WHEEL

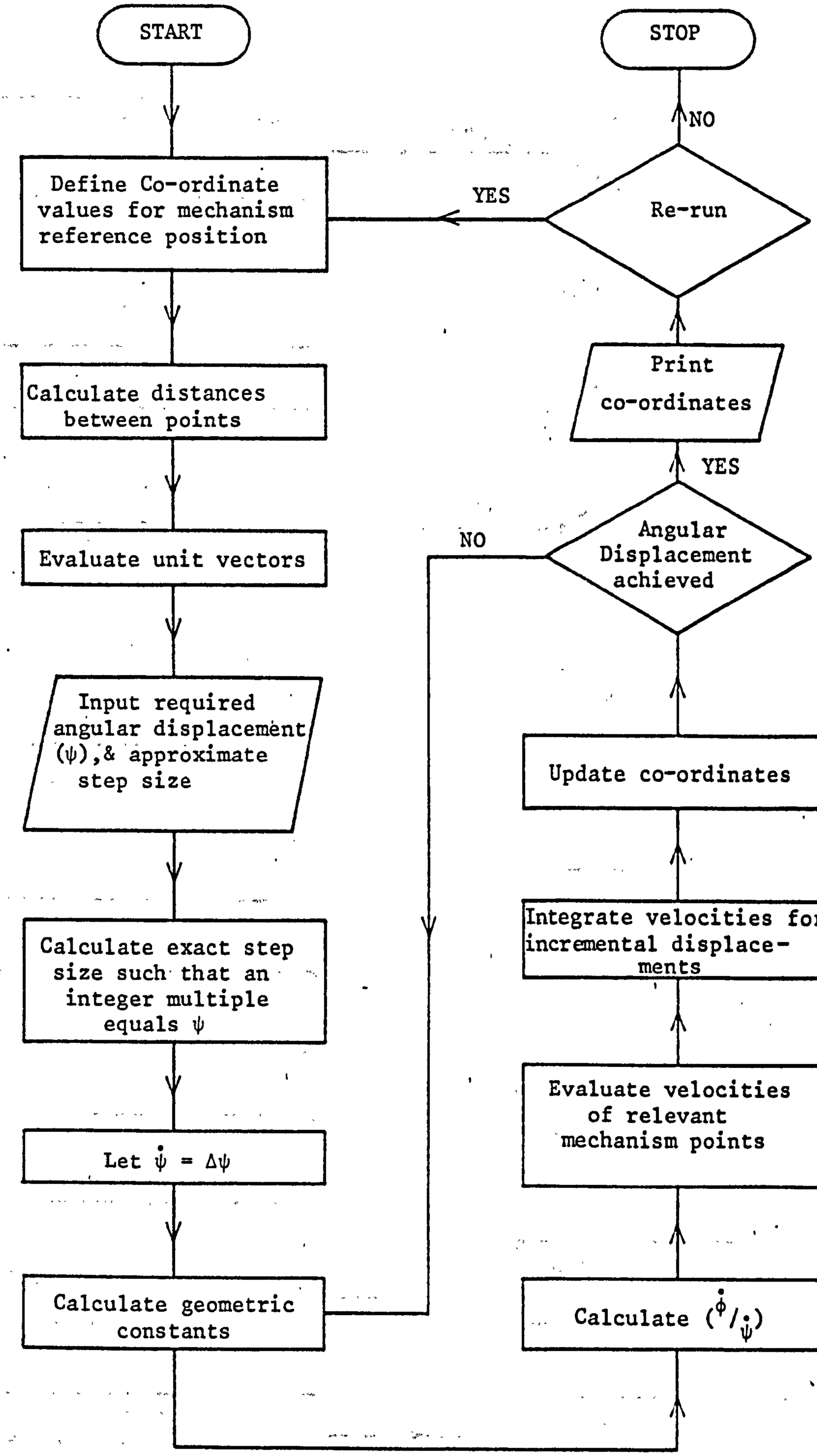

Fig.41. Flow chart for program KINEM1

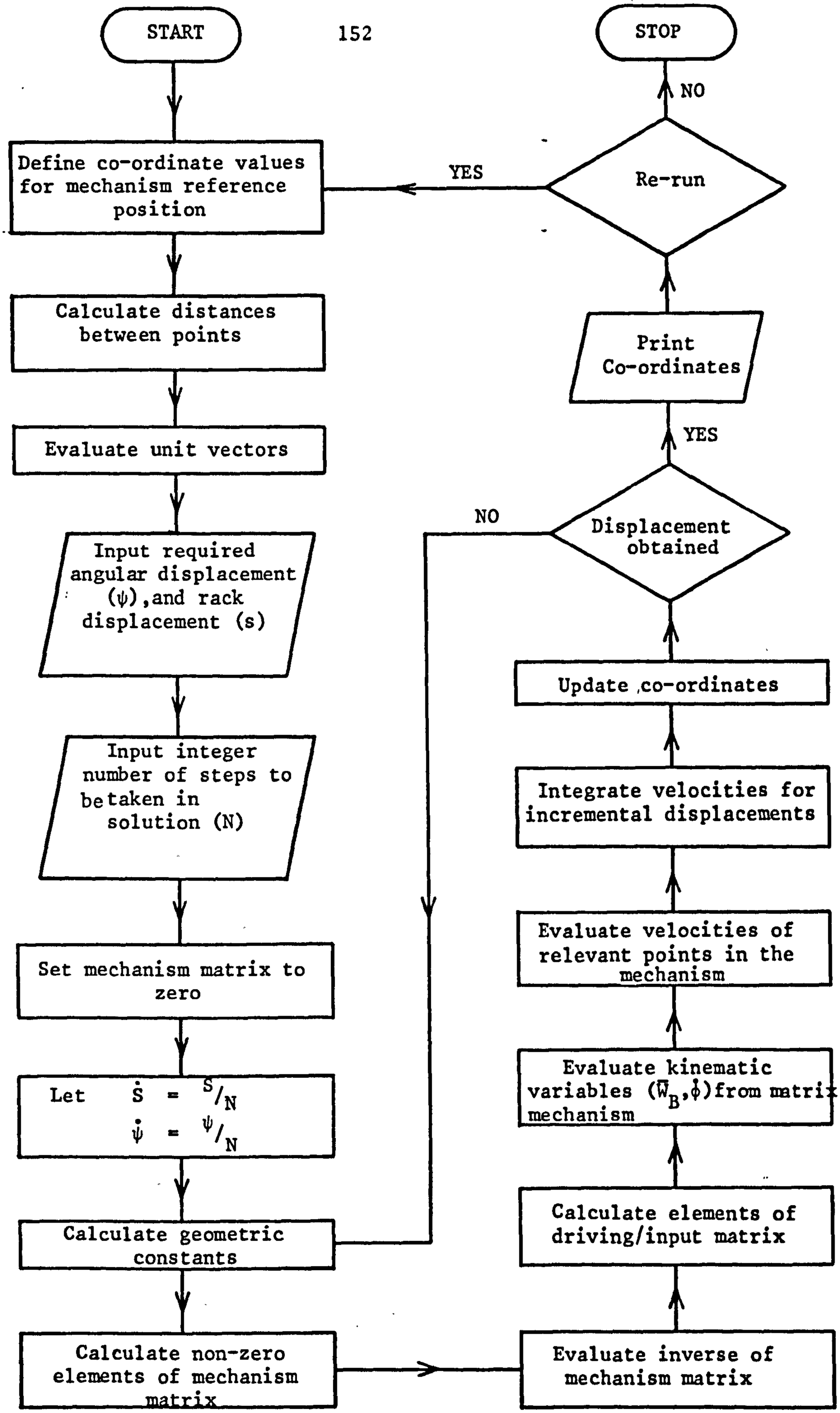

Fig.42. Flow chart for program KINEM2

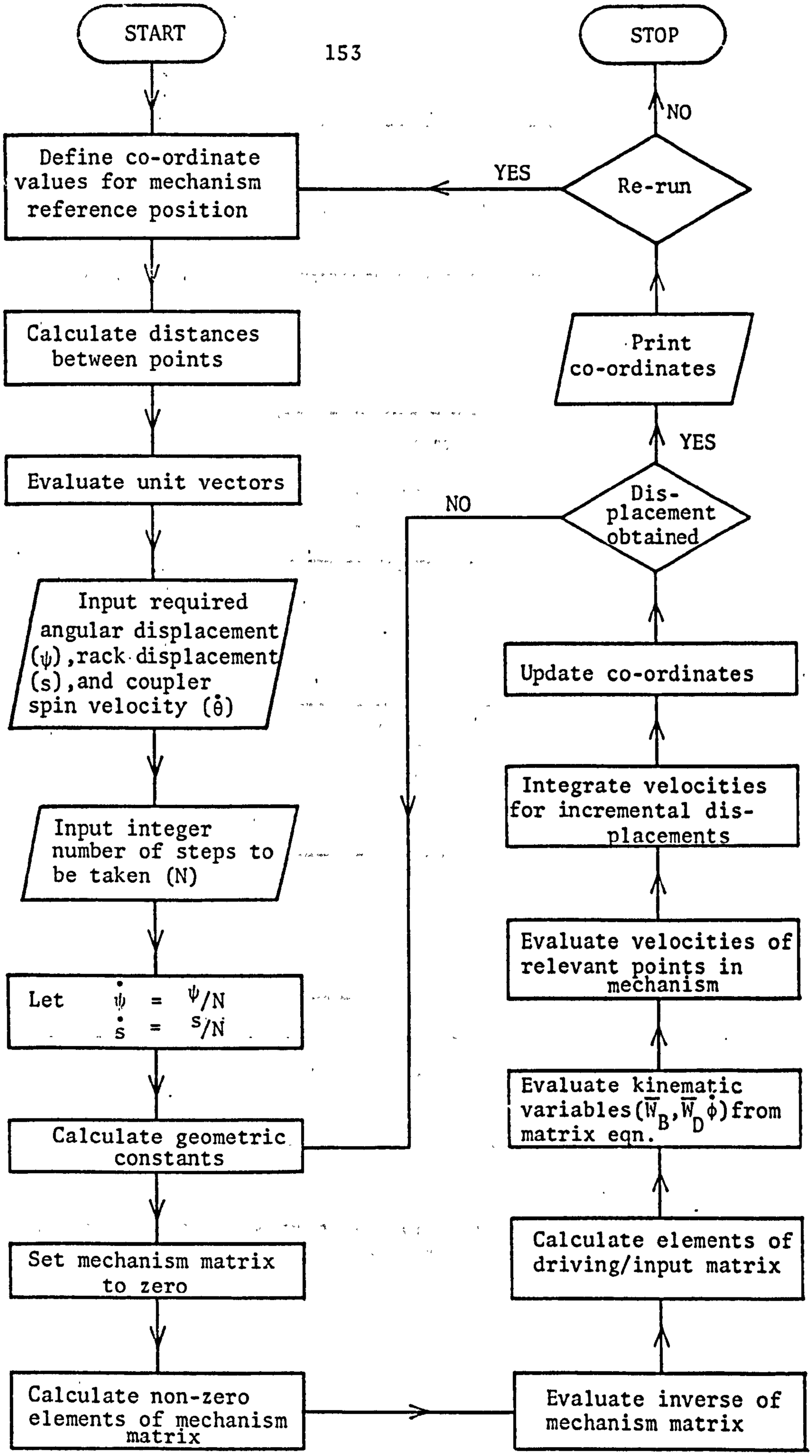

Fig. 43. Flow chart for program KINEM3

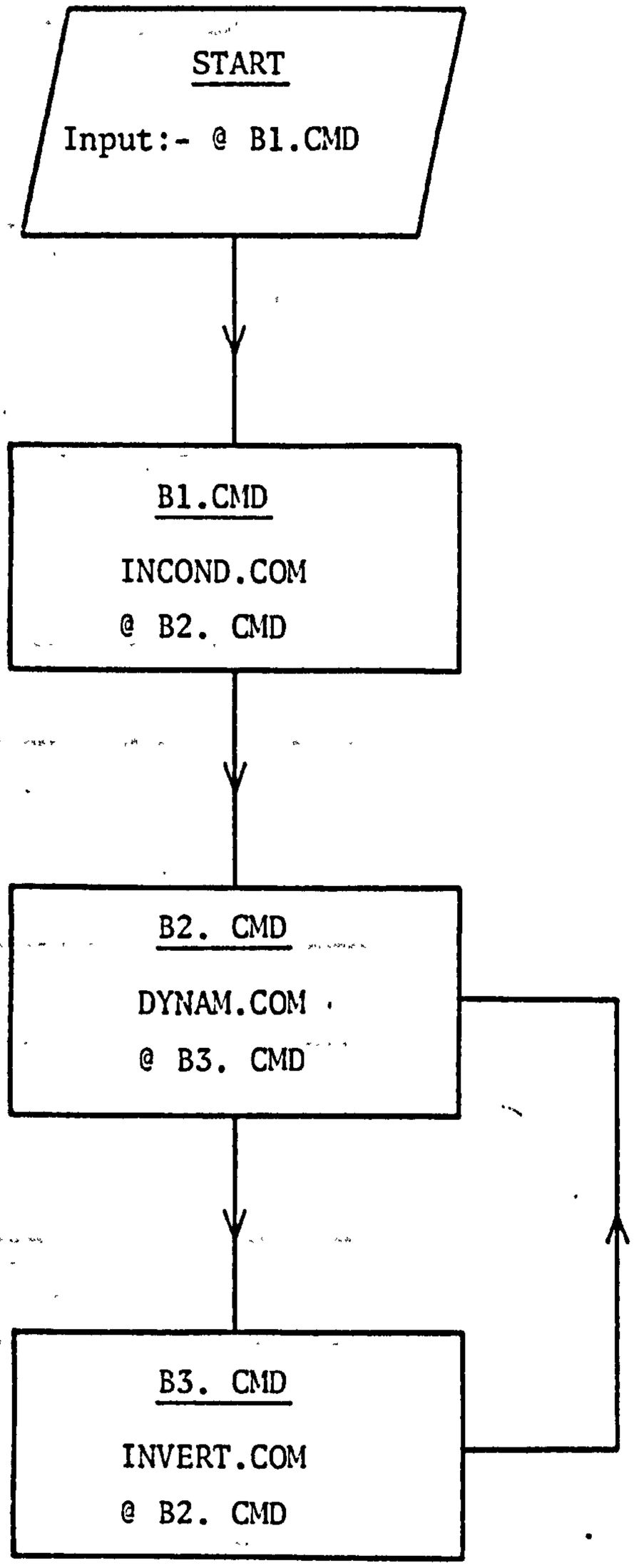

Fig.44.Flow chart indicating batch mode operation when running the set of dynamic simulation programs under the CDOS software

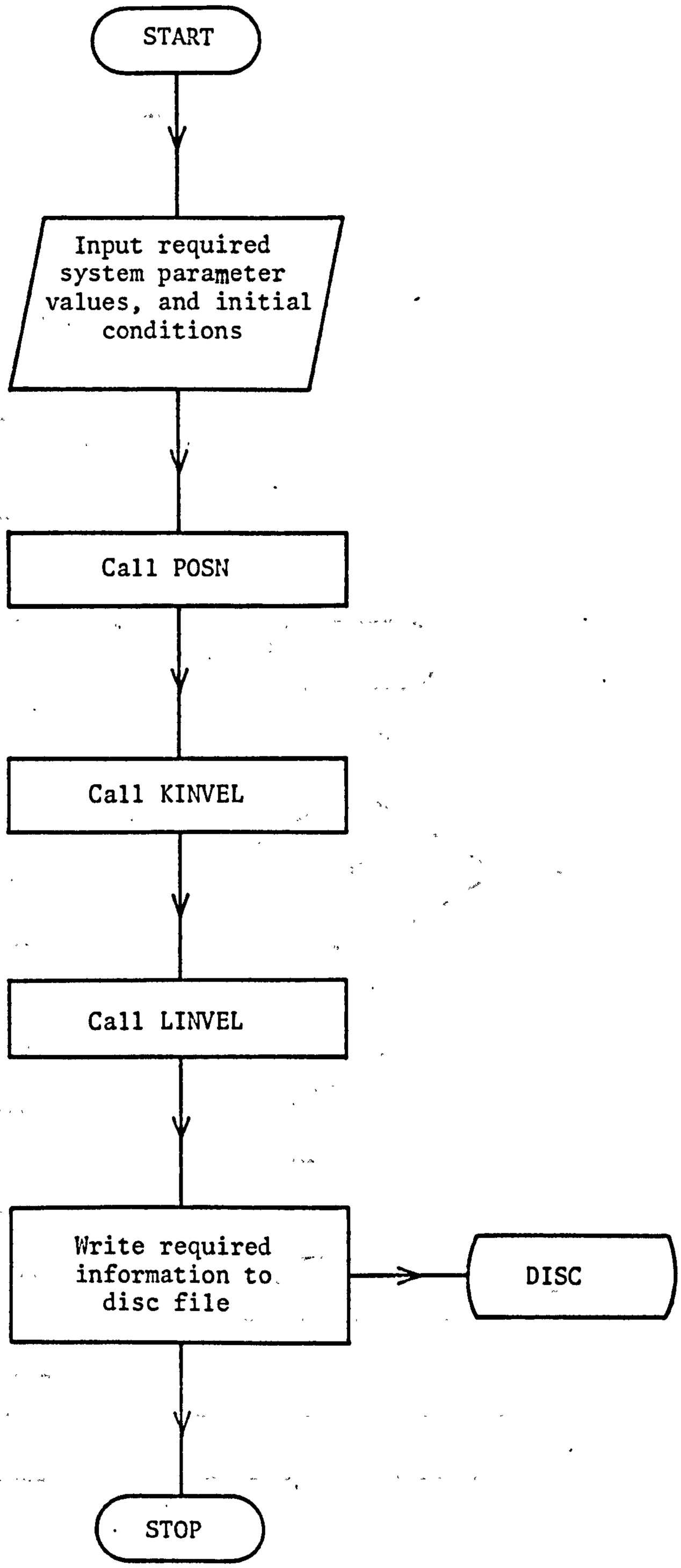

Fig.45. Flow chart for program INCOND

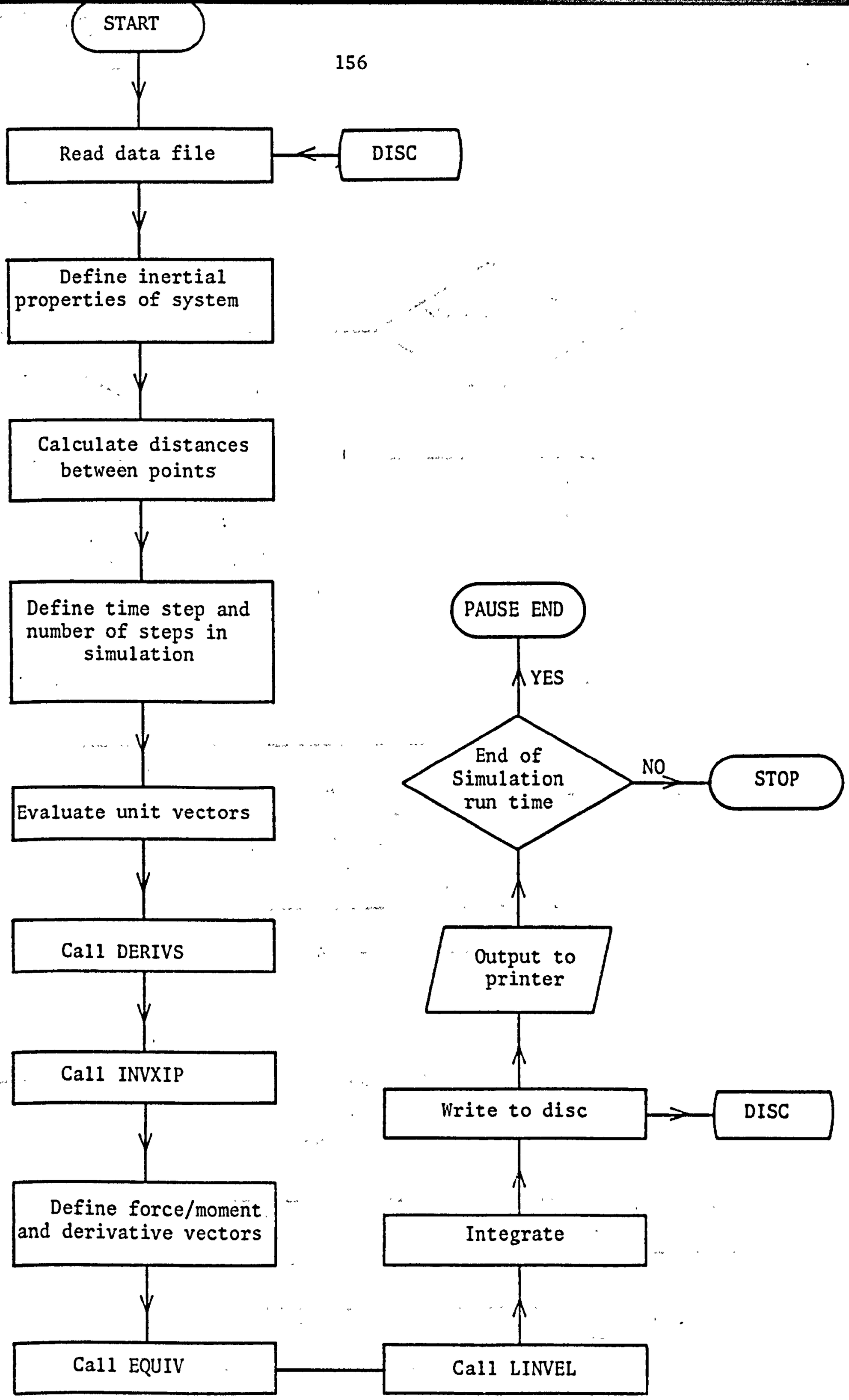

Fig.46. Flow chart for program DYNAM

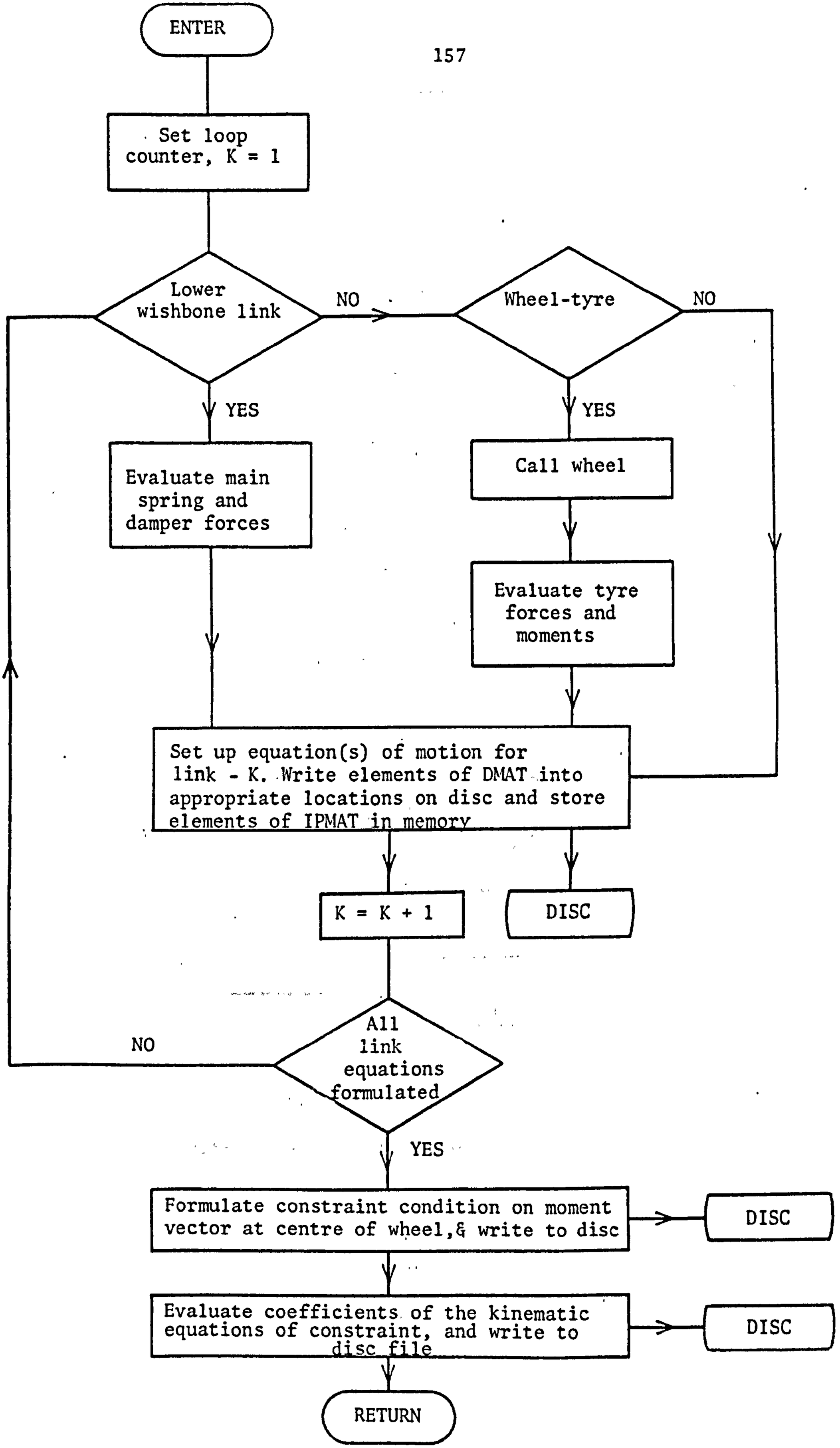

Fig.47. Flow chart for subroutine DERIVS

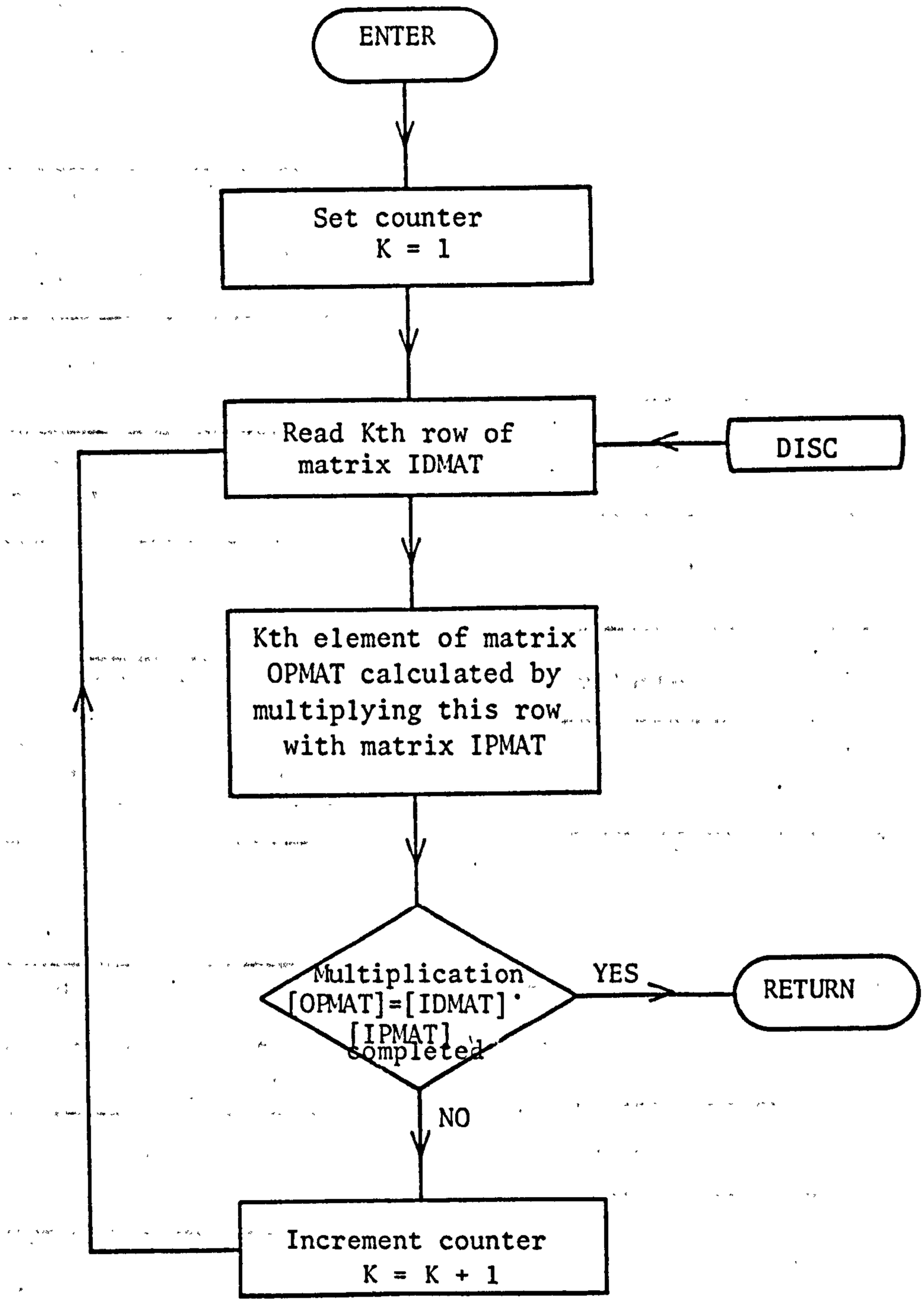

Fig.48. Flow chart for subroutine INVXIP

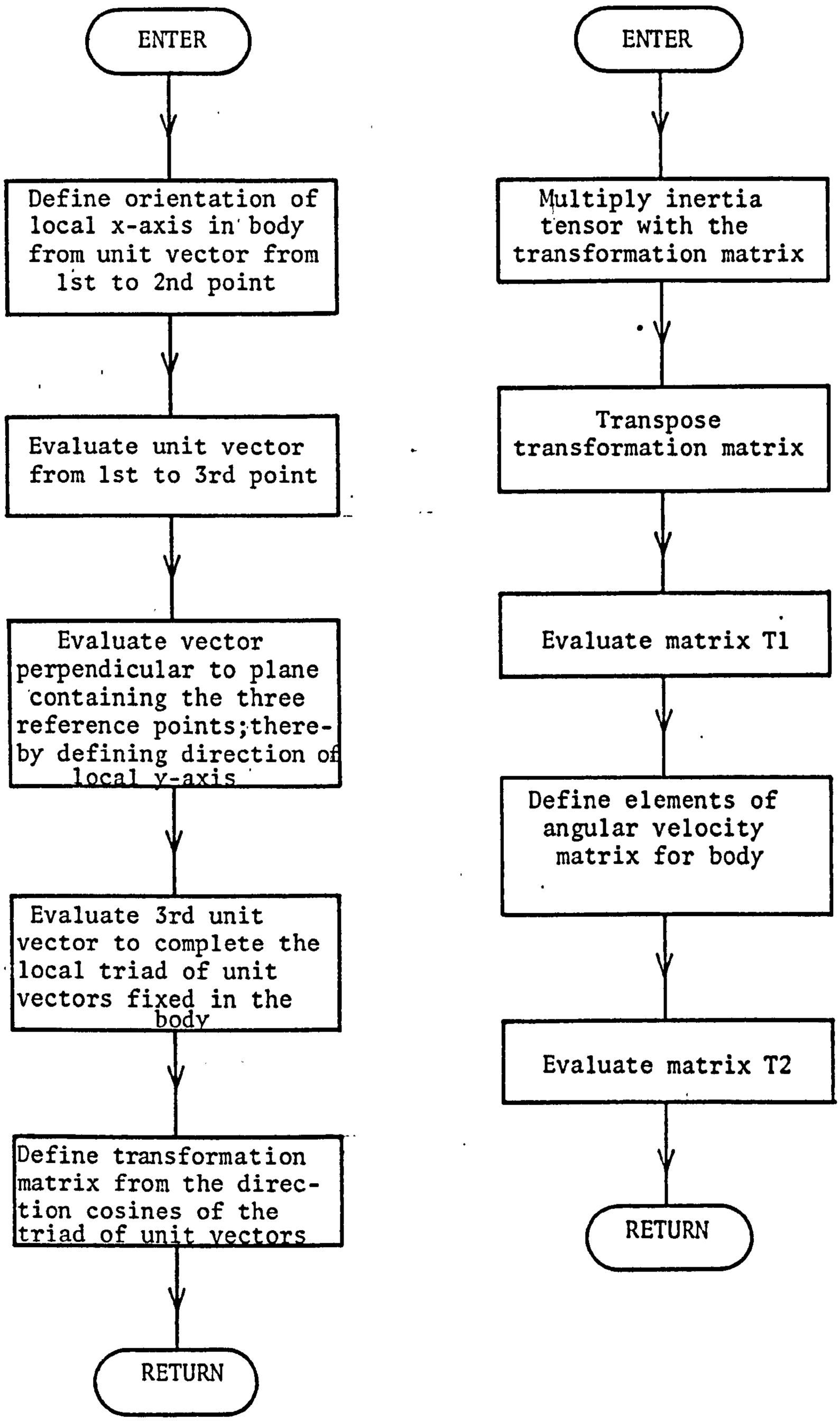

Fig.49. FLOW CHARTS FOR SUBROUTINES TMAT AND TFORM

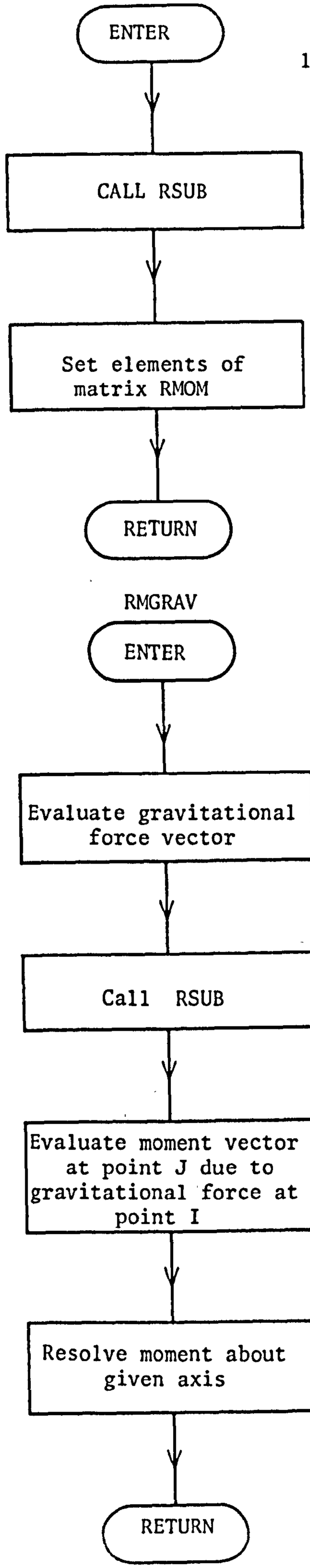

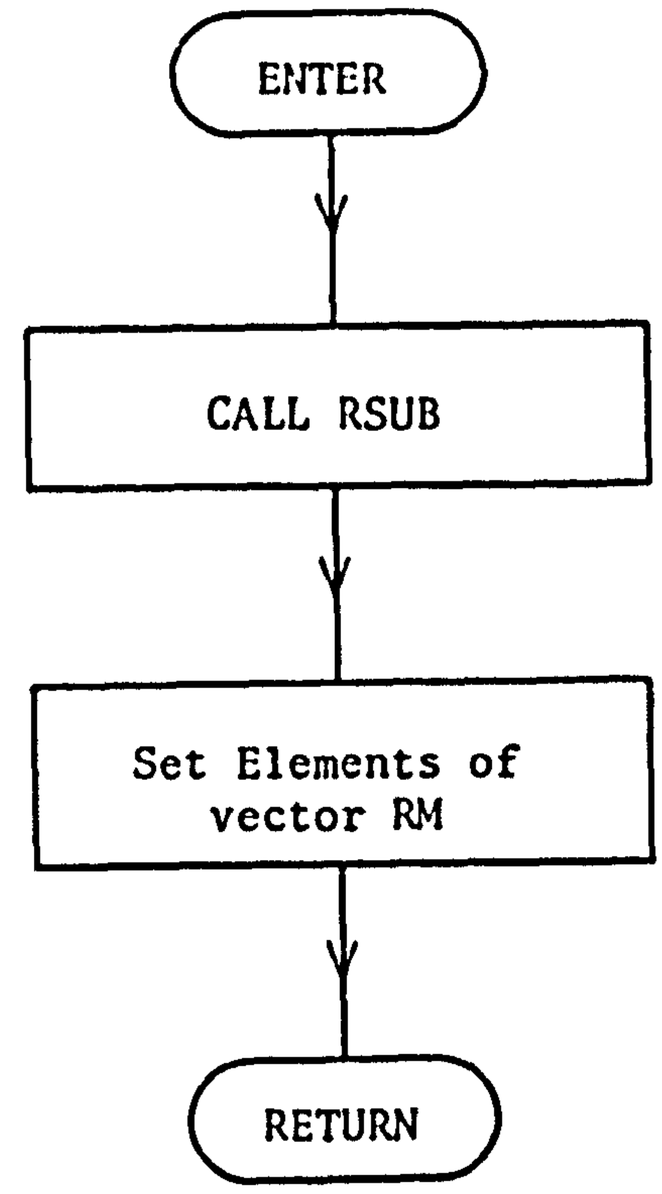

Fig.50 Flow charts for subroutines MOMENT, RESMOM, and RMGRAV

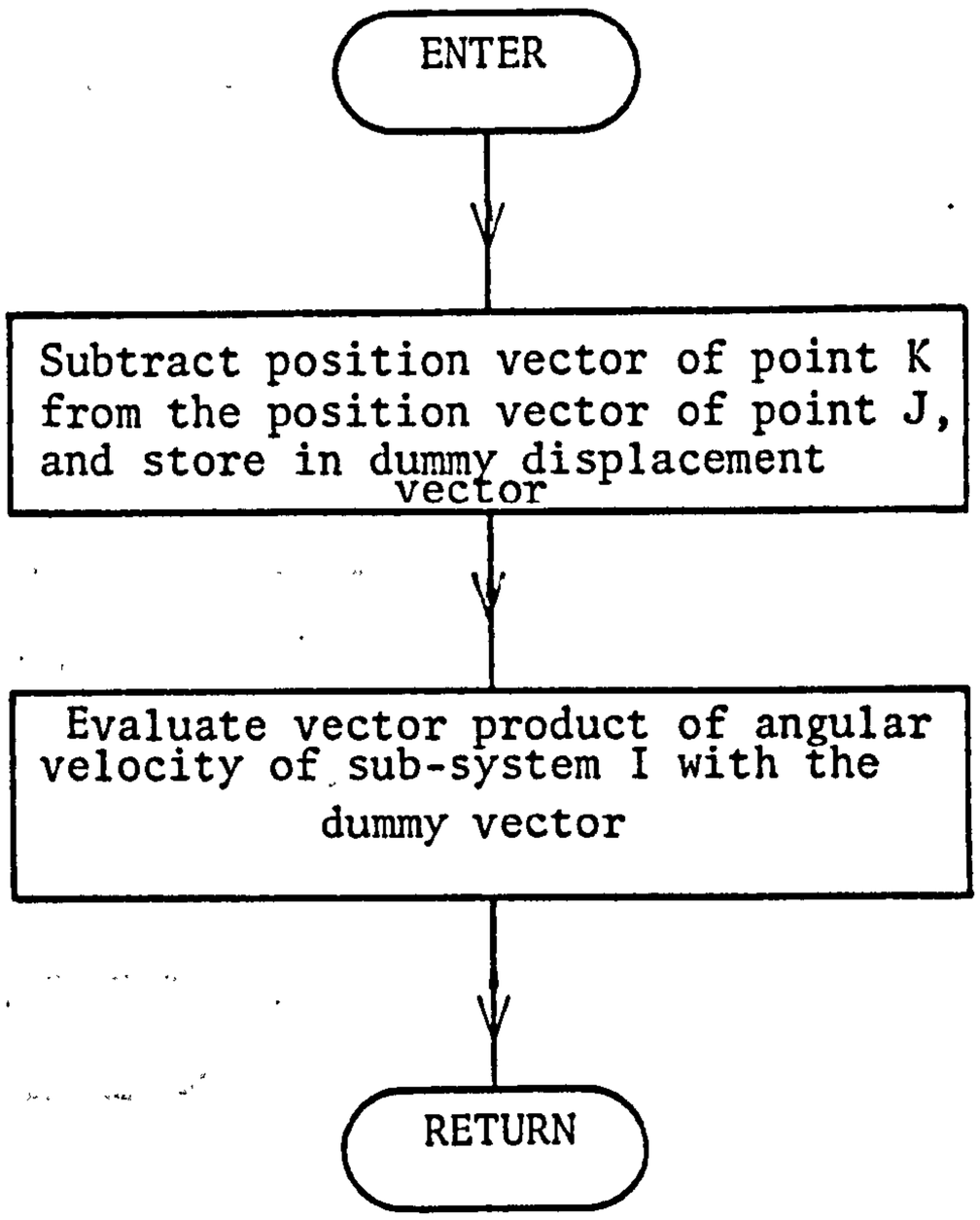

WXRR

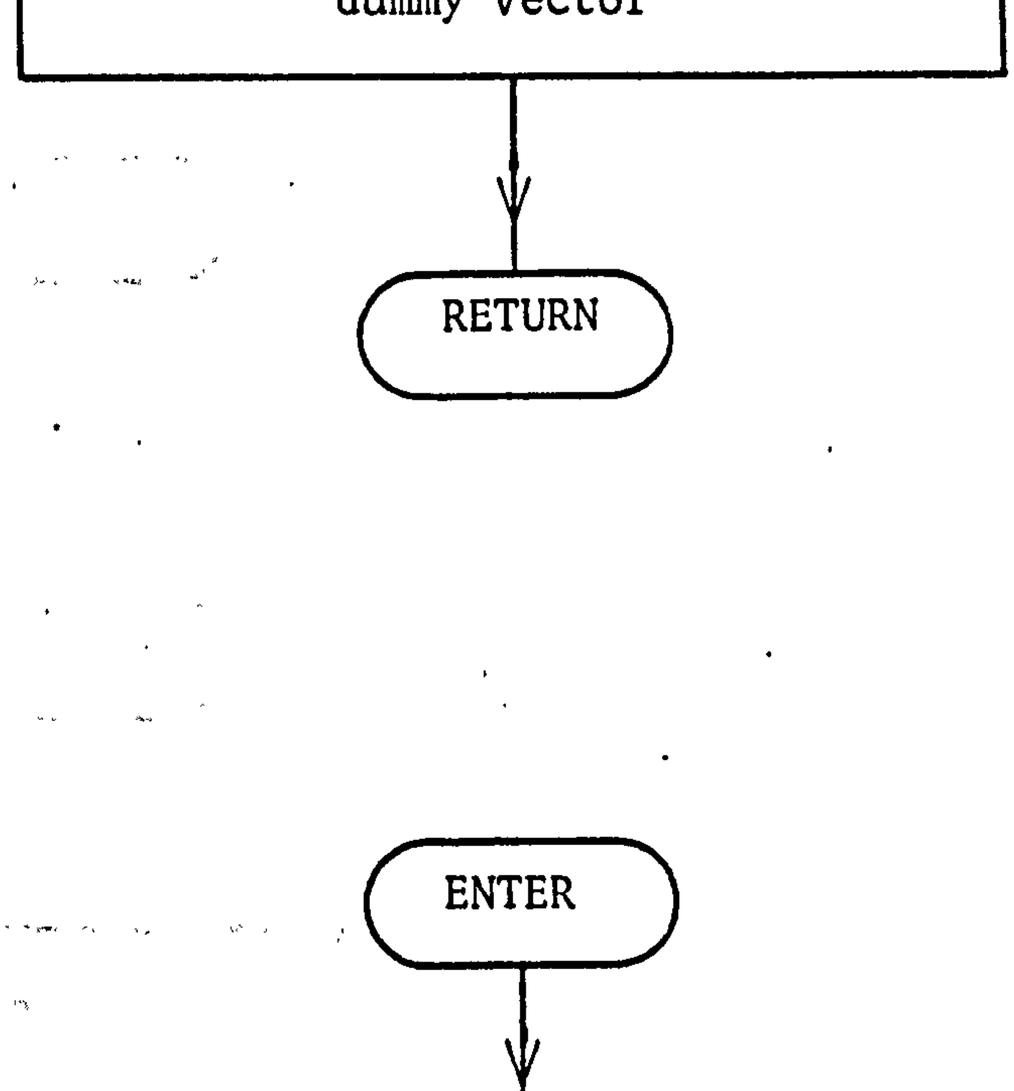

WXVV

Fig.51. Flow charts for subroutines WXRR and WXVV

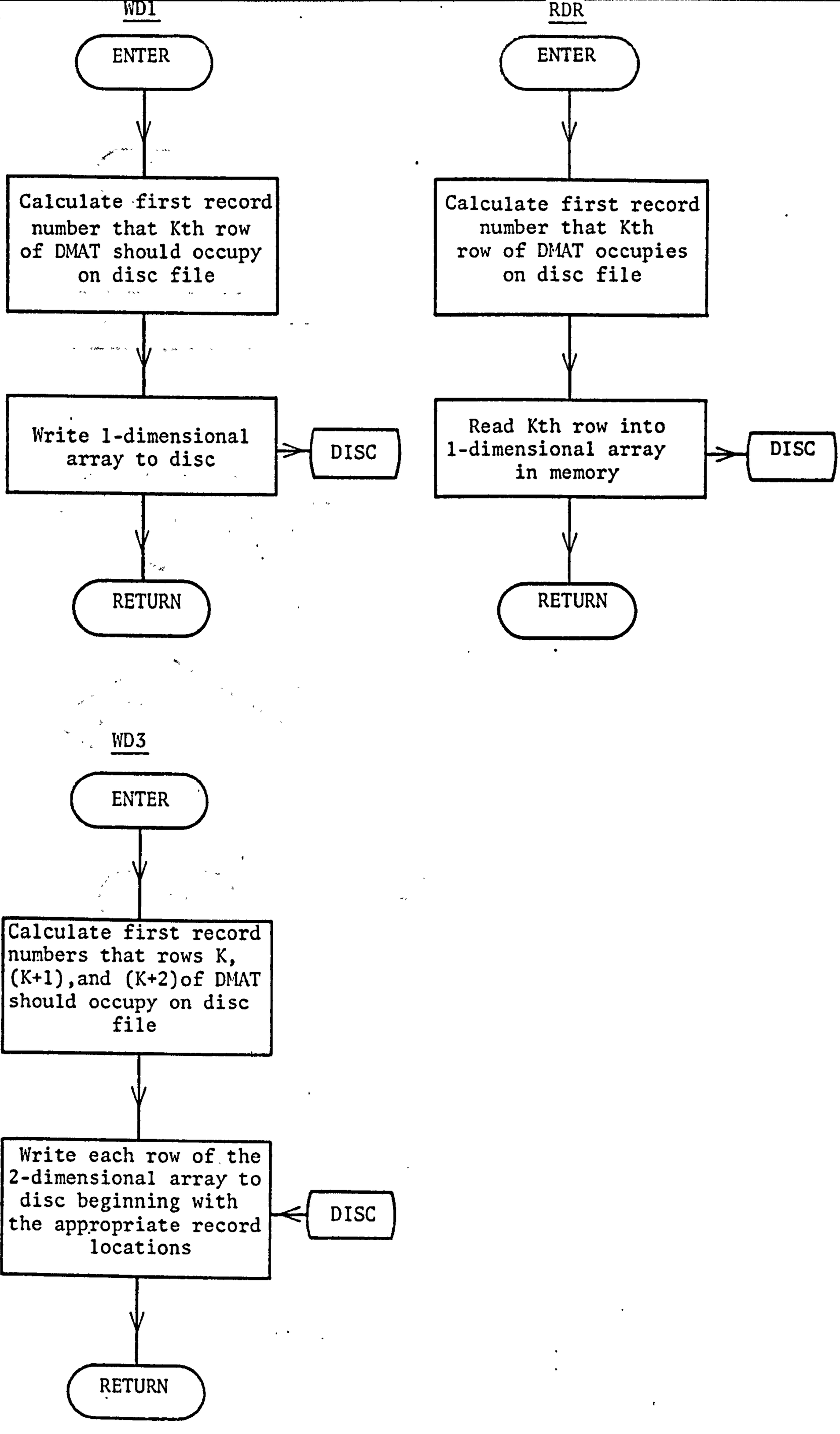

Fig.52 Flow charts for subroutines WD1, WD3 and RDR

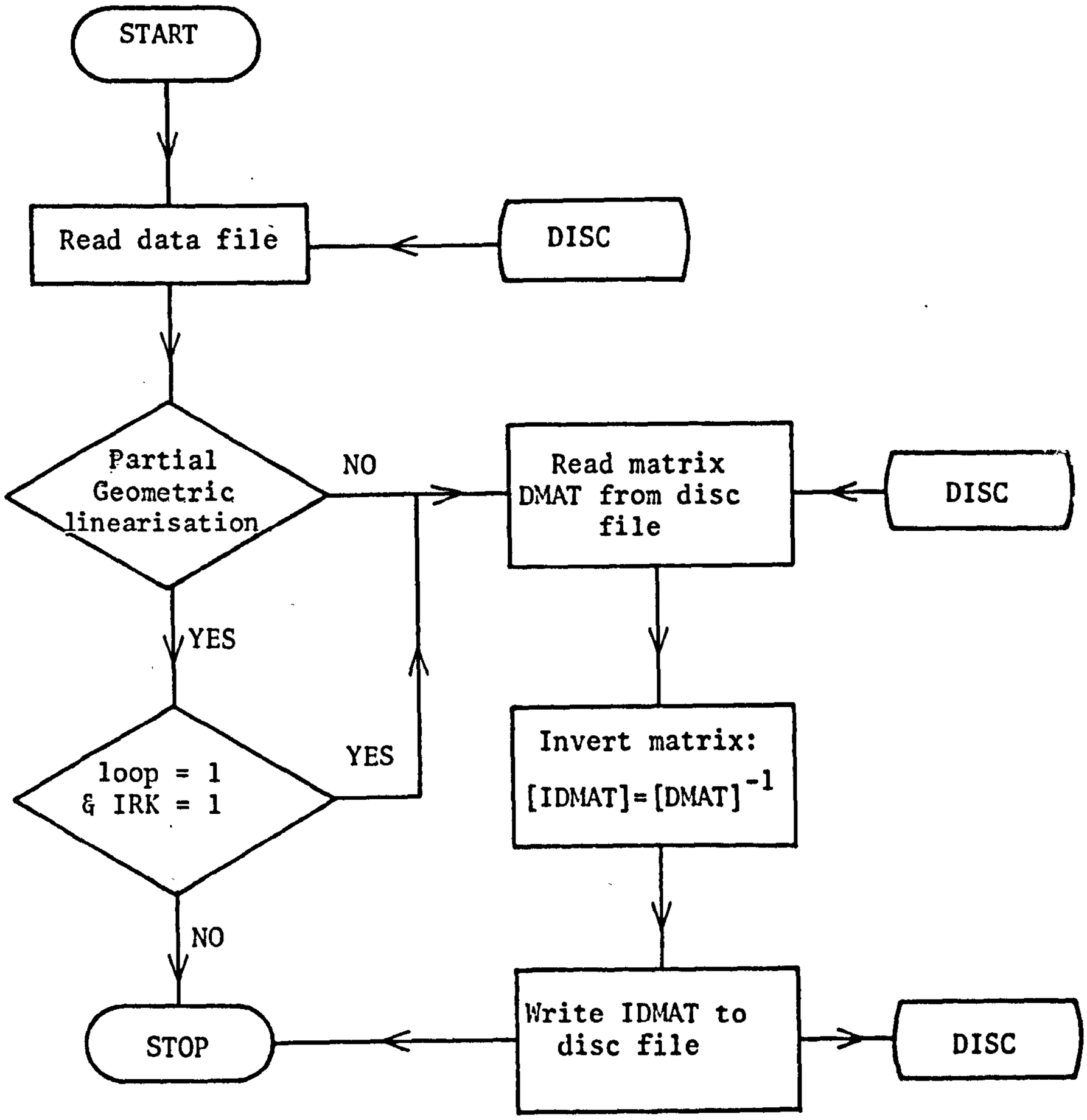

Fig.53. Flow chart for program INVERT

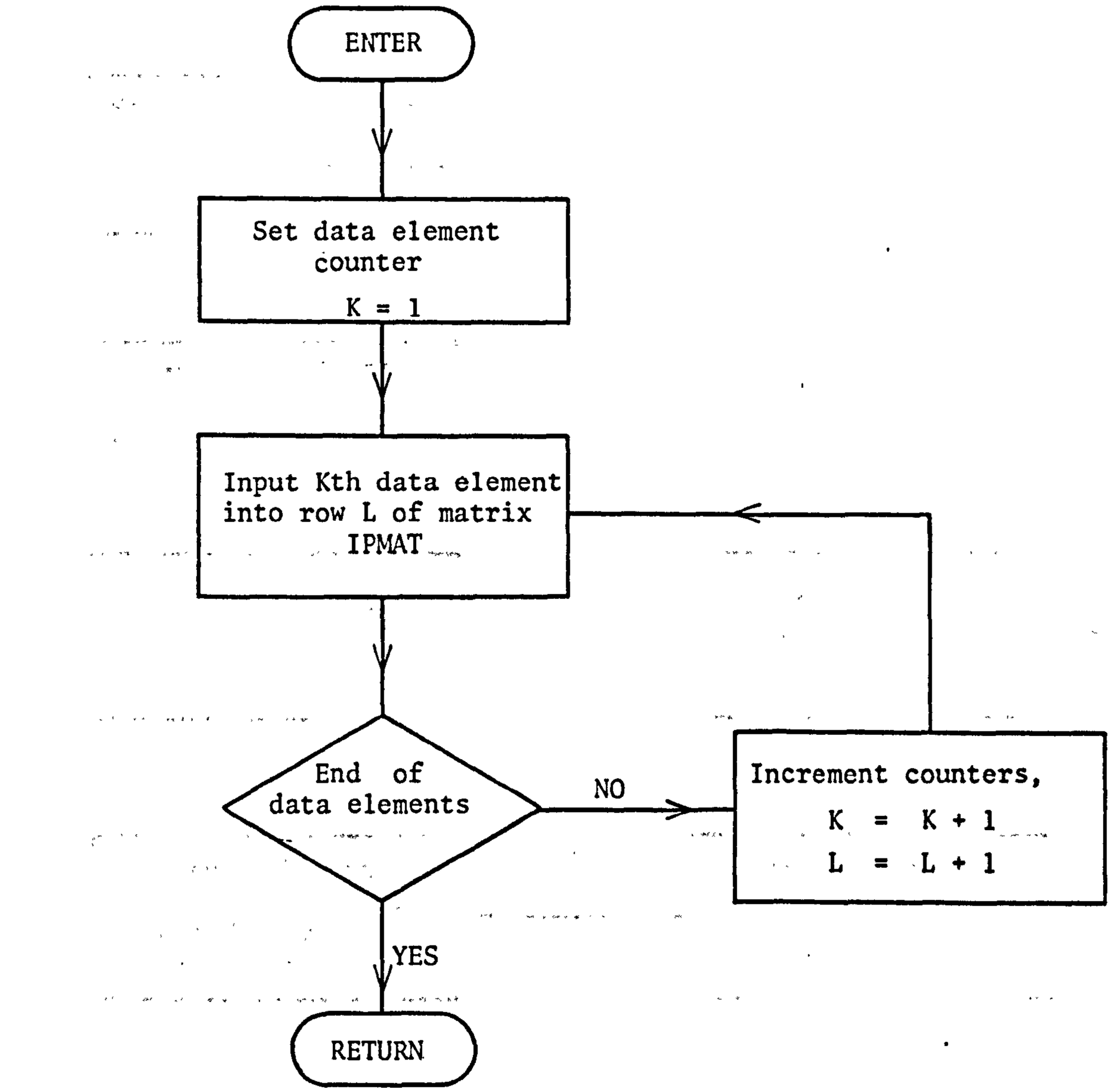

Fig.54. General flow chart for PIPMAT set of subroutines

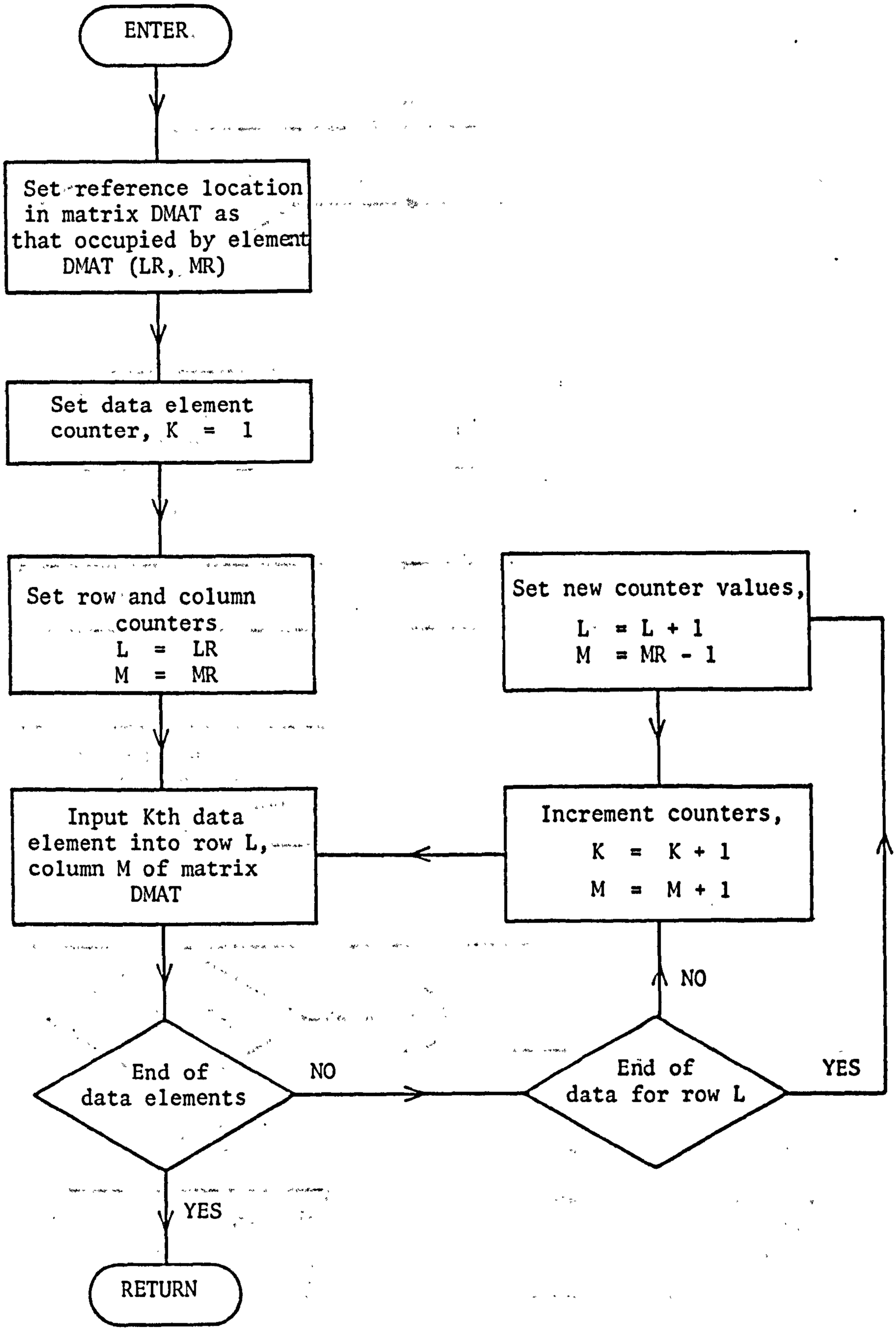

Fig.55.General flow chart for PDMAT set of subroutines

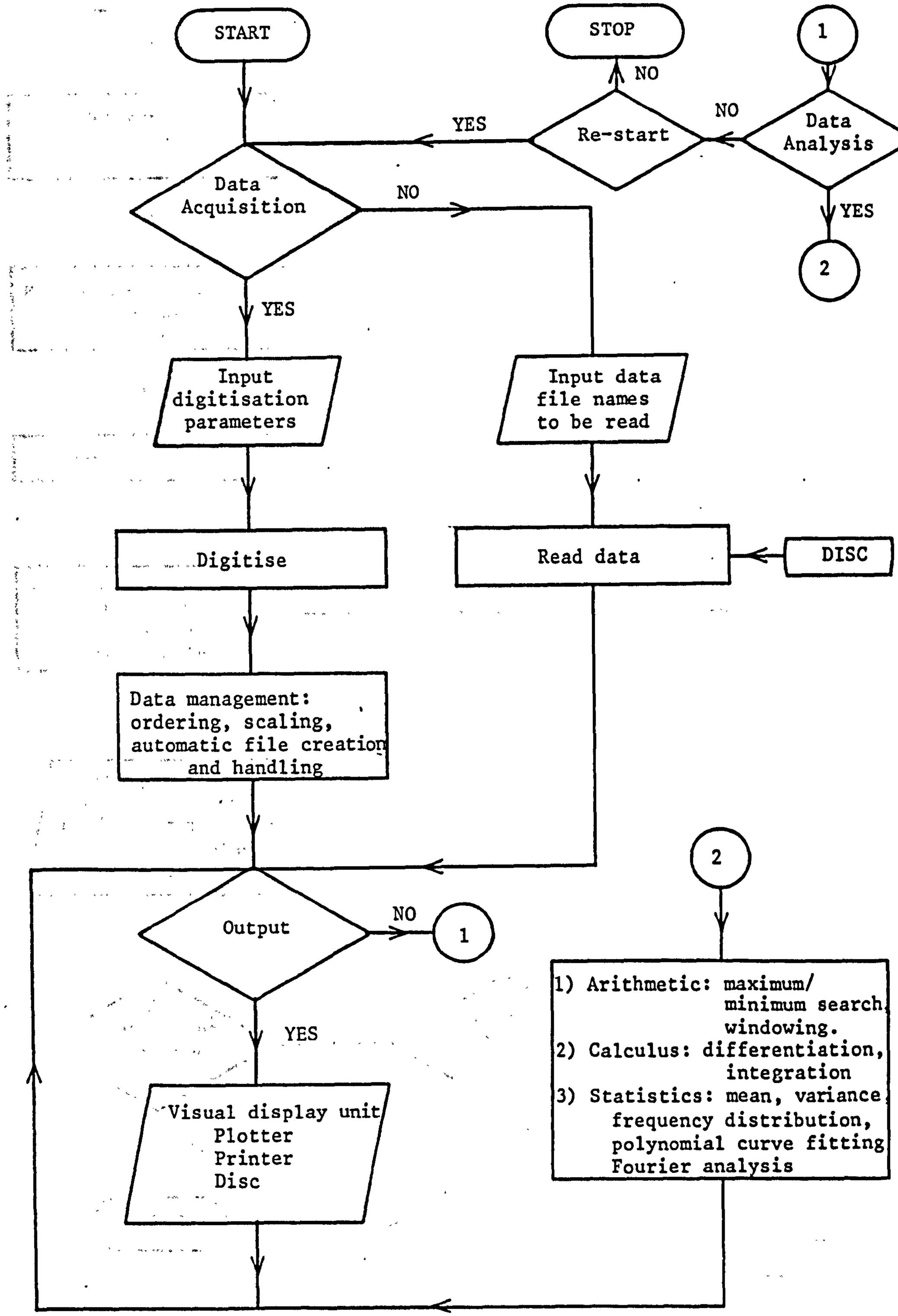

Fig.56. Flow chart for program SCAN

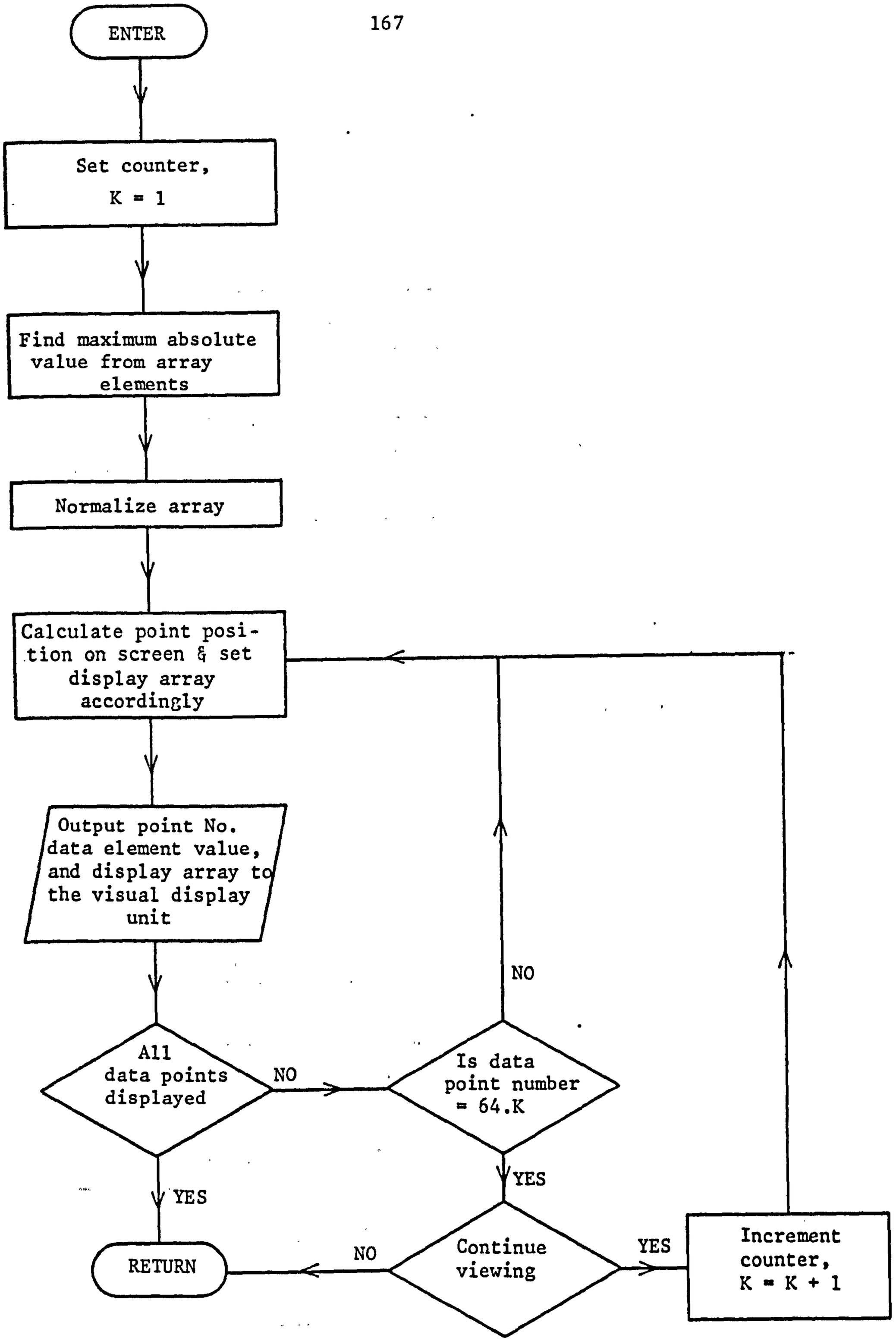

Fig.57 Flow chart for subroutine VIEW

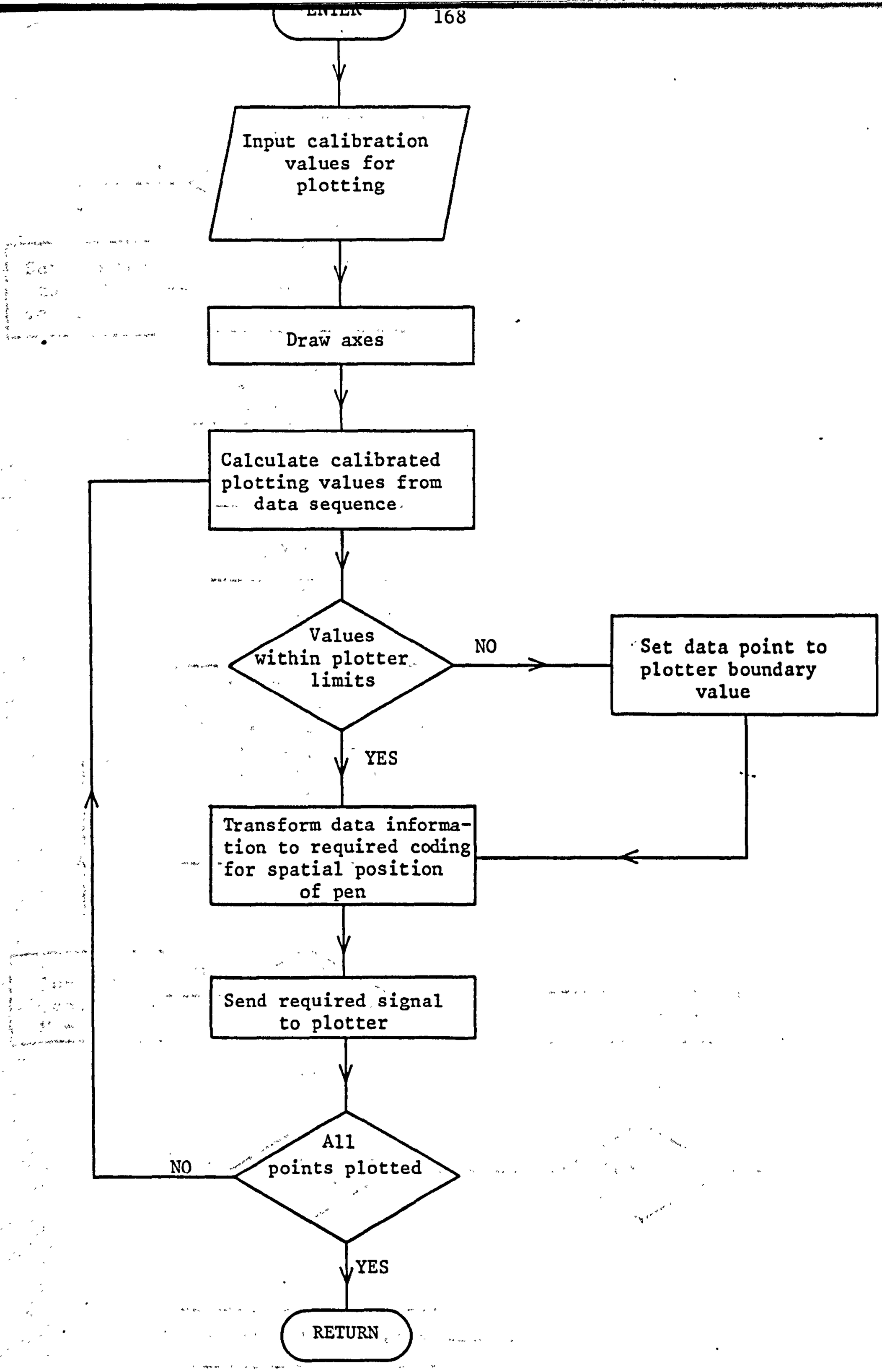

Fig.58 Flow chart for subroutine PLOT

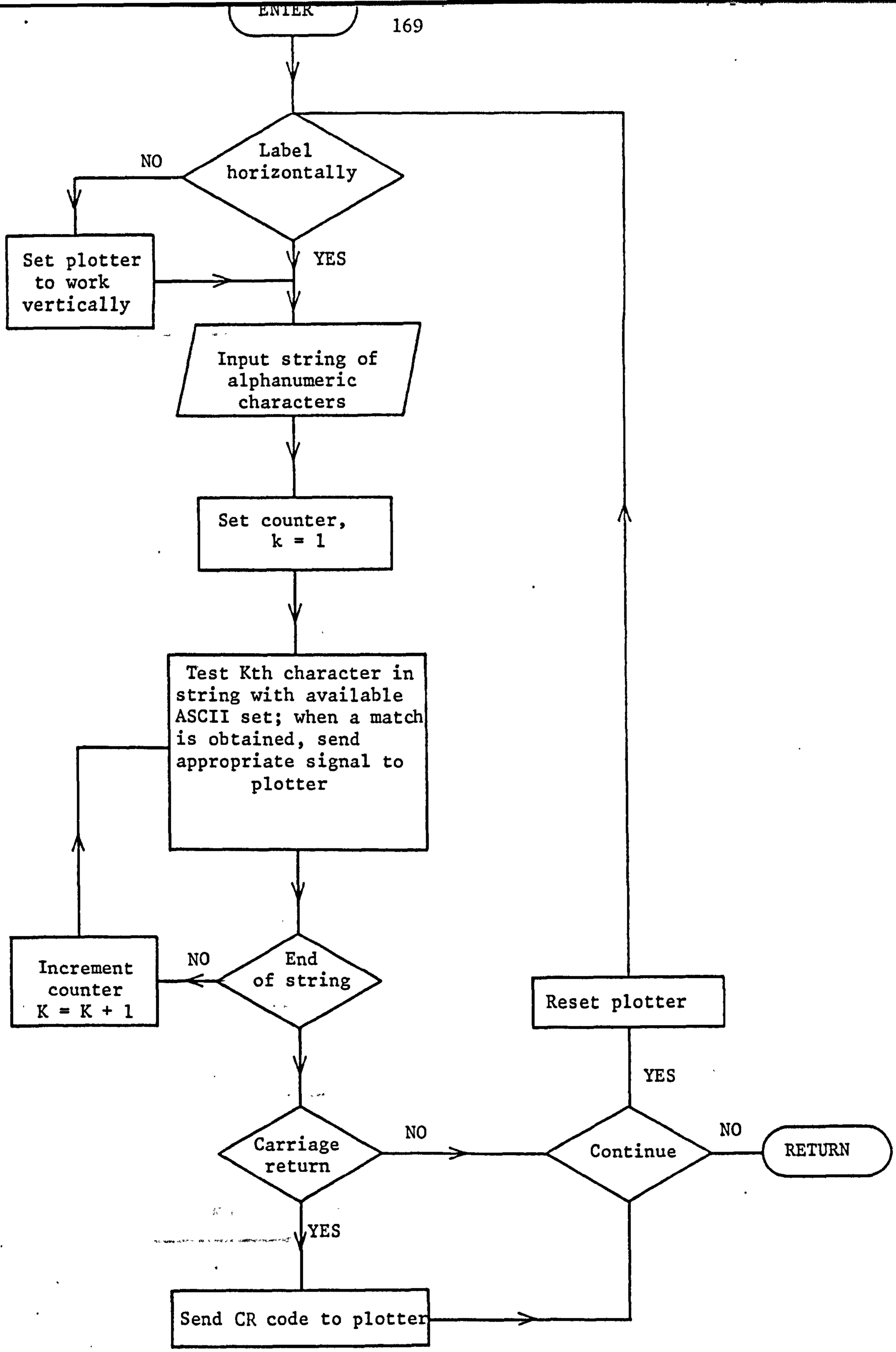

Fig.59 Flow chart for subroutine LABEL

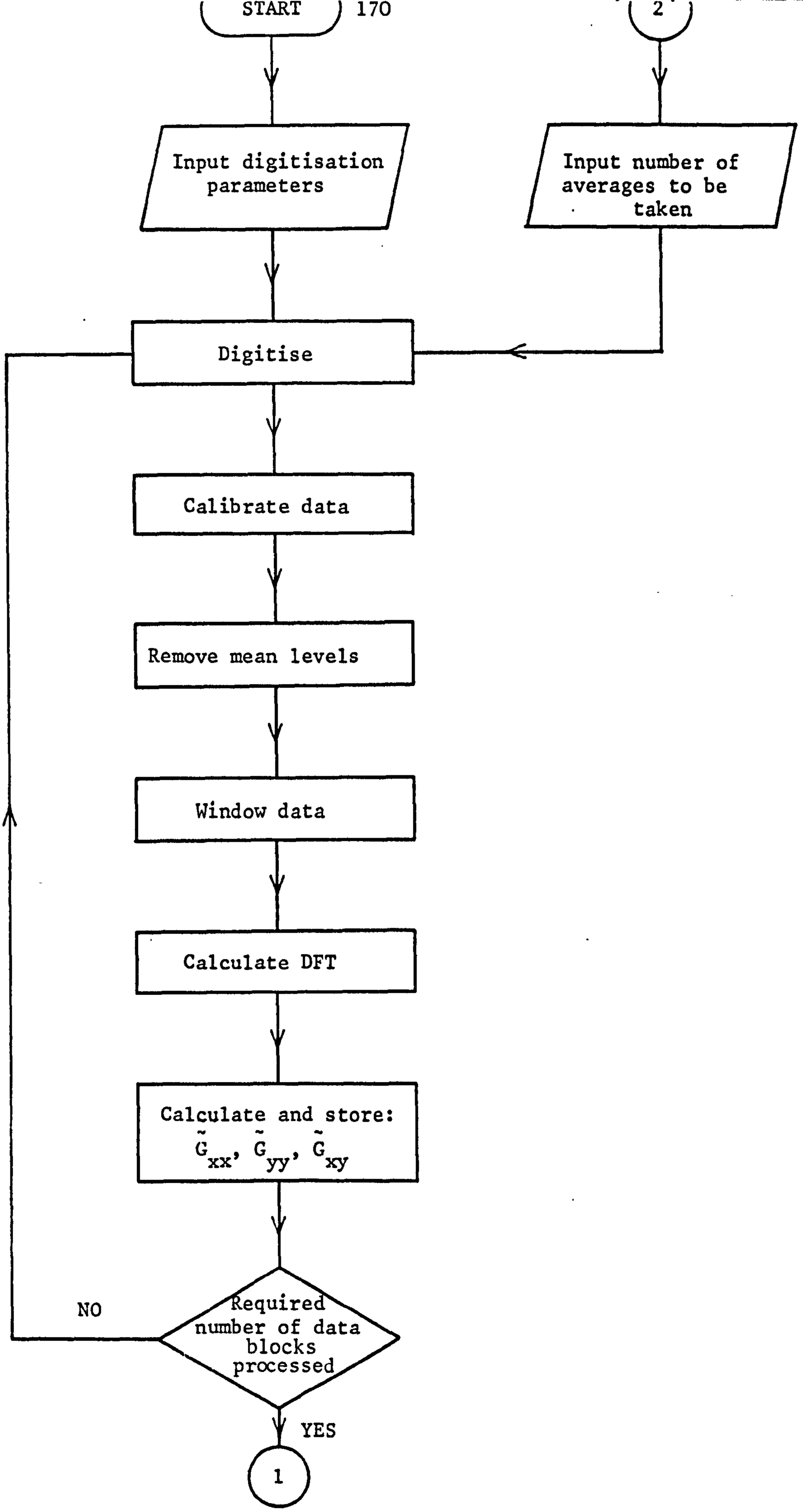

Fig.60 Flow chart for program FRF

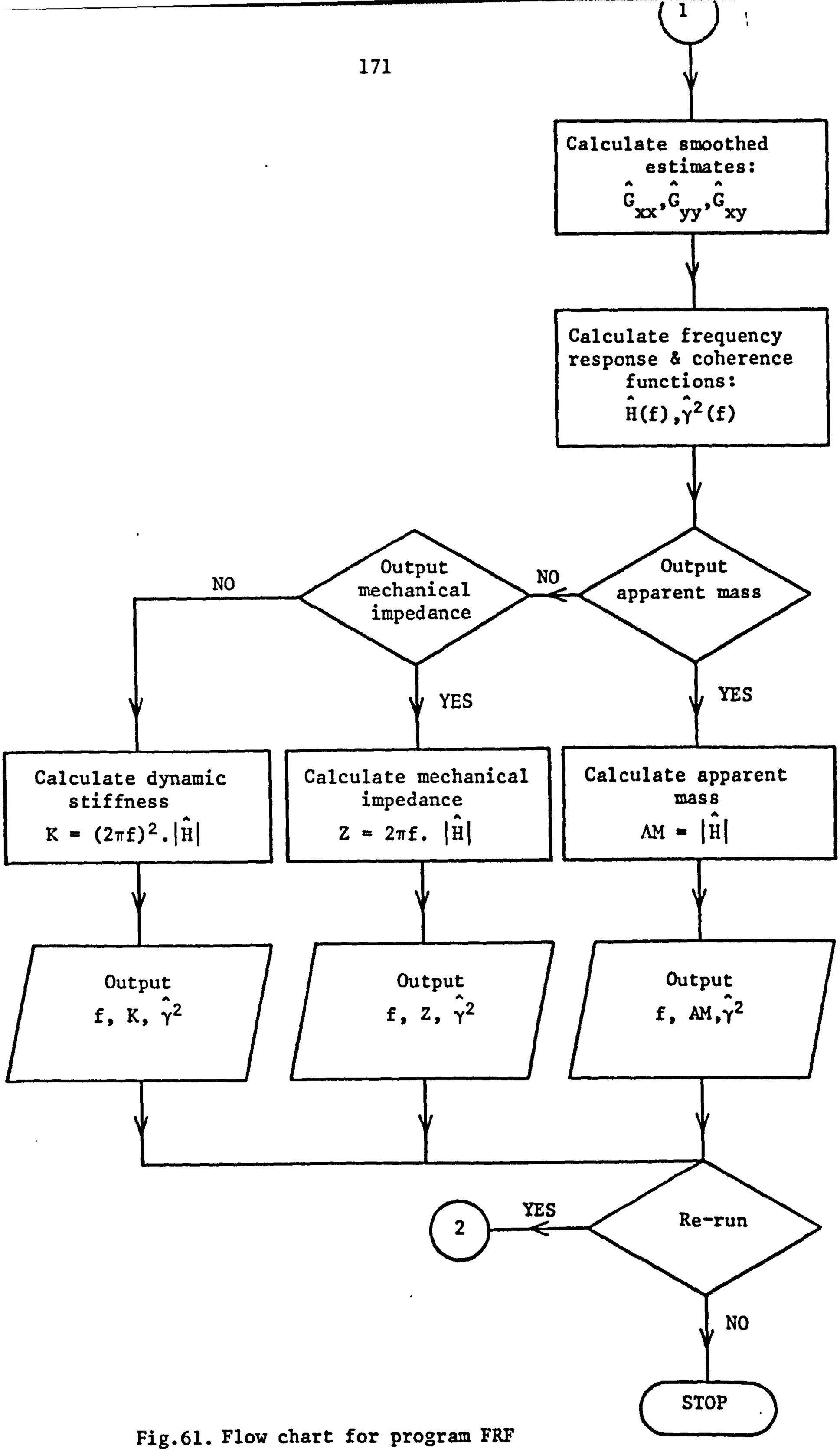

Fig.61. Flow chart for program FRF

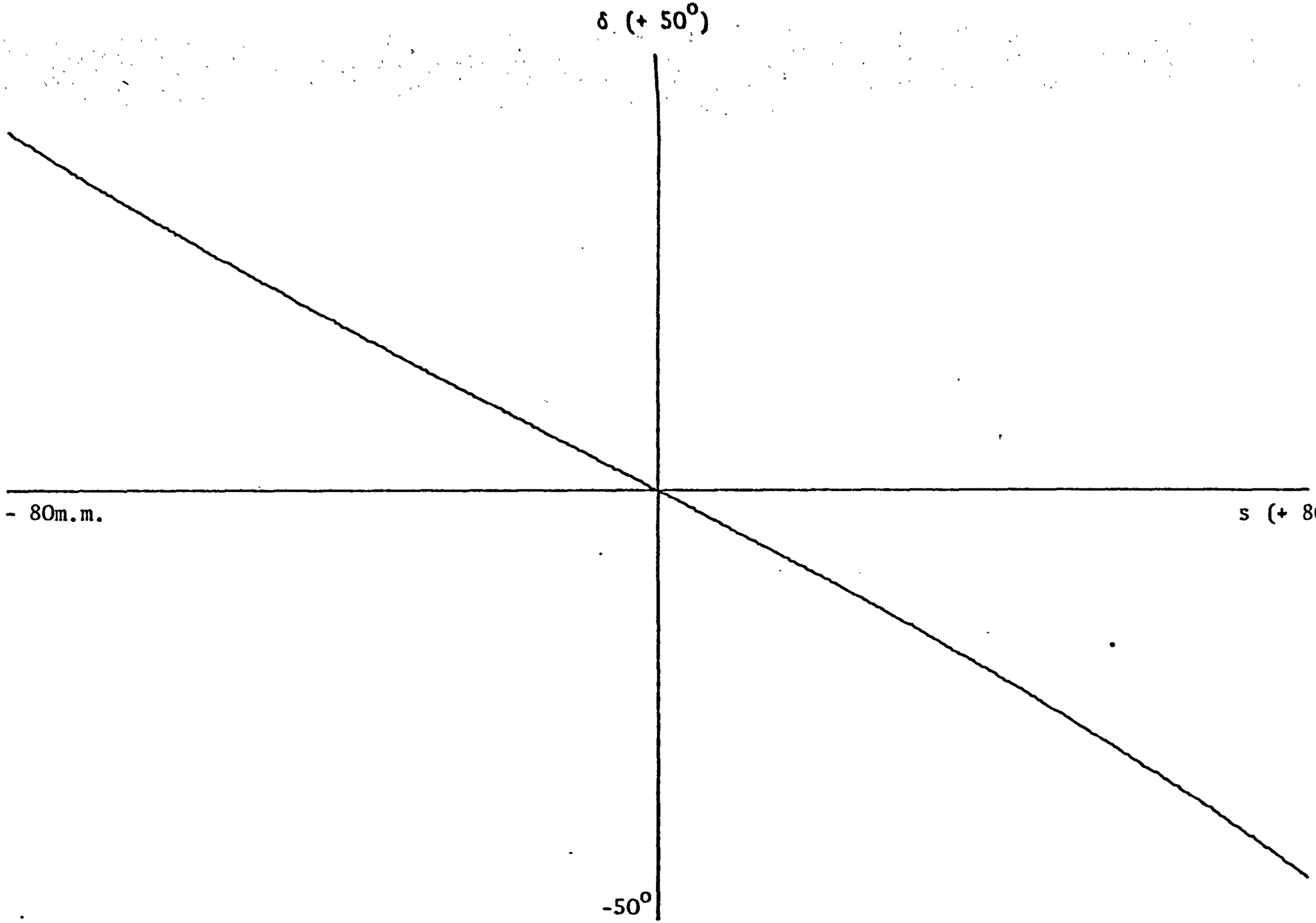

KINEMATIC RELATIONSHIP BETWEEN STEER ANGLE (δ) AND RACK DISPLACEMENT (s) FOR ZERO UPPER WISHBONE LINK ANGLE (ψ = 0)

Fig. 62

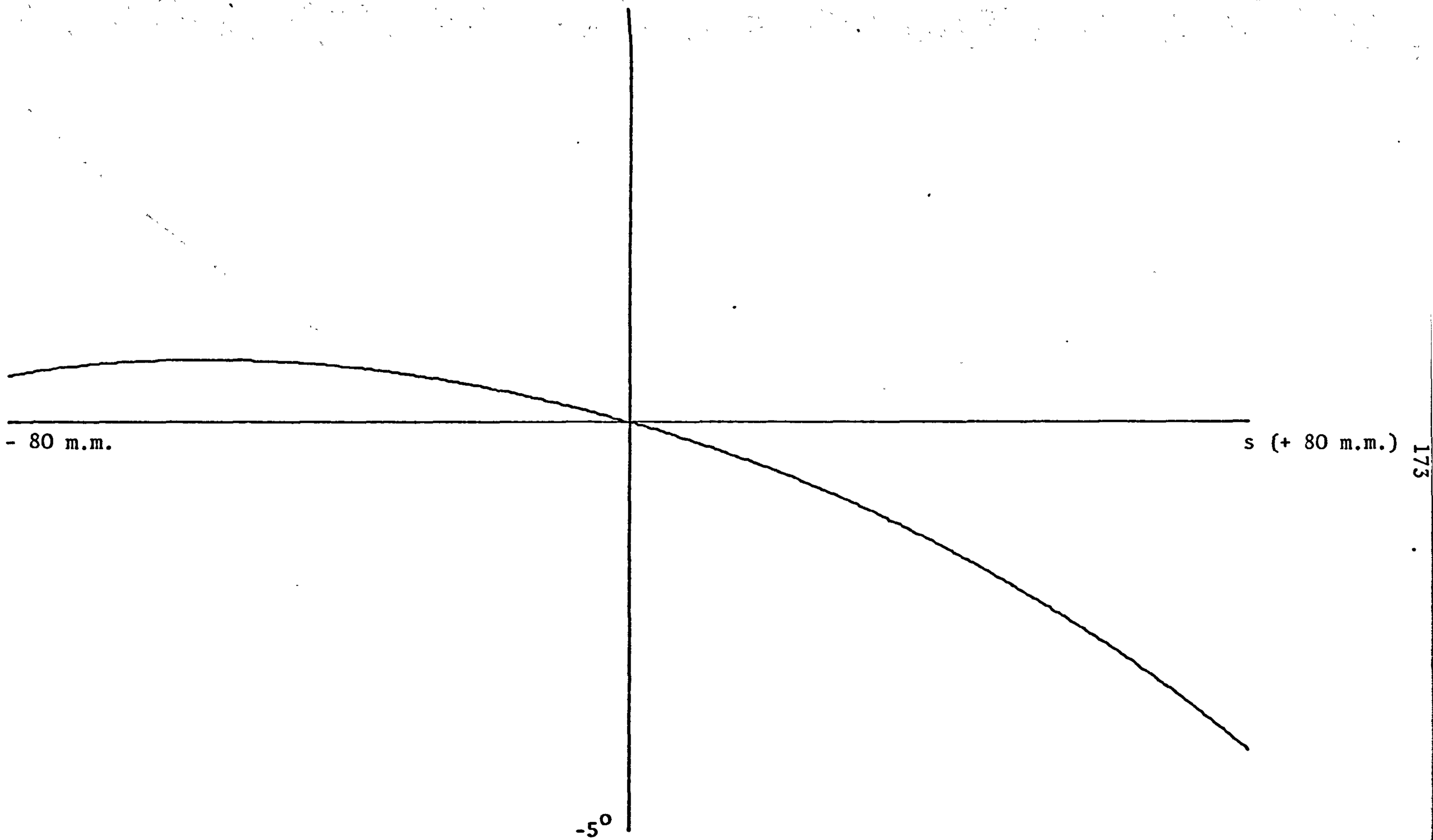

KINEMATIC RELATIONSHIP BETWEEN CAMBER ANGLE (ϕ) AND RACK DISPLACEMENT (s)
FOR ZERO UPPER WISHBONE LINK ANGLE (ψ = 0)

Fig.63

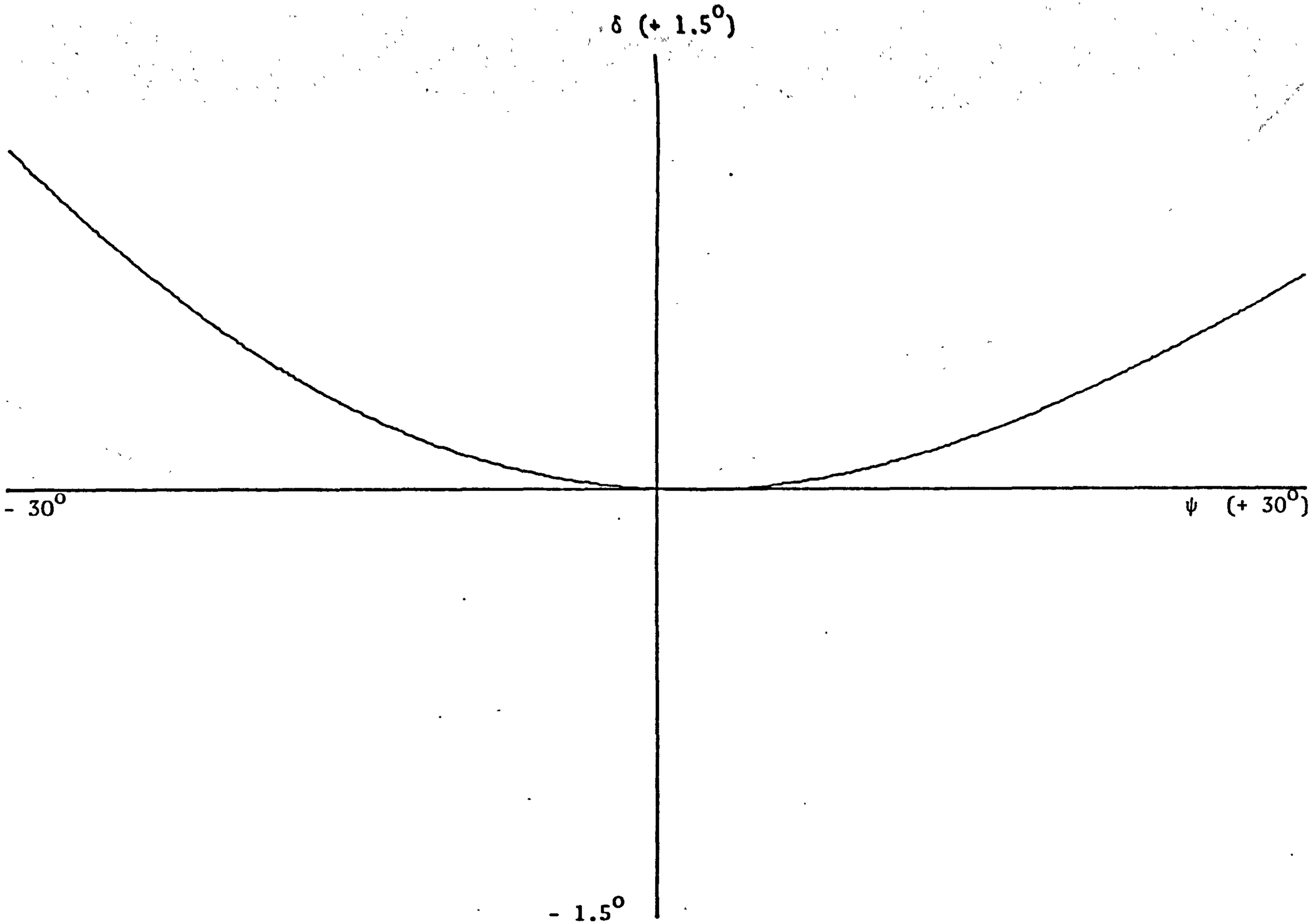

KINEMATIC RELATIONSHIP BETWEEN STEER ANGLE (δ) AND UPPER WISHBONE LINK ANGLE (ψ)
FOR ZERO RACK DISPLACEMENT (s = 0)

Fig.64

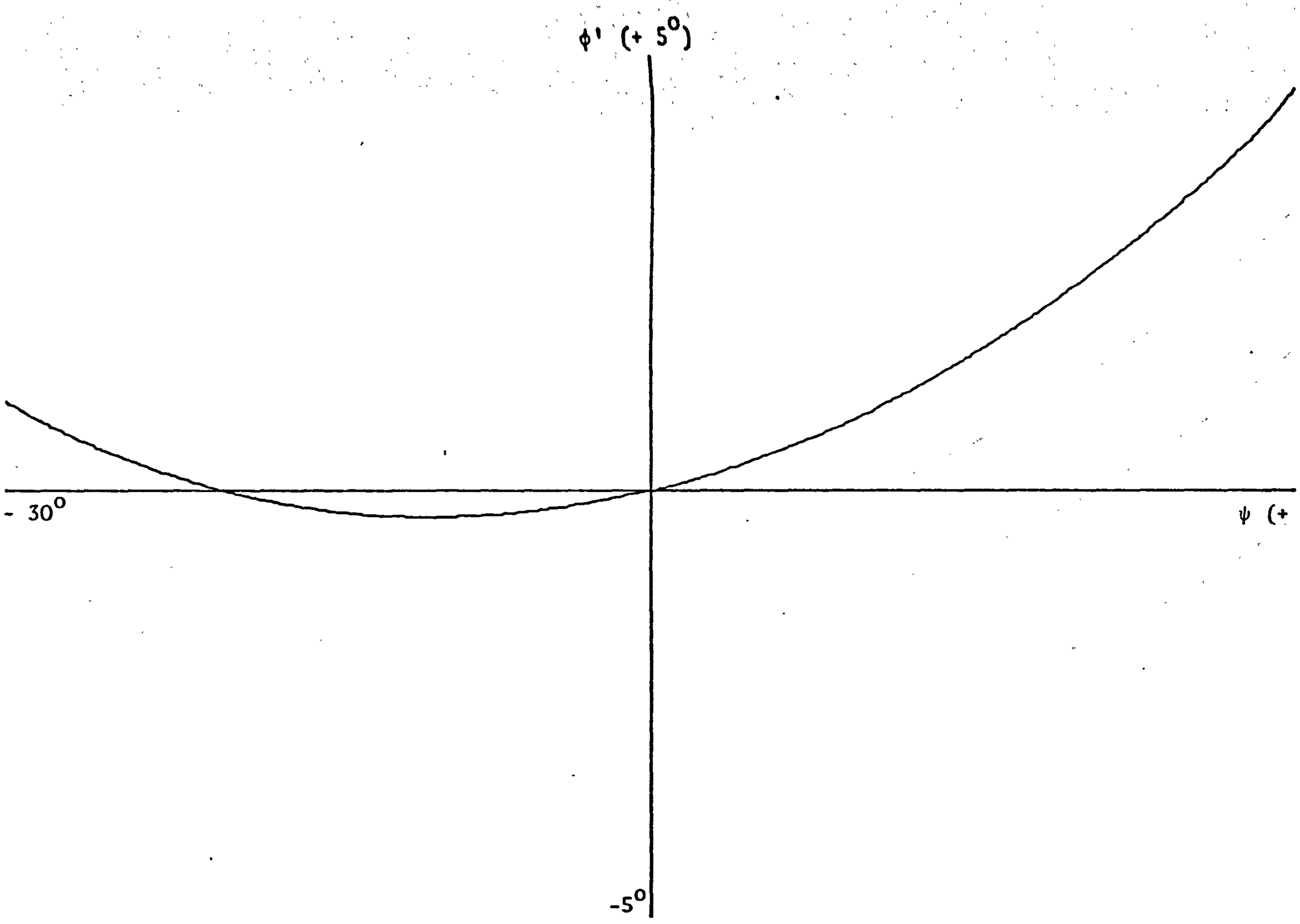

KINEMATIC RELATIONSHIP BETWEEN CAMBER ANGLE (ϕ') AND UPPER WISHBONE LINK ANGLE (ψ) FOR ZERO RACK DISPLACEMENT (s = 0)
Fig.65

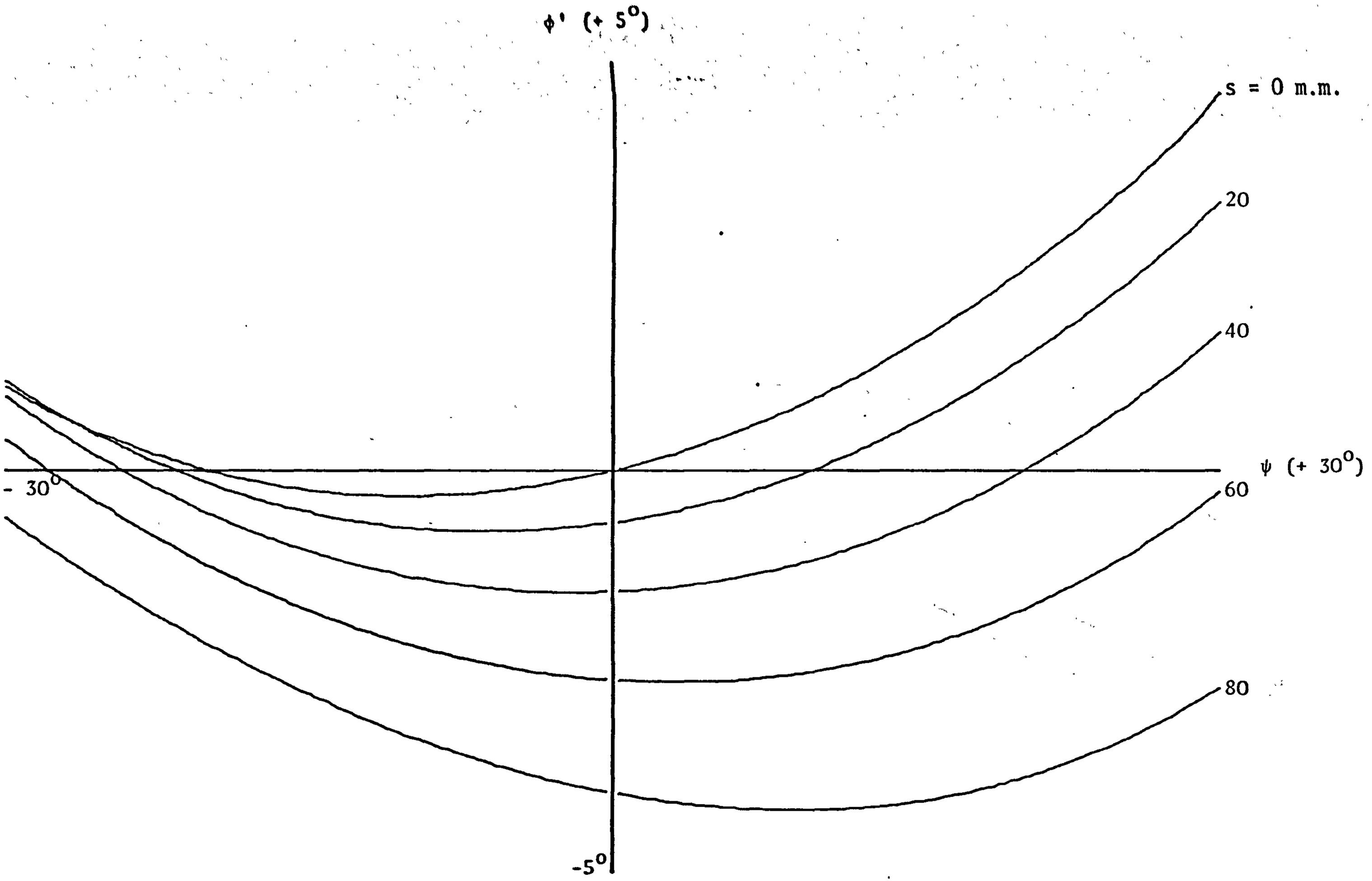

KINEMATIC RELATIONSHIP BETWEEN CAMBER ANGLE (ϕ') AND UPPER WISHBONE LINK ANGLE (ψ) FOR VARIOUS FIXED RACK DISPLACEMENT VALUES.

Fig.66

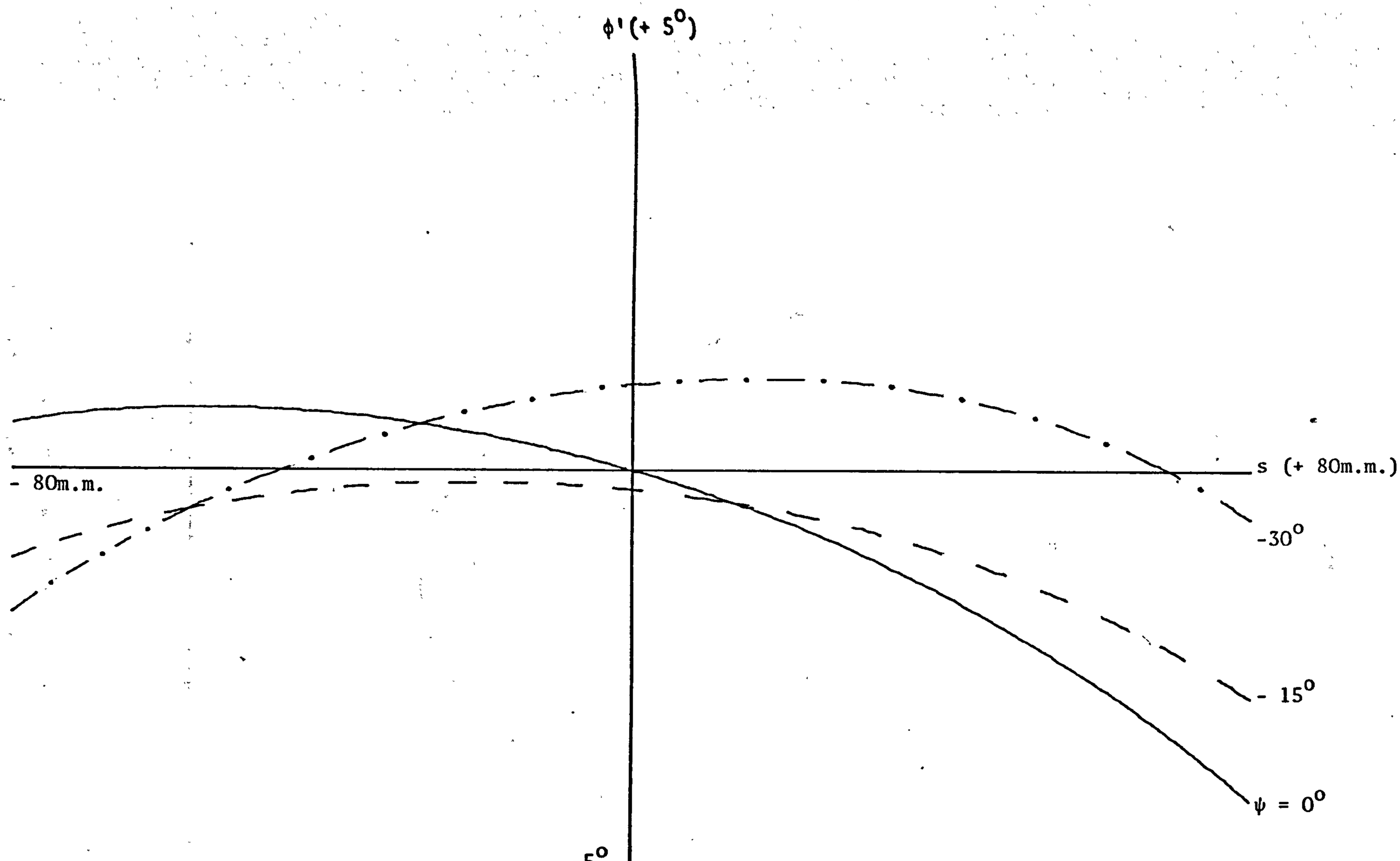

KINEMATIC RELATIONSHIP BETWEEN CAMBER ANGLE (ϕ') AND RACK DISPLACEMENT (s)
FOR VARIOUS FIXED UPPER WISHBONE LINK ANGLE VALUES

Fig. 67

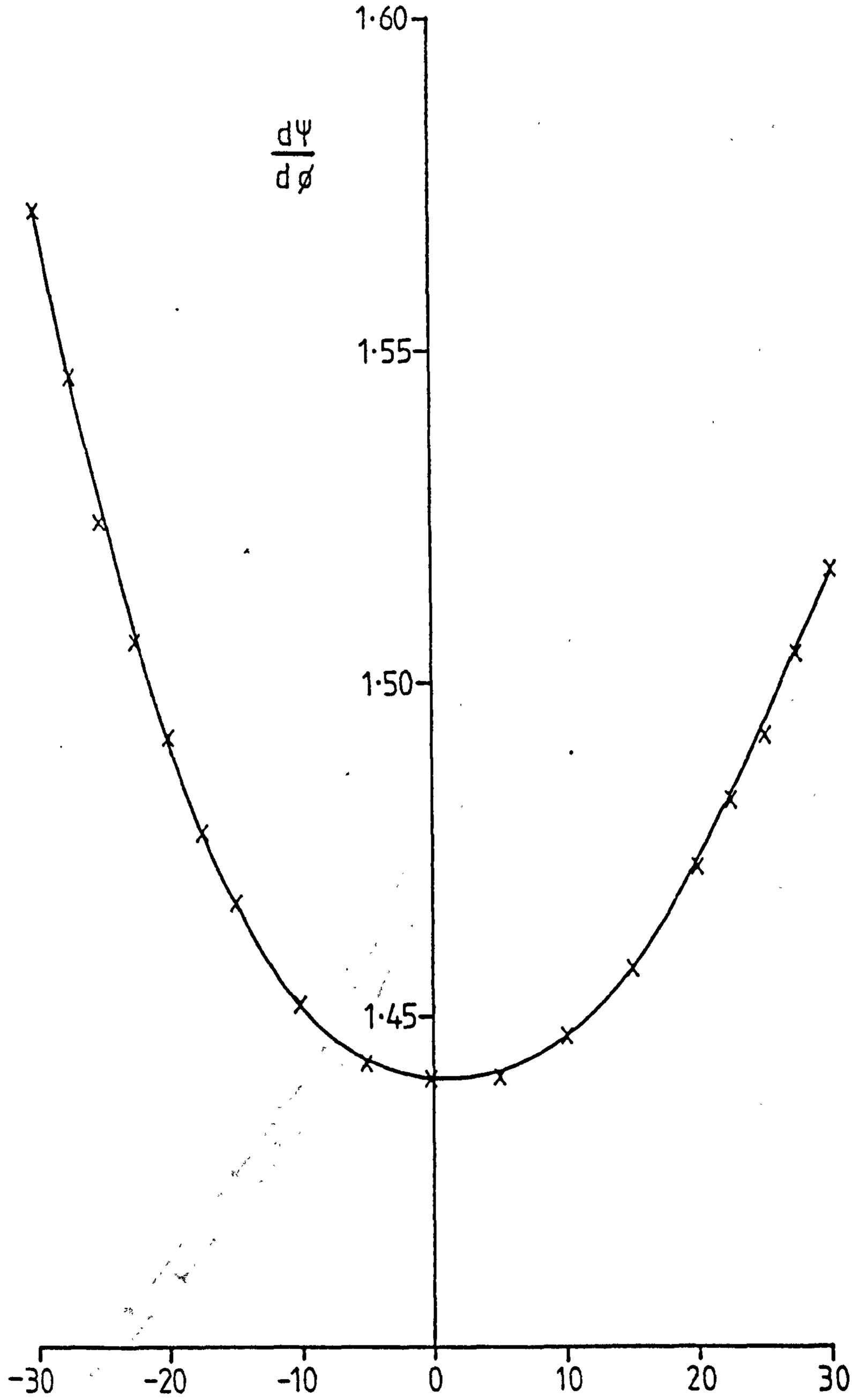

Rate of change of upper wishbone link angle (ψ) with respect to lower link angle (ϕ) as a function of the mechanism orientation.

Fig. 68

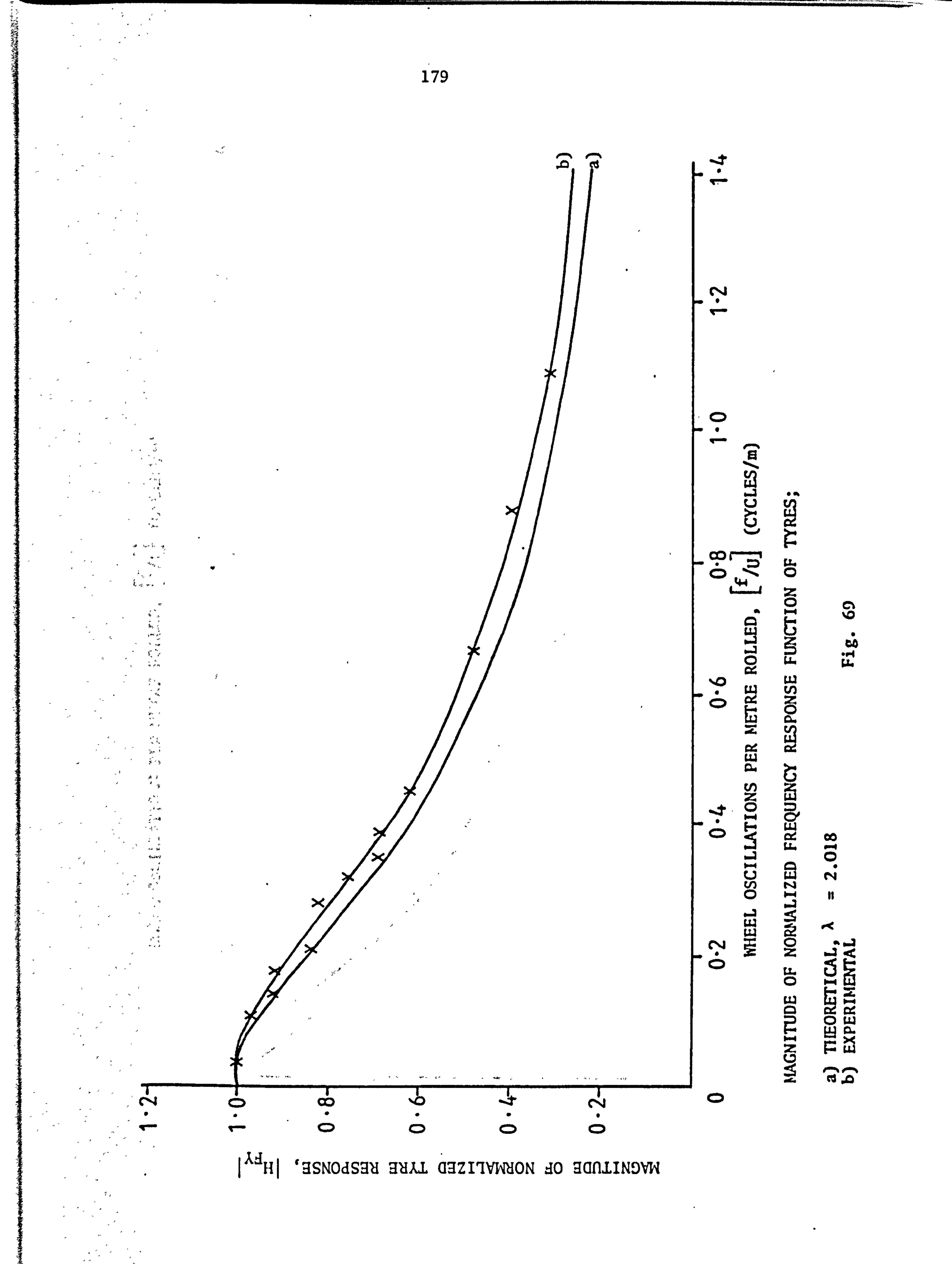

MAGNITUDE OF NORMALIZED FREQUENCY RESPONSE FUNCTION OF TYRES;
a) THEORETICAL, $\lambda = 2.018$
b) EXPERIMENTAL

Fig. 69

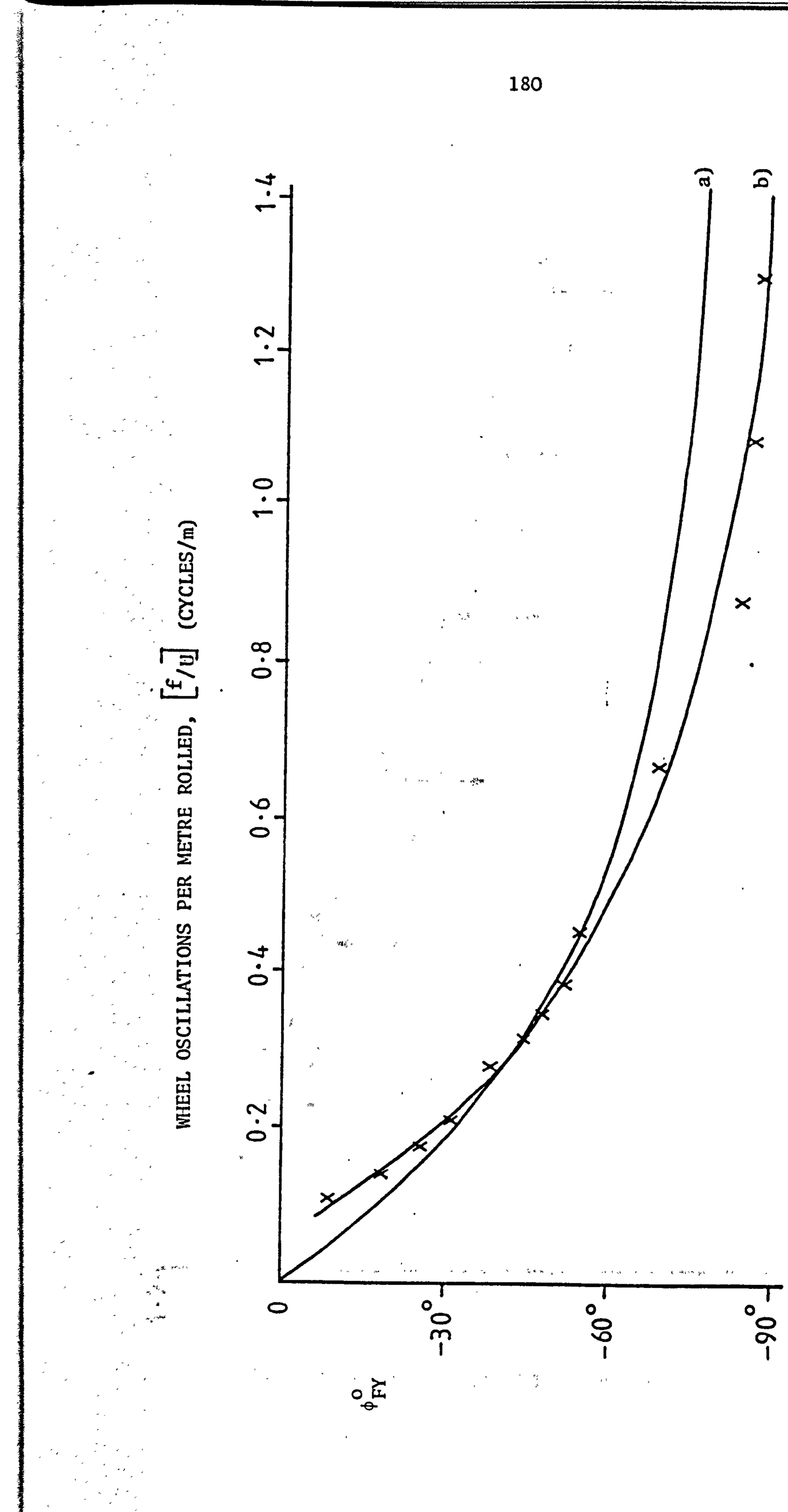
WHEEL OSCILLATIONS PER METRE ROLLED, $\left[\frac{f}{v}\right]$ (CYCLES/m)
0·2
0·4
0·6
0·8
1·0
1·2
1·4
0
−30°
−60°
−90°
ϕ_{FY}^{o}
a)
b)
x
PHASE OF NORMALIZED FREQUENCY RESPONSE FUNCTION OF TYRE;
a) THEORETICAL, λ = 2.018
b) EXPERIMENTAL

Fig. 70

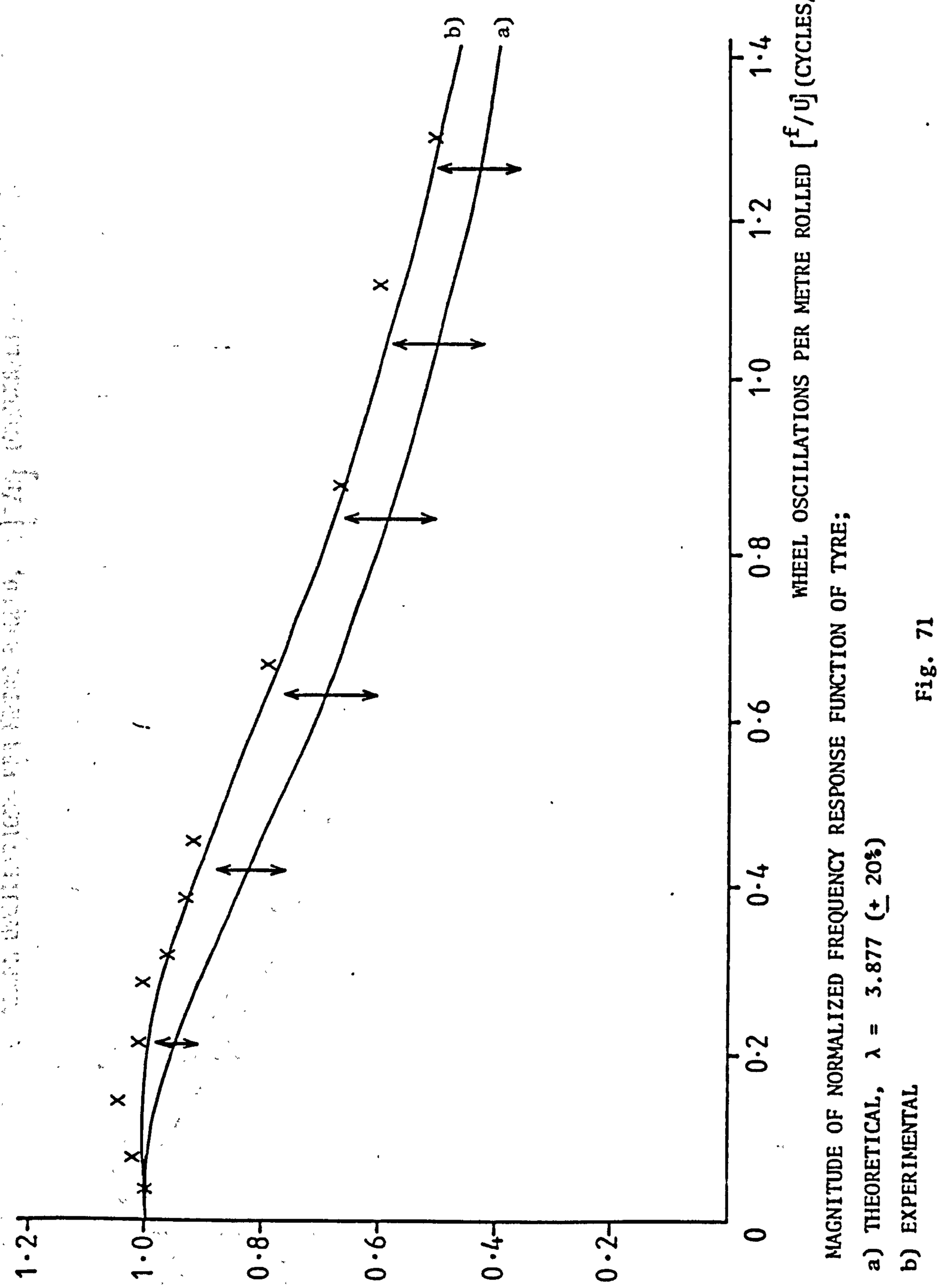

MAGNITUDE OF NORMALIZED FREQUENCY RESPONSE FUNCTION OF TYRE;
a) THEORETICAL, λ = 3.877 (± 20%)
b) EXPERIMENTAL

Fig. 71

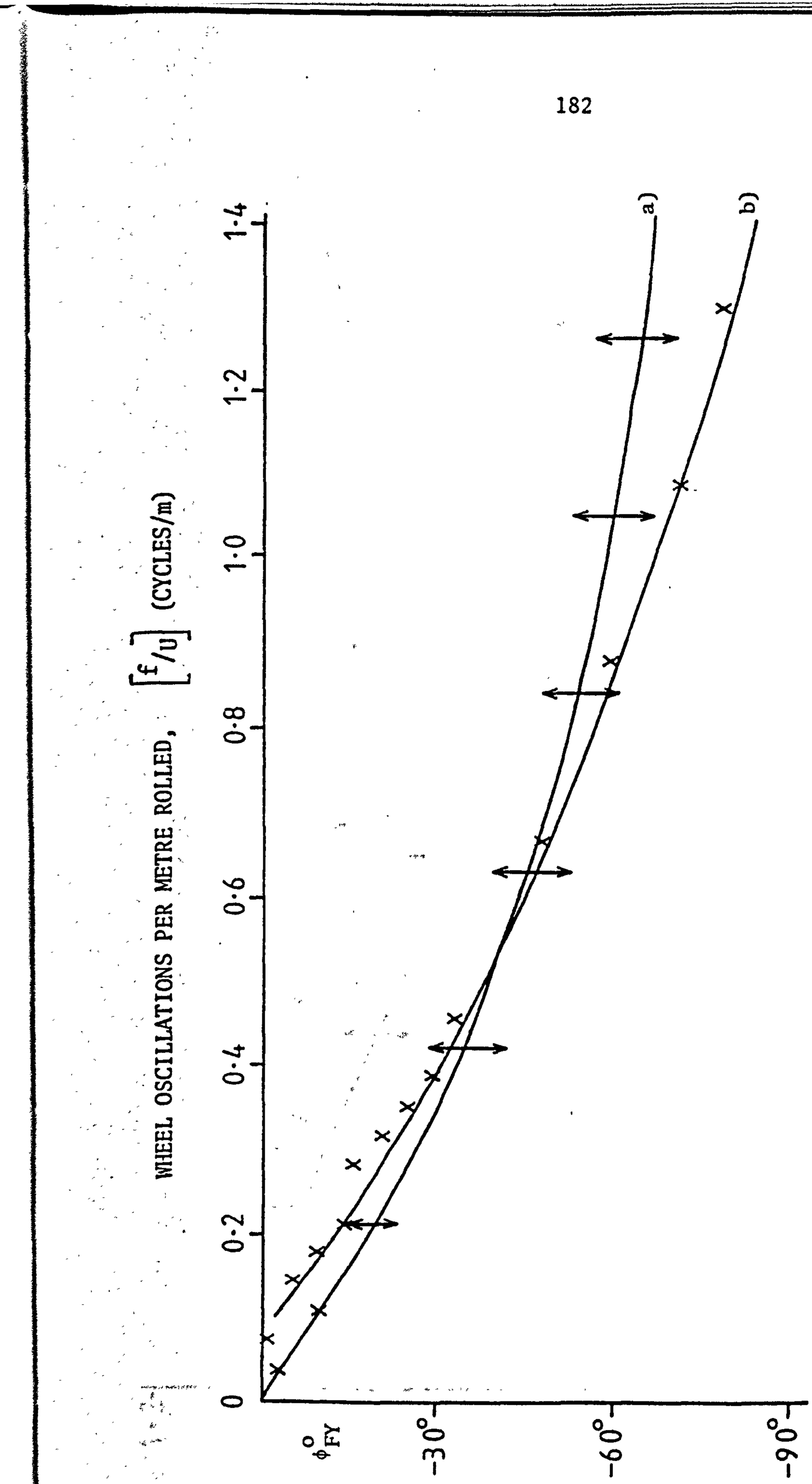

PHASE OF NORMALIZED FREQUENCY RESPONSE FUNCTION OF TYRE;

a) THEORETICAL, λ = 3.877 (± 20%),

b) EXPERIMENTAL

Fig. 72

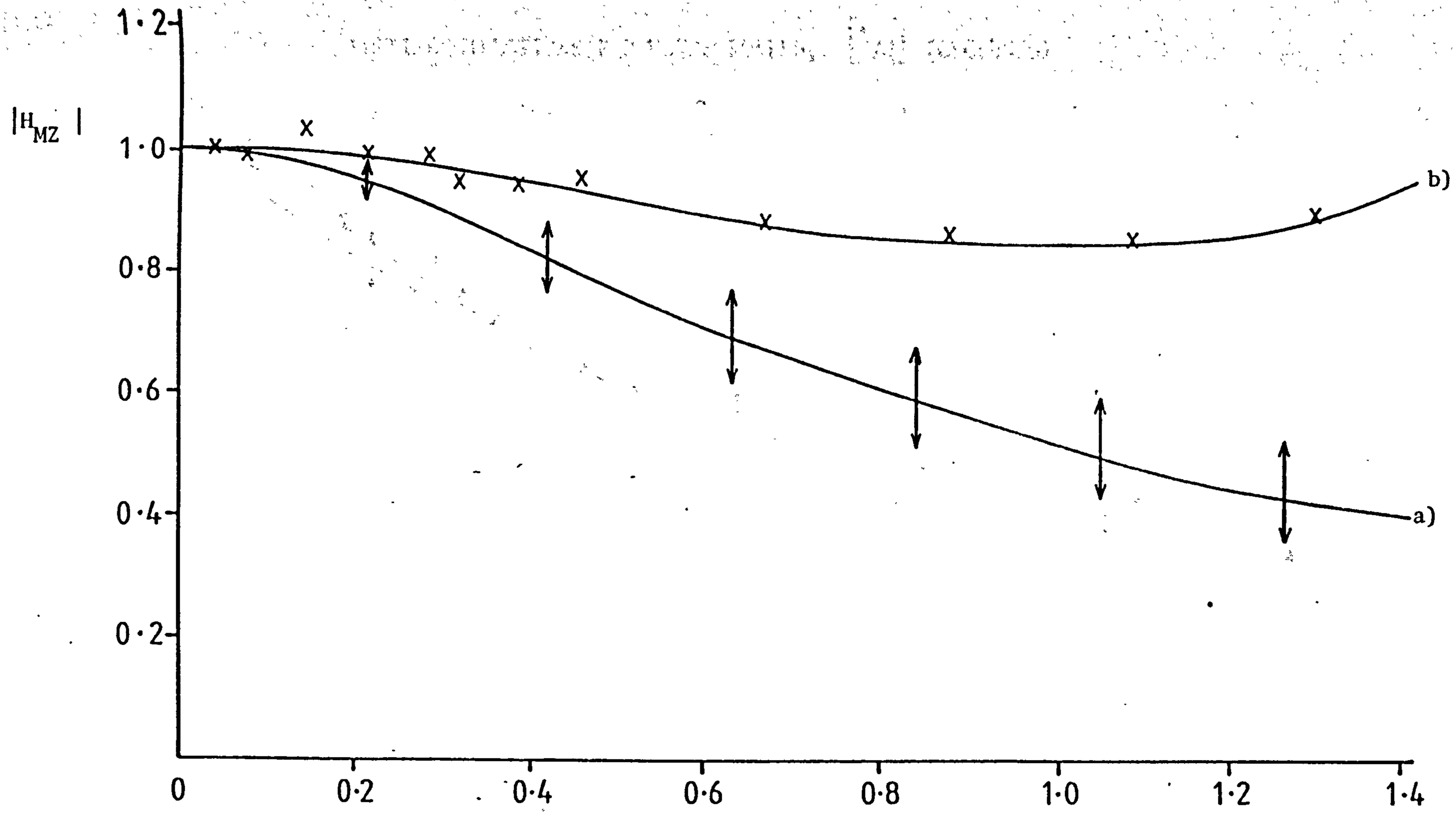

MAGNITUDE OF NORMALIZED FREQUENCY RESPONSE FUNCTION OF TYRE;

a) THEORETICAL, $\lambda = 3.877$ ($\pm$ 20%)

b) EXPERIMENTAL

Fig. 73

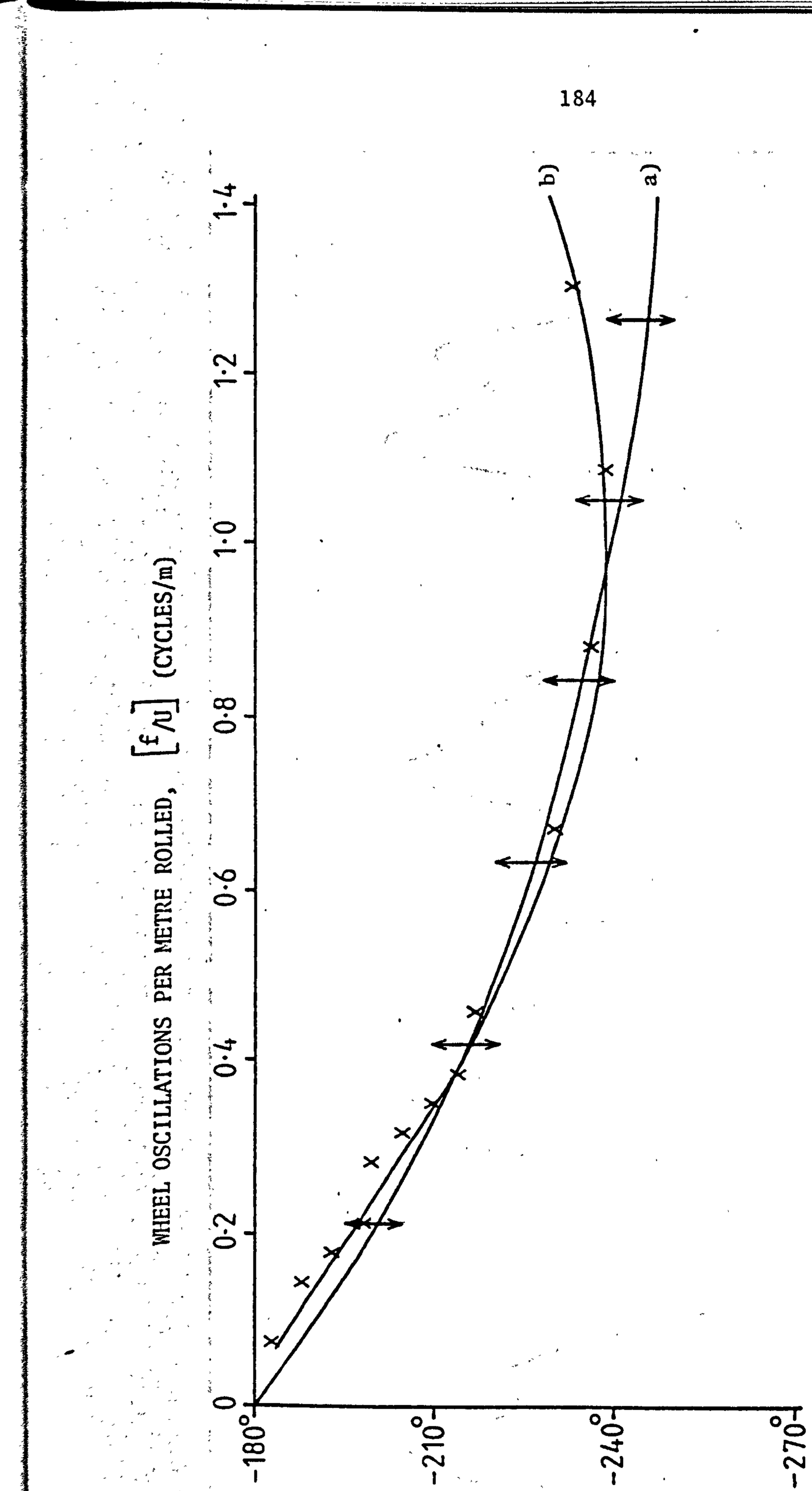

PHASE OF NORMALIZED FREQUENCY RESPONSE FUNCTION OF TYRE;

a) THEORETICAL, λ = 3.877 (± 20%)

b) EXPERIMENTAL

Fig. 74

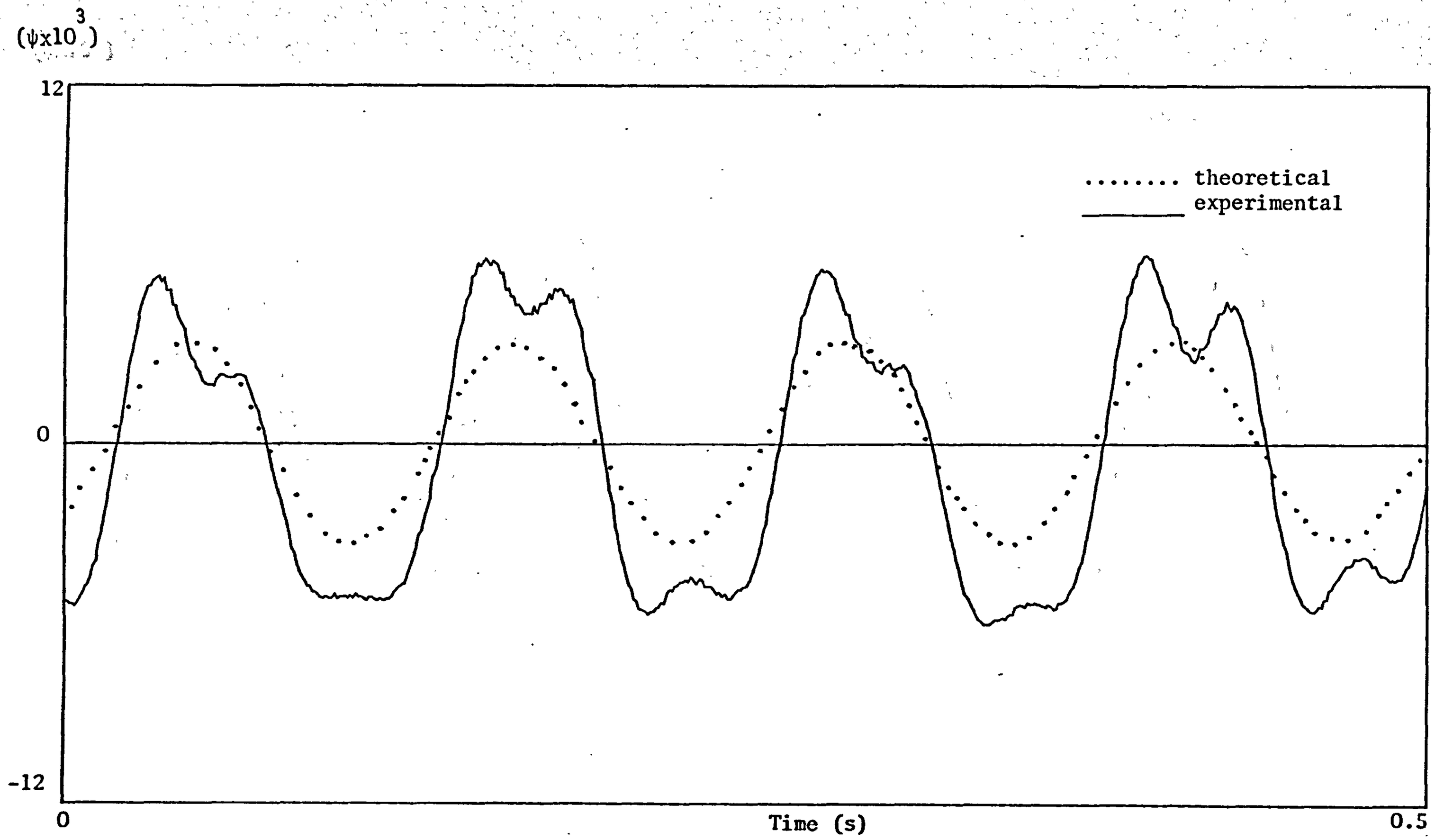

Fig. 75

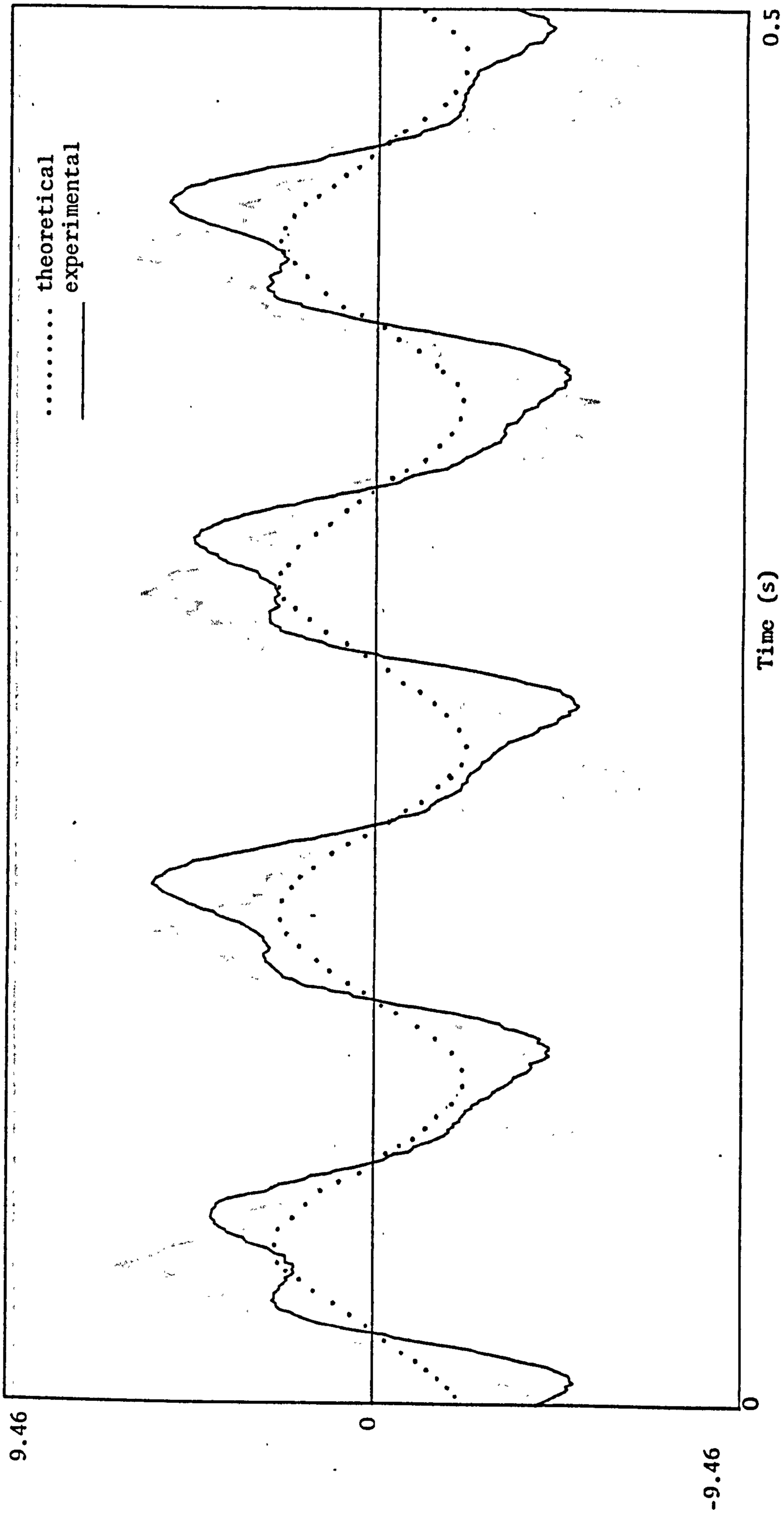

Fig. 76

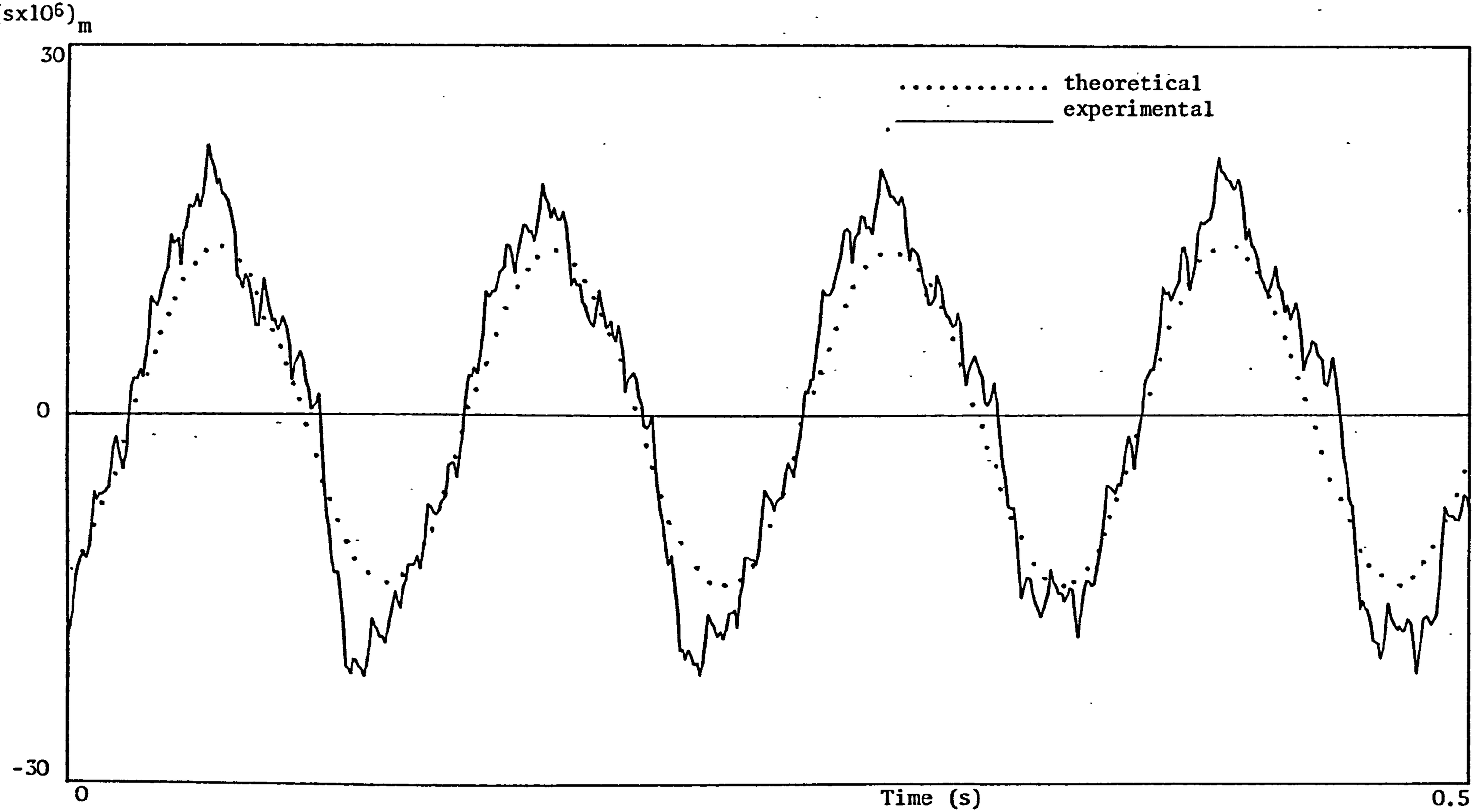

Fig. 77

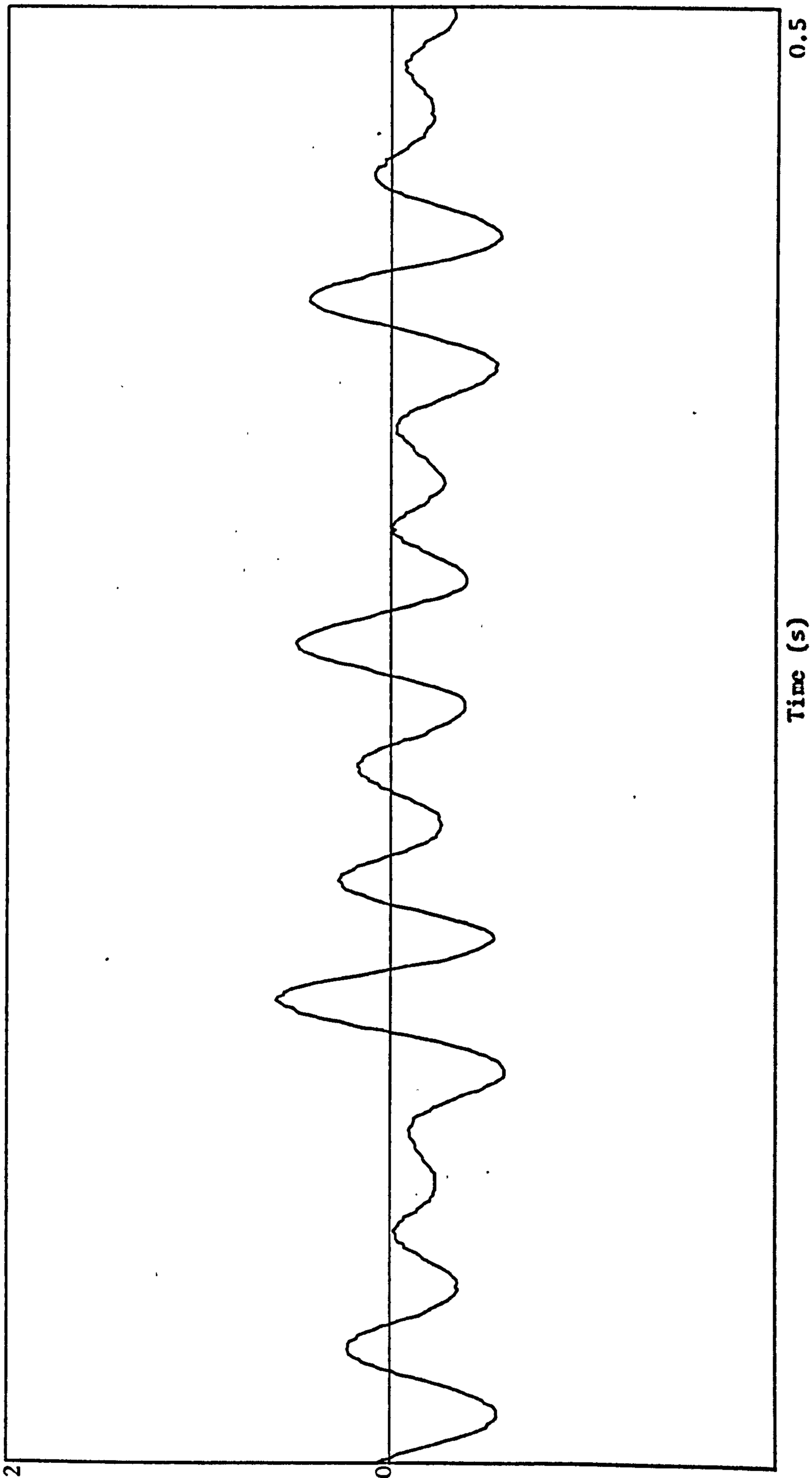

Fig. 78

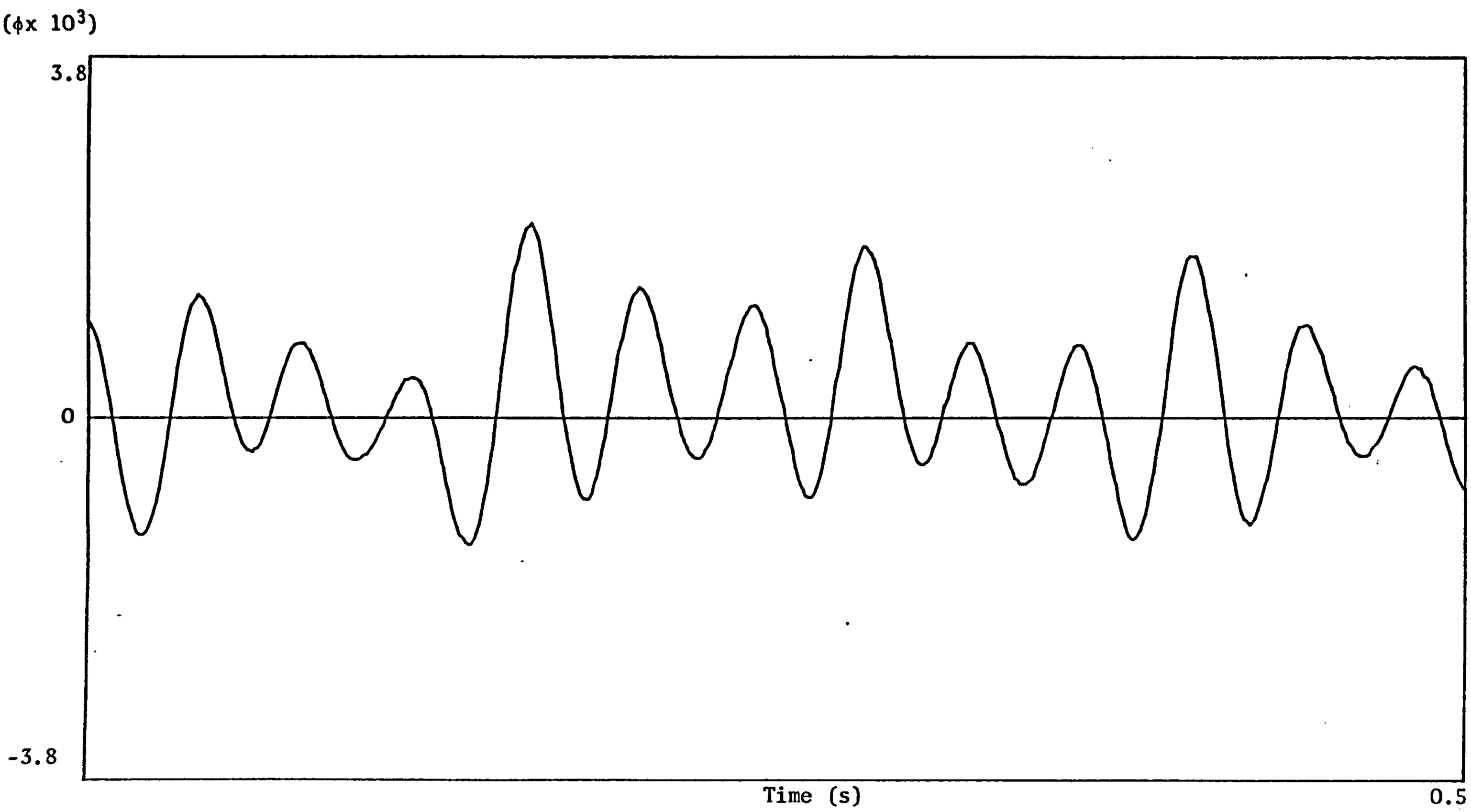

Fig. 79

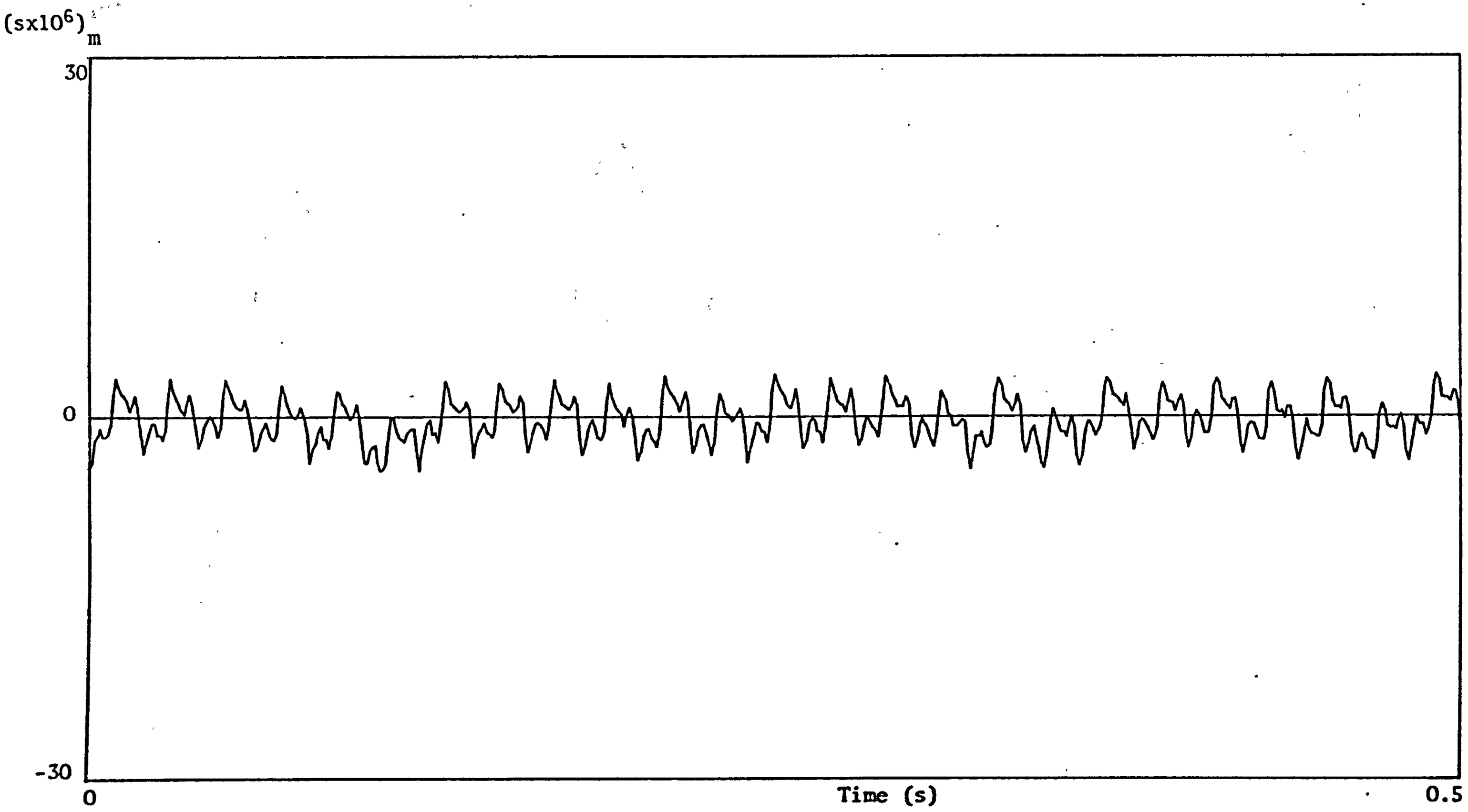

Fig. 80

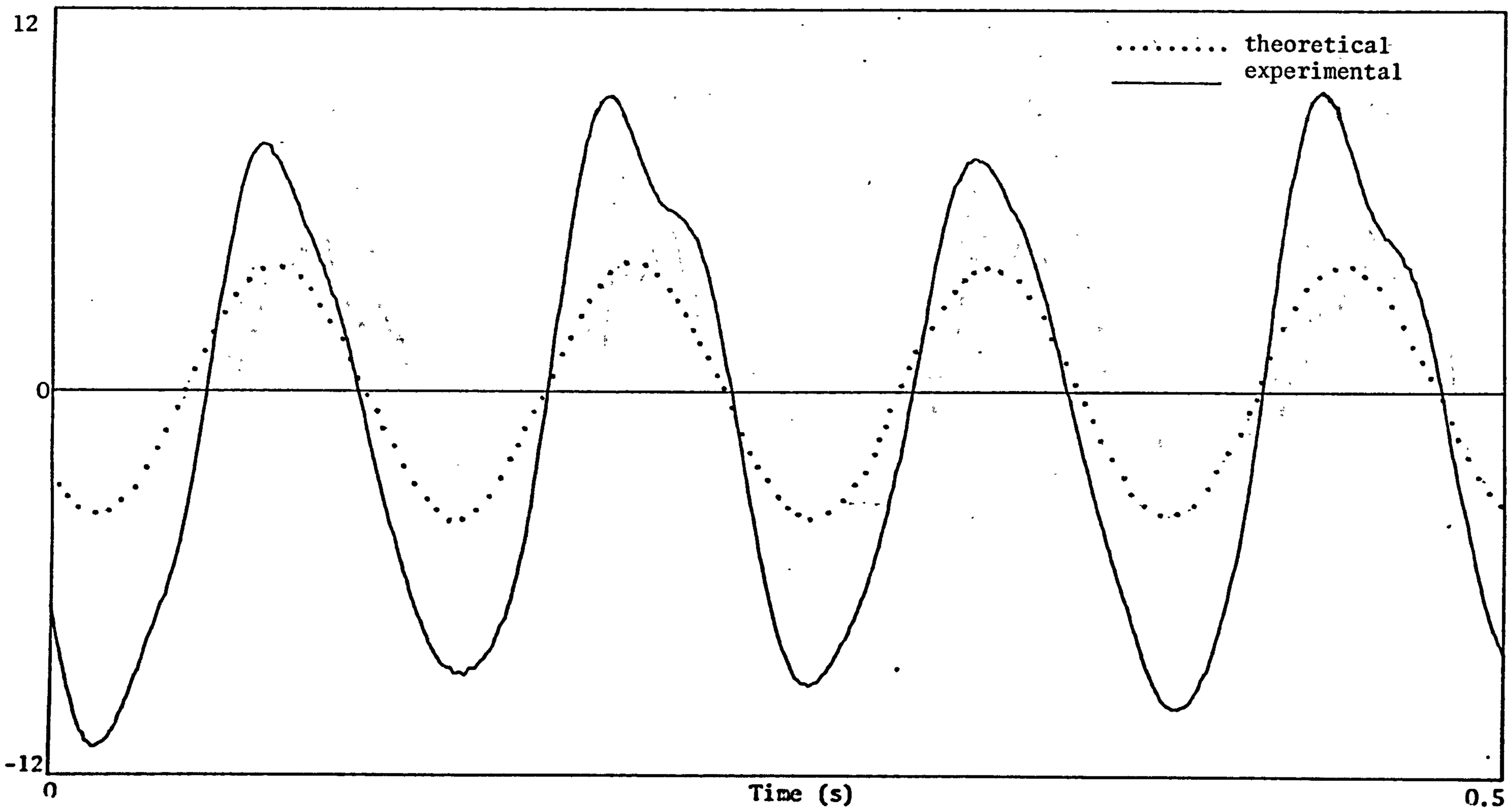

Fig. 81

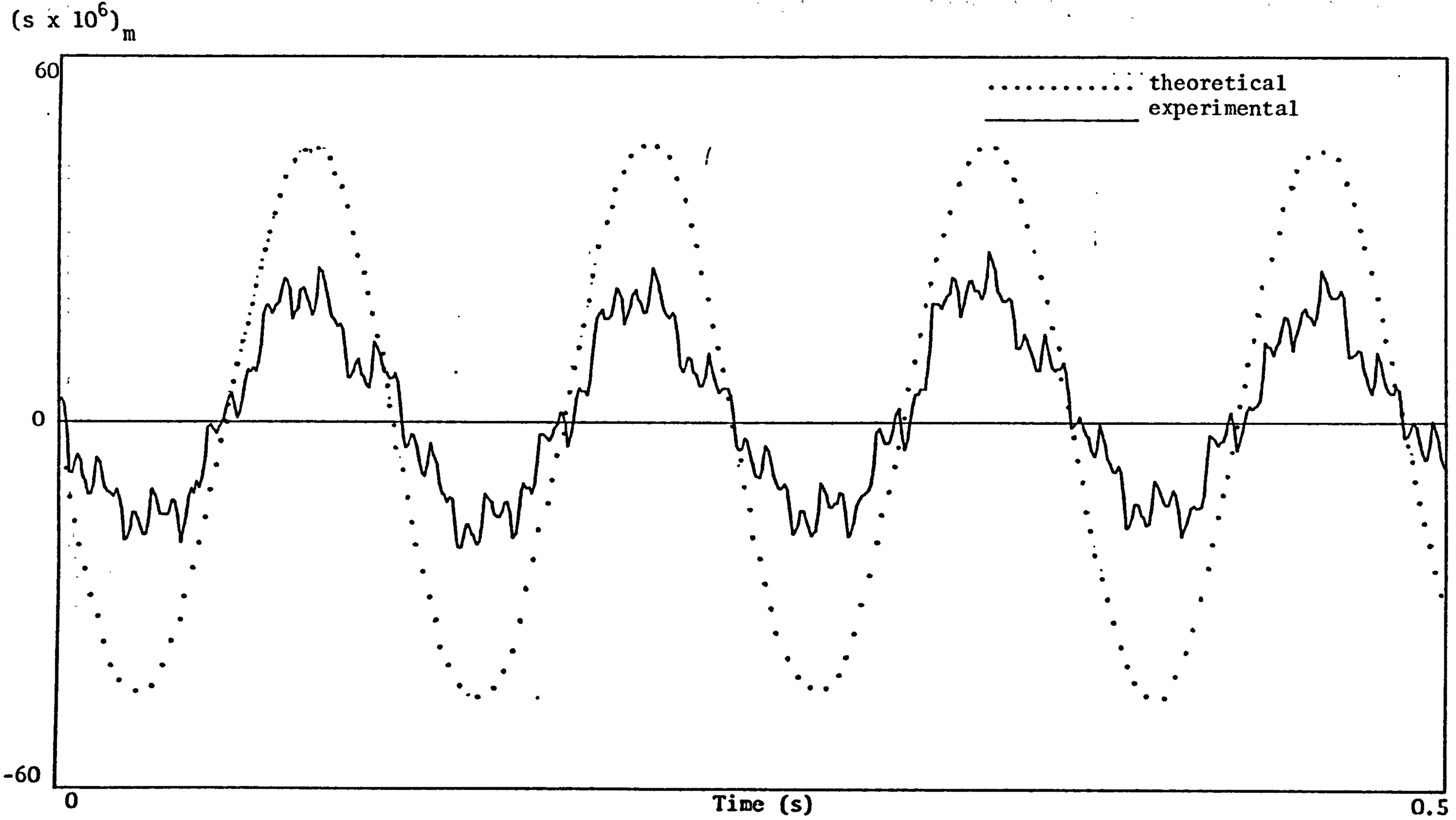

Fig. 82

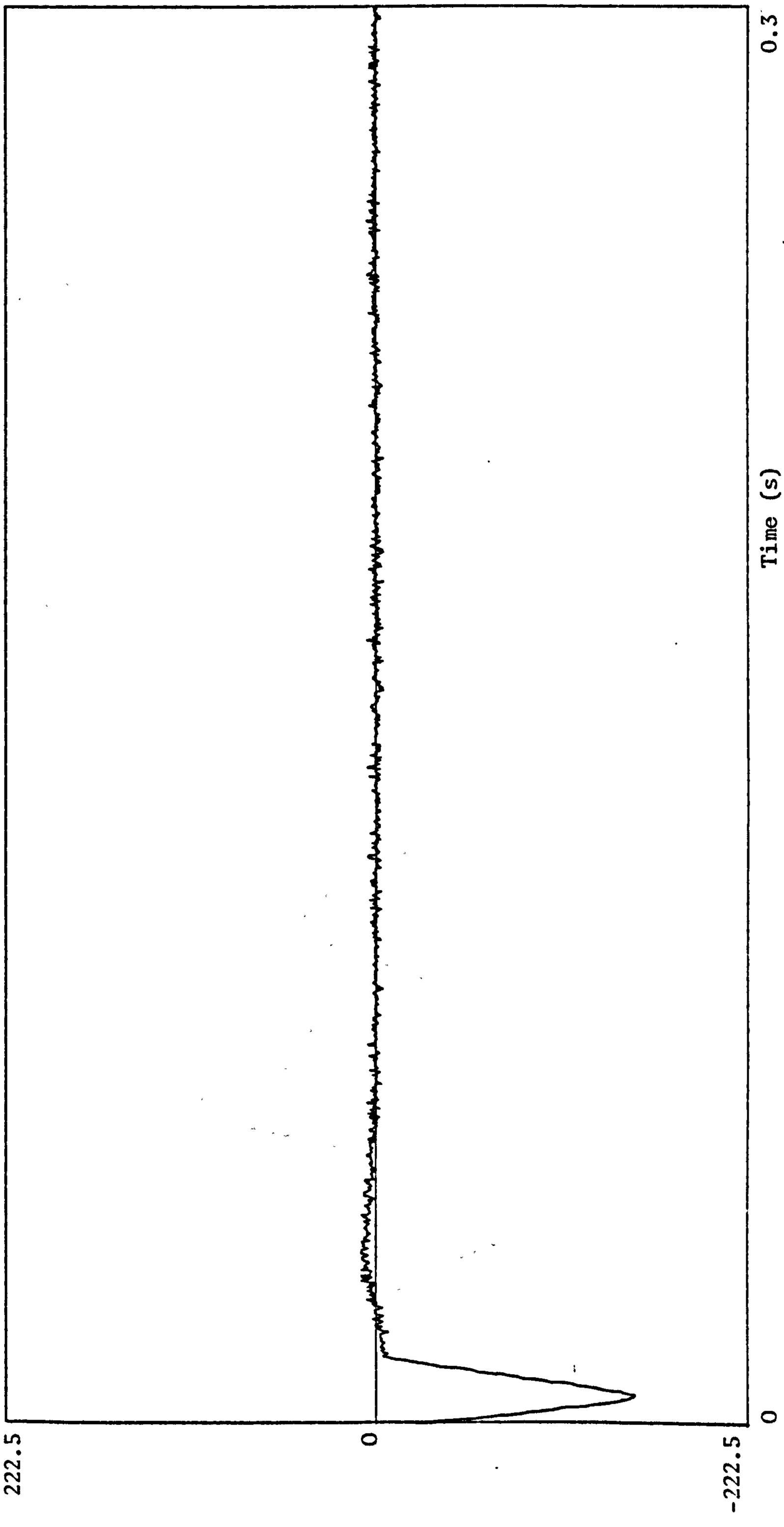

Fig. 83

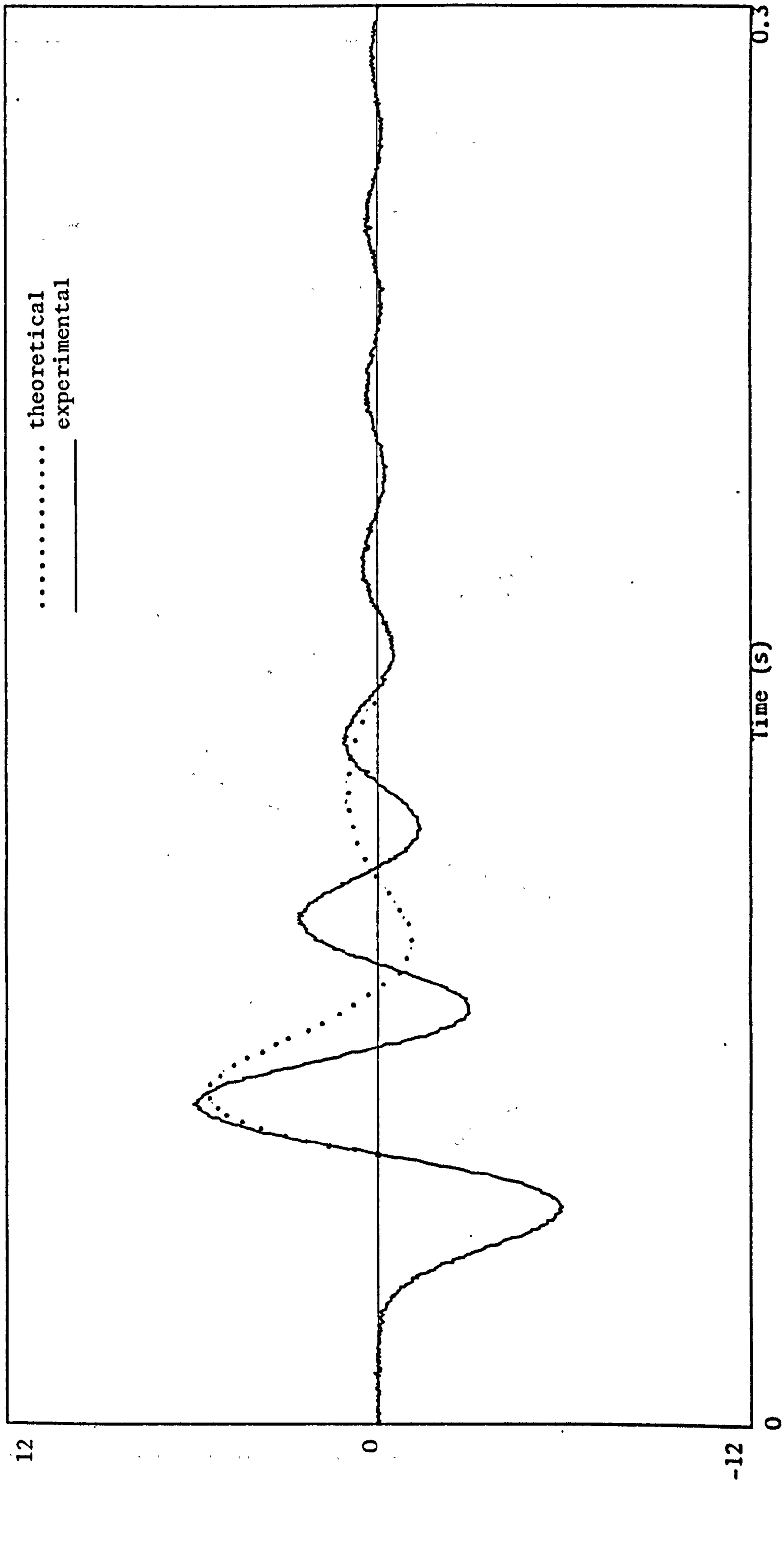

Fig. 84

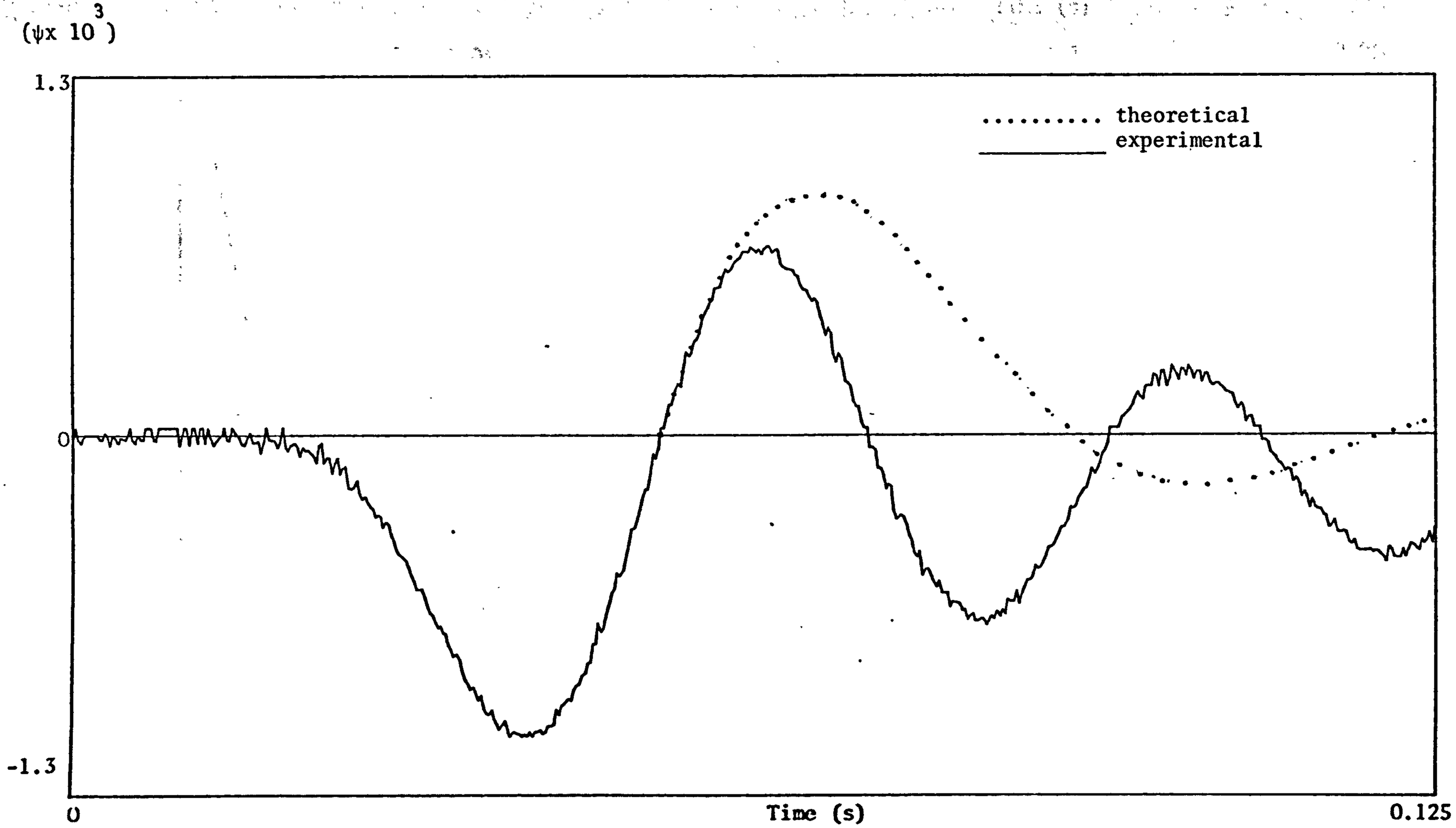

Fig. 85

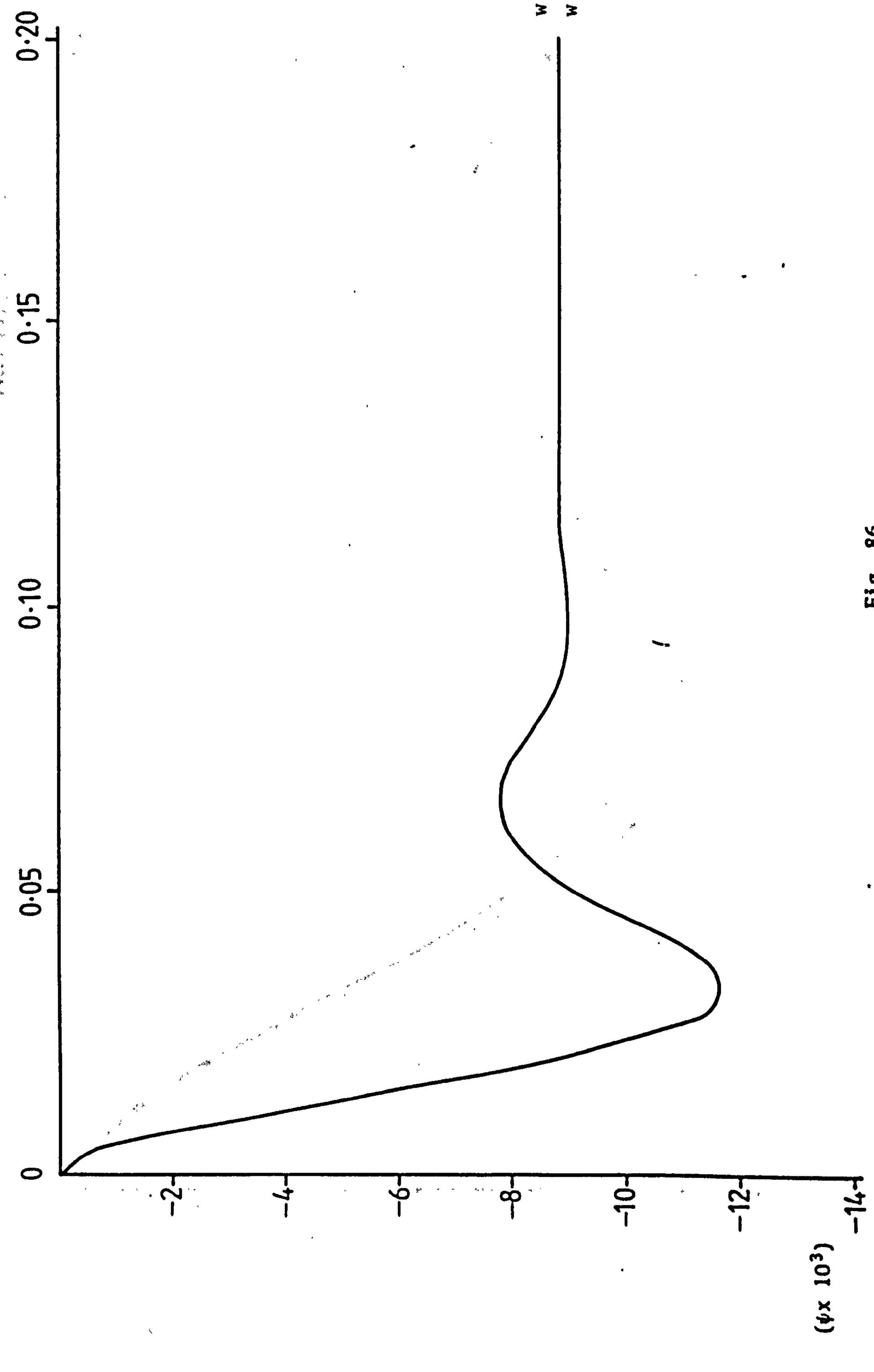

Fig. 86

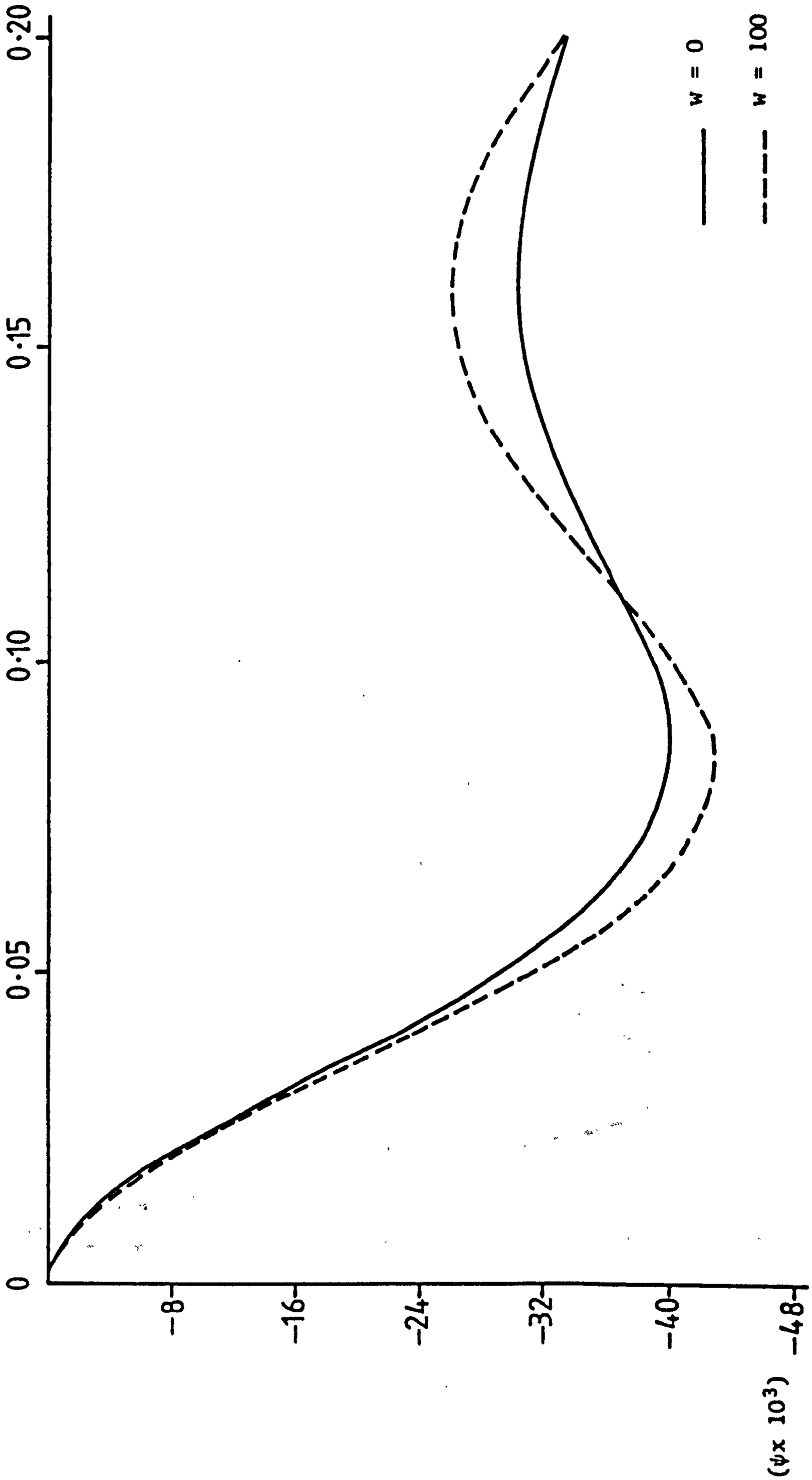

Fig. 87

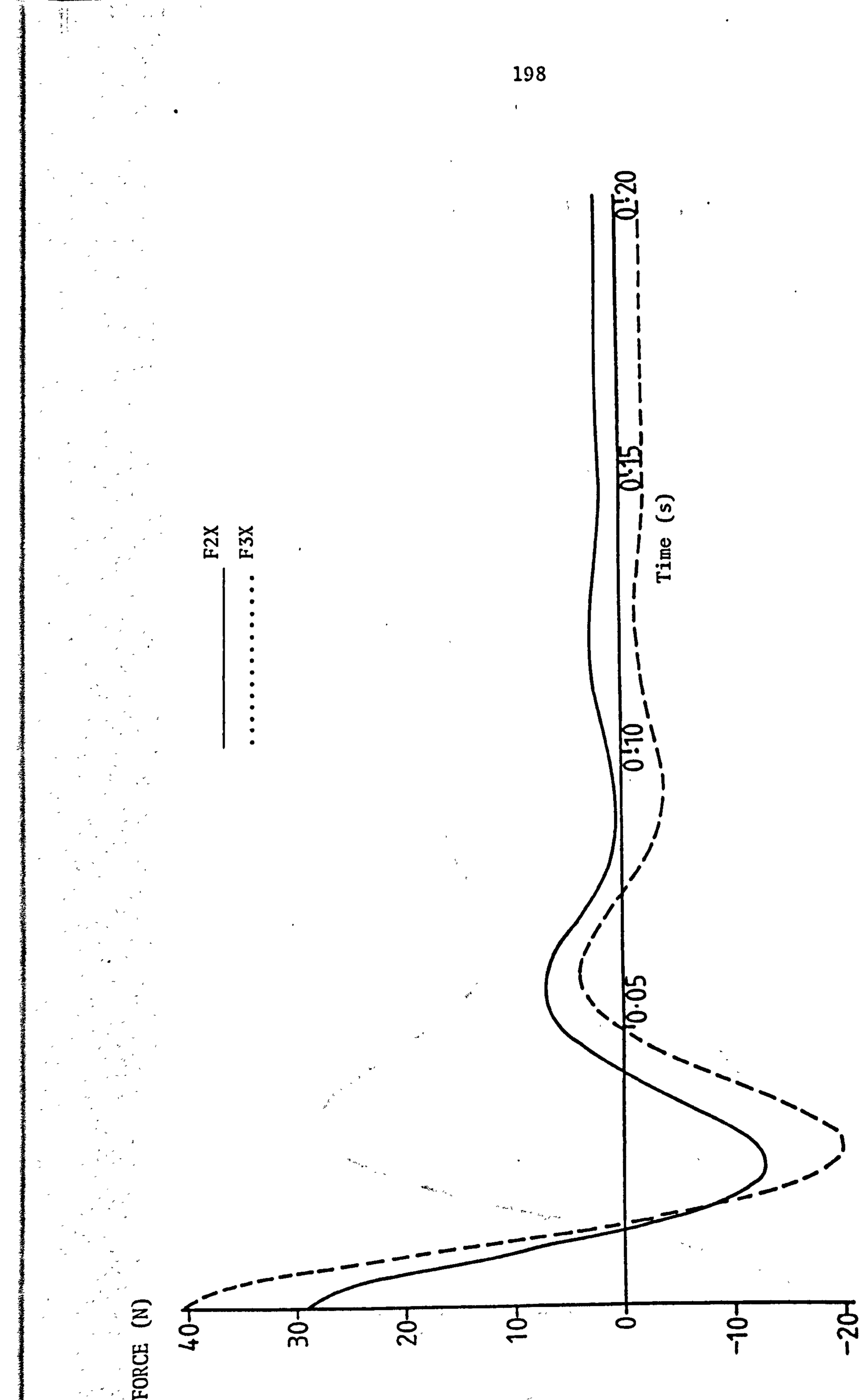

Fig. 88

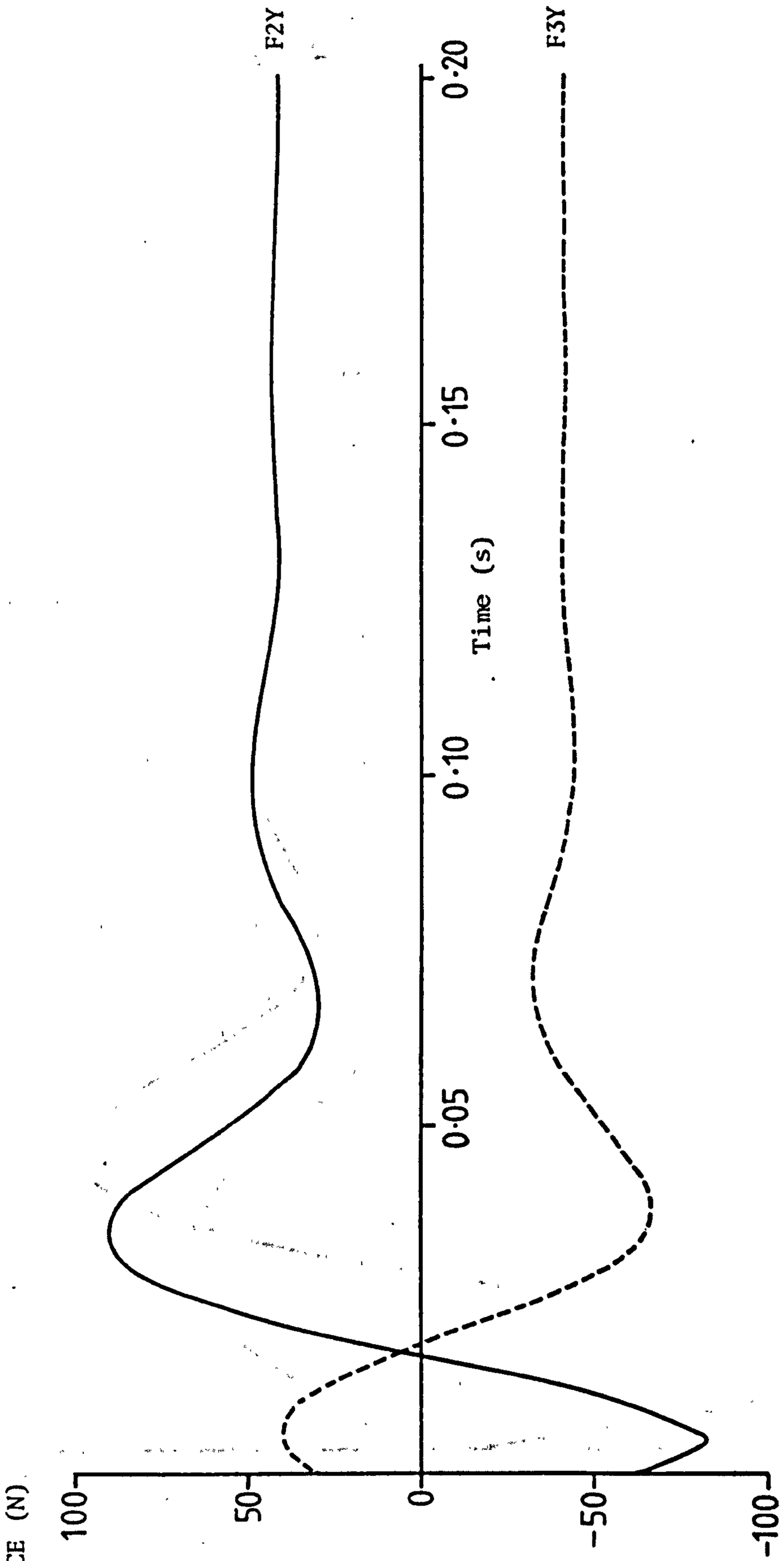

Fig. 89

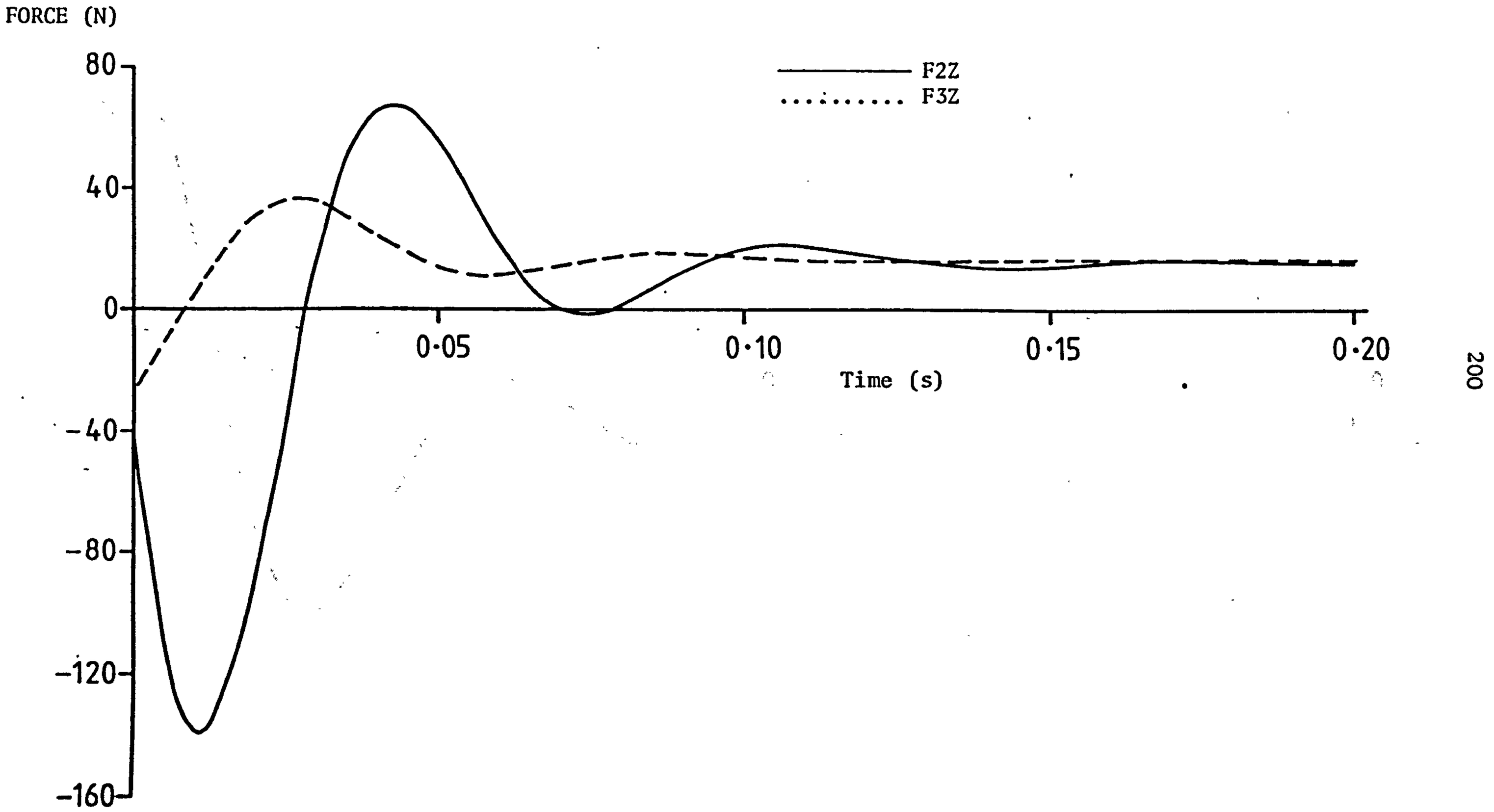

Fig. 90

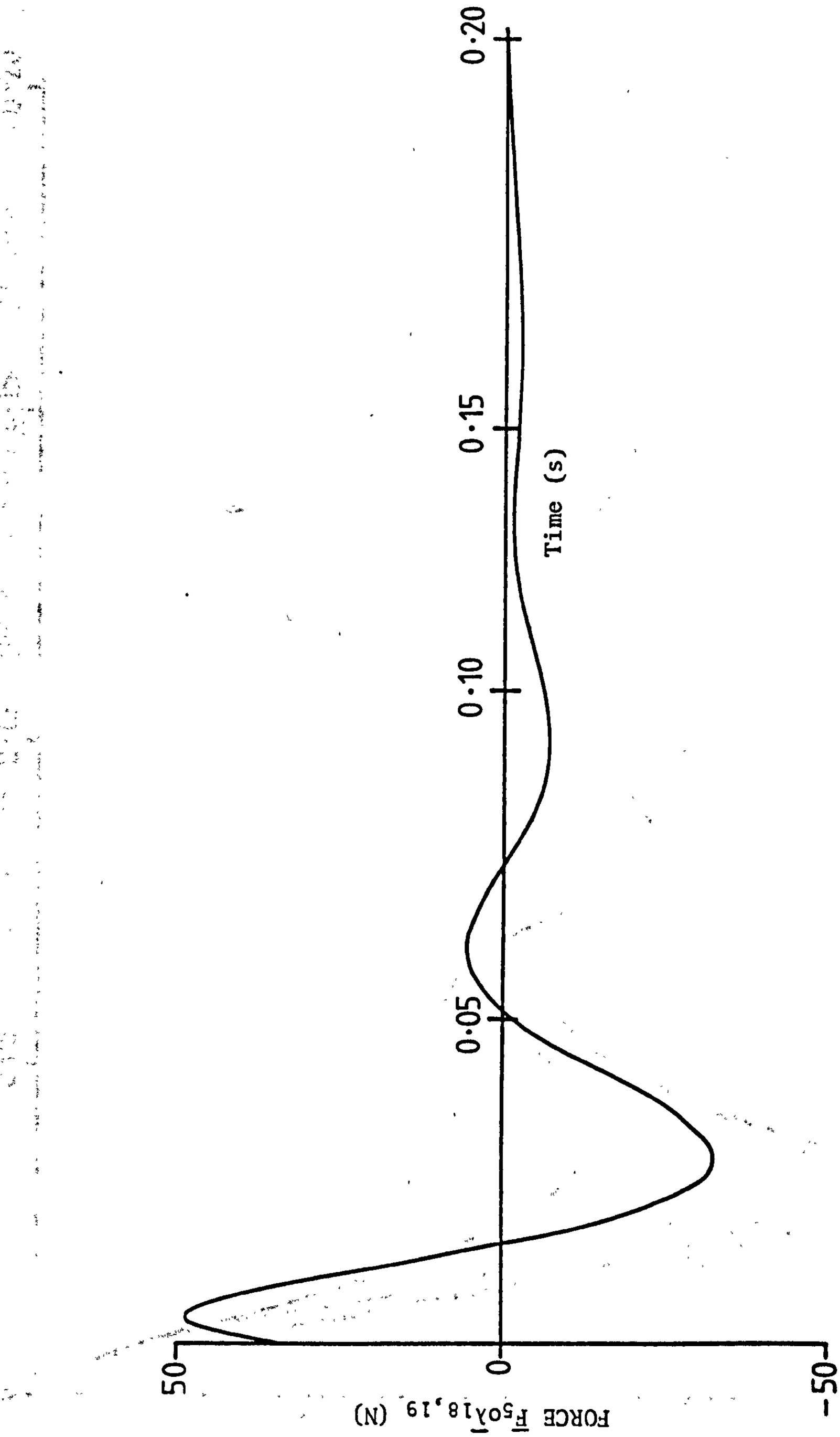

Fig. 91

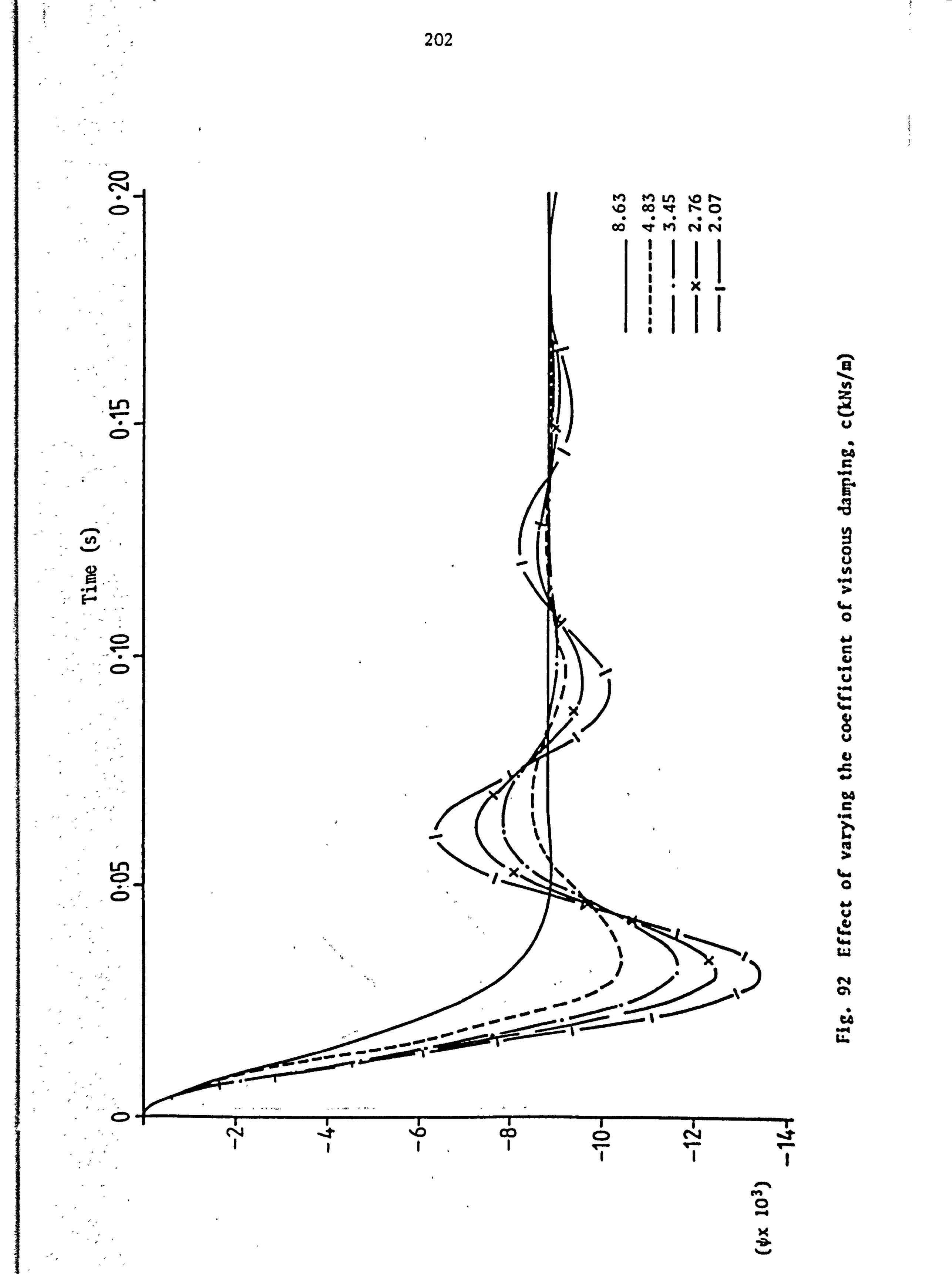

Fig. 92 Effect of varying the coefficient

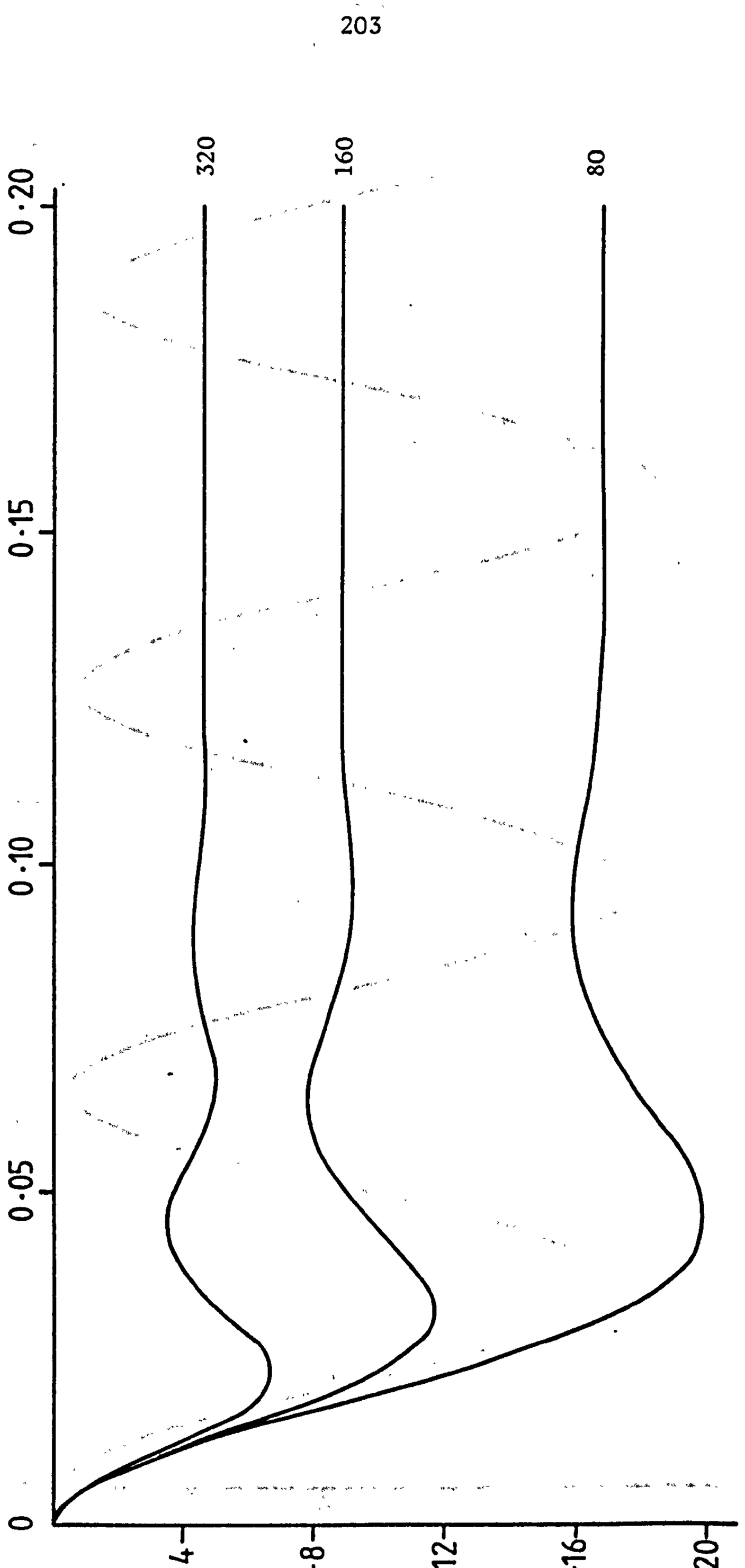

Fig. 93 Effect of varying the vertical stiffness of the pneumatic tyre; k_{TZ} (kN/m)

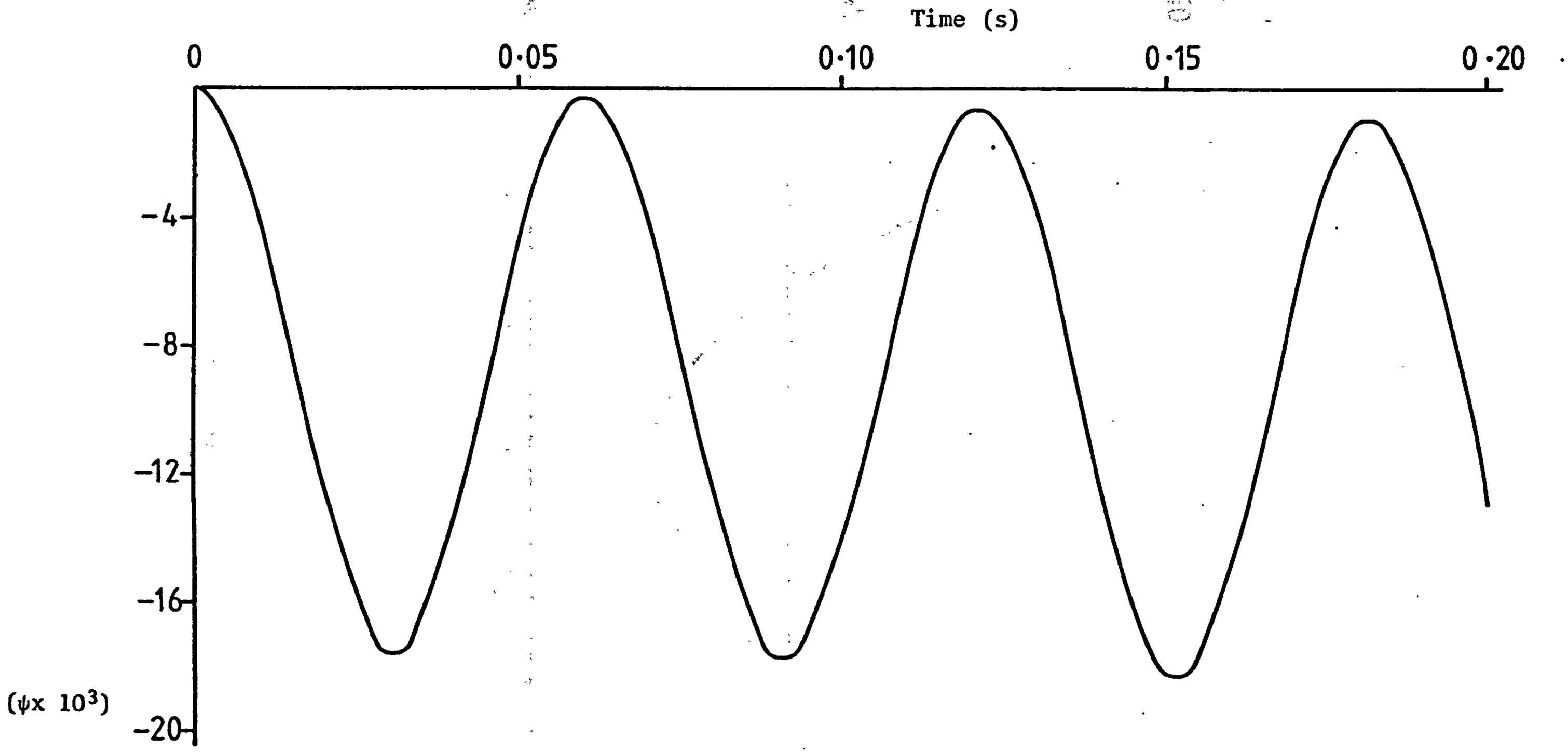

Fig. 94 Response of reference model with no damping

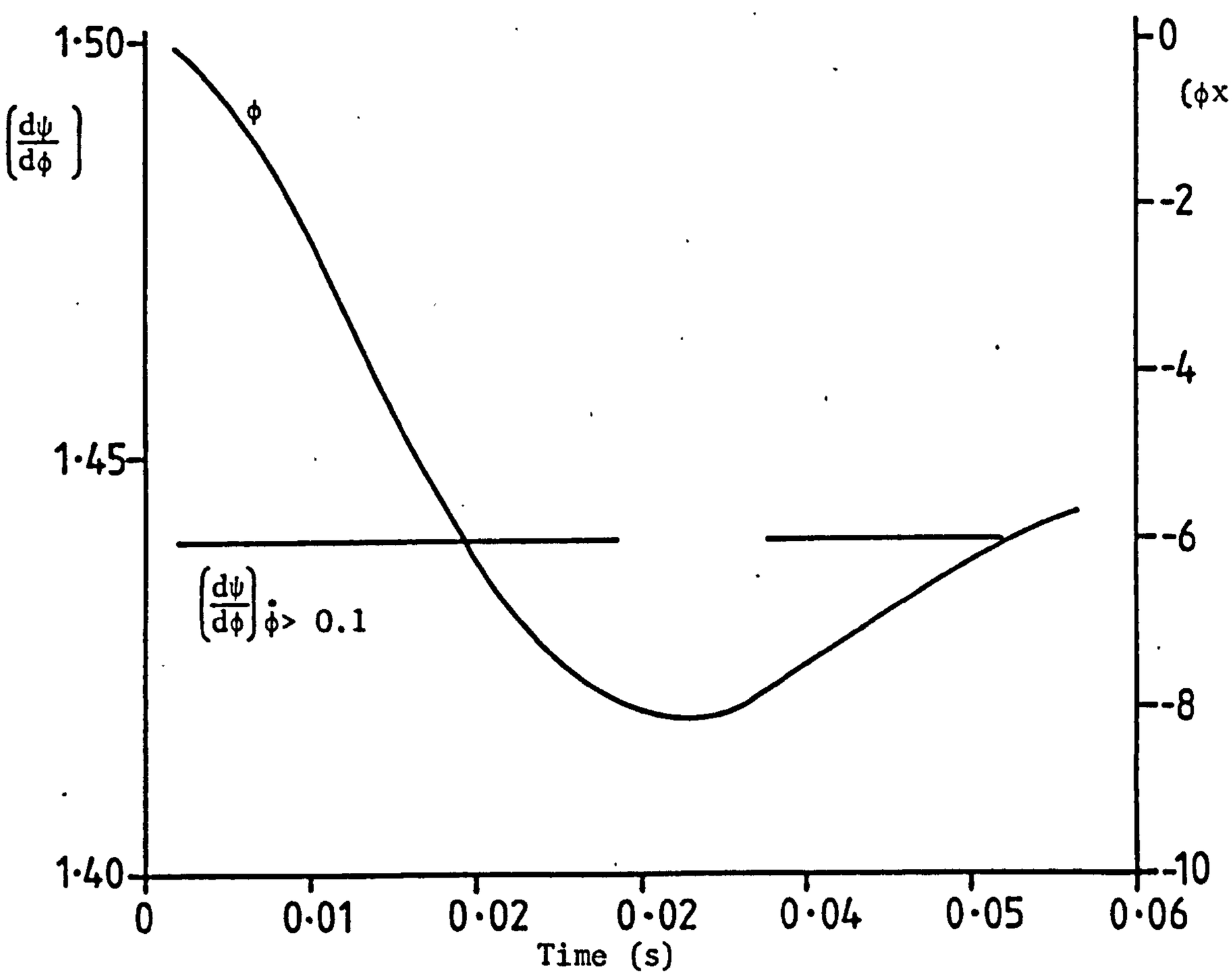
1·50
1·45
1·40
$\left(\frac{d\psi}{d\phi}\right)$
ϕ
$\left(\frac{d\psi}{d\phi}\right)\dot{\phi} > 0.1$
0
-2
-4
-6
-8
-10
($\phi \times 10^3$)
0
0·01
0·02
0·02
0·04
0·05
0·06
Time (s)

Fig. 95

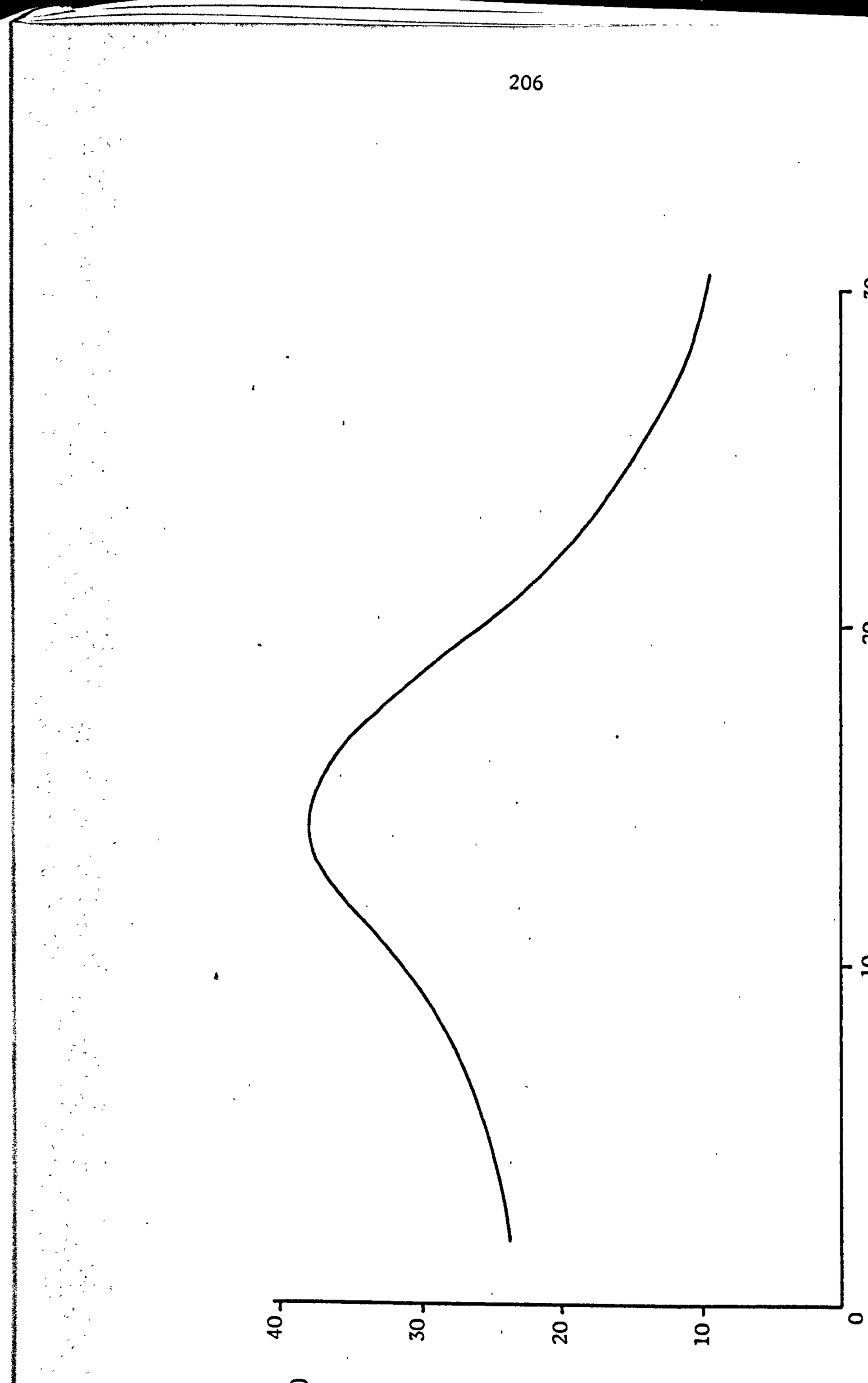

Fig. 96